Plasma Physics Series

Series Editor: **Professor E W Laing**, University of Glasgow

Advisory Panel
Dr J Lacina, Czechoslovak Academy of Sciences
Professor M A Hellberg, University of Natal
Professor A B Mikhailovskii, I V Kurchatov Institute of Atomic Energy
Professor K Miyamoto, University of Tokyo
Professor H Wilhelmsson, Chalmers University of Technology

Other books in the series

An Introduction to Alfven Waves
R Cross

MHD and Microinstabilities in Confined Plasma
W M Manheimer and C N Lashmore-Davies

Transition Radiation and Transition Scattering
V L Ginzburg and V N Tsytovich

Plasma Diagnostics based on Forward Angle Scattering
L Sharp, J Howard and R Nazikian

Radiofrequency Heating of Plasmas
R A Cairns

Plasma Physics via Computer Simulation
C K Birdsall and A B Langdon

Electromagnetic Instabilities in an Inhomogeneous Plasma
A B Mikhailovskii

Forthcoming titles

Physics of Intense Beams in Plasmas
M V Nezlin

Plasma Physics Series

Tokamak Plasma:
A Complex Physical System

B B Kadomtsev

I V Kurchatov Institute of Atomic Energy, Moscow, Russia

Translation Editor: **Professor E W Laing**

Institute of Physics Publishing
Bristol and Philadelphia

British Library Cataloguing in Publication Data. A catalogue record for this book is available from the British Library.

ISBN 0-7503-0234-8

Library of Congress Cataloging-in-Publication Data

Kadomtsev, B.B.
Tokamak plasma: a complex physical system / B. B. Kadomtsev; translation editor, E. W. Laing.
p. cm. – (Plasma physics series)
Includes bibliographical references and index.
ISBN 0-7503-0234-8
1. Plasma confinement. 2. Tokamaks. I.Title. II. Series.
QC718.5.C65K33 1992
621.48'4–dc20 92-29978
CIP

Published by IOP Publishing Ltd, a company wholly owned by the Institute of Physics, London

IOP Publishing Ltd, Techno House, Redcliffe Way, Bristol BS1 6NX, UK,
US Editorial Office: IOP Publishing Inc., The Public Ledger Building, Suite 1035, Independence Square, Philadelphia, PA 19106

Typeset by in TEX by IOP Publishing Ltd
Printed in Great Britain by Bookcraft, Bath

Contents

Notation vii

Acknowledgments xi

1 Introduction 1

2 Tokamak Evolution 4

3 Concept of Tokamaks and their Status 9

3.1 Nuclear Fusion 9
3.2 Magnetic Confinement 11
3.3 Charged Particles and Fields 16
3.4 Elementary Plasma Dynamics 20
3.5 Plasma Equilibrium 24
3.6 Plasma Stability 30
3.7 Operational Limits 35
3.8 Plasma as a Complex System 37
3.9 Physics of Confinement 40
3.10 Edge Plasma 47
3.11 Current Drive 49
3.12 Tokamak Reactor 54

4 Plasma Equilibrium 57

5 Plasma Stability 64

5.1 Kink Instability 65
5.2 Tearing Instability 73
5.3 Flute Instability 77
5.4 The Ballooning Instability 81
5.5 Internal Kink Mode 85
5.6 Drift Instabilities 85

6 Plasma as a Complex System 90

6.1 Dimensional Approach 92
6.2 Dimensional Analysis of Tokamaks 95
6.3 Murakami and Hugill Numbers 100
6.4 Dimensional Analysis of Energy Confinement 102

7 Non-linear Plasma Activity 109

7.1 Mirnov Oscillations 109
7.2 Saw-tooth Oscillations 110
7.3 Disruption Instability 114
7.4 Fan Instability 117
7.5 'Fish-bone' Instability 119
7.6 Edge Localized Modes 121
7.7 MARFE 122

8 Plasma Thermal Insulation 124

8.1 Neoclassical Theory of Transport 124
8.2 Bootstrap Current 129
8.3 Confinement Modes 132
8.4 Scalings 143
8.5 Thermal Conductivity, Diffusion and Viscosity 147

9 Plasma Self-organization 151

9.1 Profile Self-consistency 151
9.2 Optimal Profiles 153
9.3 Spontaneous Breakdown of Symmetry 161
9.4 Physics of Transport 177

10 Heating and Current Drive 183

10.1 Ohmic Heating 183
10.2 Lower Hybrid Resonance 184
10.3 Ion-cyclotron Resonance 185
10.4 Electron-cyclotron Resonance 186
10.5 Neutral Injection 188
10.6 Other Schemes of Heating 189

11 The Burning Plasma 191

12 Conclusion 194

References 199

Index 207

Notation

a	-minor radius, horizontal half-width of plasma cross section
$A = R/a$	-aspect ratio
A_i	-ion atomic mass
b	-vertical half-width of plasma
$\boldsymbol{B}$	-magnetic field vector
B	-absolute value of the field, toroidal field in simplified relations
B_0	-field on magnetic axis; $B = R_0 B_0/R$, where R_0 is the major radius of magnetic axis
B_0, B_T, B_φ	-toroidal magnetic field
B_z	-vertical equilibrium field
B_θ	-poloidal field component
$B_p = B_\theta(r = a)$	-poloidal field on plasma edge
$\boldsymbol{B}^*$	-auxiliary field for perturbation with helical symmetry; B^*_θ is its azimuthal component
c	-light velocity
D	-diffusion coefficient
e	-electron charge
$\boldsymbol{E}$	-electric field vector
E_f	-neutral beam energy
$\mathcal{E}_\psi$, $\mathcal{E}_\phi$	-energy of magnetic field and of plasma compression at weak oscillations (eq (255))
f_{ce}	-electron-cyclotron frequency
f_{ci}	-ion-cyclotron frequency
f_{LH}	-lower hybrid frequency
f_L	-L-mode enhancement factor of energy confinement
F_i, F_e	-ion and electron tuning factors of magnetic pumping and magnetic noise decay (eq (294))
g	-Troyon factor
H	-Hugill number
I	-plasma current
I_φ	-total current flowing through a circle with radius R (eq (86))
$I_c = 5Ba^2/R$	-plasma current corresponding to $q_a = 1$

$I_N = I/Ba$ –normalized current
j, J –local current density
j_s –current density averaged over cross section
k –wave number
$K = b/a$ –plasma elongation
$K_i = a^2/\rho_i^2$ –square ratio of plasma radius to mean ion Larmor radius
l_i –internal inductance per unit length
$L_i = 2\pi R l_i$ –internal inductance
m_e, m_i –electron mass, ion mass
$M = \bar{n}_e R/B$ –Murakami number
n_e, n_i –local electron density, local ion density
$\bar{n}_e$ –chord mean density value
$\langle n_e \rangle$ –averaged over volume plasma density
$N_D = n(T/e^2 n)^{3/2}$ –non-dimensional number, proportional to the number of particles in a Debye sphere
$p = n_e T_e + n_i T_i$ –plasma pressure
p_n –neutron load on the wall
P –plasma heating power
P_{OH} –ohmic heating power
P_f –fusion power
P_α –alpha-particle heating power
$q = B_T r/B_\theta R$ –local safety factor
$q_a = B_T a/B_p R$ –safety factor
$q_{eff} = q_* = 5B_T ab/IR$ –the same but for elongated cross section (in simple equations—q)
$Q = P_f/P$ –ratio of fusion power to plasma heating power
$Q_{DT}*$ –predicted value of Q for D–T plasma
r –variable minor radius
r_s –resonance point, where $q(r_s) = m/n$; inversion radius of saw-tooth oscillations
$r_0 = e^2/m_e c^2$ –electron classical radius
R –variable radius in cylindrical coordinate system
R_0 –plasma major radius
$S = rq'/q$ –local shear
t –time
T_e, T_i –electron temperature, ion temperature
$T_0 = T(0)$ –temperature at plasma centre, where $r = 0$
u –normalized phase velocity of drift waves
U –loop voltage
v –hydrodynamic velocity
v_e, v_i –mean thermal velocity of electrons, ions; $v_j = \sqrt{2T_j/m_j}$
v^* –drift phase velocity
V –plasma volume
w –half-width of magnetic island
W_T –plasma thermal energy
W –heat flux to the chamber wall

$x = r - r_s$ –distance from resonance point
$y = r\theta$ –coordinate along the magnetic surface cross section
Z_{eff} –effective charge number of plasma ion component: $Z_{eff} = \Sigma n_j Z_j^2/n_e$
$\alpha = -8\pi p' r/B^2$ –normalized plasma pressure gradient
α –amplitude of helical perturbation of poloidal flux eq (120))
α_z –decay index of equilibrium field B_z
β –ratio of plasma pressure to that of magnetic field $\beta = 8\pi\langle p\rangle/B_T^2$, $\beta_\theta = 8\pi\langle p\rangle/B_\theta^2$, $\beta_p = 8\pi\langle p\rangle/B_p^2$
β_α –ratio of alpha-particle pressure to magnetic field pressure
γ –adiabatic index; for plasma $\gamma = 5/3$
γ_{CD} –non-inductive current drive efficiency
Γ –vortex density
Γ_n –particle flux
Γ_e –electron heat flux
Γ_i –ion heat flux
δ –triangularity of plasma cross section
Δ –Shafranov shift (eq (82))
Δ' –logarithmic discontinuity jump of $\tilde{\psi}$ (eq (117))
$\epsilon = r/R$ –local toroidicity
η –resistivity
$\eta_i = \mathrm{d}\ln T_i/\mathrm{d}\ln n$ –ratio of temperature relative gradient to that of density
$\kappa = -(1/n)(\mathrm{d}n/\mathrm{d}r)$ –density relative gradient
$\kappa_T = -(1/T)(\mathrm{d}T/\mathrm{d}r)$ –temperature relative gradient
$\kappa_e = n_e \chi_e$ –electron thermal conductivity coefficient
$\kappa_i = n_i \chi_i$ –ion thermal conductivity coefficient
λ –effective potential (eq (141))
λ –mean free path length (eq (14))
$\Lambda = c/\omega_{pe}$ –London length, magnetic field penetration depth into ideal plasma
$\mu = 1/q = B_\theta R/B_T r$ –normalized angle of rotational transform
$\nu_{e,i}$ –electron and ion collision frequencies
ν_a –anomalous collision frequency
$\Pi = a^2/\Lambda^2 = 4\pi n a^2 r_0$ –non-dimensional density, number of particles per unit length (eq (160))
$\rho_{e,i}$ –Larmor electron, ion radius
$\rho_{e\theta}, \rho_{i\theta}$ –Larmor radius in poloidal field
$\sigma = 1/\eta$ –plasma electrical conductivity
$\tau = T_i/T_e$ –ion to electron temperature ratio
$\tau_E = W/P$ –energy confinement time
φ –azimuthal angle
ϕ –electric field potential
Φ –toroidal magnetic flux
Φ_e –electron thermal conductivity adjustment factor (eq (292))

χ	–flux function (eq (97))
χ_e, χ_i	–electron and ion transverse thermal diffusivities
ψ	–poloidal magnetic flux per unit length of cylindrical plasma (per radian in the torus, Chapter 4)
Ψ	–total poloidal magnetic flux in the torus (Chapter 3)
$\tilde{\psi}$	–poloidal magnetic flux perturbation
ψ^*	–magnetic flux for auxiliary field B^*
ω	–oscillation frequency
ω^*	–drift frequency
ω_{ce}, ω_{ci}	–electron and ion cyclotron frequency
ω_{LH}	–lower hybrid frequency
$\omega_{pe} = \sqrt{4\pi e^2 n/m_e}$	–Langmuir frequency
$\omega_A = k\sqrt{B^2/4\pi m_i n}$	–Alfven frequency
$\omega_{A\theta}$	–Alfven frequency in poloidal magnetic field

Acknowledgments

The author is grateful to the following for granting permission to reproduce figures included in this book.

JET Joint Undertaking for figures 6.2 and 7.4 ©EURATOM

Max-Planck-Institut für Plasmaphysik for figure 7.7

US Department of Energy, Princeton University Plasma Physics Laboratory for figure 8.8

European Physical Society for figure 8.10

General Atomics, San Diego, California for figures 3.6 and 9.9

The author and IOP Publishing Ltd have attempted to trace the copyright holder of all the figures reproduced in this publication and apologize to copyright holders if permission to publish in this form has not been obtained.

1 Introduction

From time to time, at a certain stage in the development of any branch of science, the need arises for a summing-up of the results achieved so far. A certain 'compression' of information is required, i.e. a concise presentation of major results from numerous publications which have previously appeared in the form of articles, reports and contributions to conferences. The need for such a summary has arisen now in tokamak research, and there are several reasons for this.

The first, but not the main reason, is the existence of vast amounts of information. Even for an experienced person, who has worked for a long time in a given field of research, it is often difficult to find the way through a large number of publications, to observe the similarities or contradictions among various results and, moreover, to evaluate the quality of certain published results, which, unfortunately these days, are often rather shallow.

The second, more important reason, lies in the fact that we have now reached a clear understanding of the major principles that govern the behaviour of high-temperature plasma in tokamaks. Today we can formulate these principles with a sufficiently high degree of accuracy and there is a tangible probability that the principles will 'survive' succeeding stages of experimental and theoretical studies, although it is quite reasonable to assume that they will undergo detailed study and improvement.

Finally, there is one other reason for summarizing the major results of studies in tokamaks. This reason is explained by the fact that tokamaks have passed a very important stage of their development. We have witnessed a vast number of experiments on larger new facilities. These experiments together with theoretical developments were aimed at studies of high-temperature plasma physics, which would consequently permit us to master plasma as the subject matter of future reactors.

For quantitative characteristics of such plasma it is very convenient to use the value of Q—the ratio of fusion reaction power to input power, which is required to maintain plasma in a steady state. Value $Q = 1$ corresponds to the so-called 'break-even'—a state when the fusion power is equal to the plasma heating power. Break-even has been the major objective of studies so far. At the present time this goal has been practically reached: the largest European tokamak, JET, has plasma with temperature, density and level of thermal insulation of such an order that in the case of using a deuterium–tritium mixture the fusion power should be close to the power of plasma heating. The experiments with deuterium–tritium (D–T) are in their initial stage: in the first D–T shots a megawatt level of fusion power was achieved [160]. It is hoped that the calculated value of $Q \sim 1$ will be reached in the near future. Somewhat more modest, but of the same standard of deuterium plasma, were the results obtained on the American tokamak TFTR. That is why we can accept that the problem of plasma heating and confinement is solved.

But this does not mean that absolutely all problems of thermonuclear plasma physics have been solved. Additional attempts are needed to obtain a D–T plasma extended burn, to remove helium-reaction products as well as other impurities from plasma, to develop optimal schemes and scenarios of plasma heating and current drive by non-inductive methods, to obtain temperature and density profile control with the aim of decreasing the probability of current disruption, and to further increase plasma pressure as compared with magnetic field pressure. Further experiments are required which are aimed at optimization of a tokamak-reactor and at a possible transition to more promising fuels, e.g., to a low-radioactive mix of D–^{3}He.

The major task has, however, been achieved—a physical data base for a fusion reactor has been created and because of this the designs of fusion reactor-tokamaks are currently being developed. Among them the most advanced one is the design of an International Thermonuclear Experimental Reactor (ITER), which was started in 1988 on the initiative of the former Soviet Union.

Fusion reactor design activities require the continuation of studies of plasma physics and plasma technology as well as the implementation of specific R&D engineering and technological programmes for the design needs. The fusion researches attract a broad number of new scientists and engineers of various disciplines. This fact superimposes another image on the pattern of digesting the results of studies on tokamaks. To be more specific, the review should be available not only to the patriarchs in this field of science but also to young scientists and engineers who are just starting their work and

who have decided to combine their creative activity with the assessment of fusion as a real energy source. That is why the 'compression' of information should be not only a compilation like a 'guidebook' on published materials but rather a review of major ideas and of the basic knowledge accumulated so far. In any case, this was the very goal I tried to reach while preparing this book. How far I have succeeded is for the readers to judge.

One other remark. Tokamak plasma is a complex physical system. Various physical processes exist and interact simultaneously there. That is why the deeper the studies are the more sophisticated are the discovered physical phenomena. Here, similar to many paintings by the prominent artist Hieronymus Bosch, there exist many levels of perception and understanding. At a cursory glance of the picture you promptly grasp its idea. But under a more scrutinized study of its second and third levels you discover new horizons of a deeper life and it turns out that your first impressions become rather shallow. Tokamak plasma investigators go deeper and deeper and some of the details are still to be agreed upon among them. That is why in attempting to give a compressed description of tokamak physics it is rather difficult to make an unbiased account of the results obtained. For this reason I have deliberately roughened and simplified the picture. In doing so I hope to be as close to the reality of the situation as possible. This is rather difficult by itself and for me especially because I cannot completely release myself from my own ideas, feelings and perceptions. That is why the reader is recommended to accept major well-proven results with confidence and not to be so critical towards the presented explanations of details.

To make your reading easier, a list of the major symbols used in the text has been given at the beginning of the book.

2 Tokamak Evolution

A man's fate is determined primarily by his parents' standing and also by the abilities of those who taught him his first steps, first words and first ideas. The same applies to a branch of science—it is very important who the initiator and developer of that branch was: the depth and magnitude of the spirit of those who established that branch of science determine the level of that branch.

In this regard tokamaks were fortunate. Their originators were prominent physicists—theoretician Tamm and, one of the greatest thinkers of our time, Sakharov. In his lecture [1] on the occasion of the Nobel Peace Prize award Sakharov recollects that period of his life as follows: 'Twenty-five years ago I was fortunate together with my teacher, Nobel Physics Prize winner Tamm, to launch the research into fusion reactions in our country. Now this work has expanded tremendously. Various trends are being studied, ranging from classical schemes of magnetic thermal insulation to laser methods'.

The main idea of the fundamental works by Sakharov and Tamm was the idea of magnetic thermal insulation: a high-temperature plasma immersed in a strong magnetic field should have a strongly decreased thermal conductivity across the magnetic field due to the fact that the trajectories of charged particles look like compact helical lines wound on the magnetic field lines. There is no thermal insulation in the longitudinal direction and that is why magnetic lines should be closed in such a way that a magnetic flux tube would have a toroidal form. But here another difficulty arises: the toroidal magnetic field is non-uniform, and in a non-uniform field charged particles undergo a systematic drift, so that thermal insulation is destroyed. To restore thermal insulation, Sakharov proposed to generate an additional current either along the conducting coil which is situated on the circular axis of the torus or simply along the plasma ring. A field configuration composed of mutually enclosed toroidal magnetic surfaces was well-known and even described in a textbook

by Tamm. This proposal to generate an additional current had defined a major step towards tokamak concept but still much effort was needed to bring it up to the present level.

Studies on controlled fusion reaction with magnetic plasma confinement were started soon after the idea of magnetic thermal insulation had been formulated. Experimental work was headed by Artsimovich and theoretical studies by Leontovich. The first experiments went along a simpler way of pinches—self-compressed gaseous discharges. Only when numerous instabilities of magnetically-confined plasma were observed did the interests of the experimentalists turn to the initial Tamm–Sakharov idea. In 1955 Golovin and Yavlinsky and a group of young and vigorous scientists started experiments on the toroidal facility TMP [5] where a toroidal discharge which was excited by an azimuthal electric field was immersed in a strong enough toroidal magnetic field. To avoid column shift along the major radius Sakharov proposed to use a conducting shell. Inductive currents in the shell were to facilitate the plasma column positioning. Somewhat later a new term was proposed which unified major elements of a plasma facility: the tokamak—a toroidal chamber with magnetic coils.

The first results obtained on toroidal discharges were not very inspiring to anyone, except the experimentalists themselves: the plasma was impure and cold. A metallic chamber made of Cr–Ni stainless steel appeared to be more attractive: plasma became purer. But the laws of plasma physics were unknown, which was the reason why the theory was developed by its own logic almost independently of experiment. The idea of plasma column stabilization by a strong longitudinal magnetic field was theoretically proved to be very important [6]. After the Geneva conference of 1958, when all fusion research was declassified, this idea quantitatively formulated by Shafranov [7], was combined with a similar discovery by Kruskal and was called the Kruskal–Shafranov criterion. Shortly after this the theoretically predicted stability was confirmed by the experiments conducted by Gorbunov and Razumova [8].

At the Geneva conference Soviet physicists became acquainted with the remarkable idea of stellarators, put forward by the well-known American astrophysicist Spitzer. In a stellarator toroidal drift of particles is compensated by external helical magnetic fields. Soviet physicists returned from the Geneva conference inspired: tokamak geometry seemed to them simpler and, correspondingly, more promising. The possibility of using a limiter to constrain the plasma column which was successfully proven in stellarators opened new ways of improving plasma quality. Step by step maturing of tokamaks started with the operation of new facilities T-2, T-3, TM-2.

Plasma parameters were improved, being accompanied by the development of theory and deeper perception of processes occurring in tokamak plasma. In parallel with the development of science the technology was also improved and diagnostic tools were expanded.

For many years the major objective of tokamak studies was physics of confinement, i.e. physics of transport phenomena in plasma: thermal conductivity, diffusion, impurities transfer. At that time the Bohm diffusion relation persistently dominated in stellarators and the prospects of magnetic confinement were rather grim. The first non-Bohm type scaling, i.e. a simplified empirical dependence of confinement time upon the major plasma parameters was proposed by Gorbunov, Mirnov and Strelkov—the so-called GMS-scaling. Compared with Bohm formulae it was much more optimistic. Artsimovich having recognized in this a principal difference between the two concepts stated at the Novosibirsk conference of 1968 that plasma confinement in tokamaks is better than predicted by Bohm formulae. He started to develop his investigations in a way that would permit better understanding of this difference. Since the measurement of the electron temperature based on the value of the longitudinal electrical conductivity did not seem to be very reliable, he invited a group of experimentalists from England with newly-developed laser diagnostics. The high electron temperature in the T-3 tokamak was confirmed. In parallel with the experiments, the theory was also being developed. The Soviet and foreign theoreticians studied various types of plasma instabilities including a broad class of relatively slow drift instabilities. Galeev and Sagdeev developed a more precise theory of collisional transport which was called neo-classical theory [9].

This progress enabled Artsimovich to draw up certain conclusions of tokamak physics studies in a review in *Nuclear Fusion* [10]. Following on from the comparison of theory and experiments in T-3 and T-4, ion component confinement agreed fairly well with the classical theory and the electrons showed anomalous transport which could be described by an empirical formulae of pseudo-classical diffusion.

Somewhat earlier, in 1967, two short articles (in Russian) appeared in *Uspekhi Fizicheskikh Nauk* (*Soviet Physics Uspekhi*) [11,12]. In the first publication Artsimovich gave a positive assessment of the status and prospects of tokamaks. He emphasized, in particular, that in order to improve plasma parameters and to get a deeper understanding of plasma confinement physics it was necessary to develop methods of additional plasma heating (additional to ohmic heating). In the second publication, written by myself, I supported the idea that instabilities in tokamak plasmas did not hinder the achievement of good plasma confinement which is required for a fusion reactor, i.e. the confinement could be two orders of magnitude better than according to the Bohm formulae. To get this result, however, plasma dimensions should be large enough so that the product of the minor radius and longitudinal magnetic field would be of the order of 10 mT. It is interesting to note, that this value of $aB \sim 10$ mT was chosen by the International Thermonuclear Reactor (ITER) Team for elongated plasma cross section and improved 'H-mode' confinement regime.

Experimental studies showed a slow but steady progress. Soon the stellarator in Princeton Laboratory was modified into an ST tokamak, which immediately resulted in a drastic improvement of plasma parameters. After this many plasma laboratories throughout the world started to build tokamaks.

In 1975 two large tokamaks were commissioned: T-10—at the I V Kurchatov Institute of Atomic Energy and PLT at Princeton Plasma Physics Laboratory. A high-temperature and pure enough plasma was immediately obtained in T-10: temperature grew up to 1 keV, energy confinement time was increased four-fold as compared with T-4. That was a clear demonstration of the advantages of going to larger scale plasmas. Very soon, devices for additional plasma heating by means of neutral injection were installed on PLT facility, and ion temperature was easily raised to multi-keV values. Other heating methods were initiated and implemented: ion-cyclotron resonance heating, electron-cyclotron resonance (ECR) heating with the help of gyrotrons, heating and current drive at lower-hybrid resonance etc.

Apart from being practical, the use of additional heating turned out to be very important for magnetic confinement physics studies. Quite unexpectedly, it was found that additional heating in contrast to purely ohmic heating leads to a definite degradation of plasma confinement. This was very accurately demonstrated in a small facility ISX-B in Oak Ridge. There it was also shown that the degree of degradation was very sensitive to plasma conditions at its periphery. It took much effort to study these phenomena both in small and large tokamaks. Plasma confinement under an ohmic heating regime was studied scrupulously in comparatively small facilities of T-11 and ALCATOR type [13,14]. Respectively, similar scalings were obtained: T-11 and neo-ALCATOR ones [15,16] which were confirmed later on larger devices. But, of course, studies of plasma confinement with additional heating are of major interest.

The first experiments were not particularly encouraging. After the discovery of the regime of improved confinement in ASDEX [17], the so-called H regime, the prospects appeared to be more optimistic. As for the regime of 'not so good' confinement it was named the L

regime (L—low, H—high). Successive experiments in other tokamaks including large ones, confirmed the existence of the H regime and broadened the number of other possible modes of improved plasma confinement.

The ASDEX facility is one of the first facilities with a poloidal divertor, i.e. a special tool for plasma impurities removal. (The first poloidal divertor was installed in a small T-12 tokamak at the I V Kurchatov Institute [152].) The idea of a divertor was initially proposed by Spitzer in relation to stellarators. In tokamaks, to maintain axial symmetry, this idea naturally evolved into the poloidal divertor. Together with elongation of plasma cross section, proposed initially for confinement improvement [18] and later proved to be useful from other points of view the poloidal divertor turned out to be a very convenient tool for improvement of plasma parameters and its confinement capability.

In the 1980s several large tokamaks were commissioned: TFTR in USA, JET in Europe, JT-60 in Japan and somewhat later two tokamaks with superconducting coils—TORE SUPRA in France and T-15 in the former USSR. These large facilities started a new phase in tokamak studies and prepared a scientific basis for design and subsequent construction of an experimental thermonuclear reactor.

3 Concept of Tokamaks and their Status

The initial physical concept of the tokamak was an extremely simple one: a plasma ring with a toroidal current immersed in a strong toroidal magnetic field seems to be safely confined and permanently heated. However, even the first attempts to implement this idea had shown that the tokamak plasma is a much more sophisticated object than could be imagined from the abstract theoretical model. Plasma represents a very complicated world of non-linear self-organized matter with quite unusual behaviour. Tokamak plasma is really one of the best examples of the so-called complex physical system. Being such a complex system it can be easily produced in a laboratory and can be diagnosed and investigated in detail.

Initially the family of small tokamaks and later the tokamaks of medium and large sizes had clarified many mysterious phenomena in magnetically confined high-temperature plasma. At present we have an extensive experimental data base and enough theoretical understanding to explain the major effects in plasma.

3.1 Nuclear Fusion

The tokamak concept was proposed in connection with the idea of controlled nuclear fusion. The question is how to assess the huge source of nuclear energy of light elements in the form of quiet controlled burn of nuclear fuel.

When we talk about slow controlled burn we mean in fact burning at such a rate that the time for fuel refreshment is of the order of one minute. If only a few percent of fuel was really burned during this time, then the typical scale for the fuel burn is of the order of $10^{-3}\ s^{-1}$.

The highest rate of fusion reactions takes place in the deuterium–tritium (D–T) mixture. The D–T reaction looks like

$$D + T \rightarrow He^4 + n + 17.6\,(MeV) \qquad (1)$$

where its products are the helium nucleus and the neutron. Most of the energy released, i.e. 14.1 MeV, is taken by the neutron and the rest, 3.5 MeV, is left with He^4.

The nucleus, deuteron and triton are positively charged. Therefore to obtain an appreciable yield of nuclear reaction the initial relative velocity of nuclei should be high enough to pass through the Coulomb barrier.

The optimal energy for the D–T collisions is of the order of 10 keV. If this energy corresponds to the energy of thermal motion of particles, then the temperature of the D–T mixture has to be very high. At very high temperatures the hydrogen atoms, including its heavy isotopes, are split into their constituent parts—electrons and ions. Such a mixture of electrons and ions is called plasma. This high temperature plasma serves as the ignition for controlled nuclear fusion.

The temperature in plasma physics is measured usually in electronvolts or in kiloelectronvolts. Neither kelvin nor fahrenheit are convenient for high temperatures in plasma. Thus,the thermal energy of plasma electrons or ions is equal to $\frac{3}{2}T$ without the Boltzmann constant. The temperature $T = 1$ keV corresponds to 1.16×10^7 K. Therefore, the optimal temperature for a D–T reaction temperature of 10 keV is about one hundred million kelvin.

If we denote by n the density of ions, i.e. the number of ions per cm^{-3}, then the specific power of fusion reactions for 50%–50% mixture of deuterium and tritium can be written as

$$P/V = \tfrac{1}{4}n^2\langle\sigma v\rangle\mathcal{E}_0. \qquad (2)$$

Here P is the total fusion power, V is plasma volume, $\mathcal{E}_0 = 17.6$ MeV is the energy yield of a single reaction, $\langle\sigma v\rangle$ is averaged over Maxwellian distribution product of the D–T fusion cross section and relative velocity of nuclei and n is the ion density. We can represent relation (2) in the form

$$P/V = \frac{1}{16}p^2\frac{\langle\sigma v\rangle}{T^2}\mathcal{E}_0 \qquad (3)$$

where $p = 2nT$ is the total plasma pressure, including both ion and electron components (we assume similar temperatures for ion and electron components and the absence of impurities).

The expression $\langle\sigma v\rangle/T^2$ has a smooth maximum in the region 8–18 keV, so that the optimal temperature for the D–T reaction at a given plasma pressure is about 10 keV.

The typical scale for nuclear cross section is 1 barn = 10^{-24} cm^2. For a D–T reaction at a temperature of about 10 keV, the D–T fusion cross section is even lower than $\sim 10^{-26}$ cm^2, i.e. much less than the nuclear characteristic energy value. As for ion thermal velocity it is of the order of 10^8 $cm\,s^{-1}$ at $T \sim 10$ keV, so that if we are interested in the nuclear reaction rate of the order of $10^{-3}n$ $cm^{-3}\,s^{-1}$, n has to be of the order of 10^{14} cm^{-3} (see relation (2)). At this value of particle density the power density (2) is about 1 W cm^{-3} or 1 MW m^{-3}. These are the typical values for controlled D–T fusion in particular, based on the tokamak concept.

To be energetically favourable the fusion reaction rate has to be higher than the energy losses from plasma. The fusion energy yield $\mathcal{E}_0$ is three orders of magnitude higher than the mean thermal energy. Thus the characteristic confinement time of plasma energy τ_E has to be not less than 10^{-3} of complete burn time. The latter value is of the order of $10^3(10^{14}/n)$ s cm^{-3}, so that for D–T self-sustained fusion reaction we have a necessary condition

$$n\tau_E > 10^{14}\,(cm^{-3}\,s). \qquad (4)$$

This is known as the Lawson criterion.

As we see again the density of 10^{14} particles per cm^3 is the most natural one for tokamak plasma. That is why the value 10^{14} cm^{-3} or 10^{20} m^{-3} can be reasonably used as a unit for density measuring. In the subsequent text we shall express the particle density just in these units and then Lawson criterion looks very simple: $n\tau_E > 1$. Here τ_E is measured in seconds and n in 10^{20} m^{-3}.

3.2 Magnetic Confinement

Plasma density of the order of 10^{14} particles per cubic centimetre is about five orders of magnitude lower than air density. Therefore to produce such a plasma a chamber with a very high vacuum is needed. The chamber is filled with the D–T mixture which has to be heated to a temperature of the order of one hundred million degrees kelvin. To maintain this temperature for quite a long time is a very difficult task. Indeed, even a simple thermal gas expansion at velocities of around 10^8 $cm\,s^{-1}$ would cool a plasma of 1 metre size during 1 microsecond. We need at least 10^6 times better insulation.

This task is fulfilled by magnetic confinement accompanied by magnetic thermal insulation.

Let the magnetic vacuum chamber approximate an infinitely long cylinder (figure 3.1). In the absence of the magnetic field (see figure 3.1(a)) plasma particles can reach the walls very quickly, but

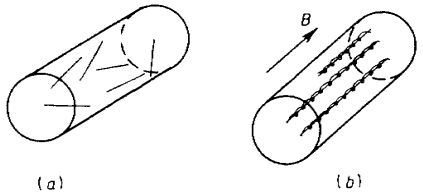

Figure 3.1 Trajectories of charged particles (a) without and (b) with a strong magnetic field.

this picture is drastically changed if a strong magnetic field directed along the cylinder is added (see figure 3.1(b)). Such a field prevents free motion of charged particles in a transverse direction. The ion trajectories look like helical lines stretched along the cylinder. In other words, the strong magnetic field is able to confine charged particles in a transverse direction. The motion of charged particles is described by the equation

$$m\frac{\mathrm{d}\boldsymbol{v}}{\mathrm{d}t} = e\boldsymbol{E} + \frac{e}{c}\boldsymbol{v}\times\boldsymbol{B}. \tag{5}$$

Here m is the mass of a particle, e is its electric charge, $\boldsymbol{v}$ is its velocity, $\boldsymbol{E}$ is the electric field vector, and $\boldsymbol{B}$ is the magnetic field vector. CGS units are used in (5) hence the appearance of the velocity of light in the expression for the Lorentz force.

If the electric field is absent then only the Lorentz force is present. It acts in the $\boldsymbol{v}\times\boldsymbol{B}$ direction so that the particle moves freely in the longitudinal direction.

As for the transverse direction, the circular motion of the particle is produced by the Lorentz force. Let ρ be radius of Larmor motion. Then the centripetal acceleration $m\omega_c v$ is equal to the Lorentz force evB/c and leads to the following expression for angular frequency:

$$\omega_c = eB/mc. \tag{6}$$

This is called the Larmor or cyclotron frequency. The Larmor radius is equal to

$$\rho = v_\perp/\omega_c \tag{7}$$

where $v_\perp$ is the transverse component of the particle velocity. As we see, the Larmor radius increases with the transverse energy $\mathcal{E}_\perp = mv_\perp^2/2$ as the square root of energy. If this energy is the energy of thermal motion then the average value of Larmor radius is

proportional to the square root of temperature. For the deuterons we have

$$\rho \simeq \sqrt{T}/2B \ (\mathrm{cm}). \tag{8}$$

Here the ion temperature is measured in keV, B in tesla, and ρ in centimetres. For the typical value of magnetic field in tokamaks, $B = 5$ T and the temperature $T = 10\,\mathrm{keV}$ the estimate (8) gives $\rho \approx 0.3\,\mathrm{cm}$. This is much less than the typical value of the tokamak chamber radius by an order of one metre. The electron Larmor radius is still smaller than the ion radius. Thus, the strong magnetic field can confine the charged particles quite safely.

It is easy to check that the positively charged ion rotates in the clockwise direction if the magnetic field is directed towards us. The x, y coordinates of a particle are $\{x, y\} = \rho\{\cos\omega_c t, -\sin\omega_c t\} + \{x_c, y_c\}$, and components of the velocity $\{v_x, v_y\} = v_\perp\{-\sin\omega_c t, -\cos\omega_c t\}$ where x_c, y_c are the coordinates of the Larmor centre. The point $\{x_c,\ y_c\}$ is called the guiding centre. In the case of a homogeneous magnetic field it moves along the magnetic field line with the longitudinal component of velocity $v_\parallel$. Each rotating charged particle produces a tiny current loop. If many particles are involved they can produce a macroscopic current density which is called the Larmor current density. To find the Larmor density we have to sum all the elementary currents. For instance, the y-component of the Larmor current density is $j = \langle env_y\rangle$ where n is the ion density, v_y is the y-component of Larmor velocity and averaging is produced over all particles passing through the given x point. If the plasma is homogeneous, the average value of the Larmor current density is equal to zero, but when a gradient in the x direction exists a current density arises. To find it we have to use the distribution function $f(x, v_y, v_\perp)$ instead of n while averaging the elementary currents over many particles.

Let $f_0(x_c,\ v_\perp)$ be the distribution function of the guiding centres. When the mean Larmor radius is small, this function does not greatly differ from the particle distribution function. More exactly, this difference is small and can be taken into account in the linear approximation with respect to the Larmor radius. We have for a single particle $x = x_c + \rho\cos\omega_c t$; $v_y = -v_\perp\cos\omega_c t$, so that $x_c = x + \omega_c^{-1}v_y$. The ion distribution function is equal simply to the guiding centre distribution with x_c expressed through x. In the linear approximation we have $f = f_0 + \omega_c^{-1}v_y\,\mathrm{d}f_0/\mathrm{d}x$. Thus, the averaged current density is equal to

$$j_y = \langle efv_y\rangle = \frac{c}{B}\cdot\frac{\mathrm{d}}{\mathrm{d}x}\langle mv_y^2 f_0\rangle.$$

The average over a Maxwellian distribution of mv_y^2 is equal to T, so that

$$j_y = \frac{c}{B}\frac{\mathrm{d}}{\mathrm{d}x}(nT). \tag{9}$$

The nT product is simply the ion pressure. A similar expression is also valid for the electron current. Thus the total current density is doubled as compared with (9). Relation (9) contains three different components of different vectors and can be written in the vector form

$$\nabla p = \frac{1}{c} J \times B. \tag{10}$$

Here p is total plasma pressure. Relation (10) shows that the plasma pressure gradient is supported by the ampere force. Thus the simple fact that each Larmor gyration is retained by the magnetic field leads immediately to the macroscopic equilibrium equation (10). If we remember that $\boldsymbol{j} = \frac{c}{4\pi}\nabla \times \boldsymbol{B}$ then for the case when $\boldsymbol{B}$ has only a z component depending upon x, y variables we can represent relation (10) in the form

$$\nabla(p + B^2/8\pi) = 0. \tag{11}$$

It follows that

$$p + B^2/8\pi = \text{constant} = B_0^2/8\pi \tag{12}$$

where B_0 is the magnetic field value outside of plasma, i.e. at $p = 0$. We see that plasma pressure cannot exceed the value $B_0^2/8\pi$, that is, the magnetic field pressure outside the plasma. Thus plasma is really confined by the magnetic field pressure. The magnetic field inside plasma is weaker than the vacuum magnetic field. In other words, plasma behaves like diamagnetic matter and Larmor current defined by relation (9) is called the diamagnetic current.

Now let us introduce a very important dimensionless value, namely, the ratio of plasma pressure to the magnetic field pressure

$$\beta = 8\pi p/B^2. \tag{13}$$

In tokamaks this value is usually much less than unity. The maximum value reached up to now was demonstrated in the DIII$-D$ tokamak: $\beta = 44\%$ was claimed to be reached there at the plasma centre.

Thus, a strong magnetic field is a very convenient tool for confining high-temperature plasma, or, more precisely, to prevent thermal expansion of plasma. Now we have to take care of its thermoinsulation: plasma should not be cooled too fast by thermal fluxes to the chamber walls.

The thermal fluxes may be produced by binary collisions of plasma charged particles. Such collisions can interchange particles with different energies providing the net thermal flux to the wall.

Let us estimate the rate of plasma cooling. The thermal diffusivity of ions χ_i can be estimated as $\chi_i \propto \rho_i^2 \nu_i$, where ρ_i is their mean Larmor radius and ν_i is the ion–ion collision frequency.

To find the collision frequency $\nu_i = v_i/\lambda_i$, we have to know the mean free path $\lambda_i = 1/n\sigma_i$ for ions (v_i is the ion thermal velocity and σ_i is the cross section of ion–ion collisions). At first glance the ion–ion collision cross section could be estimated as $\pi(e^2/T)^2$ because the e^2/T value corresponds to the minimal distance of ions while approaching each other at collisions. In fact this value has to be increased by a factor $L \sim 10$ which arises due to the long-distance nature of Coulomb forces and is called the Coulomb logarithm. Thus we have the following estimate for the ion mean free path in CGS units

$$\lambda_i = T^2/\pi L e^4 n. \tag{14}$$

If we measure again n in 10^{14} cm^{-3} and T in keV this relation is approximately equal to

$$\lambda_i \simeq 10^4 T^2 n^{-1} \text{ (cm)}. \tag{15}$$

At the temperature $T \sim 10$ keV and the density $n \sim 1$ (in units 10^{14} cm^{-3}) we obtain from (15) $\lambda_i \sim 10^6$ cm, so that the ion–ion collision frequency is not very high: $\nu_i \sim v_i/\lambda \sim 10^2\,\mathrm{s}^{-1}$. Remembering that ρ_i is of the order of 0.3 cm at $T = 10$ keV and $B = 5$ T we estimate ion thermal diffusivity as $\chi_i \sim 10\,\mathrm{cm}^2\,\mathrm{s}^{-1}$. This is a very low value. It shows that the energy confinement time $\tau_E \sim a^2/4\chi$ can reach the desired value of the order of several seconds at a quite modest size of vacuum chamber radius $a > 10$ cm. At a reactor size of plasma column of about one metre the classical collisional thermal flux would be almost two orders of magnitude better than needed for fusion plasma thermal insulation.

Electron thermal diffusivity is even lower than the ion thermal diffusivity because the electron Larmor radius is much smaller than the ion one.

Thus, for an infinite straight cylinder the physics of plasma magnetic confinement looks very attractive from the point of view of controlled nuclear fusion applications.

To proceed from the ideal picture of an infinitely long cylinder to a closed configuration it seems that it would be sufficient to take some section of this cylinder and to bend it into a torus. Unfortunately the bending of the magnetic field lines produces toroidal inhomogeneity of the magnetic field strength which drastically changes plasma properties. Before considering these plasma features we have to learn something new about particles and fields.

3.3 Charged Particles and Fields

To confine plasma it is necessary to confine each of its particles. Therefore to discuss plasma confinement we have to analyse the motion of single particles.

As we know, each charged particle rotates over the Larmor gyration producing a tiny circular current loop. This current induces magnetic field which is directed against externally applied field. We can say that the Larmor gyration is seen from a long distance as a small magnet with moment μ. It can be calculated directly, but in case anybody has forgotten how to do this, we can propose a somewhat artificial but nevertheless very simple approach.

Let the magnetic field be directed along the z axis and be slowly varying along the x axis. We can find the F force along the x-direction by averaging the x component of the Lorentz force $F = \frac{e}{c}\langle v_y B\rangle$. We know that, $v_y = -v_\perp \cos\omega_c t$ and $x = \rho\cos\omega_c t$ when the guiding centre is placed at the point $x_c = 0$ and $F = -(e/2c)v_\perp \rho\, \mathrm{d}B/\mathrm{d}x$, i.e. the particle is expelled in the direction of the weaker magnetic field. We can say that the charged particle has a diamagnetic moment

$$\mu = \frac{ev_\perp}{2c}\rho = \frac{mv_\perp^2}{2B}. \tag{16}$$

This expression is proportional to the ratio of energy to frequency and corresponds to the so-called adiabatic invariant. It is conserved when the external magnetic and electric fields are slowly varying.

It is easy to see that the value of $\Phi = \pi\rho^2 B$ is equal to the magnetic flux through the Larmor gyration. This flux is also conserved by the motion of a charged particle in the strong magnetic fields.

The energy of the diamagnetic momentum μ in the magnetic field is equal to $\mathcal{E}_\perp = \mu B = mv_\perp^2/2$. It is exactly equal to the transverse kinetic energy of particle. This means that instead of a gyrating particle we can consider a tiny Larmor circle as a quasi-particle with mass m, charge e and magnetic moment μ. When the magnetic field is inhomogeneous in the longitudinal direction then a longitudinal force $-\mu\,\mathrm{d}B/\mathrm{d}z$ appears which again is directed towards the weaker of magnetic field. We have for longitudinal motion

$$m\frac{\mathrm{d}v_\parallel}{\mathrm{d}t} = -\mu\frac{\mathrm{d}B}{\mathrm{d}z}. \tag{17}$$

Multiplying this relation by $v_\parallel$ we obtain

$$\frac{\mathrm{d}}{\mathrm{d}t}\frac{mv_\parallel^2}{2} = -\mu v_\parallel\frac{\mathrm{d}B}{\mathrm{d}z} = -\mu\frac{\mathrm{d}B}{\mathrm{d}t} \tag{18}$$

where the derivative B with respect to time is taken along the particle path. As μ =constant, it follows from (18) that $\mathcal{E} = \mathcal{E}_\perp + \mathcal{E}_\parallel$ =constant, where $\mathcal{E}_\perp$ and $\mathcal{E}_\parallel$ are the transverse and longitudinal components of energy. We see that the total energy is constant. This is quite a natural result because the Lorentz force cannot produce any work perpendicular to the velocity vector.

Equation (17) shows that the particle is repelled from the strong field region. If, for instance, the particle was initially moving in the direction of stronger magnetic field it gradually slows down and stops completely at the point $B_{\max}$ where $v_\parallel = 0$, i.e. $\mu B_{\max} = \mu B + mv_\parallel^2/2$. Such a reflection of the particle is called the magnetic mirror effect. It is used in mirror devices for fusion research.

Now we are ready to consider the charged particle motion in a pure toroidal magnetic field. Such a field decreases with distance R from the symmetry axes as R^{-1}. Due to this field inhomogeneity the charged particle is expelled with the force $-\mu\mathrm{d}B/\mathrm{d}R = \mu B/\mathrm{R}$. The particle moves freely along the magnetic field line but due to the curvature of the field line a centrifugal force $mv_\parallel^2/R$ appears. It is again directed along the radius R.

If some force is acting on the charged particle in a very strong magnetic field the particle responds by drifting in the perpendicular direction to this force and to that of the magnetic field.

If we introduce the cylindrical frame of reference, R, φ, z, the drift will be directed along the z axis. Drift velocity can be found very easily: the Lorentz force produced by this drift motion should balance the externally applied force. Remembering expression (16) for μ we obtain the following expression for the drift velocity

$$v_\mathrm{d} = (v_\parallel^2 + v_\perp^2/2)/\omega_c R. \tag{19}$$

This velocity is directed along the vertical z-axis and is called the toroidal drift. Averaged over Maxwellian distribution the mean value of this drift is equal to

$$\langle v_\mathrm{d}\rangle = \frac{cT}{eB}\frac{2}{R}. \tag{20}$$

This is of the order of $v_j\rho_j/R$, where v_j is the mean thermal velocity and ρ_j is the mean Larmor radius for j-species. For instance, if $\rho_\mathrm{i} \simeq 0.3\,\mathrm{cm}$ and $R = 300\,\mathrm{cm}$, the averaged drift is three orders of magnitude less than the thermal velocity but at $v_\mathrm{i} \simeq 10^8\,\mathrm{cm\,s^{-1}}$ it is still too high.

Thus a purely toroidal magnetic field is not valid even for single-particle confinement. We will see later that for plasma the situation becomes even worse.

Thus, for plasma toroidal confinement a more complicated geometry is needed in a closed magnetic trap. In tokamaks this complication relates to the existence of the poloidal magnetic field produced by current induced in a plasma ring. But before we consider this more complicated configuration we continue our acquaintance with the charged particles and fields. If an electric field exists in addition to a strong magnetic field then the longitudinal component of this field $E_\parallel$ simply accelerates the particle along B, whereas the perpendicular component $E_\perp$ produces the so-called electric field drift

$$v_d = cE \times B/B^2 \tag{21}$$

which is sometimes called simply 'E cross B drift'.

Expression (21) is written under the assumption that the electric field is a homogeneous one, but in fact the same relation is valid when E is produced by a very short wavelength perturbation: the corresponding value of E relates simply to the value averaged over a particle orbit.

An interesting effect appears when both electric and magnetic drifts are simultaneously present. Let the magnetic drift (19) be directed along the z axis. If the electric field is directed along the same axis the electric drift (21) is directed radially and is equal to $-cE/B$. Being shifted along the R radius the particle conserves its adiabatic invariant μ and angular momentum $M_\varphi = mv_\parallel R$. Thus, the total energy of particle

$$\mathcal{E} = mv^2/2 = M_\varphi^2/2mR^2 + \mu B \tag{22}$$

decreases when R increases. This energy change can be considered as a result of the work produced by the electric field along the toroidal drift motion. Indeed, from (22) we have at $\mu=$ constant and $B \propto R^{-1}$:

$$\dot{\mathcal{E}} = -\left(\mu B + \frac{M^2}{mR^2}\right)\frac{\dot{R}}{R} = -\left(\frac{mv_\perp^2}{2} + mv_\parallel^2\right)\frac{\dot{R}}{R} \tag{23}$$

where the dot means the derivative over time. But $\dot{R} = -cE/B$ so that $\mathcal{E} = ev_dE$, where v_d is given by expression (19). Thus, the radial shift with conserved μ, M is accompanied by the work produced by the electric field. This field can be generated by the charged particles themselves. We may consider here a very simple example.

Let the charged particles, both positively and negatively charged, fill a tiny toroidal magnetic tube. We assume for simplicity that all particles have the same $v_\perp^2$ and $v_\parallel^2$. Being initially electrically neutral, this tube starts to generate the electric field E due to charge

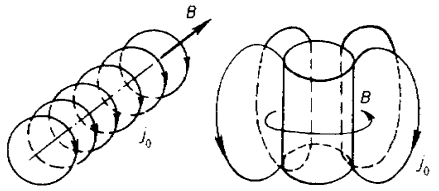

Figure 3.2 The longitudinal magnetic field inside (a) a straight cylinder and (b) the torus.

separation: the differently charged particles have oppositely directed toroidal drifts (19). The electric field E leads to radial motion of all tubes with velocity $v = cE/B$. We can claim that the work produced by E on each particle per second, namely, eEv_d has to be equal to vF, where $F = m(v_\parallel^2 + v_\perp^2/2)R^{-1}$ is the radial force, acting on each particle. Thus we can say that due to energy conservation $mv\dot{v} = vF$. In other words all the particles are accelerated in a radial direction by the force F.

This means that the quasi-neutral tube of charged particles can be thrown out to the walls much faster as compared with the drift velocities. The same conclusion is valid for quasi-neutral plasma when F has to be averaged with the Maxwellian distribution function. It is easy to check that a plasma with density $n = 10^{14}$ cm^{-3} is definitely quasi-neutral: any reasonable electric fields can be built up at very small charge separation.

Note, that during the radial tube motion the size of each Larmor circle increases proportionally to R so that the cross section of the full tube also increases. The magnetic flux of this tube is conserved so that we can say that the plasma is tied to the magnetic field lines.

Now to be prepared for subsequent discussion of the tokamak concept we have to remember some features of magnetic fields.

The simplest example of a vacuum magnetic field is a homogeneous field produced by an infinitely long solenoid. We can consider this solenoid as a series of superconducting rings with currents j_0 (see figure 3.2(a)).

If we have N rings per unit length then the averaged surface current j_s in the solenoid is equal to $j_s = Nj_0$. Magnetic field in such a solenoid is equal to

$$B = \frac{4\pi}{c}j_s = \frac{4\pi}{c}Nj_0. \tag{24}$$

Outside the solenoid magnetic field is equal to zero so that the average value of field inside the ring conductor is equal to half the value in (24). Keeping this in mind, we can find the ampere force F acting on the surface area of solenoid

$$F = \frac{1}{2c} B j_s = B^2/8\pi. \tag{25}$$

Thus we can say that magnetic field has a pressure which acts on the surface of the solenoid playing the role of the magnetic field container.

In addition to transverse pressure magnetic field lines have a tension along the lines. This fact is most easily seen when the toroidal magnetic field is placed between two superconducting cylinders of radii R and $R + \mathrm{d}R$. Toroidal magnetic field decreases with R as R^{-1}, so that at the external cylinder the magnetic pressure will be less than at the internal cylinder by the value $2\mathrm{d}R\,R^{-1}B^2/8\pi$. If we select a sector with angle $\mathrm{d}\varphi$ we see that the force acting on the internal wall of this sector, $F_i = R\mathrm{d}\varphi B^2/8\pi$, is higher than the force acting on the external cylinder $F_e = (R+\mathrm{d}R)\mathrm{d}\varphi(1-2\mathrm{d}R/R)B^2/8\pi$. The equilibrium exists only if we take into account the centripetal force produced by tension of the magnetic field: $F = \mathrm{d}T\mathrm{d}\varphi$, where $\mathrm{d}T = \mathrm{d}RB^2/8\pi$ is the tension of the field lines inside the $\mathrm{d}R$ layer, so that the tension per unit area is equal to $B^2/8\pi$.

Now let us bend the straight solenoid (figure 3.2(a)) into a toroidal one (figure 3.2(b)). To avoid collapse of the rings produced by tension of the magnetic field lines we have to use a support cylinder. If the rings are considered to be elastic strings then each coil will appear as shown in figure 3.3(b). Namely, it has a D-shape with the straight section attached to the support cylinder. Such D-shaped coils have no shear stresses when only toroidal field is present.

As we will see later, when tokamak plasma is placed in equilibrium an additional vertical field is needed. In this case the toroidal field coils undergo the overturning moment which has to be unloaded by a special mechanical structure. For plasma shaping even more complicated poloidal fields are needed. Toroidal and poloidal fields in tokamak are mutually perpendicular and not linked with each other.

3.4 Elementary Plasma Dynamics

Plasma is a complicated form of matter. Its dynamics is the dynamics of charged particles in the magnetic and electric fields generated

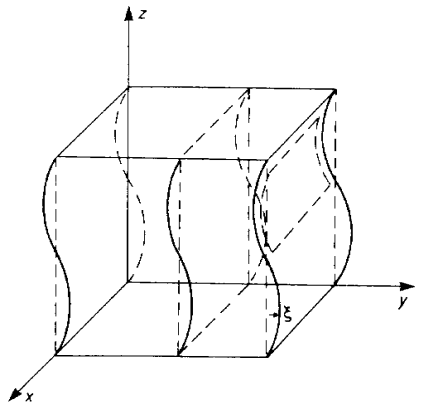

Figure 3.3 Magnetic-field-line distortion when the plasma is shifted along the y direction with periodic dependence upon z.

by particles themselves. There is a more or less precise method of describing plasma dynamics. It consists of a kinetic-equations approach supplemented by Maxwell equations for self-consistent fields. This general approach or its simplified version of the so-called MHD equation, i.e. magnetohydrodynamics, will be used throughout this book. Here we consider only some very simple examples of plasma dynamics to get some intuitive basis for understanding plasma physics .

The simplest case of plasma dynamics is its expulsion from a purely toroidal magnetic field, but as a starting point we take an even simpler case when the longitudinal magnetic field is homogeneous and directed along the z axis. Let us assume that the plasma motions are also homogeneous along the z axis. Plasma may move with the so-called electric drift when transverse electric fields are generated. When the magnetic field perturbations are very small the electric field is vortexless and can be described by electric potential φ, so that the electric drift is given by the relation

$$v_\perp = \frac{c}{B} e_z \times \nabla\phi. \tag{26}$$

It is easy to check that this motion is incompressible, i.e. $\mathrm{div} v_\perp = 0$. The vortex of the velocity field (26) is equal to

$$\Gamma = (\nabla \times v_\perp)_z = \frac{c}{B}\Delta_\perp\phi. \tag{27}$$

But when $\mathrm{d}\varphi/\mathrm{d}z = 0$ the expression $\Delta_\perp\varphi$ is proportional to the electric charge density, i.e. to the difference between the ion and

electron densities. There are no reasons for this charge density to be changed if no longitudinal currents are present, so that the vorticity Γ will move together with the plasma and

$$\frac{d\Gamma}{dt} = \frac{\partial \Gamma}{\partial t} + v_\perp \nabla \Gamma = 0. \tag{28}$$

In other words, the plasma vorticity is simply transported with the plasma when no particle collisions are present and both species are simply shifted by the electric drift. When plasma is homogeneous and of constant density equation (28) can be written in the form

$$m_i n_0 \frac{d\boldsymbol{v}_\perp}{dt} + \nabla F = 0 \tag{29}$$

where F is an arbitrary function of x, y, t variables and plays the role of pressure. It is easy to check that for the incompressible two-dimensional motion equation (28) can be obtained from (29) by the simple operation curl $= \boldsymbol{e}_z \times \boldsymbol{\nabla}$.

Thus two-dimensional motions of the collisionless plasma in the strong magnetic field look like incompressible flow of ordinary liquid.

Now if the toroidal curvature is included, equation (29) has to be supplemented by the toroidal expulsion force

$$m_i n \frac{d\boldsymbol{v}_\perp}{dt} + \nabla F = 2p\boldsymbol{R}/R^2 \tag{30}$$

where p is the kinetic plasma pressure and $\boldsymbol{R}$ is the toroidal radius-vector. The right-hand side looks like a gravitational force with the p playing the role of mass density. It is easy to imagine how such a fluid is moving.

Now let us consider a very simple example when the plasma motion is not a homogeneous one along the z direction. For simplicity we consider only small perturbations of initially homogeneous stationary plasma.

The plasma perturbations can be described by the plasma displacement ξ related to the velocity $\boldsymbol{v} = d\xi/dt$. We assume that the displacement along the y axis is a periodic function of z, as shown in figure 3.3. The waved surfaces in figure 3.3 correspond to the initial planes distorted by the subsequent plasma displacement. It is easy to see that the magnetic field lines are curved together with the waved surfaces. Indeed, any closed contour on the surfaces, for instance, represented by a dotted line in figure 3.3, has no magnetic flux because the collisionless plasma has zero resistivity and initial flux through this contour was zero.

Thus all the magnetic lines are bent to be on the same magnetic surfaces which are deformed in their turn by plasma displacements. This effect of the displacement of magnetic field lines together with plasma is called tied magnetic lines. Sometimes people say the magnetic field is frozen into plasma. The distortion of magnetic field lines produces immediately the strong forces acting on the plasma because a transverse current density is generated. Indeed if $\xi \simeq \exp(-i\omega t + ikz)$ then the perturbed magnetic field is $B = B_0\, d\xi/dt = ikB_0\xi$ and the corresponding current density is equal to $j_x = -(c/4\pi)(\partial B_y'/\partial z) = (ck/4\pi)B_0\xi$. Thus from the plasma motion equation with the ampere force taken into account

$$m_i n_0 \frac{d^2\xi}{dt^2} = \frac{1}{c}\boldsymbol{j} \times \boldsymbol{B}$$

it follows that the frequency ω is equal to

$$\omega = \frac{B_0 k}{\sqrt{4\pi m_i n_0}}.$$

The value $c_A = B_0/\sqrt{4\pi m_i n_0}$ is called the Alfven velocity and the corresponding wave is called the Alfven wave. In plasma with low β-value this velocity is larger than the ion thermal velocity. This means that any perturbation of magnetic field lines propagates along these field lines very rapidly, faster than the speed of sound. Thus, plasma in a strong magnetic field is almost rigid with respect to its bending along the magnetic field.

From these two examples it is seen that plasma in a magnetic field is a very unique physical object. It looks like a fluid across the magnetic field and is elastic but almost rigid while deforming along the magnetic field lines.

We have assumed above that the plasma resistivity is zero. This is indeed very close to reality: the resistivity of fusion plasma is less than copper resistivity at room temperature by six orders of magnitude. This feature was quite clear at the initial stage of plasma physics research. However, the precise value of the laboratory plasma resistivity was not at all well-known for a long period and arguments were presented in favour of the existence of an anomalously high value of resistivity. I remember that Piotr Kapitsa, Nobel Prize Winner for the discovery of superfluidity, underlined many times that the basic physics of plasma has to be started with very simple experiments. In particular, he insisted that it is necessary to measure the plasma resistivity value by special experiments.

It turned out that the tokamak itself is the best experimental instrument for these measurements. The plasma resistance in tokamaks was measured with quite good accuracy. It was shown that its

value is close to the classical Spitzer value with toroidal neoclassical corrections taken into account. In other words, the classical plasma resistivity is not affected by low-level turbulence which is sufficient for anomalous cross-field transport . Thus, at least in this respect, the properties of plasma are quite well known.

We shall consider more complicated plasma features in subsequent chapters.

3.5 Plasma Equilibrium

Tokamak is the most natural concept of magnetic confinement. Plasma is produced in the form of an axisymmetrical torus, of circular cross section in the simplest case. Plasma is confined by a combination of magnetic fields: toroidal (along plasma turn) and poloidal (across the current turn). A schematic view of a tokamak is shown in figure 3.4. A strong toroidal magnetic field is generated by a toroidal field coil system. Inserted into the coil system a toroidal vacuum chamber is filled with hydrogen or its isotopes under relatively low pressure. This gas forms a kind of a closed secondary transformer coil, with a primary winding on the iron core. When current is driven through the primary winding an inductive electric field is produced inside the chamber, directed along the chamber. When the value of this field is high enough, an electric gaseous break-down occurs and a closed plasma ring is formed. Then the current increases and heats plasma up to high temperatures. In this way, the primary winding serves as an inductor for current drive and ohmic heating of plasma. In addition to the inductor, which should not create stray transverse fields in the chamber, there are special windings to produce poloidal fields in the plasma: these are needed to control the position and shape of plasma.

The value of magnetic flux swing (volt-second) in the primary transformer winding is an important parameter of a tokamak. In an actual pulse the magnetic flux has to be allocated both for resistive volt-second consumption during plasma initiation and inductive flux linkage during current ramp-up, LI/c, where I is the plasma current and L is the total (external and internal) plasma inductance. The remaining part of the total flux swing may be used for ohmic current drive: usually, loop voltage U is of the order of ~ 1 V (in medium-size tokamaks), and, thus, pulse duration under ohmic current drive is of the order of the remaining volt-seconds. It is desirable to have this duration as long as possible, but the volt-second capability is constrained by the inductor size and by the maximum value of the inductor magnetic field.

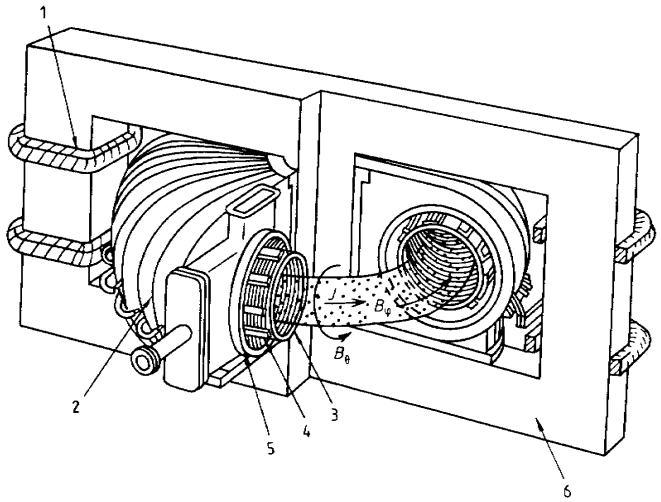

Figure 3.4 Schematic diagram of a tokamak: 1—primary transformer circuit; 2—toroidal field coils; 3—liner; 4—poloidal field coils; 5—copper shell; 6—iron transformer core.

Geometrical parameters of the plasma torus are its radii: the minor radius a and the major radius R. The value $R/a = A$ is called the aspect ratio. The current I flowing in the plasma produces its own (poloidal) magnetic field B_θ, which at the boundary of the plasma is equal to $B_\mathrm{p} = 2I/ca$ in CGSE units (c—velocity of light). In MKS units $B_\mathrm{p} = I/5a$, where I is measured in MA, a in metres and B_p in T.

A strong longitudinal magnetic field is used in tokamaks, so that $B_\mathrm{p}^2 \ll B^2$. The plasma pressure is weak compared with magnetic field pressure. These specific features impose certain constraints on the tokamak plasma dynamics.

Let us consider now the forces acting on the plasma torus. To begin with, we consider first an ideal case when there is either no current in the plasma or that it is negligible. It is obvious that the plasma cannot be in a steady state under such conditions. Indeed, plasma as a gas tends to expand. The longitudinal magnetic field frozen into plasma hinders its direct expansion along the minor radius. However, plasma with the frozen-in magnetic field can expand in the direction of the major radius R. The toroidal magnetic field decreases with R as R^{-1}. Magnetic field is frozen into plasma so that when displacing along R the plasma cross section S increases proportionally to R. In addition the length of the plasma turn also increases with R. Therefore the plasma volume V changes with R according

to a quadratic law. Any plasma magnetic tube follows the same law. When displaced along the major radius the total work produced by all plasma tubes is equal to $\langle p\rangle \mathrm{d}V = \langle p\rangle V 2\,\mathrm{d}R/R$, where $\langle p\rangle$ is the mean value of plasma pressure averaged over the volume. Let F_p be a force acting on plasma ring in the radial direction. We can relate it to the unit length i.e. we take $F_\mathrm{p} 2\pi R\,\mathrm{d}R = \langle p\rangle \mathrm{d}V$. Since $V = 2\pi^2 a^2 R$ and a^2 is proportional to R, we derive:

$$F_\mathrm{p} = \langle p\rangle \frac{2\pi a^2}{R} = \frac{2}{R}\langle p\rangle \pi a^2. \tag{31}$$

This force could be compensated by an additional current across the plasma in the vertical direction so that the ampere force of this current and of the longitudinal magnetic field would be directed towards the axis of symmetry. However, such a current would destroy the thermal insulation by heat convection with current carrying electrons.

It is worthwhile considering plasma behaviour in purely toroidal field in more detail because something similar can occur in each tokamak at the early initial phase of the shot.

The radial force acting on each plasma tube and being equal to $2p/R$ per unit cross section area is similar to the gravitational force acting on an inhomogeneous liquid. If the pressure p of some tube is higher than that of the neighbouring environment then this tube will be expelled in the radial direction. On the contrary, if this pressure is lower than the surrounding pressure the tube is pushed in the direction of smaller radii. This is a direct result of plasma polarization due to toroidal drift: the higher the plasma pressure the larger the field built up. Thus in initially non uniform plasma a specific convection develops which tends to stratify the plasma in such a manner that the pressure is a monotonically increasing function of R, not depending upon z.

If the vacuum chamber is conductive and axially symmetric then it is an equipotential. Hence the tangential component of electric field is zero at the wall so that the normal component of electric drift, at the wall, is also zero. Therefore, the plasma cannot be thrown out directly on the wall and direct loss of plasma with the MHD velocity is absent. Slower plasma loss can be produced by toroidal drift. The plasma pressure near the walls decreases and subsequently plasma tubes are pushed inside the plasma core generating a plasma convection. Such a combination of convective transfer of fresh plasma tubes towards the walls with subsequent electron–ion recombination on walls leads to plasma leakage. As a result at such slow convection, the plasma losses can be strongly suppressed as compared with its direct expulsion along the R-radius with thermal velocity.

In a tokamak configuration the longitudinal plasma current is present and the direct expansion of the plasma column in the direction of the major radius is prevented by the ampere force $(1/c)IB_z$, where I is the plasma longitudinal current and B_z is the vertical magnetic field produced by poloidal field coils.

In fact in addition to the force (31) the force F_B of electromagnetic expansion also needs to be compensated. The poloidal magnetic field energy is equal to

$$\mathcal{E}_\mathrm{p} = \frac{LI^2}{2c^2} \tag{32}$$

where L is the plasma inductance, and the corresponding F_B force per unit length of the plasma column is equal to:

$$F_B = \frac{I^2}{4\pi R c^2}\frac{\partial L}{\partial R}. \tag{33}$$

If the poloidal coils generating field B_z, are located close enough to the plasma column, only the internal inductance has to be taken into account: $L_\mathrm{i} = 2\pi R l_\mathrm{i}$ where l_i is inductance per unit length. The value of l_i does not depend on R since the relative distribution of frozen-in magnetic field inside the plasma is conserved during the displacement of the plasma along R. Thus, the equilibrium equation could be written as

$$F_\mathrm{p} + F_B = \langle p\rangle \frac{2\pi a^2}{R} + \frac{l_\mathrm{i}}{R}\frac{I^2}{2c^2} = \frac{1}{c}B_z I. \tag{34}$$

The poloidal magnetic field on the boundary of the plasma is equal to $B_\mathrm{p} = 2I/ca$. Thus equilibrium condition (34) may be written as

$$\beta_\mathrm{p} + 0.5 l_\mathrm{i} = B_z Rc/I. \tag{35}$$

Here we use a specific symbol for the ratio of the mean plasma pressure to the poloidal magnetic field pressure at the plasma boundary:

$$\beta_\mathrm{p} = 8\pi\langle p\rangle / B_\mathrm{p}^2. \tag{36}$$

In expression (35) the internal inductance l_i is simply a number which depends on the current density profile: $l_\mathrm{i} = 0.5$ for uniform current and it increases with current shrinking. In modern tokamaks the equilibrium field B_z is automatically controlled in such a way that the column is centred with respect to displacement along the major radius. Thus the value of R is known and equation (35) may be used for the experimental measurement of β_p by measuring l_i and B_z.

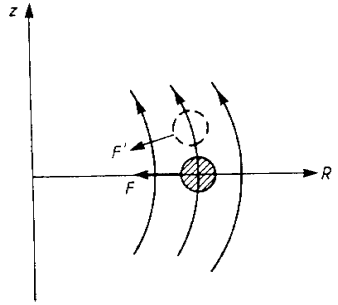

Figure 3.5 Equilibrium magnetic barrel-type field lines. When the plasma torus is shifted vertically the restoring force F' generates a vertical component directed towards the median plane.

If the equilibrium field is 'barrel-like', i.e. increasing on both sides from the median plane, then it provides vertical column stability: such a field has a radial component at $z \neq 0$ which tends to push the column back to a stable position when it is displaced along z (see figure 3.5). The field 'barrel-likeness' means also that B_z decreases along the major radius, i.e. the decay index $\alpha_z = -(R/B)(\mathrm{d}B_z/\mathrm{d}R) > 0$. When the field decay index increases the effect of vertical stability becomes stronger. But if a_z is very large then the stability along R may be lost. Indeed, to ensure stability along R the right-hand side of (34) should increase when R increases (since $l_i \simeq$ constant and β_p, as may be shown, changes weakly with R). When the plasma is shifted along the major radius the total current decreases as $1/R$ as a result of magnetic flux conservation inside plasma, i.e. $2\pi R l_i I =$ constant. That is why, to ensure radial stability, B_z should not decay faster than R^{-2} (see (35)), i.e. the field decay index should not be higher than 2.

The plasma position control may be strengthened with the help of a feedback system. In the first tokamaks the effect of plasma positioning was achieved with the help of the conducting shell: when the column was displaced, image currents were generated in the shell and the magnetic field of such currents pushed plasma back to the initial equilibrium position. Modern tokamaks have on-line systems to control plasma equilibrium which actively centre the plasma in respect of its radial displacements.

The poloidal magnetic field coil system may be used also to shape the plasma cross section. A circular form is simplest but is not the optimal form. To increase plasma stability it is desirable to locate it

in the region with the maximum magnetic field strength, i.e. to push it towards the inboard chamber contour. Then D-shaped plasma is formed: its cross section is elongated along the vertical axis and takes some triangularity as is shown for example in figure 3.6 for the D-IIID device cross section. This facility has a D-shaped chamber and plasma of the same configuration. If plasma has a non-circular cross section symbol a is used for the plasma half-width in the equatorial plane. Half-height is denoted by b, and elongation by $K = b/a$. Triangularity, i.e. the degree of D-shapeness is denoted by δ.

In figure 3.6 the contour lines show the cross sections of magnetic surfaces. Inside the loop-line, named the separatrix, these surfaces represent nested tori and beyond the separatrix the magnetic surfaces are open ones and the magnetic lines may continue up to the chamber walls. Thus, a configuration with a poloidal divertor is established, when the magnetic lines outside the separatrix divert to the walls. In figure 3.6 the separatrix has only one X-point: this is a point where the poloidal field component is zero. In some cases instead of a single-null configuration, a double-null divertor configuration may be used which is symmetrical in respect of the $z = 0$ plane.

The elongated plasma shapes with the divertor are used in many tokamaks, e.g., JET, PBX-M, ASDEX, JT-60-U etc. The maximal elongation of $K = 2.5$ was reached in DIII-D for a single-null configuration. JET operates at K up to 1.8 although more typical are the values of 1.4–1.7. The elongation allows the increase of the current plasma at the same geometric dimensions of a, R and of the toroidal magnetic field B value. The gain expressed in the current value which could be achieved with non-circular plasmas, reaches the values in the range 2–3. However, it is difficult to attain a greater elongation because of vertical instability of the plasma column. Indeed the elongation seems to be produced by coils with currents in the same direction as in the plasma. These currents are located above and below the plasma ring and because the parallel currents attract, the vertical displacement of the plasma leads to its 'sticking' to the corresponding poloidal field coil. A rather effective feedback system is needed to prevent plasma vertical instability.

In this respect the DIII-D facility has a very effective configuration: the poloidal magnetic field coils are located inside the toroidal magnetic field coils close to the plasma. Since the two systems of the coils are mutually linked, the toroidal coils of the facility were made to be dismantable.

In large tokamaks with a strong toroidal field the poloidal field coils are located outside the toroidal field coils. Correspondingly, the inductor solenoid is located at the axis of symmetry with the

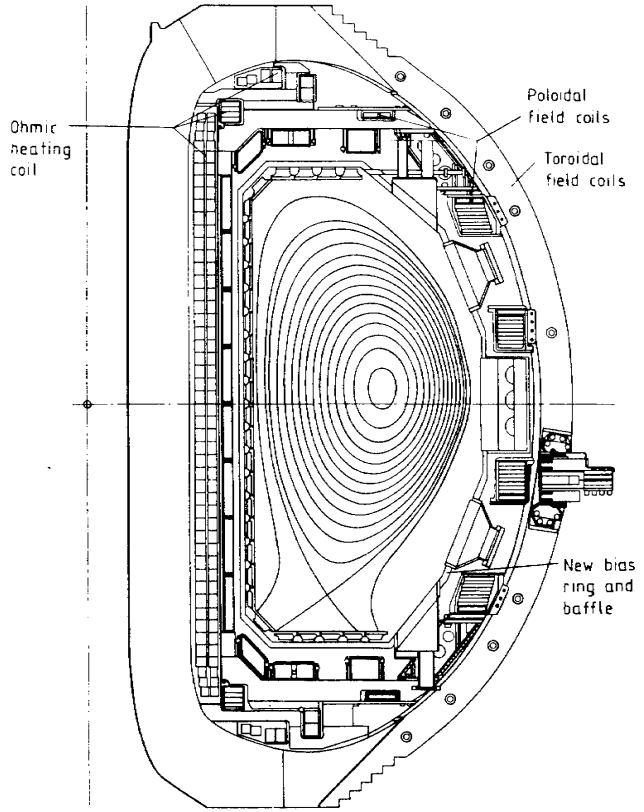

Figure 3.6 DIII-D tokamak elevation [147].

toroidal field coils placed around an inductor. Taking the DIII-D configuration as an example, one may observe another specific feature of modern tokamaks: an inductor without an iron core can be used in such devices. By removing the iron core, the magnetic field of the inductor can be increased to values higher than the iron saturation field, i.e. considerably higher than $2T$.

3.6 Plasma Stability

The major advantage of the tokamak configuration is the possibility

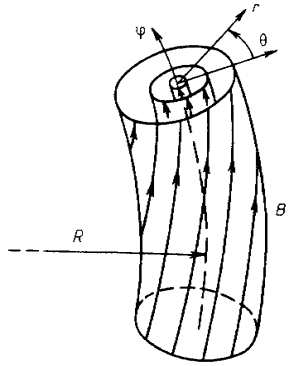

Figure 3.7 Magnetic field lines and coordinates r, θ and ϕ for a tokamak with a circularly-shaped plasma.

of stabilizing MHD-instabilities by a strong toroidal magnetic field. Let us consider the tokamak magnetic field geometry in more detail. Figure 3.7 represents a simplified picture of magnetic lines. When the plasma cross section is circular, magnetic field lines are located on the nested toroidal surfaces of circular cross section. Let us introduce a system of coordinates r, θ, φ as is shown in figure 3.7. A magnetic line with $r = 0$ is closed and is called a magnetic axis. The value of the toroidal magnetic field B_T on this axis is considered as a main characteristic of a tokamak as viewed from its ability to confine stable plasma. The toroidal field decreases with the major radius as $1/R$, but assuming that the aspect ratio $A = R/a$ is high enough, we can neglect this variation of B in the first approximation.

The magnetic field lines are located at the magnetic surfaces winding on them as helical lines: under angle displacement $\mathrm{d}\varphi$ along the torus, the magnetic line rotates by angle $\mathrm{d}\theta$ in the poloidal direction. Since the arc length along φ is equal to $R\,\mathrm{d}\varphi$, and along θ is equal to $r\,\mathrm{d}\theta$ their ratio is equal to the ratio of the components of the corresponding fields: $R\,\mathrm{d}\varphi/r\,\mathrm{d}\theta = B_T/B_\theta$. Hence $\mathrm{d}\theta/\mathrm{d}\varphi = B_\theta R/B_T r$. Thus, after a complete round along the torus, angle θ will change as $\Delta\theta = 2\pi B_\theta R/rB_T$. This angle is called the rotational transform angle. Let us use the following notation:

$$q = \frac{1}{\mu} = \frac{B_T r}{B_\theta R} \tag{37}$$

where $B_\theta = B_\theta(r)$. Then the rotational transform angle will be written as $2\pi\mu = 2\pi/q$.

The value of q is of great importance in a tokamak. Geometrically it may be defined as the ratio of the number of magnetic-line rotations along the major and minor azimuths. If a magnetic line becomes closed after m rotations, i.e. q becomes equal to a rational fraction of m/n, then such a surface is rational. For example, on the surface with $q = 2$ a magnetic line rotates poloidally at $\Delta\theta = \pi$ after a single toroidal rotation and becomes closed after the second rotation along φ. If q is irrational, the magnetic line is never closed and the definition of q as the ratio of a numbers of rotations should be understood asymptotically, i.e. as the limit when the number of rotations tends to infinity.

The radial variation of q in tokamaks usually looks like a monotonously growing function of the radius r, including the region outside the current channel, where $q \sim r^2$. The q value on the boundary of plasma column $r = a$ is denoted by q_a. Afterwards, when the global plasma characteristics as a whole are meant, the index a is omitted. The value of q_a may also be expressed as

$$q_a = \frac{B_T a}{B_p R} = \frac{cB_T a^2}{2IR} \tag{38}$$

where $B_p = B_\theta(a)$, I is the plasma current and c is the velocity of light (the CGSE system of units is used). In MKS units, this ratio is

$$q_a = \frac{5B_T a^2}{IR} \tag{39}$$

where B_T is measured in T, a and R are in metres and I is in MA.

Equation (39) may also be written as

$$q_a^{-1} = I/I_c \qquad I_c = 5B_T a^2/R. \tag{40}$$

Thus, q_a^{-1} value may be considered as a dimensionless current.

The $q(r)$, $\mu(r)$ values can be introduced using another definition which is more universal. Let us introduce toroidal, Φ, and poloidal, Ψ, magnetic fluxes:

$$\Phi = \pi r^2 B_T \qquad \Psi = 2\pi R \int_0^r B_\theta \mathrm{d}r. \tag{41}$$

The increments of these fluxes for an increase $\mathrm{d}r$ in r are, respectively, $\mathrm{d}\Phi = 2\pi r B_T\,\mathrm{d}r$ and $\mathrm{d}\Psi = 2\pi R B_\theta\,\mathrm{d}r$.

Comparing these flux ratios with (7) we find that:

$$\mu = 1/q = \frac{\mathrm{d}\Psi}{\mathrm{d}\Phi}. \tag{42}$$

This is a much more convenient representation. Let us assume for instance that with 'frozen-in' magnetic fluxes we will deform the plasma column cross section to a D-shape (figure 3.6). Relation (42) will not be changed because the field topology is conserved. Thus, the relation (42) is more universal and that is why it is used for plasmas of non-circular cross section. In order to mark these more exact values of μ and q, they are sometimes labelled with an index Ψ, namely μ_Ψ, q_Ψ.

As we have already noted, when the poloidal divertor is present the transverse magnetic field tends to zero near the X-point of the separatrix. That is why the separatrix magnetic line asymptotically approaches the X-point and does not make even a single poloidal rotation when the number of rotations along the major azimuth φ tends to infinity. It means that $\mu = 0$ on the separatrix. When approaching the separatrix from inside $\mu_\Psi \to 0$, $q_\Psi \to \infty$. That is why the q_Ψ value on the separatrix seems to be misleading. However, when approaching the separatrix the q_Ψ function tends to infinity very slowly according to the logarithmic law and a reasonable characteristic of the edge q-parameter may be its value beneath the separatrix but not very far from it. For this reason the $q_{0.95}$ value is used which represents the value of q on the magnetic flux point $\Psi = 0.95\Psi_s$, where Ψ_s- is the value of Ψ on the separatrix. For non-circular plasmas sometimes another expression is used:

$$\mu_s = q_s^{-1} = \frac{\pi R}{5B_T} j_s \tag{43}$$

where j_s is the current density averaged over the cross section. For plasma of circular cross section this expression coincides with (39) whereas for the elongated cross section with $K = b/a \neq 1$ one may use a simplified expression

$$\mu_{eff} = q_{eff}^{-1} = \frac{IR}{5Bab}. \tag{44}$$

The q_{eff} value is called a cylindrical or engineering value of q, since it contains the simplest plasma parameters which are used for engineering design of tokamaks. Equation (44) similarly to (40) may be written as $q_{eff}^{-1} = I/I_c$, where $I_c = 5Bab/R$. The q_a value defined by the equation (39) or, respectively, by (44) for a non-circular cross section is called the safety factor. As was shown by Shafranov and Kruskal, the tokamak plasma is unstable at $q_a < 1$ in respect of helical perturbations. That is why plasma current cannot exceed the limit

$$I_c = 5Bab/R \tag{45}$$

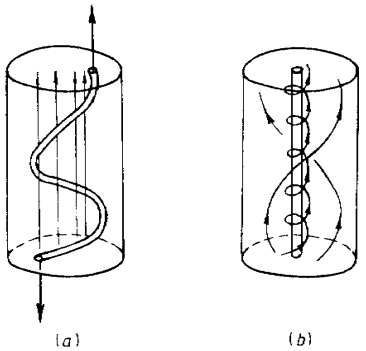

Figure 3.8 When the helical conductive filament (a) is stretched vertically the magnetic field lines become helical (b).

which corresponds to the value of $q = 1$. The kink-mode stability condition

$$q_a > 1 \tag{46}$$

was named the Kruskal–Shafranov criterion.

To clarify the physical cause of this instability we consider the following 'Gedanken experiment'. Let helical superconductive filament be placed in a strong longitudinal magnetic field (figure 3.8(a)).

If the two ends of this filament are pulled apart (see figure 3.8(a)) the magnetic field lines deform into helices of the same sign of screw, left or right. When the filament becomes a straight string all the magnetic lines are helical. It means that a current I is induced. We can easily evaluate this current.

Let us choose some section of the initial helix with length L and number of turns equal to N. Let a be the filament radius and b the radius of the cylindrical superconductive casing. If we take the loop shown by the dotted line in figure 3.8 we have to accept that the total magnetic flux is invariable during the filament deformation. Its initial value is equal to $N\pi R^2 B$ where R is the initial radius of the helical line guiding cylinder. The final value of the flux through the same dotted line loop is determined by the azimuthal magnetic field and is equal to $2LIc^{-1}\ln(b/a)$. Therefore, the filament current value is equal to $I = \pi R^2 cB(2l\ln(b/a))^{-1}$, where $l = L/N$ is the pitch of the initial helix.

The magnetic field energy in the final stage, figure 3.8(b), is higher than that in the initial state just by the azimuthal magnetic field energy.

Now we consider the backward deformation from the state shown in figure 3.8(b), where the current is flowing along the filament, to the state shown in figure 3.8(a) where the azimuthal magnetic field disappears completely. We can say that such a transition is energetically favourable. In other words, the state in figure 3.8(b) is unstable in respect of the helical deformation of the current-carrying filament.

A similar phenomenon can take place in a tokamak plasma. If the plasma column is very long then it is unstable in respect of helical deformation, but if $2\pi R$ becomes less than the pitch of the magnetic field line, $2\pi a B_T/B_p$, then the magnetic energy decrease outside the plasma column is balanced by the magnetic energy increase inside the plasma due to the toroidal magnetic field perturbation. The necessary stability condition, $2\pi R < 2\pi a B_T/B_p$, or $q_a > 1$ corresponds to the Kruskal–Shafranov limit.

The higher q_a, the more stable plasma is in respect of kinks. Experiments show that the stability becomes reliable only when $q_a > 2$. As a matter of fact very carefully handled plasma discharges were realized even in the region near $q = 1.3$ [19]. However, these discharges with low q-values correspond to higher plasma energy losses and were not considered to be of much interest.

3.7 Operational Limits

Plasma discharges in a tokamak can be realized only within a definite range of densities: at a given plasma current there exist a lower and an upper density limit. At low densities the electron–ion collision frequency is not sufficient to prevent the generation of so-called 'run-away' or accelerated electrons. The run-away electrons can be accelerated by the inductive electric field up to very high energies. They spoil the discharge characteristics and may be dangerous for the vacuum chamber of the tokamak. Thus the plasma density has to exceed some critical value.

At high densities the atomic processes at the plasma edge become rather important. These processes are radiation, charge-exchange and neutral atom ionization. They can lead to contraction of the plasma column: the effective plasma radius decreases and the danger of kink instability becomes real. Thus, on the current-density plane there is a limited operational region which schematically is defined by the so called Hugill plot (figure 3.9). The non-dimensional current I/I_c, i.e. $1/q_{eff}$, is plotted on the ordinate axis, and the non-dimensional density or Murakami number†

† The non-dimensional nature of M is explained in Chapter 5.

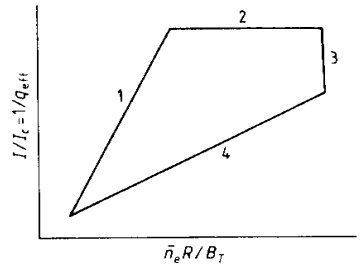

Figure 3.9 Hugill plot for tokamak plasma operation region: 1—run-away electron limit; 2—current limit; 3—Murakami density limit; 4—Hugill limit.

$$M = \bar{n}_e R/B_T \tag{47}$$

is plotted on the abscissa axis. Here $\bar{n}_e$ is the mean electron density which is measured experimentally along the central chord. It is always somewhat higher than that averaged over the volume value of $\langle n_e \rangle$. In (47), the density n_e is measured in $10^{20}\,\mathrm{m}^{-3}$, R in metres and B_T in tesla. As is seen from figure 3.9, the tokamak operational domain on the current–density plane is restricted by four limits: 1—limit of run-away electrons at low density; 2—current limit due to the MHD-instability; 3—Murakami limit at high density; 4—Hugill density limit where the Hugill number $H = q_{eff}M$ remains constant.

The limiting density is determined by the power balance on the plasma periphery, i.e. by balance of the energy flow from the central region and radiation and ionization losses. When additionally heated the plasma density limit usually increases approximately as $\sqrt{P}$, where P is the total plasma heating power.

There is one other tokamak plasma limit, which is not directly related to the limits on the Hugill diagram, namely, the pressure limit. The pressure limit is related to the so-called ballooning instability: tokamak magnetic lines of the outer region are convex with radius of curvature $\sim R$. That is why at the higher pressures a 'swelling' may occur on magnetic surfaces there. Without going into theoretical detail, which can eventually be supported by numerical calculations, the value of the pressure limit may be estimated with the help of simple arguments. Namely, if the bundle of magnetic lines (with the effective length $\sim qR$) experiences a 'swelling' on the outer region, it will be drawn back by the magnetic tension of $\sim B_T^2/8\pi qR$, and the cause for 'swelling' is plasma pressure gradient $\propto p/a$.

Thus, the instability occurs at $\beta = 8\pi p/B_T^2 \sim a/qR$. Since $q \sim q_a \sim B_T a^2/IR$, the expression for the limiting value of β, i.e. β_c, is

approximately

$$\beta_c = g\frac{I}{aB_n} \equiv gI_N \tag{48}$$

where $I_N = I/aB_T$ is the normalized current. The g coefficient (sometimes the notation β_N is used) in equation (48) is called the Troyon factor because it was F Troyon who had summarized in a simple formula, (18), the results of numerical calculations for various plasma-pressure radial-distribution profiles and various shapes of plasma column cross section. The g-factor slightly changes with q_a, pressure profile and shape of plasma. Roughly, it may be considered as constant and equal to $g \approx 3\%$. The normalized current I_N differs from the previously introduced ratio of I to the maximum current I_c

$$I_N = I/aB_T = (I/I_c)\,5b/R. \tag{49}$$

For the most effective use of the toroidal magnetic field it is preferable to have the values of β as high as possible, i.e. to have a high I_N value. Since I/I_c is limited by the upper current limit on the Hugill diagram, b/R should be maximized according to (49), i.e. the column should be elongated vertically as much as possible. The highest β value of 10% was reached experimentally in DIII-D with strong elongation of $K = b/a = 2.3$. The values of $g = \beta_N$ exceeded 3% in DIII-D and in some discharges reached as high as 5%.

The maximum β value at the magnetic axis $\beta(0) = 44\%$ was reached when very accurate pressure profile tailoring was realized in DIII-D.

Theoretical analysis of instabilities (ballooning and kink) shows that the values of the $g = \beta_N$ -factor obtained in DIII-D may indeed reach such high values by carefully tailoring the pressure and current profiles.The maximum β value reached in DIII-D depended on the current density profile [50]. The experimental data for critical β are summarized by a simple empirical formulae $\beta_c = 4l_i I/aB_T$, where l_i is the internal inductance per unit length.

3.8 Plasma as a Complex System

For many years until now the main objective of the experiments in tokamaks was the investigation of the physics of plasma magnetic confinement, i.e. the study of processes of heat and particle transport across magnetic surfaces (the transport along the surfaces is very fast— practically comparable to thermal velocities of particles). The experimental and theoretical studies complemented each other. A huge variety of phenomena were discovered experimentally and

then theoretically explained and numerically simulated. The theoretical physicists try to go further—to construct a complete theory of thermonuclear plasma in the presence of collective effects. Much has been done here. However, numerous experiments unceasingly supply information on much finer processes in plasma, which in their turn require the further development of theoretical and numerical models. Very roughly speaking, one may say that the phenomenological clarity of the main plasma features has been achieved, but details continue to be explained.

Many experiments have shown that tokamak plasma represents a very complicated object: many collective processes occur in plasma simultaneously—processes initiated by instabilities of different natures. The most powerful of these is the so-called disruptive instability. It develops while approaching the stability limits on the Hugill plot. During disruption the magnetic configuration collapses totally: instead of mutually enclosed magnetic surfaces the magnetic islands, i.e. helical configurations embedded between main magnetic surfaces, start to grow with subsequent total stochastization of magnetic lines. Then plasma thermal quench is produced by thermal electrons moving along the stochastized magnetic lines. Simultaneously, but somewhat more slowly, the plasma current decays: a current quench takes place.

If one does not approach the stability limits and handles plasma carefully one can avoid the disruption instability (to be more precise, drastically reduce the probability of disruptions). However, less pronounced effects of MHD-activity might persist. Among them, first of all, are the so-called saw-tooth oscillations which look like periodically repeated processes near the magnetic axis. Each period consists of two phases. At first, a comparatively slow heating of the plasma core leads to sharpening of the electron temperature profile. Then, during the second phase, the temperature profile flattens drastically.

One other type of MHD-activity, the so-called Mirnov oscillations, is observed outside the plasma column in the form of poloidal magnetic field periodical oscillations. These magnetic oscillations correspond to the small perturbations of magnetic surfaces inside the plasma. All these oscillations affect the plasma transport not only in the sense of a local increase of thermal conductivity and diffusion but in the form of mutual influence of different plasma regions. There are two effects which illustrate the existence of the second phenomenon very clearly: the existence of different confinement modes and the mutual influence of profiles and transport in so-called 'profile consistency' phenomenon.

The first effect was very clearly manifest in the well-known L–H transition, first discovered in the ASDEX facility [19]. The confinement of L-mode type (from the word 'low') is more universal. In practice, it is present in all tokamaks with additional heating, if special attention is not given to the processes in the peripheral plasma. The H mode (from the word 'high') was easily realized in the ASDEX configuration with poloidal divertor and later on it was discovered also in the geometry with a limiter. Compared with L mode, H mode has a sharply-emphasized modification of peripheral plasma. The density and, especially, the electron temperature on the periphery markedly increase so that 'a pedestal' is formed on the electron temperature profile. The recycling on the wall (i.e. plasma recombination with re-entry of neutrals into the column) reduces which entails a visible drop of radiation in the H_α line. But the main feature of the H mode rests with a sharp improvement of plasma confinement—2–3 times as compared with the L mode.

The density and temperature increase on the periphery resembles some kind of a barrier for particle transport. However, the confinement improvement is caused not only by this barrier but also by the global decrease of transport coefficients

There are some other regimes of improved confinement. For example, the confinement improves (especially in the ohmic heating regime) with the injection of pellets— i.e. grains of solid hydrogen or deuterium. In the ohmic regime improved ohmic confinement (IOC) was observed. In TFTR the so-called 'super shots' with improved confinement and strongly-peaked density and temperature profiles were discovered [20,21]. Recently, it was shown in TFTR [21] that the H mode could be produced not only from the L mode but from 'super shots' as well, and these modes of improved confinement retained some features of super shots, (for instance, weak dependence upon current and heating power values).

All these phenomena indicate the existence of some specific feedback or self-organization mechanisms: transport processes in various regions of the plasma column turn out to be bound to each other. In other words, in tokamak plasma not only do temperature and density profiles depend on radial distribution of sources and transport coefficients but, vice versa, profiles affect the diffusion and thermal conductivity coefficients as well.

The plasma self-organization phenomenon is clearly displayed by the so-called effect of 'profile consistency' which was first declared by Coppi [22]. He noticed, that the experimentally measured profiles of electron temperature have a bell-like form similar to a Gaussian distribution. These profile features are not the simple trivial consequence of the fact that the plasma temperature on the boundary is much lower than at the centre and its gradient on the periphery is low due to higher transports. The question is of some kind of

profile self-similarity: their width is directly related to the q_a value on the plasma column boundary and with growing of q_a the profiles get narrowed. One may say that the electron temperature profile adjusts itself in such a way that a significant part of the current flows inside the radius $r = a_*$, where $q(r = a_*) = 2$. At the boundary of the effective current channel, $r = a_*$ the q-value according to the formula $q = 5a^2 B_T/RI$ is close to 2. Hence the effective radius of the current channel is proportional to the square root of current, $a_* \sim I\sqrt{RI/B_T}$. When the q_a value grows the plasma channel contracts. This effect was demonstrated by experiments on TFTR [23] and agrees with the results of other tokamaks.

The profile self-consistency phenomenon was studied in some detail in T-10 [24,25]. This facility has a powerful gyrotron system for plasma electron component heating at the electron-cyclotron resonance frequency. By using gyrotrons with different frequencies, one may easily change the profile of the power deposition and study the response of the electron temperature profile to the heating profile. The experiments clearly demonstrate the effect of the self-consistency of the electron–temperature profile: plasma tends to maintain the same optimal profile even in spite of drastic change of the power deposition profile. The rigidity of the profile retention grows together with the value of n/I, so that one may speak of the 'limiting' profile strongly retained at high values of n/I.

3.9 Physics of Confinement

The profile effects together with the existence of different confinement regimes have clearly shown that tokamak plasma is a complex self-organizing physical system. For its description one may use the approaches advocated for other complex systems. For instance, ordinary turbulence of liquid or gas is a very complicated non-linear phenomenon. It has not been precisely described theoretically yet. However, this fact does not bother engineers, since there exist empirical formulae, which are based on dimensional analysis. The same is true for plasma. Summarizing a large quantity of results from various tokamaks and taking dimensional analysis into consideration, one may obtain the formulae for the description and prediction of plasma confinement characteristics. To find these formulae the facilities of different sizes are compared with each other. That is why the corresponding empirical formulae were named 'scalings'.

One of the most important scalings is the scaling for τ_E, i.e. energy confinement time. This value is introduced in the following way. Let W be the total plasma thermal energy: $W = \langle 3/2(n_e T_e + n_i T_i)\rangle V$.

Here n_e, n_i are electron and ion densities (they can be non-equal, if the mean charge number $Z_{eff} \neq 1$), T_e, T_i are their temperatures, angle brackets mean volume averaging and V is the plasma volume. Plasma continuously loses its energy through different channels: electron and ion thermal conductivities, diffusion, radiation, charge exchange recharging and neutral atom ionization. That is why to maintain plasma in a steady state one should launch a certain power P into it. The $\tau_E = W/P$ value is called the energy confinement time. Writing this relationship as a balance of powers, $W/\tau_E = P$, we observe that τ_E is a characteristic time of plasma cooling. The higher τ_E, the better is the confinement.

It turns out that scalings for τ_E, i.e. the dependence of energy confinement time on plasma parameters, differ markedly in regimes with ohmic and additional heating.

For ohmically heated plasma at not very high density (in the non-dimensional representation) the neo-ALCATOR scaling is valid. It summarizes many of the experimental data with sufficient accuracy and can be written as

$$\tau_E = 7 \times 10^{-2} n_e a R^2 q_{eff}. \tag{50}$$

τ_E is measured in seconds, a and R in metres, n_e in 10^{20} m^{-3} whereas q_{eff} is defined by (44). A relationship, somewhat similar to (50), was derived for the T-11 device and was named T-11 scaling or Merezhkin–Mukhovatov scaling [15].

When density increases, but still does not exceed the upper density limit on the Hugill diagram, the improvement with density is lost and confinement saturates so that the relationship (50) is not valid. Instead of being proportional to $n_e a R^2 q_{eff}$, the energy confinement time becomes proportional to aRB_T. The transition from one dependence to another occurs approximately at the density value:

$$\bar{n}_e \simeq \frac{B_T}{q_{eff} R}\sqrt{A_i/2} \tag{51}$$

where A_i is the atomic mass of ions [26].

With additional heating, confinement degrades: i.e. the energy confinement time decreases with power. There are many empirical scalings, i.e. various dependences of τ_E on the main plasma parameters for tokamak data with additional heating. The first of them was proposed by Goldston in 1984 [27] for the L mode of confinement. It is in reasonable agreement with the experimental data from medium-size and large tokamaks. There are many other scalings which at first glance seem to be considerably different from the Goldston scaling.

However, as the ITER team has shown [28], these differences are not so essential—they hide the existence of parameter combination which vary insignificantly from one facility to another. Eventually, the L-mode scaling was defined accurately enough. There exist also H-mode scaling laws. Very roughly the corresponding τ_E value is about 2–3 times the L-mode value.

The minimal values of transport fluxes can be found theoretically, taking into account only Coulomb collisions between charged particles. Proposed first by Galeev and Sagdeev and improved further by the American theoreticians, the so-called neoclassical theory allows the calculation of transport coefficients in a quiet plasma with nested toroidal magnetic surfaces. The experimentally measured fluxes usually exceed the neoclassical values. As for the ion thermal conductivity, it slightly exceeds the neoclassical value and sometimes even approaches this value. The electron thermal conductivity and diffusion, however, are almost two orders of magnitude higher than the neoclassical values. To describe this high degree of anomaly one may apply the ideas based on turbulent processes in plasma with various types of instabilities.

We can presume that the macroscopic instabilities are stabilized with the help of profile tailoring when not approaching the operational limits. The concern is caused by the very fine-scale so-called microscopic instabilities which cannot destroy the plasma as a whole but can produce a small-scale turbulence entailing enhanced transport.

We start the discussion with the very simple case: plasma of low pressure in a homogeneous magnetic field. For both components of plasma, ions and electrons, the equilibrium with the guiding centres at rest means that a so-called Larmor current (9) is present. Let $\langle \boldsymbol{v}_\mathrm{i} \rangle$ be the averaged ion velocity and $\langle \boldsymbol{v}_\mathrm{e} \rangle$ be the averaged electron velocity. For each component we have, taking the electric field into account,

$$\nabla p_\mathrm{i} = en\boldsymbol{E} + \frac{e}{c} n \langle \boldsymbol{v}_\mathrm{i} \rangle \times \boldsymbol{B} \tag{52}$$

$$\nabla p_\mathrm{e} = -en\boldsymbol{E} - \frac{e}{c} n \langle \boldsymbol{v}_\mathrm{e} \rangle \times \boldsymbol{B}. \tag{53}$$

We assume that ion and electron densities are equal.

The sum of these two equations is equal to the equilibrium equation (10) since $\boldsymbol{j} = en(\langle \boldsymbol{v}_\mathrm{i} \rangle - \langle \boldsymbol{v}_\mathrm{e} \rangle)$.

When the electric field is absent the averaged velocities $\langle \boldsymbol{v}_\mathrm{i} \rangle$ and $\langle \boldsymbol{v}_\mathrm{e} \rangle$ correspond just to Larmor drifts and are directed opposite to each other. The guiding centres do not move in the radial direction. More realistic is the case when only ions are at rest, i.e. $\langle \boldsymbol{v}_\mathrm{i} \rangle = 0$. As

we see from equation (52) the ions are confined in fact by the electric field in this case. For instance, if the temperature is constant and density is a function of the minor radius r, we obtain from (52)

$$n = n_0 \exp(-e\phi/T) \tag{54}$$

where ϕ is the electric potential, i.e. $\boldsymbol{E} = -\nabla\phi$. If the density decreases towards the walls the potential ϕ has to be a rising function of the radius. In other words, the plasma is negatively charged. The ions are confined by the negative electric field and corresponding electron expulsion is balanced by their additional drift across the magnetic field.

We see that the ion guiding centres are rotating in the electron drift direction when the averaged ion velocity $\langle v_\mathrm{i} \rangle$ is zero. We can say that we have in fact a very slow plasma rotation. The order of magnitude of the rotation velocity is the Larmor drift

$$v_D \sim \rho v/a \sim cT/eBa. \tag{55}$$

Here ρ is the averaged Larmor radius and v is the thermal velocity of either ions or electrons.

This slow flow of plasma may be either stable or unstable in the linear approximation. But in both cases we can imagine that the plasma may transit into the turbulent mode of flow: many examples of ordinary fluid motion demonstrate this possibility very well. Plasma has a very low dissipation rate so that its turbulent behaviour is quite a natural one.

By analogy with an ordinary liquid the assumption can be made that the cross-field transport is produced by convection with velocities of the order of (55), so that the diffusion coefficient D may be estimated as $D \sim \lambda v_D$, where λ is so-called mixing length. If λ is proportional to the plasma radius a we obtain:

$$D = \alpha \frac{cT}{eB}. \tag{56}$$

This is the well-known Bohm formula for plasma diffusion. Bohm proposed this relation using the results of experiments with arc discharges in strong magnetic fields. He proposed the numerical value $\alpha = 1/16$ for the dimensionless factor α in (56).

It is interesting to note that Bohm diffusion was supported by many early experiments in the so-called stellarators, i.e. toroidal magnetic traps which differ from tokamaks. But fortunately the tokamak plasma is confined much better than was predicted by the Bohm formula.

The reason is that Bohm diffusion builds up only when no constraints are present that could suppress the free plasma motion with the drift velocity (55). This is not so in tokamak geometry. As we know, the tokamak magnetic configuration looks like a family of nested magnetic surfaces. To diffuse across the field, plasma has to cross a series of such surfaces between the plasma core and the walls. This could be done by convection, but convection is produced by electric drift. For the radial motion the electrical field should have a component which is directed tangentially to the magnetic surfaces. However, this component of electric field is constrained due to the very high electric conductivity of plasma: plasma tends to be equipotential along the magnetic field lines.

There is only one exception when the high longitudinal electric conductivity cannot prevent the build up of the tangential component of electric field. This is the case when the safety factor $q(r)$ is in fact equal to a constant rational number, $q(r) = \text{constant} = m/n$. In this case all the magnetic lines are closed. Therefore, longitudinal currents cannot take off the electric charge from plasma tubes. We obtain a situation similar to the pure toroidal magnetic field. Again, cross-field convection can develop and Bohm diffusion can be produced.

The case $q = m/n = \text{constant}$ is unique and cannot be realized generally. In the general case $q(r)$ is a function of the minor radius. It can coincide with the radial number $q = m/n$ at some resonance point $r = r_s$. But even very near to this point $q(r)$ is different from the m/n value. The rate of q variation can be characterized by the quantity

$$S = \frac{r}{q}\frac{\mathrm{d}q}{\mathrm{d}r} \tag{57}$$

which is called 'shear'. The value of q near the resonant point can be represented as

$$q = \frac{m}{n} + q'x = \frac{m}{n}(1 + \frac{xS}{r_s}). \tag{58}$$

Here $x = r - r_s$ is the distance from the resonant point.

Very close to the r_s point the electric potential looks like an arbitrary function of the cross section point extended along the magnetic field lines as a screw with m grooves. But when $r - r_s$ increases the magnetic field lines cease to be closed and the electric field is weakened as a result of longitudinal electric conductivity action. The conductivity value is very high in a high temperature tokamak plasma. That is why Bohm diffusion is strongly suppressed in tokamaks, at least, inside the high temperature core. The supressing of D as compared with the Bohm value can be taken into account by formula (56) with the correspondingly diminished α-factor. If it is assumed to be some small constant number we obtain the suppressed Bohm diffusion. This value corresponds to the much smaller scale of the mixing length λ, but again λ is proportional to plasma minor radius a. If λ becomes of the order of the ion Larmor radius, $\lambda \simeq \rho_i$, then we obtain the so-called gyro-reduced Bohm diffusion, when α in (56) is proportional to the small ratio ρ_i/a. Both suppressed Bohm and gyro-Bohm transport coefficients are not very much different from the experimental values. But their dependence upon the plasma temperature and the magnetic field values does not agree with experiments.

The preliminary analysis of different instabilities and their role in tokamak plasma transport phenomena was performed by Pogutse and myself [54] several years ago. It was shown that many modes can be stabilized in the high-temperature tokamak plasma and the most dangerous ones left are the so-called ion temperature gradient mode (ITGM) and the dissipative trapped electron mode (DTEM). These instabilities continue to be the subject of detailed consideration among plasma theoreticians. They indeed may play an important role in plasma transport, but I believe that the main cause of the enhanced transport in tokamaks is quite different.

As will be argued in Chapter 9, the electron component of tokamak plasma destroys the nested magnetic surface structure. Instead of smooth surfaces many so-called magnetic islands appear which split the surfaces and produce a great number of helical magnetic tubes. Such surface destruction is a result of specific filamentation of current density. It could be said that the initial, very symmetric, geometry breaks down spontaneously.

Spontaneous break-down of symmetry is well-known in different branches of physics. It takes place, for instance, in ferromagnetics, type-II superconductors, rotating superfluids and so on. In tokamak plasma the symmetry break-down arises as a consequence of the fact that the plasma is very far from thermodynamic equilibrium. Possessing a very low dissipation rate the plasma prefers to generate a non-linear pattern with magnetic surface destruction.

The physical picture looks like this. If a small perturbation of magnetic fields is present it can be considered as a superposition of harmonics like $\exp(im\theta + in\varphi)$ where θ and φ are poloidal and toroidal azimuthal angles, and m and n are integers. The small perturbation can be considered as a linear one everywhere but the resonant point $q(r_s) = m/n$. At this point a family of helical magnetic tubes is generated (figure 3.9(b)) which looks like an island-chain

in cross section. Therefore, the perturbed magnetic configuration is filled with many island chains. Due to plasma inhomogeneity the magnetic configuration perturbations are accompanied by plasma density perturbations. As a result corresponding electric fields appear.

Let us assume that this structure has a very fine-scaled structure with dimensions much less than the mean ion Larmor radius. When electric fields are present the ions are able to move across the magnetic field. If the ions are shifted by these fields in the direction of the major radius, R, i.e. in the direction of lower magnetic field, their energy is diminished due to conservation of the adiabatic invariant $\mu = mv_\perp^2/B$. As it was argued in section 3.3. the longitudinal energy also decreases when the ions are shifted along R. Thus when small-scale electric fields are present, ions can diminish their energy, being toroidally shifted. This energy loss is transferred to the fluctuations. In other words, when the shift of ions along R is possible we have a direct pumping of fluctuations by ions.

More detailed analysis of Chapter 9 shows that such a pumping takes place when the island-chains fill all the plasma cross section and are touching each other. Both ions and electrons are at the margin of stochasticity in this case. Ions pump the noise and electrons lead to their decay. As a result of a very delicate balance of pumping and decay the self-organized configuration is maintained. It has a broken magnetic symmetry: an initial azimuthally symmetric configuration is filled with a huge number of helical filaments. This pattern is very sensitive to external influence. That is why transport in tokamak plasma is so sensitive to profile modifications and edge plasma activity.

The picture described above predicts the energy-confinement time dependence upon different parameters of plasma which is in qualitative agreement with experiments. It gives in addition a clue to understanding many phenomena of tokamak plasma self-organization.

The scalings experimentally found are safe enough and allow the prediction of plasma parameters for the experimental thermonuclear reactor. For example, the ignition and D–T plasma burn is predicted for ITER from the existing database with a sufficient degree of confidence. However, to assess the ignition, some additional experiments on plasma optimization at the ITER reactor itself would be needed.

The present status of high-temperature plasma magnetic confinement in tokamaks is shown in figure 3.10. On the abscissa axis the ion temperature at the centre of the plasma column $T_i(0)$ is plotted, measured in keV, and on the ordinate axis the confinement parameter $n_d(0)\tau_E T_i(0)$ is plotted where $n_d(0)$ is the deuteron density at the centre of the plasma column, measured in $10^{20}\,\mathrm{m}^{-3}$ and τ_E is the energy confinement time. The maximal value of this parameter equal to 9 was reached in JET. The Q_{DT*} value which is equal to the ratio of the calculated D–T reaction power ratio (when using D–T instead of deuterium) to the plasma heating power, reaches the value of the order of unity in JET. In TFTR this value is close to 0.5. Thus, these two facilities are close enough to 'break-even', $Q_{DT*} \sim 1$, which was preset in their design objectives as a major goal. A record ion temperature value of $\sim 30\,\mathrm{keV}$, i.e. twice as high as is required for the D–T reaction ignition, was first reached in TFTR [29] and later on in JET. The first experiments with D–T fuel on JET have demonstrated Q value of 0.15 with a reasonable projection to $Q \sim 1$ [160]. Several facilities are routinely working at multi-keV temperatures with the help of different additional heating methods. One may say that the problem of plasma heating and confinement in tokamaks is almost solved.

When approaching a fusion reactor two new important physics problems emerge: impurity control and steady-state non-inductive current drive.

3.10 Edge Plasma

Impurity control depends very strongly on the plasma-wall interaction and edge plasma behaviour. This can be argued in the following way.

If the plasma ions are at rest, i.e. their averaged macroscopic velocity is zero, then ions are confined by the electric field only. Let us consider again the simplest case of a homogeneous temperature inside the plasma core. Then for the ion density we have a Boltzmann distribution (54). For impurities the same law is valid but the ion charge e has to be replaced by the Z value, the charge number of an ion, so that we have an equilibrium

$$n_z = n_z(0)\,(n_H/n_H(0))^Z\,. \tag{59}$$

Here n_z is the density of impurities with charge number equal to Z and n_H is the hydrogen (or deuterium) density. We see that impurities have a tendency to be accumulated near the centre of the plasma. The central value $n_z(0)$ of impurity density depends upon the total number of impurity ions. If impurities are continuously supplied by the wall the impurity accumulation becomes dangerous one for high-temperature plasma.

The problem is that impurities produce higher radiation losses which are higher for larger Z-numbers. Radiation power is a decreasing function of temperature so that radiation losses are larger

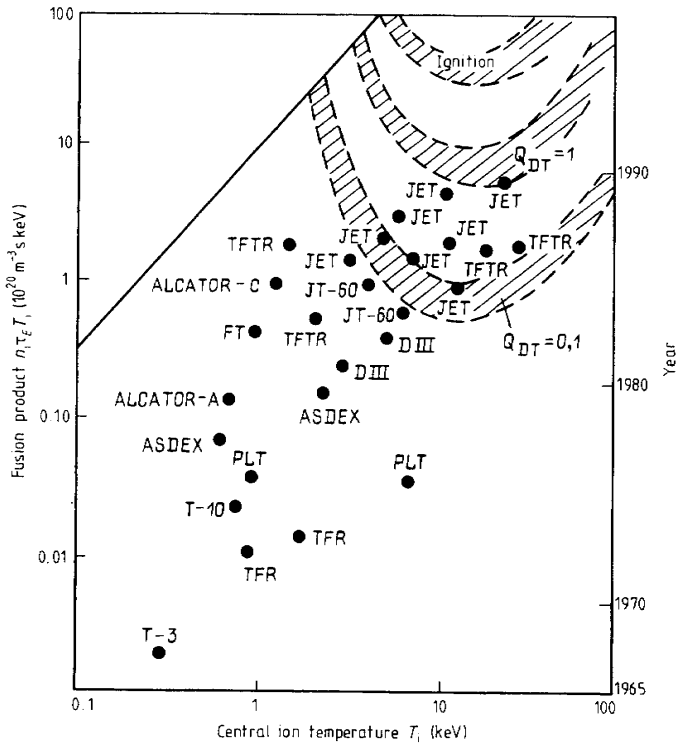

Figure 3.10 Progress in tokamak parameters. (See also the review paper [147].)

on the plasma periphery. This feature leads to the shrinking of the plasma column making it less stable. The impurities are quite undesirable also from the point of view of fusion because they dilute the hydrogen plasma. Each heavy ion provides Z electrons so that at a given plasma pressure each heavy ion replaces Z hydrogen ions. All this means that the fusion plasma has to be very clean.

The medium- and high-Z impurities are released from the walls due to sputtering: bombardment of walls by high energy ions knocks out atoms from the solid surface. The freshly released atom is ionized very close to the wall so that it has a high probability of returning back to the wall. This process leads to redeposition of the wall material. The atoms which penetrate deeper into the plasma are further ionized and their charge number increases. Some of them can reach the hot plasma core. In a quiet plasma impurity accumulation

at the centre could occur. But in fact a tokamak plasma is not quiet at all, so that thermodynamic equilibrium (59) is not reached. Outwardly directed diffusion flow captures the impurity ions and protects the plasma core from impurity accumulation.

Thus the most pleasant mode of plasma confinement is where some slight turbulence is maintained in the plasma so that both hydrogen ions and impurities have enhanced diffusion flux towards the walls. Some level of plasma turbulence is maintained by the edge plasma itself. Experiments show that a high level of fluctuations is present near the plasma edge. Some of the fluctuations have a quite irregular feature, but others display a regular behaviour. For instance, so-called edge localized modes (ELM) look like a series of spikes similar to the saw-teeth of relaxation oscillations. Many complicated physical phenomena take place in the edge plasma and the main objective of the corresponding researches is to use all these phenomena in the optimal way.

The most convenient tool for impurity control is the poloidal divertor, i.e. such a configuration which has open magnetic surfaces outside the so-called separatrix—the last closed magnetic surface (see figure 3.6). The divertor configuration allows the plasma-wall interaction surface to be isolated from the plasma edge. The divertor has to fulfil two functions: to unload the thermal flux from the plasma and to screen plasma from the impurity influx. If the plasma density inside the divertor chamber is high enough, both these functions can be realized. However, for a reactor plasma the matter is not so simple and continues to be a focus of present plasma experiments.

In fusion D–T plasma it is necessary to take care of the helium exhaust: the ash of the fusion reactions has to be expelled from the plasma in order not to poison it. This function can be laid again on the divertor.

3.11 Current Drive

In most tokamak devices the plasma current is generated and maintained with the help of an inductive current drive. When the inductive coils are used to change the magnetic flux inside the inductor then an oppositely directed magnetic field flux between the inductor and plasma appears. The variation of this flux with time entails the appearance of an induced electric field directed along the toroidal azimuth.

Each plasma electron is accelerated by this field according to the equation of motion:

$$m_e \frac{\partial v}{\partial t} = -eE - \nu_e m_e v. \tag{60}$$

Here v is the longitudinal electron velocity and ν_e is the electron–ion collision frequency. If the density of electrons is equal to n then their current density $j = -env$.

According to the Maxwell equation

$$\frac{\partial B}{\partial t} = -c\nabla \times E \tag{61}$$

the inductive electric field is caused by the magnetic field variation with time.

Let us use again the cylindrical frame of reference neglecting the toroidal curvature of plasma column. The electric field is directed along the z-axis and the current density has the same direction. Equation (60) can be expressed in the form

$$\frac{\partial J}{\partial t} + \nu_e J = \nu_e \sigma E \tag{62}$$

where $\sigma = e^2 n/\nu_e m_e$ is the electric conductivity. On the left-hand side of (62) the first term prevails when the current density changes much faster than the collision frequency. We consider first the case where $\partial J/\partial t = \nu_e \sigma E$. We express E in (61) with the help of this relation and take into account the Maxwell equation

$$J = \frac{c}{4\pi}\nabla \times B \tag{63}$$

where we have neglected the term with the time derivative of the electric field. Now we can transform (61) into the following relation:

$$\frac{\partial B}{\partial t} = -\frac{c^2 m_e}{4\pi e^2 n}\frac{\partial}{\partial t}\nabla \times \nabla \times B. \tag{64}$$

If we assume that $n =$ constant and use the relation $\nabla \cdot B = 0$, we can rewrite (64) in the form

$$\frac{\partial B}{\partial t} = \Lambda^2 \Delta_\perp \frac{\partial B}{\partial t} \tag{65}$$

where $\Lambda^2 = c^2/\omega_{pe}^2 = c^2 m_e/4\pi e^2 n$ is the collisionless skin layer thickness or London length and ω_{pe} is the plasma Langmuir frequency. Relation (65) is well-known in the theory of superconductivity. It shows that magnetic field penetrates into plasma only to a depth Λ.

Indeed, according to (65) the poloidal component of magnetic field looks like $B_p(t)\exp(-x/\Lambda)$, where x is the distance from the plasma edge and $B_p(t)$ is a given poloidal field value at the plasma boundary. The value of Λ is very small. For instance, at $n = 10^{14}\,\mathrm{cm}^{-3}$ $\Lambda \simeq 0.05$ cm. As for the value of the collision frequency, $\nu_e = v_e/\lambda_e$ it can be estimated with the help of (15) taking into account that λ_e and λ_i are of the same order of magnitude. At $n = 10^{14}\,\mathrm{cm}^{-3}$ and $T = 10\,\mathrm{keV}$ the value of ν_e is of the order of $\sim 5 \times 10^3\,\mathrm{s}^{-1}$. This is a very high value so that for slow current rise and time variations it is more appropriate to drop the first term on the right-hand side of relation (62). In this case we have simply $J = \sigma E$ and relation (61) takes the form

$$\frac{\partial B}{\partial t} = -\nabla \times \left(\frac{c^2}{4\pi\sigma}\nabla \times B\right). \tag{66}$$

When the poloidal magnetic field has a B_θ component only, relation (66) can be written as

$$\frac{\partial B_\theta}{\partial t} = \frac{\partial}{\partial r}\left(\frac{c^2}{4\pi}\frac{1}{r}\frac{\partial}{\partial r} r B_\theta\right) \tag{67}$$

while the J value is equal to $J = (c/4\pi)(1/r)(\partial/\partial r)(rB_\theta)$. If the poloidal field $B_p = B_\theta(r = a)$ is held to be constant at the plasma boundary the current density relaxes to the value $J = \sigma E$ value at $E =$ constant. As we know, σ is proportional to $T_e^{3/2}$ since λ_e is proportional to T_e^2, so that the steady state current density as a function of the minor radius r looks like $T_e^{3/2}$. The electron temperature is bell-shaped and the same is true for the $J(r)$ distribution.

The rate of current density relaxation is described by equation (67) from which we can estimate the skin-time value

$$\tau_s \approx a^2/4D_s \tag{68}$$

where $D_s = c^2/4\pi\sigma$ is the magnetic field diffusion coefficient. We see that

$$\tau_s \simeq \pi a^2 n r_0 \tau_e \tag{69}$$

where $\tau_e = \nu_e^{-1}$ is the average collision time and $r_0 = e^2/m_e c^2$ is the so-called classical radius of the electron. We see that (69) contains the dimensionless parameter $\pi a^2 n r_0$ which is called 'the electron line density'. We shall use the parameter $\Pi = a^2/\Lambda^2 = 4\pi n a^2 r_0$ instead of 'electron line density'. The Π parameter shows how large the plasma size is compared with the collisionless skin-layer depth.

Now let us estimate the skin time for the plasma with $n = 10^{14}\,\mathrm{cm}^{-3}$, $T_e = 10\,\mathrm{keV}$, and $a = 100\,\mathrm{cm}$. We find that $\pi a^2 n r_0 \simeq 10^6$,

$\tau_e = \nu_e^{-1} \simeq 2 \times 10^{-4}$ so that $\tau_s \simeq 200\,\mathrm{s}$. We see that this value is almost two orders of magnitude larger than the energy confinement time needed for a thermonuclear reactor.

Let us represent the equation (61) for the poloidal magnetic field component B_θ in the form of a continuity equation

$$\frac{\partial B_\theta}{\partial t} + \frac{\partial}{\partial r}(V_E B_\theta) = 0 \tag{70}$$

where $V_E = cE/B_\theta$ is the electric drift in the poloidal magnetic field. This drift velocity is sometimes called Ware-pinching. If the longitudinal magnetic field were absent, each charged particle would be drifting just with this velocity.

Equation (70) can be considered as a continuous flow of poloidal magnetic field lines towards the centre of the plasma column. When E = constant, the flux $V_E B_\theta$ of the magnetic field lines is also constant. The change of total poloidal magnetic flux $\psi = \int_0^a B_\theta dr$, as we see from relation (70), is balanced by the influx of magnetic field lines through the plasma boundary $V_E B_\theta = -cE(r = a)$. Meanwhile the magnetic line loops disappear at the centre. In the steady state it is necessary to maintain the constant influx of lines to prevent the current decay by the tightening of magnetic line loops. In other words, we have to supply the new magnetic loops between the plasma and inductor. To do this it is necessary to increase the magnetic flux inside the inductor. But this flux is limited by the maximum value of the inductor magnetic field due to stress limitation.

Thus the inductive current drive can maintain the plasma current for a restricted period of time only. Afterwards a new discharge pulse can be produced. The pulse mode operation is not appropriate for future fusion reactors. That is why the different schemes of non-inductive current drive attract attention of many researches.

The hope of adapting non-inductive current-drive schemes is based on two circumstances. The first is the very low electric resistivity of plasma leading to very large skin-time value and the second is the very low electron-current velocity J/en as compared with the sound velocity. Both of these facts mean that small deviations from thermodynamical equilibrium can lead to various driving forces.

One of these forces is produced by the plasma pressure gradient. It is called 'bootstrap current' and will be explained in more detail in Chapter 10. Its physics is based on the existence of so-called trapped particles. These particles with very small longitudinal component of velocity are oscillating between the magnetic mirrors near the minimum magnetic field value at given magnetic surfaces, i.e. near the outer circumference of the torus. The trapped particles are not

confined by the toroidal magnetic field and their toroidal expulsion is balanced by their drift along the toroidal azimuth. The current produced by such toroidal drift is diamagnetic, being directed in the same direction as that induced by ohmic current drive.

Another, more active, approach is based on the shaping of the electron distribution function with the help of external tools. Such an influence can change the electron equation of motion (62) in favour of relaxation to the state with $v \neq 0$. Thus this mechanism can be really considered as a driving force generation.

For the current drive different additional heating tools may be used. The non-inductive current drive I_{CD} may be represented as:

$$I_{CD} = \gamma_{CD} P / \langle n_e \rangle R \tag{71}$$

where $\langle n_e \rangle$ is the mean volume electron density measured in $10^{20}\,\mathrm{m}^{-3}$, R is the major radius measured in metres, and P is the power in MW launched in plasma for the current drive. The γ_{CD} coefficient is the current drive efficiency. The reversed dependence of the non-ohmic current on density is a common unfavourable feature of all the current drive schemes.

The physical reason for such a dependence is quite clear. The current carrying electrons have an angular momentum which is proportional to the product IR. This momentum is damped by collisions with the main bulk plasma being at rest. Just to restore this momentum an external power supply is needed. As the collision frequency is proportional to the plasma density the momentum balance leads to an expression similar to (71). The efficiency γ_{CD} may have a favourable dependence on electron temperature for such schemes of non-inductive current drive when the thermal electrons in addition to beams participate in the current carrying.

The best results on current drive were obtained in the Japanese tokamak JT-60, where $I_{CD} = 2\,\mathrm{MA}$ was maintained using electromagnetic waves at the lower hybrid resonance. The current drive efficiency has been raised up to the value of $\gamma_{CD} = 0.34$ at a moderate density [30].

For current drive at higher densities some other schemes could be used: neutral injection, electromagnetic waves at ion-cyclotron and electron-cyclotron resonances. Some of these have already been tried, and others are being developed.

Thus, tokamak experiments are performed at a very sophisticated level. The possibility of plasma heating up to temperatures of the order of $\sim 30\,\mathrm{keV}$ has been shown, the operational limits of plasma steady state confinement have been established, and a reliable data-base has been created which is sufficient for the design and construction of an experimental thermonuclear reactor. Progress in plasma

Table 3.1 Main ITER parameters developed during the conceptual design.

Major plasma radius	$R = 6.0\,\mathrm{m}$
Plasma half-width	$a = 2.15\,\mathrm{m}$
Elongation	$b/a = 2$
Toroidal field	$B_0 = 4.85\,\mathrm{T}$
Nominal plasma current	$I = 22\,\mathrm{MA}$
D–T reaction power	$P_f = 1000\,\mathrm{MW}$

physics is based on many advanced technologies: magnetic systems, including superconducting ones, plasma heating systems, control systems etc. A well-developed theoretical basis and many numerical models permit the description of a variety of complex non-linear phenomena in a high-temperature tokamak plasma.

3.12 Tokamak Reactor

The present level of fusion research is sufficient for realization of plasma burning and construction of an experimental fusion reactor. There are several designs for studying D–T reaction burning as well as several experimental reactor designs. The most thoroughly developed design of the experimental reactor is the International Thermonuclear Experimental Reactor (ITER) [149,150]. A diagram of the ITER scheme is shown in figure 3.11.

ITER represents a large complex engineering structure. Its parameters were chosen to provide a thermonuclear reaction burn in the first phase of ITER operation and a steady-state operation by means of non-inductive current drive as a final goal.

The major ITER technical objective is to obtain all technical information for the subsequent construction of DEMO— the first power thermonuclear reactor.

ITER is an experimental reactor but it has all the systems of a future power reactor so that figure 3.11 can be used to get the first impression of the main features of a future fusion power reactor with magnetic confinement of plasma.

We see that the toroidal plasma is placed in a big toroidal vacuum chamber. Plasma has an elongated shape with separatrix separating the closed magnetic surfaces from the open ones. The divertor configuration is foreseen to accomplish the impurity control and to solve the problem of helium ash exhaust. Future power reactors will have a steady-state mode of operation. ITER will operate in the long-pulse mode having the steady-state operation as a goal. Heating of

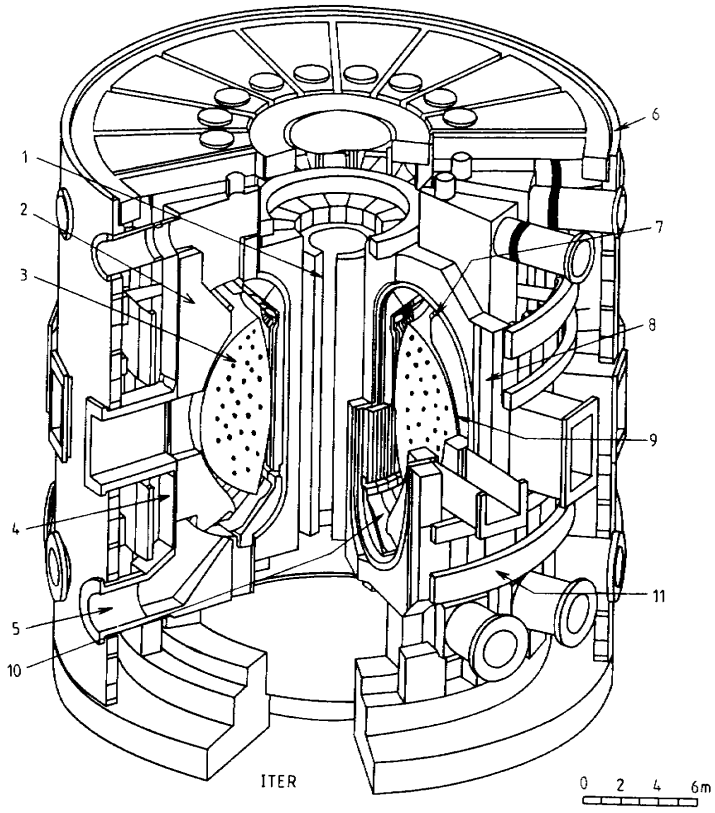

Figure 3.11 ITER elevation view: 1—inductor; 2—blanket; 3—plasma; 4—vessel; 5—plasma exhaust (gas-pumping); 6—cryostat; 7—active control coils; 8—toroidal field coils; 9—first wall; 10—divertor plates; 11—poloidal field coils [149].

the plasma and non-inductive current drive are achieved with the help of a multi-function heating and current drive system. The first option is based on 1.3 MeV negative-ion neutral beams working together with lower hybrid and electron cyclotron resonance schemes. The second option uses ion cyclotron heating. The current-drive systems will be used to study very long pulses and steady-state discharges. The plasma will be continuously refreshed with the help of D–T pellets—tiny grains of frozen hydrogen accompanied by pump-

ing of gas, i.e. the product of the electron–ion recombination on the divertor plates.

Systems of toroidal field coils and poloidal field coils are used for plasma confinement. The goal of achieving extended burn (ultimately, steady-state) dictates the use of superconducting-coil systems. As we see, the toroidal and poloidal systems are not linked with each other: all the large poloidal field coils are placed outside the toroidal field coils. All the coils have a common cryostat.

The burning plasma is surrounded by an integrated structure of blanket and shield. Tritium needed for the D–T reactions could be produced by the fusion reactor itself. For this purpose, a tritium breeding blanket can be used which contains lithium compounds. The nuclear reactions of fusion neutrons with the lithium nuclei can generate tritium with a breeding ratio greater than unity, if the chemical composition of the blanket is appropriately adjusted.

The ITER programme has three major research objectives. The first objective is to demonstrate controlled ignition and extended burn in a D–T plasma with steady-state operation as an ultimate goal. The second objective is to demonstrate technologies essential for a reactor in an integrated system. The third goal is to perform integrated testing of the high heat flux nuclear components required in the practical utilization of fusion power. ITER has to provide all the technical information needed for development of DEMO—the first fusion power reactor.

4 Plasma Equilibrium

If tokamak plasma parameters are within the stability region, plasma reaches an equilibrium when the pressure gradient is balanced by the ampere force:

$$\nabla p = \boldsymbol{J} \times \boldsymbol{B}/c. \tag{72}$$

Here $\boldsymbol{J}$ is the current density, $\boldsymbol{B}$ is the magnetic field vector, the cross denotes the vector product and c is the velocity of light. CGSE units are used here. Using MKS units and measuring the current in MA, the value of c should be replaced by 10. Multiplying (72) by $\boldsymbol{B}$ and $\boldsymbol{J}$ we obtain:

$$\boldsymbol{B} \cdot \nabla p = 0 \qquad \boldsymbol{J} \cdot \nabla p = 0. \tag{73}$$

These relations may be considered as a statement that the pressure is constant along the magnetic field lines and current lines: the ampere force does not act in these directions. Relations (73) also mean that the magnetic field lines and current lines are located on the surfaces p = constant, these surfaces are the magnetic surfaces. In a tokamak with quiet plasma the magnetic surfaces are toroidal and nested. When the minor radius tends to zero the torus shrinks into a line which is called the magnetic axis. All the magnetic surfaces embrace this axis.

If the aspect ratio (R/a) is high enough the equilibrium along the minor and the major radii can be considered separately. When considering the equilibrium along the minor radius one may neglect the plasma column curvature. This means that $a/R \to 0$, and, for circular cross section, the magnetic surfaces can be considered as circular cylinders, r = constant. The equilibrium condition will be as follows:

$$\frac{\mathrm{d}p}{\mathrm{d}r} + \frac{\mathrm{d}}{\mathrm{d}r}\left(\frac{B_\mathrm{T}^2}{8\pi}\right) + \frac{B_\vartheta}{r}\frac{\mathrm{d}}{\mathrm{d}r}\left(\frac{rB_\vartheta}{4\pi}\right) = 0. \tag{74}$$

The toroidal magnetic field in a tokamak is strong enough and therefore it slightly differs from the initial vacuum value. Let

$B_T = B_T^0 + \Delta B_T$ where B_T^0 = constant and ΔB_T is small. Retaining the linear terms only we can replace (74) by the relation

$$4\pi \frac{dp}{dr} + B_T^0 \frac{d}{dr}(\Delta B_T) + \frac{B_\theta}{r} \frac{d}{dr}(rB_\theta) = 0. \tag{75}$$

Equilibrium condition (75) relates three functions p, B_θ, B_T so that it may be interpreted as an equation for ΔB_T at a given $p(r)$ and $B_\theta(r)$. In other words, equilibrium along the minor radius does not impose any constraints on the profiles of pressure and of current density as functions of the minor radius. Let $\Delta\Phi_i$ be the difference in magnetic flux in the plasma compared with its vacuum value:

$$\Delta\Phi_i = \int_0^a 2\pi r \Delta B_T \, dr. \tag{76}$$

Let us multiply (75) by $2rdr$ and integrate the result over the column region, i.e. from zero up to $r = a$. The first component, after integration by parts, gives $8\pi\langle p\rangle a^2$, where the angle brackets denote a volume average. The third component gives the value of $a^2 B_\theta^2(a) = 4a^2 I^2 c^{-2}$. The second component, after integration by parts, gives the following expression:

$$B_T^0 \left[2a^2 \Delta B_T(a) - \int_0^a 4r \Delta B_T dr \right].$$

Let r_c be the radius of the magnetic field toroidal coils. Since the longitudinal magnetic field beyond the plasma column is uniform, the value of $B_T(r)$ remains the same in a circle of radius r, $a < r < r_c$. Therefore, the total longitudinal flux change is

$$\Delta\Phi = \Delta\Phi_i + \pi(r_c^2 - a^2)\,\Delta B_T(a). \tag{77}$$

We assume that $\Delta\Phi = 0$ since flux is fixed by the toroidal magnetic field coils. Then (77) allows us to express ΔB_T in terms of $\Delta\Phi_i$, so that the result of integration of (75) may be written as:

$$C B_T^0 \Delta\Phi_i = I^2/c^2 - 2\pi\langle p\rangle \tag{78}$$

where the constant $C = r_c^2 B_T^0 / 2\pi a^2 (r_c^2 - a^2)$. The value of the longitudinal flux change is easily measured experimentally. Thus, expression (78) allows us to measure a volume average of plasma pressure. As we can see from (78), the longitudinal current creates paramagnetism—strengthening of the flux inside plasma while the plasma pressure leads to diamagnetism. That is why measuring $\langle p\rangle$ with the help of the value of $\Delta\Phi_i$ actually means using a diamagnetic signal.

Let us also note another feature which is important for the understanding of tokamak physics. The value of the longitudinal magnetic field energy change in a linear approximation with respect to ΔB_T is equal to:

$$\Delta\mathcal{E}_T = \int_0^{r_c} \frac{B_T^0 \Delta B_T}{4\pi} 2\pi r \, dr = \frac{B_T^0}{4\pi}\Delta\Phi = 0. \tag{79}$$

As the total magnetic flux is constant, the toroidal magnetic energy is constant too. This statement has a much broader meaning: at any changes of pressure and of the poloidal field in tokamaks the strong toroidal magnetic field plays the role of an external constraint and energetically is not involved in these processes.

Let us now consider the equilibrium along the major radius. For the column as a whole, the equilibrium is determined by (5) which can be written as:

$$\beta_p + 0.5 l_i = 2B_z R / B_p a. \tag{80}$$

Here $\beta_p = 8\pi\langle p\rangle / B_p^2$, l_i is the internal inductance, $B_p = B_\theta(a)$ is the poloidal field at the plasma boundary and B_z is the vertical equilibrium field.

Equation (80) could also be used for the internal magnetic surfaces if it were modified appropriately. Indeed, let us consider some internal torus of minor radius r (see figure 4.1(a)). This torus is affected by a force F_p which pushes it along the major radius (see formula (31)). However, similar to the Archimedes force applied to an object immersed in a liquid, the upward force is determined by the excess pressure compared with the pressure $p(r)$ at the point r. Thus, for the torus of radius r instead of (31) we have

$$F_p = (\bar{p} - p) 2\pi r^2 / R \tag{81}$$

where $\bar{p}(r) = r^{-2} \int_0^r 2pr \, dr$ is the mean value of pressure inside radius r. Thus, for the internal torus under β_p in (80) one should assume the value $\beta_p = 8\pi(\bar{p} - p)/B_\theta^2(r)$. Here l_i is the internal inductance: $l_i = 2c^2\mathcal{E}_p/I^2$, where $\mathcal{E}_p$ is the energy of the poloidal magnetic field equal to $\langle B_\theta^2\rangle \pi a^2 / 8\pi$. Therefore, l_i for the whole column may be written as $\langle B_\theta^2\rangle / B_p^2$. For the internal torus of radius r, l_i in equation (80) should be replaced by $\bar{B}_\theta^2 / B_\theta^2$, where the bar again marks averaging over the internal torus.

Let us remember that to assure equilibrium for the whole column a vertical field B_z is needed. This increases the poloidal field on the

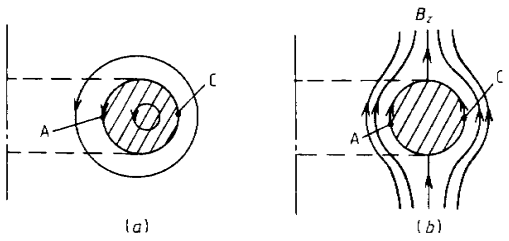

Figure 4.1 Relationship between magnetic surface displacement and an effective vertical equilibrium field B_z. Radially dependent displacement (r) of magnetic surfaces leads to the change (a) of the poloidal magnetic field: $\delta B_\perp = B_\perp \Delta'(r)\cos\theta$. It is equivalent to the superimposition of an additional vacuum field (b). The equivalent vertical magnetic field B_z far from the surface is half that at points A and C..

outer plasma contour and decreases it at the inner one. Similarly the internal torus should be 'supported' by the outer poloidal field. In other words the torus is shifted along the major radius in order to amplify the poloidal field on its outer contour and to reduce the poloidal field at the inner one. This radial displacement of magnetic surfaces is called the Shafranov shift. Let us denote the magnetic surface displacement by $\Delta(r)$. For the radial force to appear directed towards the symmetry axis, the displacement of the internal surfaces should be larger than that of the external ones, as seen in figure 4.1(a). At a slight displacement the distance between adjacent surfaces, initially equal to $\mathrm{d}r$, becomes $\mathrm{d}r - \Delta'\mathrm{d}r$ at point A and $\mathrm{d}r + \Delta'\mathrm{d}r$ at point C, where $\Delta' = \mathrm{d}\Delta/\mathrm{d}r$. The field at point A decreases and becomes equal to $B_\theta(1+\Delta')$, while the value of field at point B increases to $B_\theta(1-\Delta')$, where B_θ is the initial unperturbed poloidal field. Thus, at the points A and C a vertical field $\Delta' B_\theta$ is produced. Now we have to find the equivalent equilibrium field B_z, i.e. the additional vacuum field perturbation outside of the column of radius r. The appropriate additional vacuum field is shown in figure 4.1(b).

This field controls the radial position. The position control field is considered as a superposition of the homogeneous magnetic field B_z and the field of a magnetic dipole placed at the centre of the shaded circle in figure 4.1(b). The magnetic dipole value is adjusted in such a way that the magnetic lines of the additional field do not intersect the circle contour. It is easy to see that the additional field strength

at the points A and C is twice the homogeneous control field B_z far from the circle. Thus we can put $B_z = -\frac{1}{2}\Delta' B_\theta$.

Substituting all the calculated values into the radial equilibrium equation (80) which is related now to the torus of radius r, we obtain an equation for the displacement Δ'

$$-\Delta' = \frac{r}{R}\left\{\frac{8\pi(\bar{p}-p)}{B_\theta^2} + \frac{\bar{B}_\theta^2}{2B_\theta^2}\right\}. \tag{82}$$

As is seen, displacement Δ' grows with β_θ and may reach a value of the order of a when $\beta_\theta \sim R/a$.

In a tight torus the aspect ratio cannot be considered as a very high value. Therefore, a separate consideration of the equilibrium along minor and major radii is not valid, but the vector equation (72) due to axial symmetry may be transformed to a simpler scalar Grad–Shafranov equation.

To derive this equation, we can use a cylindrical system of coordinates R, φ and z. Let B_φ be the toroidal magnetic field, which is equal to $2I_\varphi/cR$ in CGSE units, where I_φ is the total current flowing through a horizontal plane stretched on the circle of radius R. The current I_φ is constant on the magnetic surface. Furthermore, the poloidal magnetic field divergence is equal to zero:

$$\frac{\partial}{R\partial R}(RB_R) + \frac{\partial B_z}{\partial z} = 0. \tag{83}$$

Therefore, the poloidal magnetic field may be expressed using the poloidal magnetic flux

$$B_R = \frac{1}{R}\frac{\partial \psi}{\partial z} \qquad B_z = -\frac{1}{R}\frac{\partial \psi}{\partial R}. \tag{84}$$

As we see, $\boldsymbol{B}\nabla\psi = 0$, i.e. the function ψ is constant on a magnetic surface. Consequently, the current I_φ may be considered as a function of ψ. By using (84), the azimuthal current density $\boldsymbol{J} = (c/4\pi)\nabla \times \boldsymbol{B}$ can be expressed via ψ:

$$J_\varphi = \frac{c}{4\pi R}\Delta^*\psi \tag{85}$$

where the operator Δ^* is defined by $\Delta^* = R(\partial/\partial R)(1/R)(\partial/\partial R) + (\partial^2/\partial z^2)$. Since the plasma pressure is also constant on a magnetic surface and may also be considered as a function of ψ, the pressure gradient $\nabla p = p'\nabla\psi$, where $p' = \mathrm{d}p/\mathrm{d}\psi$. Now we can project the

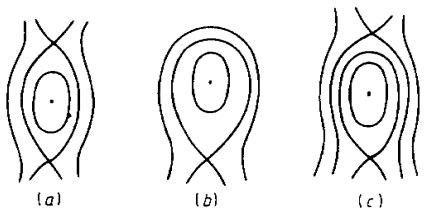

Figure 4.2 Divertor configurations: (*a*) double null, (*b*) single null, (*c*) semi-double null.

vector equation (72) on the direction of $\nabla\psi$ and obtain the Grad–Shafranov equation:

$$\Delta^*\psi + 4\pi R^2 p' + \frac{4}{c^2} I_\varphi I'_\varphi = 0. \tag{86}$$

A prime here means differentiation with respect to ψ. This equation is convenient for numerical calculations of equilibrium configurations with arbitrary plasma shapes.

Equation (86) contains a large quantity I_φ related to the toroidal magnetic field. It is not difficult to observe that the equilibrium does not depend on the absolute value of the toroidal field: if I_φ increases, the derivative I'_φ automatically decreases and the equation is unchanged for given $(I_\varphi^2)'$. The equilibrium toroidal magnetic field may be changed in the broad range consistent with the condition $I_\varphi^2 > 0$.

From the point of view of reactor applications divertor configurations are most important. Figure 4.2(*a*) shows schematically the tokamak magnetic-surface cross section for the case of a double-null divertor, and figure 4.2(*b*) for a single-null one. The latter is in fact an internal part of a more general divertor configuration (see figure 4.2(*c*)) which is called a semi-double-null divertor. When the vertical asymmetry is reduced, the semi-double-null divertor configuration tends to a double-null one. If the separatrix is 'pressed' towards the internal contour, a D-configuration is formed which, in addition to the elongation $K = b/a > 1$, also possesses a triangularity. The triangularity value δ is determined as shown in figure 4.3.

Due to cross field diffusion, MHD-equilibria described by (72) resemble, in fact, a slow flow of plasma towards the walls. The convection velocity is many orders of magnitude less than the particle mean thermal velocity. The closer to the plasma edge, i.e. the less the density of particles, the higher is the convection velocity. It reaches a particularly high value in the vicinity of the limiter, which restricts

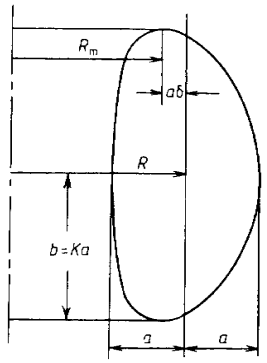

Figure 4.3 Parameters of D-sl.aped plasma: $K = b/a$—elongation.

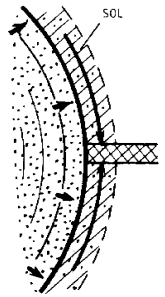

Figure 4.4 Scrape-off layer (SOL).

the plasma column. As is shown in figure 4.4, a layer is formed here, which rests on the edge of the limiter and is called the scrape-off layer (SOL). The particles which enter into the SOL are swept towards the limiter with velocities close to thermal. Since the cross-field convection velocity of the magnetized plasma is very low compared with the sonic velocity, SOL is very shallow.

5 Plasma Stability

From the practical point of view any equilibrium is real only when it is stable. An unstable equilibrium is just an abstract idealization: if slight deviations from the equilibrium start to grow then the equilibrium will not exist for a long time. Since the plasma is a very mobile medium with an enormous number of collective degrees of freedom, numerous instabilities are inherent. They have been studied and classified in detail. One should clearly understand that all those instabilities, although they have a common source, i.e. a strong thermal non-equilibrium of high-temperature plasma, are rather different. Global instabilities related to large-scale plasma perturbations are most dangerous. They are usually called MHD-instabilities, because for their description one may use the magnetohydrodynamic approximation or, to be more precise, gaseous dynamics for compressible plasma.

MHD-instabilities may lead to complete plasma collapse. If they are eliminated, then microscopic instabilities of slower growth may develop. One may live with them since they do not lead to plasma collapse but only enhance transport fluxes, i.e. diffusion and thermal conductivity. In this case the plasma equilibrium can be maintained only on average: in spite of macroscopic MHD-stability various phenomena of a collective nature may occur in plasma. They are, as a rule, very erratic and related to chaotic turbulent processes. Nevertheless, the study of instabilities even in a linear approximation is of great interest. In respect of large-scale perturbations, plasma should be stable while the studies of micro-instabilities could be a first step to the understanding of non-linear noise and turbulence.

It is reasonable to start the analysis of instabilities with large-scale MHD-modes. Tokamak plasma has two origins of instabilities, i.e. two energy sources for excitation of oscillations: the magnetic energy of plasma current and plasma thermal energy. At high pressures they start to interact with each other but at low pressure they can be studied separately. The poloidal field magnetic energy excites the

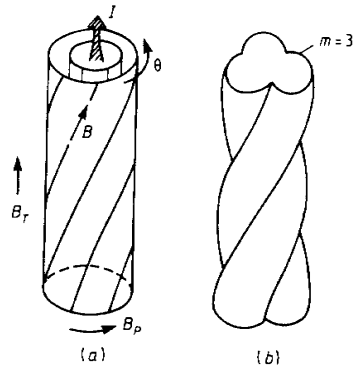

Figure 5.1 Helical perturbation of the tokamak plasma considered as a cylindrical column of length $2R$ with identical ends: (a) initial start; (b) perturbation of the $m = 3$ mode.

helical instabilities, while the thermal energy excites the flute and ballooning modes.

5.1 Kink Instability

Tokamak plasma kink instability is the most strong and dangerous. To understand its physical nature many simplifications can be used (although to describe plasma of non-circular cross section precisely, a numerical analysis should be done).

Instead of a toroidal column we will analyse a straight cylinder of length $L = 2\pi R$ with identified ends (see figure 5.1(a)). We will use a cylindrical system of coordinates r, θ and z, where the vertical z coordinate replaces $R\varphi$ in the previously used coordinate system (figure 3.7). Alongside the new z coordinate we will also use a φ coordinate. Let us superimpose a small perturbation on the cylindrical column. The perturbation should be periodic in the θ, φ angles, so that it must represent a sum of harmonics of the form $\exp(im\theta - in\varphi)$, where n and m are integer numbers. Let us call this perturbation the m/n mode. The m-number specifies the 'entry' of a helical perturbation. For example, when $m = 3$ we obtain a 'three-thread entry' screw (figure 5.1(b)). When $m = 1$ the column winds along the screw together with the magnetic axis.

The non-perturbed magnetic lines (figure 5.1(a)) are helical, so that a question naturally arises: how is the helical symmetry of magnetic lines related to helical perturbations? The magnetic lines

have $d\theta = q^{-1}d\varphi$, i.e. they correspond to the relation $q\theta - \varphi =$ constant. It follows that at the point where

$$q = m/n \tag{87}$$

the magnetic line pitch coincides with the helical perturbation pitch. In general q is a function of the radius r, so that condition (87) becomes valid at some point $r = r_s$. This point is called a resonance point, and the corresponding magnetic surface is also called a resonance, or rational point, since q is expressed as a rational fraction (87). The r_s resonance point may be located either outside or inside the plasma column. It turns out, that these two cases differ strongly. The kink instability refers to a case when $r_s > a$. If $r_s < a$, i.e. the resonance point is inside the plasma then such instability is called a tearing instability, or a tearing mode.

The kink instability was studied in detail by Shafranov [7] at the initial stage of tokamak investigations and later on it was scrupulously analysed (including the non-circular plasma) by means of numerical simulations.

5.1.1 *Reduced MHD Equations*

Theoretical description of kink modes can be performed with the help of the magnetohydrodynamic equations. For an ideal plasma, i.e. neglecting dissipative processes, these equations are:

$$m_i n \frac{d\boldsymbol{v}}{dt} + \nabla p = \frac{1}{c}\boldsymbol{j} \times \boldsymbol{B} \tag{88}$$

$$\boldsymbol{j} = \frac{c}{4\pi}\nabla \times \boldsymbol{B} \tag{89}$$

$$\operatorname{div} \boldsymbol{B} = 0 \tag{90}$$

$$\frac{\partial \boldsymbol{B}}{\partial t} = \nabla \times \boldsymbol{v} \times \boldsymbol{B} \tag{91}$$

$$\frac{\partial n}{\partial t} + \operatorname{div}(n\boldsymbol{v}) = 0. \tag{92}$$

The equations are written in the CGSE-system, using standard notation.

It turns out, that for a tokamak these equations may be simplified, using the fact that the longitudinal component of the magnetic field $B_z = B_T$ strongly exceeds the transverse component $B_\perp$- the field in $r - \theta$ plane. From the point of view of physics this simplification consists of excluding fast magnetosonic waves which cannot be excited by natural plasma motion.

The reduced equations were first proposed by Pogutse and myself in 1973 [31]. Later they were used by Rosenbluth and his coauthors [32,33], by Strauss [34] and other authors. These equations are called the reduced MHD equations. In some Russian papers they are known as the Kadomtsev–Pogutse equations while in papers by American authors, as the Strauss-equations. Later on various corrections of a higher order were introduced in the simplified equations, but still, the most clear qualitative picture of helical plasma flows, including non-linear ones, is obtained with the help of the simplest zero-approximation in the B_T^{-1} expansion. The idea of simplification is the assumption that the strong longitudinal field $B_z = B_T$ is considered as constant, and plasma is allowed to move only in the transverse direction, so that $v_z \equiv 0$. Under these assumptions the z component of equation (91) reduces to the following statement:

$$\operatorname{div} \boldsymbol{v}_\perp = 0 \tag{93}$$

and equation (90) takes a simple form

$$\operatorname{div} \boldsymbol{B}_\perp = 0. \tag{94}$$

Making a natural assumption, that all the values change slowly along the z axis, i.e. $\partial/\partial z \sim (B_\perp/B_T)\nabla_\perp$, one may carry out a strict expansion of the initial equations in inverse powers of B_T. Then equations (88) and (91) are simplified to the form

$$m_i n \frac{d\boldsymbol{v}}{dt} + \nabla_\perp P = \frac{1}{4\pi}(\boldsymbol{B} \cdot \nabla)\boldsymbol{B}_\perp \tag{95}$$

$$\frac{\partial \boldsymbol{B}_\perp}{\partial t} = \nabla \times (\boldsymbol{v} \times \boldsymbol{B}_\perp) + B_T \frac{\partial \boldsymbol{v}}{\partial z} \tag{96}$$

where P is the sum of the plasma and magnetic field pressures, and $\boldsymbol{B} \cdot \nabla = B_T \cdot \nabla_z + \boldsymbol{B}_\perp \cdot \nabla_\perp$. The equations (93)–(96) are called the reduced MHD equations.

They may be simplified even further if we assume that $n = n_0 =$ constant across the plasma column. With such an assumption we are losing some detail of plasma column evolution with time, but all the energetic part, which is essential for instability build-up and evolution of non-linear flow, is conserved.

According to (93) and (94) one can introduce two scalar functions χ and ψ

$$\boldsymbol{v}_\perp = \boldsymbol{e}_z \times \nabla\chi \qquad \boldsymbol{B}_\perp = \boldsymbol{e}_z \times \nabla\psi \tag{97}$$

where $\boldsymbol{e}_z$ is a unit vector along the vertical axis. With this new notation, equations (95) and (96) are reduced to two scalar equations

$$m_i n_0 \frac{d\Gamma}{dt} = \frac{1}{c}(\boldsymbol{B}\cdot\nabla)j \tag{98}$$

$$\frac{d\psi}{dt} - = B_0 \frac{\partial \chi}{\partial z}. \tag{99}$$

Here $d/dt = \partial/\partial t + v_\perp \nabla_\perp$, Γ is the vortex density: $\Gamma = (\nabla \times v_\perp)_z = \Delta_\perp \chi$ and j is the longitudinal current density

$$j = \frac{c}{4\pi}\Delta_\perp \psi. \tag{100}$$

The scalar equations (98) and (99) are sometimes called the Strauss equations.

5.1.2 *Linear Approximation*

To study the kink instability, equations (98) and (99) should be linearized. In the linear approximation for perturbations of the form $(-i\omega t + im\theta - in\varphi)$, they take the form

$$\omega m_i n_0 \Delta_\perp \tilde{\chi} = -\frac{B_\theta}{4\pi r}(m - nq)\Delta_\perp \tilde{\psi} + \frac{m}{rc} j' \tilde{\psi} \tag{101}$$

$$\omega \tilde{\psi} = -\frac{B_\theta}{r}(m - nq)\tilde{\chi} \tag{102}$$

where small perturbation values are marked with a ~ sign and $q = RB_\theta / rB_T$ and $j' = dj/dr$.

The case of a uniform distribution of current density, j = constant, q = constant is especially simple. Eliminating $\tilde{\chi}$, we find

$$\{\omega^2 - \omega_A^2 (m - nq)^2\}\Delta_\perp \psi = 0 \tag{103}$$

where the notation $\omega_A^2 = B_\theta^2 / 4\pi m_i n_0 r^2$ has been introduced. We have two possible solutions. With

$$\omega^2 = \omega_A^2 (m - nq)^2 \tag{104}$$

the value of $\Delta_\perp \psi$ may be arbitrary. These are the well-known Alfven waves. If ω^2 is not equal to (104), then $\Delta_\perp \psi = 0$, which entails the plasma boundary perturbation. We will consider this case in more detail.

Suppose that the plasma column is not surrounded by a conducting shell. Then we have:

$$\tilde{\psi} = \begin{cases} \tilde{\psi}_a (r/a)^m & \text{at } r < a \\ \tilde{\psi}_a (a/r)^m & \text{at } r > a \end{cases} \tag{105}$$

The χ function looks similar. We see that the $\tilde{\psi}$ derivative has a discontinuity at the boundary:

$$\Delta' = \frac{1}{\tilde{\psi}}\frac{d\tilde{\psi}}{dr}\bigg|_{a+0} - \frac{1}{\tilde{\psi}}\frac{d\tilde{\psi}}{dr}\bigg|_{a-0} = -2m/r. \tag{106}$$

The discontinuity of the derivative of the perturbed magnetic flux implies the existence of a surface current, which affects the plasma owing to its interaction with the poloidal field.

In order to find another matching condition, one should integrate equation (101) over the narrow interval, which includes the point $r = a$. Going back to the derivation of (98) from (95) one can see that one derivative on r should be placed outside density $n(r)$. That is why the equation (101) can be easily integrated over r between $a - 0$ and $a + 0$:

$$-\omega m_i n_0 \frac{m}{a}\tilde{\chi}_a = \frac{B_p m}{2\pi a^2}(m - nq)\tilde{\psi}_a - \frac{m}{2\pi} B_p \tilde{\psi}_a \tag{107}$$

where $B_p = B_\theta(r = a)$.

Eliminating χ_a from (107) by means of (102) we obtain a dispersion equation:

$$\gamma^2 = -2(m - nq)(m - 1 - nq) \tag{108}$$

where $\gamma^2 = -2\omega^2/\omega_A^2$ is the normalized growth rate of kink perturbations.

The upper row of figure 5.2(a) shows the dependence of growth rate upon nq at different values of m. As we see, for any nq there exists some m that corresponds to instability.

This unfavourable conclusion is the consequence of the simplified assumption that j_0 = constant. If the current is non-uniform and, moreover, a conducting shell is present, the situation changes for the better as is shown in the lower part of figure 5.2(b). In other words, there appear windows of stability in which tokamak should operate. These windows are present only at $q_a > 1$.

In the presence of toroidicity, neighbouring m modes are linked to each other, but the possibility of a stable state is preserved. Thus, the kink instability does not prevent stable plasma confinement, however, it has a chance to destroy plasma instantly when it is treated carelessly.

5.1.3 *Magnetic Bubbles*

The physics of kink instability can be more easily understood by considering its non-linear phase, which extends beyond the linear approximation. To do so, it is sufficient to consider a class of non-linear

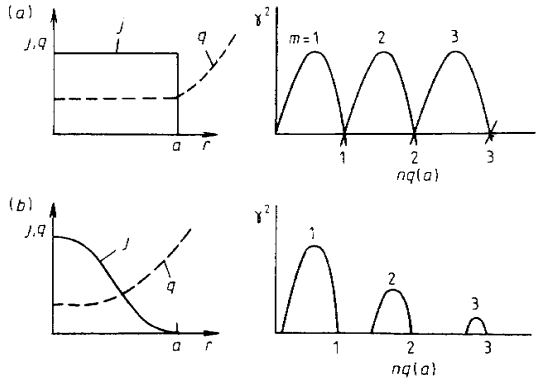

Figure 5.2 Growth rates of ideal MHD kink modes for different current density profiles: (*a*) homogeneous current density distribution; (*b*) natural current profile with decreased current density near the walls.

flows with helical symmetry when all the variables are functions of t, r, $\theta - n\varphi/m$. Thus, the derivative with respect to z in equations (95) and (96) can be replaced by $-(n/mR)\partial/\partial\theta$. It is convenient to introduce an auxiliary magnetic field

$$\boldsymbol{B}_\perp^* = \boldsymbol{B}_\perp - \frac{B_\mathrm{T}}{R} r \boldsymbol{e}_\theta \qquad (109)$$

where $\boldsymbol{e}_\theta$ is a unit vector along the minor azimuth. Equations (95) and (96) convert to a compact form in which $\boldsymbol{B}_\perp$ is simply replaced by $\boldsymbol{B}_\perp^*$, and the second component on the right-hand side of (96) disappears. Thus, we obtain truly two-dimensional equations: flows in each plane simply repeat each other rotating at an angle of $\Delta\theta = (n/m)\Delta\varphi$ when φ changes along the z axis.

The simplest one is the case when the q value is constant over the cross section and is equal to m/n. Hence, $B_\theta = rnB_\mathrm{T}/mR$ in this case so that the auxiliary field (109) is equal to zero and will remain zero. That is why magnetic field does not generate internal forces imposed on plasma: plasma motion consists of compressionless flute-type displacements which are constant along the magnetic force lines. It is clear that in this case work can be produced by the external magnetic field only. It is easy to see that the external magnetic field may form a flute on the plasma boundary and then penetrate into plasma as a bubble (figure 5.3).

In the linear approximation according to (108) we have no instability: growth rate is equal to zero at $m - nq = 0$. However, non-linear perturbation may grow in time.

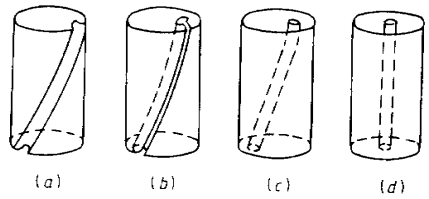

Figure 5.3 Non-linear kink instability and helical bubble injection into plasma.

The magnetic lines inside the bubble being helical initially, straighten up at later stages of plasma deformation. This means that generally this process is favourable from the energetic point of view. When the bubble is large enough, it may capture the whole poloidal magnetic field from the external region between plasma and the shell: for an external observer the plasma current will disappear. In fact it is cancelled out by the surface current in the opposite direction on the plasma edge. The helical vacuum 'snake' of figure 5.3 is free of current but its magnetic field has helical magnetic lines: the poloidal field is produced by the bulk plasma outside the bubble. In the reduced-MHD approximation the 'snake' has neutral equilibrium: any positions of figure 5.3(*c*,*d*) are energetically equivalent. While straightening the helical bubble from figure 5.3(*c*) to (*d*), the magnetic field energy inside the 'snake' diminishes but the distortion of expelled lines leads to an increase of energy. Thus the net effect results in marginal stability behaviour.

It means that the energy of plasma with a 'snake' can be calculated with the help of the axially symmetrical state of figure 5.3(*c*). We can compare this energy with initial one without a helical perturbation. If the final energy is less than the initial one the 'snake' formation is energetically favourable.

For the case $q(r) = m/n$ = constant over the plasma column the helical bubble has m-order symmetry and looks like m small circles in each cross section. The initial distribution of the poloidal magnetic field is given in figure 5.4(*a*). When the bubbles merge in a single cavity at the plasma centre a tubular configuration is produced with the poloidal field distribution of figure 5.4(*b*). The new plasma radius a_* is somewhat larger so that $a_*^2 = a^2 + r_0^2$, where r_0 is the radius of a single bubble. Magnetic field inside the plasma increases in the region $a < r < a_*$ but the external magnetic field decreases. To find the new external field value and the new plasma current we can proceed in the following way.

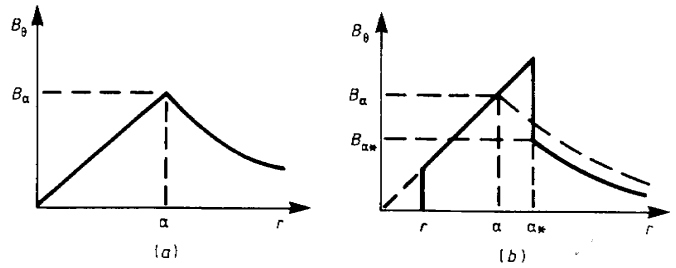

Figure 5.4 Poloidal magnetic field distribution in the initial state (a) and in the final state (b) with a single cylindrical bubble.

Let us consider a cylindrical plasma column of length $L = 2\pi Rm$. In such a column each of the m bubbles before their coalescence experiences n rotations along the minor azimuth and has identical ends, so that it can be considered as closed. If we stretch a helical membrane between the plasma edge and a conductive shell then this membrane will have the same helical symmetry as the plasma itself. The total magnetic flux through this membrane is conserved during the helical deformation of plasma because the tangential component of electric field is equal to zero both on plasma and conductive shell boundaries. With the help of this constraining condition it is not difficult to find the value of the external poloidal field and its energy. It turns out that the vacuum magnetic energy decrease is larger than the energy increase inside the plasma, which means that the bubble formation is energetically favourable.

The simple picture described above corresponds to the case when q = constant throughout the plasma. In fact the $q(r)$ safety factor is a function of the minor radius. Thus it takes the rational values $q = m/n$ at some discrete singular points. Near these points helical perturbations can develop. Such perturbations look like 'snakes' if the bubble-type entity is filled with cold plasma. Such a type of 'snake' was discovered on the JET device after pellet injection [37]. Figure 5.5 demonstrates this phenomenon which lasted for a considerable time.

Bubble formation is the simplest idealized model of a disruptive instability, i.e. a total current termination produced by helical mode disruption. The real process of disruption is accompanied by plasma turbulent oscillations, but its final state looks like a complete conversion of poloidal magnetic field energy into plasma kinetic energy and the latter is eventually transferred to the walls.

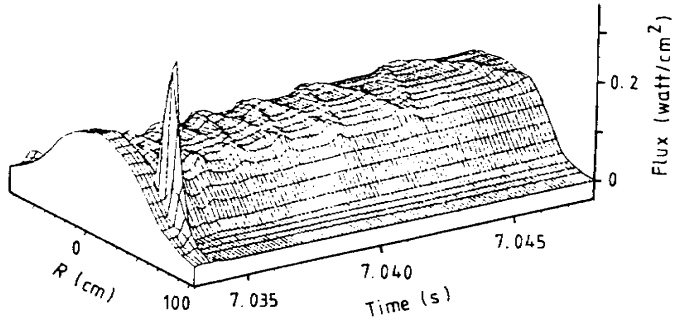

Figure 5.5 Soft x-ray (vertical camera, 140 μm thick Be filter) around the time of pellet injection showing the initial peak from ablation and the subsequent 'snake' oscillations [37].

5.2 Tearing Instability

If the rational point $q(r_s) = m/n$ is inside the plasma, then the so-called tearing instability may develop. If the plasma resistivity is not zero the tearing-instability leads to the break-up of magnetic surfaces. That is the reason why this is called a tearing instability.

A tearing mode is slow: the magnetic-surface break-up is produced by reconnection of magnetic lines due to the plasma resistivity. That is why it is much slower compared with the ideal MHD modes.

Since this process is slow, it may be described by an equilibrium equation of type (95) or (98). Let us again introduce an auxiliary field B^* and corresponding flux ψ^* by formulae similar to (97). Then the kink equilibrium condition will be of the form

$$\boldsymbol{B}^* \nabla j = (\nabla \psi^* \times \nabla j)_z = 0. \tag{110}$$

Here j may mean the value

$$j^* = (c/4\pi)\Delta_\perp \psi^* \tag{111}$$

since the difference between ψ^* and ψ according to (109) can be written as

$$\psi^* = \psi + \frac{B_T r^2}{2R}\frac{n}{m} \tag{112}$$

so that $\Delta_\perp \psi^* = \Delta_\perp \psi$ + constant. From (110) and (111) it follows that the equilibrium condition is satisfied when

$$\Delta \psi^* = F(\psi^*) \tag{113}$$

where $F(\psi^*)$ is an arbitrary function of ψ^*.

At first sight equation (113) seems to be rather simple. However, there are a number of various solutions of it, including non-trivial ones [38]. The magnetic bubbles, i.e. vacuum 'helical snakes', belong to one of the classes of such solutions. If those 'snakes' are filled with plasma, different from the bulk plasma, then they are called 'plasma snakes'. Just this 'snake' is shown in figure 5.5.

Equation (113) describes equilibria which are slightly different from a cylindrical one. They can be treated by linear approximation. Let us assume that $\psi^* = \psi_0^* + \tilde{\psi}$, where ψ_0^* is the equilibrium value, and $\tilde{\psi}$ is a small correction. The ψ_0^* function depends only on r, and $\tilde{\psi}$ depends also on $\theta - (n/m)\varphi$. The flux $\tilde{\psi}$ is small, so that equation (113) can be linearized:

$$\Delta_\perp \tilde{\psi} = \frac{\mathrm{d}F}{\mathrm{d}\psi^*}\bigg|_{\psi_0^*} \tilde{\psi} \tag{114}$$

The derivative

$$\frac{\mathrm{d}F}{\mathrm{d}\psi_*} = \frac{\mathrm{d}F}{\mathrm{d}r}\left(\frac{\mathrm{d}\psi_*}{\mathrm{d}r}\right)^{-1} = -\frac{4\pi}{c} j'(B_\theta^*)^{-1}$$

where j' is the non-perturbed current derivative with respect to the the radius r and

$$B_\theta^* = B_\theta - B_\mathrm{T} nr/mR. \tag{115}$$

It is easy to see that the equation obtained by this analysis

$$B_\theta^* \Delta_\perp \tilde{\psi} + -j'\tilde{\psi} = 0 \tag{116}$$

is the same as (101) when $\omega = 0$—a fact to be expected.

Equation (116) has a singularity at the point r_s, where $q(r_\mathrm{s}) = m/n$ and $B_\theta^* = 0$. Therefore we can assume the following. First we find a regular solution of $\tilde{\psi}_\mathrm{i}$ inside the plasma up to point r_s, then the solution of $\tilde{\psi}_\mathrm{e}$ outside r_s including the external region between plasma and the conducting shell. Using these solutions we find the value of the difference between the derivatives:

$$\Delta' = \left(\frac{1}{\tilde{\psi}_\mathrm{e}}\frac{\mathrm{d}\psi_\mathrm{e}}{\mathrm{d}r}\right)_{r_\mathrm{s}+0} - \left(\frac{1}{\tilde{\psi}_\mathrm{i}}\frac{\mathrm{d}\psi_\mathrm{i}}{\mathrm{d}r}\right)_{r_\mathrm{s}-0}. \tag{117}$$

This value is sufficient to find a stationary solution. Namely we may assume $\tilde{\psi} = \tilde{\psi}_\mathrm{i}$ at $r < r_\mathrm{s}$ and $\tilde{\psi} = \tilde{\psi}_\mathrm{e}$ at $r > r_\mathrm{s}$ when matched as $\tilde{\psi}_\mathrm{i}(r_\mathrm{s}) = \tilde{\psi}_\mathrm{e}(r_\mathrm{s})$. Hence, equation (114) will be satisfied, but the

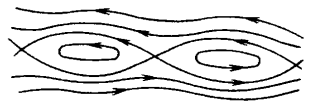

Figure 5.6 Magnetic surfaces with no island structure.

current density, i.e. $\Delta\tilde{\psi}$, has a singularity. In other words, on the rational surface a surface current j_s along the non-perturbed magnetic field is generated

$$j_\mathrm{s} = \frac{c}{4\pi}\int_{r_\mathrm{s}-0}^{r_\mathrm{s}+0} \Delta_\perp\tilde{\psi}\mathrm{d}r = \Delta'\tilde{\psi}(r_\mathrm{s}). \tag{118}$$

This solution is correct for a very small perturbation but it should be analysed in more detail for finite $\tilde{\psi}$.

To do so, let us examine the behaviour of ψ_0^* in the vicinity of point r_s. For convenience, we introduce distance from the rational surface $x = r - r_\mathrm{s}$. According to (115), in the vicinity of the rational surface we have

$$B_\theta^* = -B_\theta\frac{q'}{q}x \qquad \psi^* = \psi^*(r_\mathrm{s}) - B_\theta\frac{q'}{q}\frac{x^2}{2} \tag{119}$$

where B_θ is the poloidal magnetic field value at the point r_s and q is the derivative with respect to r. Note that $B_\theta = \mathrm{d}\psi/\mathrm{d}r$.

Let the $\tilde{\psi}$ dependence on the angle θ (in a certain cross section, $\varphi = 0$) be chosen as

$$\tilde{\psi} = \alpha\cos\theta \tag{120}$$

where the positive constant α is the amplitude of the ψ perturbation at a point r_s. Let us now examine the nature of $\psi^* =$ constant lines

$$-B_\theta\frac{q'}{q}x^2 + 2a\cos\theta = \text{constant}. \tag{121}$$

These lines are shown in figure 5.6.

We can see that the perturbation leads to rupture and splitting of the magnetic surfaces. Only outside the separatrix do magnetic surfaces form a family of nested toroidal surfaces, inside the separatrix a series of magnetic islands is formed, i.e. closed surfaces with helical structures. The separatrix corresponds to a surface, assigned by the constant on the right-hand side of (121) equal to -2α. Thus, the separatrix may be represented by the equation:

$$x^2 = 4\alpha\frac{q}{B_\theta q'}\cos^2(\theta/2). \tag{122}$$

It is seen from here, that the half-width w of the island, which is equal to the separatrix half-width at $\theta = 0$, is

$$w = \sqrt{4\alpha q / B_\theta q'}. \tag{123}$$

The island half-width increases as the square root of the perturbation amplitude.

Let us go back to the equilibrium equation $\Delta_\perp \psi = F(\psi)$. It shows that the current density should be constant on the magnetic surfaces. Therefore, the surface current is seen as the current localized on the r_s surface only by an observer situated far enough from the island. In fact this current is composed of the currents inside and outside the separatrix, but close to it. Without going into detail, let us note that an approximate solution can be found analytically. An example of such a solution will be given in Chapter 9. The equivalent surface current value for narrow islands may be considered as the perturbed current density integrated over a narrow layer with width $\sim w$.

Now let us remember that plasma has low resistivity η . To maintain a current j some longitudinal electrical field E is required. This has to be taken into account in the equation describing the magnetic field evolution, (96). For the above-defined flux function ψ^* of the auxiliary field $B^*_\perp$ the resistivity is taken into account through

$$\frac{\mathrm{d}\psi^*}{\mathrm{d}t} = \frac{\partial \psi^*}{\partial t} + (v\nabla)\psi^* = \frac{c^2}{4\pi}\eta \Delta_\perp \psi^*. \tag{124}$$

According to this equation the current density perturbation inside the island can be maintained only by a corresponding variation of $\tilde{\psi}$ with time. From (124) it is seen that, inside the island, where $\Delta_\perp \tilde{\psi} \propto \tilde{\psi}\Delta'/w$,

$$\frac{\partial \tilde{\psi}_*}{\partial t} \propto \eta \frac{c^2}{4\pi} r_s \tilde{\psi}^* \Delta'/w.$$

Since $\tilde{\psi} \sim w^2$, we have

$$\frac{\partial w}{\partial t} \sim \frac{c^2 \eta}{4\pi}\Delta'. \tag{125}$$

As we see, the island width increases linearly with time when $\Delta' > 0$ and decreases when $\Delta' < 0$. Such a regime of magnetic island evolution is called a Rutherford regime [39].

Thus, when $\Delta' > 0$ the island structure builds up in plasma. This process is called a tearing instability. When the islands become large, such an almost linear approximation is not valid. However, if one is not too rigorous, one we may use the following trick. Let us calculate

the value of Δ' by the formulae (115) not just at the point r_s, but, correspondingly, at $r_s + w$ and $r_s - w$. When Δ' determined in this way is zero, the island reaches a steady state.

Thus, according to single-fluid hydrodynamics with finite resistivity the tearing instability develops only when $\Delta' > 0$. This means that harmonics with very high m numbers are not dangerous. Indeed, when m is high then the term with j' in equation (116) for $\tilde{\psi}^*$ can be neglected, so that the solutions in the vicinity of r_s behaves as r^{+m} and r^{-m} respectively. Thus the value of $\Delta' = -2m/r_s$ and the perturbation should decay. In other words the surfaces are self-repaired in this approximation.

5.3 Flute Instability

Now let us consider instabilities which are caused by plasma pressure. The simplest one is called a convective, or flute, instability [40,41]. This instability can be clearly analysed for the case with closed magnetic lines. This analysis is similar to the analysis of plasma equilibrium in toroidal geometry.

Let the magnetic lines of the magnetic configuration be closed, and plasma pressure low, so that $\beta \ll 1$. Let us select a closed magnetic tube with plasma and assume that it is surrounded by a vacuum field. Such a tube tends to expand both in transverse and longitudinal directions, i.e. it tries to increase its volume $V = \int S \mathrm{d}l$ where S is the tube cross section. Since the flux $\Phi = SB$ along the tube is constant its value can be represented in the form $V = \Phi \int \mathrm{d}l/B$. Thus, plasma tends to increase the integral $U = \int dl/B$. In a toroidal vacuum field this integral is proportional to R^2. That is why the radial force affecting the tube can be found with the help of the relation for work $p\mathrm{d}V = VF_R \mathrm{d}R$, from which we find:

$$F_R = p(V'/V) = p(U'/U) = 2p/R. \tag{126}$$

This force is similar to the gravitational force, with the mass density replaced by pressure p. Similar to a liquid with a non-uniform density in a gravitational field, the plasma equilibrium in a pure toroidal field exists only for a stratified distribution when $p = p(R)$. If $p' > 0$, this equilibrium is stable, and if $p' < 0$, a convective instability occurs.

The physics of this instability is very simple. When some tube with plasma is shifted a distance ξ, its internal pressure $p(R)$ will differ from the plasma surrounding pressure $p(R + \xi)$ by a value $\delta p = -\xi p'$. If $p' < 0$, $\delta p > 0$, the net force taking into account the 'buoyancy force' will lead to further displacement of such a tube.

Thus the main characteristic of a magnetic trap for a low pressure plasma is pU. A plasma tube tends to expand along the direction of increasing U. Thus the 'minus U' value appears in the role of potential energy. If the function U for some magnetic configuration of a magnetic trap increases from the centre towards the periphery then this configuration has an 'average magnetic hill'. If on the contrary the function U decreases towards the trap boundaries an 'average magnetic well' is realized. It is clear that the magnetic well configuration is preferable.

Let us consider tokamak configuration from this point of view. We begin with the most simple idealization considering the straight cylinder of $L = 2\pi R$ length. In zero approximation with respect to the ratio B_θ/B_T the function U is equal to $2\pi R/B_T$ = constant, so that to find the $U(r)$ dependence we have to take into account the second-order terms in respect of the ratio B_θ/B_T.

Let us assume at first that the current density is constant so that $q = m/n$ = constant too. The length of magnetic line l is given by $l = 2\pi\sqrt{R^2 + r^2q^{-2}}$. We have to find the magnetic field value with the same accuracy. It means that we have to take into account the radial inhomogeneity of the longitudinal magnetic field. Using the radial equilibrium equation (74) for the case of low-pressure plasma and homogeneous current density distribution we find $B_T^2 = B_0^2 - 2B_\theta^2$, where B_0 is the magnetic field value at the centre. Remembering that $q = B_T r/B_\theta R$ we find $B = \sqrt{B_T^2 + B_\theta^2} = B_0\sqrt{1 - r^2/q^2R^2}$. Thus the value of U is approximately equal to $2\pi RB_0^{-1}(1 + r^2/q^2R^2)$. We see that the function U increases towards the periphery so that the straight cylinder configuration has an 'average magnetic hill'. As a result, each plasma tube is expelled in a radial direction by the force $F_r = pU'/U = 2\pi rp/q^2R^2$. This force can be again explained as a result of plasma tube expansion in a magnetic configuration with convex magnetic field lines. The curvature of the helical magnetic field line is equal to B_θ^2/rB^2. In tokamak geometry this is equal to r/q^2R^2. Thus the force F_r is again equal to the double curvature multiplied by pressure. This statement means that this force has the same value when the safety factor is not constant over the plasma cross section, but depends upon the minor radius.

This force can be taken into account in the reduced MHD equations. It is sufficient to add a term $2\pi rp/q^2R^2$ to the right-hand side of equation (95). Equations (98) and (101) have to be modified correspondingly. The model equation (98) for pure ballooning mode (driven by normal curvature only) looks like

$$m_i n_0 \frac{d\Gamma}{dt} = \frac{1}{c}(\boldsymbol{B}\cdot\nabla)j - \frac{2}{q^2R^2}\frac{dp}{d\theta} \tag{127}$$

and equation (101) takes the form

$$\omega m_i n_0 \Delta_\perp \tilde{\chi} = -\frac{B_\theta}{4\pi r}(m - nq)\Delta_\perp\tilde{\psi} + \frac{m}{rc}j'\tilde{\psi} + \frac{2m}{q^2R^2}\tilde{p}. \tag{128}$$

Here $\tilde{p}$ is the pressure perturbation, which can be found under the assumption that the plasma pressure is simply shifted together with the magnetic tube:

$$\tilde{p} = -\frac{m}{\omega r}\tilde{\chi}p' = -\frac{m}{\omega r}\tilde{\chi}\frac{dp}{dr}.$$

Marginal stability can be found using equations (101), (102) and (128) at ω=0. Excluding $\tilde{\chi}$, we obtain

$$\Delta_\perp\tilde{\psi} = \frac{4\pi m}{(m - nq)cB_\theta}j'\tilde{\psi} + \frac{8\pi m^2}{B^2(m - nq)^2 r}p'\tilde{\psi}. \tag{129}$$

As we see the last term has a very strong singularity near the singular point, where $q = m/n + q'x$, $x = r - r_s$. Thus we can neglect the first term on the right-hand side and equation (129) takes a very simple form

$$-\Delta_\perp\tilde{\psi} - \frac{\gamma}{x^2}\tilde{\psi} = 0 \tag{130}$$

where $\gamma = -8\pi p'r/B^2S^2$, $S = rq'/q$. S is known as the 'shear'. Relation (130) looks like a Schrödinger equation with the potential equal to $-\gamma/x^2$. If $\gamma > 1/4$, a solution exists with many nodes, and hence a helical perturbation can be constructed. Thus the necessary condition for stability, $\gamma < 1/4$, may be written as

$$\frac{8\pi p'r}{B^2} + \frac{1}{4}S^2 > 0. \tag{131}$$

This stability condition is known as the Suydam criterion. It takes into account the destabilizing effect of the magnetic hill and stabilization by the shear of magnetic field lines.

Now let us consider how U changes in real tokamak geometry. We start again with closed magnetic lines, when $q = m/n$ = constant. Since the poloidal field in a tokamak is considerably less than the toroidal one, the absolute value of the field is determined by the toroidal field decreasing as $1/R$ with the major radius. As for dl, it is equal to $Rd\varphi$ with the same degree of accuracy. From geometrical considerations it follows that $rd\theta/Rd\varphi = B_\theta/B$ so that $dl = Rd\varphi =$

$(Br/B_\theta)\,\mathrm{d}\theta$. But then $U = \int \mathrm{d}l/B = r\int \mathrm{d}\theta/B_\theta = r\,2\pi n\langle 1/B_\theta\rangle$, where m is the number of magnetic line rotations along the minor azimuth for m rotations along the major radius, and the value of $\langle 1/B_\theta\rangle$ averaged over θ when q = constant is approximately proportional to $1/r$. Thus, in the linear approximation with respect to the ratio B_θ/B the U-integral does not depend on r when q = constant and the magnetic tube is not affected by any force along the minor radius. In other words, this approximation leads to marginal stability and we have to take into account second-order terms.

The toroidal curvature R^{-1} is much larger than the helical line curvature r/q^2R^2 in straight geometry. In spite of the fact that the toroidal curvature has different signs on the inner and outer parts of a toroidal plasma turn, its averaged value may lead to a beneficial effect. The situation is similar to the well-known strong stabilization procedure in accelerators.

We have to take into account all the remaining approximation terms. Here two different competing effects appear. On the one hand, there is a ballooning effect, that is, the displacement on the external contour may be somewhat higher than on the internal one. On the other, the averaging of $1/B_\theta$ over the poloidal angle should be done more precisely taking into account the Shafranov shift. Plasma pressure leads to displacement of the equilibrium magnetic surfaces: they are approaching each other on the outer contour and move apart on the inner one. For this reason the factor Br/B_θ in relation $\mathrm{d}l = (Br/B_\theta)\mathrm{d}\theta$ becomes larger on the inner contour and, in its turn, increases the contribution of this region to U. As a result a specific effect of magnetic-well self-deepening arises [42].

This effect is very important for tokamaks, so that we will consider it in more detail. Remember that U was introduced as a ratio of plasma tube volume to its magnetic flux. If many tubes are arranged close to each other and fill some tubular volume between radii r and $r + \mathrm{d}r$ then we can put $\mathrm{d}V = U\mathrm{d}\Phi$. Here V is the volume of the plasma torus with minor radius r, and Φ is its longitudinal magnetic flux. Thus we can define U as $U = dV/\mathrm{d}\Phi$. If the toroidal magnetic surfaces have Shafranov shift Δ, then the distance between the neighbouring surfaces looks like $\mathrm{d}r(1+\Delta'\cos\theta)$, where $\Delta' = \mathrm{d}\Delta/\mathrm{d}r$. The major radius $R = R_0(1+\epsilon\cos\theta)$ where $\epsilon = r/R_0$; R_0 is the magnetic axis major radius. Hence the volume difference averaged over θ is $\mathrm{d}V = 4\pi^2R_0r\langle(1+\epsilon\cos\theta)(1+\Delta'\cos\theta)\rangle = 4\pi^2R_0r(1+\epsilon\Delta'/2)$. The averaged value of $\mathrm{d}\Phi$ is equal to $\mathrm{d}\Phi = 2\pi rB_0\langle(1+\epsilon\cos\theta)^{-1}(1+\Delta'\cos\theta)\rangle = 2\pi rB_0(1-\epsilon\Delta'/2+\epsilon^2/2)$. We have taken into account that the B field depends as R^{-1} on the major radius.

Taking into account the change in U with a homogeneous shift Δ due to toroidal dependence of $B \propto R^{-1}$ we obtain

$$U = \frac{2\pi R_0}{B_0}(1+\epsilon\Delta'-\epsilon^2/2+2\Delta/R_0). \tag{132}$$

The value of Δ is given by the relation (82). For a special simple case when the pressure has a parabolic distribution and the current density is homogeneous we obtain: $\Delta' = -\epsilon(\beta_\mathrm{p}+1/4)$, where $\beta_\mathrm{p} = 8\pi\langle p\rangle/B_\mathrm{p}^2$. In this case the part of U which depends on r can be written as

$$\delta U/U = -\epsilon^2(1+2\beta_\mathrm{p}). \tag{133}$$

We see that U decreases towards the periphery so that tokamak configuration has an averaged magnetic well and flute-type perturbations are stabilized even in the absence of shear.

When plasma pressure increases the magnetic well deepens, i.e. self-stabilizing effect appears. However, in parallel with magnetic-well self-deepening the ballooning effect of perturbations become larger when pressure increases. These two effects compensate each other significantly, so that the condition of stability in the quadratic approximation has the form

$$\frac{8\pi p'r}{B^2}(1-q^2)+\tfrac{1}{4}S^2 > 0 \tag{134}$$

where $p' = \mathrm{d}p/\mathrm{d}r$ and $S = (1/q)\mathrm{d}q/\mathrm{d}r$.

The local stability criterion (134) was obtained by Shafranov and Yurchenko [43]. The stability condition may also be found on the basis of the more general Mercier stability criterion [44]. Thus, when $q > 1$ and $p' < 0$ the flute instability is stabilized both by the magnetic well itself and also by shear.

5.4 The Ballooning Instability

When the plasma pressure increases and the value of $\epsilon\beta_\mathrm{p}$ is not very small the distortion of magnetic surfaces becomes so large that the simple approach with a rigid shift of circular surfaces is not valid. Correspondingly, the quadratic approximation in respect of the toroidal curvature is not justified and the higher-order terms have to be taken into account. It turns out that at the increase of plasma pressure the self-deepening of the magnetic well prevails over the ballooning effect. Plasma is self-stabilized. When this effect of plasma self-stabilization was discovered by Mikhailovskii and Shafranov [45,46] it was a great surprise for us plasma physics theoreticians. This effect is now quite well understood and may be illustrated by figure 5.7.

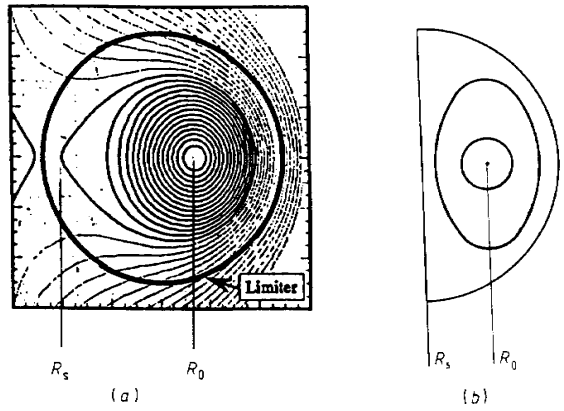

Figure 5.7 Simplified high-pressure plasma shapes: (*a*) droplet; (*b*) semicircle.

This figure shows two simplified plasma configurations at high pressure. The first one emerges more or less naturally when the plasma pressure increases inside the toroidal chamber with circular cross section. In this case the position control coils have to increase the poloidal magnetic field near the outer edge of plasma and reduce it near the inner edge. According to equilibrium condition (80) the vertical magnetic field approaches the current azimuthal field value when β_p becomes of the order of R/a. This means that at such β_p values the zero-field point can appear inside the vacuum chamber. The magnetic configuration has a separatrix with open magnetic surfaces outside the separatrix. Thus, a natural divertor configuration is produced by plasma itself. Incidentally, such a configuration has been realized in the TFTR device [47].

The second configuration, figure 5.7(*b*), is produced with the help of plasma elongation combined with triangularity. It can be imagined as a result of such positional control when only outer poloidal field coils are energized to withstand the plasma expansion along the major radius. We can imagine that plasma is heated and its pressure increases due to frozen-in magnetic field lines. All fluxes are conserved and surfaces are pushed along the major radius. Finally, only half of the circular chamber is filled by plasma.

Now we can compare the U value on the magnetic axis with the U value on the separatrix for both configurations. We have $U_0 = 2\pi R/B_0$ on the magnetic axis. As for the value of the separatrix U, it is determined by the corresponding integral along the circle

crossing all the X points, because this is the final magnetic field line of the closed surfaces. If we denote by R_s, B_s the corresponding values at the X point and take into account that $B \propto R^{-1}$, we obtain: $U_s = 2\pi R_s/B_s \simeq U_0(1+2\epsilon)$, where $\epsilon = (R_0 - R_s)/R_0$. In other words, the magnetic-well value continues to follow relation (133) even at $\epsilon\beta_p \sim 1$ when we obtain not quadratic but linear dependence of $\delta U/U$ upon toroidicity. Distortion of magnetic surfaces even helps to deepen the magnetic well.

As for plasma perturbations, they do not need to be of flute type when the plasma pressure is not low. The corresponding instability has been called 'the ballooning instability'.

The ballooning instability is closely related to plasma toroidicity. It resembles the flute instability and in a similar way it develops by means of plasma tube displacement. However, unlike the flute perturbations, the ballooning displacements of the tubes take place mainly on the outer contour of the torus. On the inner contour they seem to be fixed due to the action of magnetic well and shear.

Suppose that a certain plasma tube undergoes displacement ξ along R on the outer contour of the torus. The characteristic length of the plasma tube which is frozen in on the inner contour, is $L \sim qR$. When displacement ξ occurs the tube pressure in its new location is higher than the pressure of surrounding plasma; the difference of this value is $\delta p = -p'\xi$, where $p' = \partial p/\partial r$. Since $p' < 0$, then $\delta p > 0$ and the tube is affected by the radial force $F_R = 2\delta p/R = -2p'\xi/R$. Since the ends of the tube are frozen, the tension in the magnetic lines creates the force $F_B \simeq (B_T^2/8\pi)\xi/(qR)^2$. Equating F_R to F_B one can calculate the limiting pressure which is stable in respect of the ballooning perturbations. Since $-p' \sim p/a$, and $q \sim 5Ia/R$ we can estimate the value for the critical β: $\beta_c \sim I/10qaB$.

In addition to these local ballooning modes the global kink modes can be destabilized when plasma pressure increases. The problem is that the different helical modes with different m numbers are linked with each other in a real tokamak due to its toroidicity. When the plasma pressure increases this link becomes stronger and produces a destabilizing effect. A very rough estimation leads to the same type of dependence as for pure ballooning modes. Being more rigorous we cannot separate the kink and ballooning modes because both sources of energy, plasma pressure and poloidal magnetic field, act coherently when the plasma pressure is high enough.

The numerical calculations [48], taking into account both ballooning and kink modes, have shown that instead of the multiplier $(10q)^{-1}$, the Troyon factor g appears, which is weakly dependent on the plasma shape and on the profiles of the plasma pressure and the current density distributions

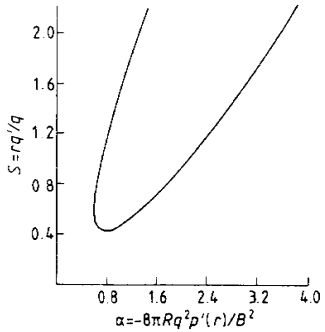

Figure 5.8 Schematic diagram for the ballooning instability region.

$$\beta_c = g\frac{I}{aB}. \tag{135}$$

The numerically calculated factor g is about 3×10^{-2}. The experimental data are in reasonable agreement with Troyon scaling but with the help of very careful plasma tailoring the g-factor can be increased.

For more optimal use of toroidal magnetic field energy it would be desirable to increase β even further. It turns out, that in principle, tokamak has such a possibility. We mean the second zone of stability which was suggested in theoretical papers [49–51]. It is based on the effects of magnetic well self-deepening and the outer connection length shortening when β increases. Figure 5.8 shows a qualitative picture of the ballooning stability region. On the abscissa axis the value $\alpha = -8\pi p'r/B^2$ is seen. When the plasma pressure is high enough one may reach the second zone of stability. Difficulty here lies in the fact that during the increase of plasma pressure one should pass through the instability zone. To diminish the instability gap between the first zone and the second, strong shaping can be used. With shaping of plasma into a D-like form with triangularity, the instability zone shrinks.

One may pass from the first zone to the second if shear S is small or even negative. Such a type of transition was studied on DIII-D [52,53], where the central core of plasma was in the second zone and its periphery in the first zone of stability. Recent experiments on DIII-D have shown that the central region can also be placed in the second zone of stability.

The maximal β value in this experiment was 11% and the central

$\beta(0)$ value defined as the central plasma pressure normalized to the vacuum toroidal field pressure at the axis reached 44%.

Figure 5.8 takes into account ideal MHD modes only. In real experiments dissipative and kinetic effects may be important. Theoretical dissipative modes analysis [54,55] has shown that they do not prevent the stability in the second zone.

Rosenbluth and others [56,154] have shown that penetration into the second zone of stability can be facilitated by use of kinetic effects: in the presence of high-energy particles their finite Larmor radius effect can help to stabilize the ballooning perturbations.

5.5 Internal Kink Mode

If $q(0) < 1$ on the magnetic axis, then according to (134) a magnetic hill should exist there. The value of the shear near the magnetic axis is small. That is why the question of the ideal $m = 1/n = 1$ mode stability arises. For an accurate theoretical description of this mode one should take into account the toroidicity of the plasma column leading to coupling of $m = 1$ and $m = 2$ modes. The relevant study was done by Bussac and co-authors [155]. They showed that the toroidal coupling of $m = 1$ and $m = 2$ modes plays a stabilizing role so that the instability can develop only when β_p is large enough. The critical β_p value depends on the current density profile and is equal to the value of the order of ~ 0.3 for a parabolic profile. In the case of very low shear the stability threshold may be reduced significantly [58] but again it depends only on the pressure gradient near the magnetic axis.

5.6 Drift Instabilities

Single-fluid magnetohydrodynamics is valid only for fast motion of plasma. To describe a class of slower oscillations, one should use either two-fluid MHD, or, which is more accurate, the Vlasov kinetic equations with self-consistent magnetic and electrical fields.

Equations of ideal two-fluid hydrodynamics are simple enough: instead of a single equation for the plasma velocity one should write two equations, for ions and electrons:

$$m_i n\frac{\mathrm{d}v}{\mathrm{d}t} + \nabla p_i = enE + \frac{en}{c}v \times B \tag{136}$$

$$\nabla p_e = -enE - \frac{en}{c}v_e \times B. \tag{137}$$

Here v is ion velocity, p_i is ion pressure, p_e is electron pressure, v_e is electron velocity, E is electric field; a term with electron inertia, being negligible, is omitted. If these equations are summed up taking into account that $p = p_i + p_e$, $j = en(v - v_e)$, we shall again obtain (88).

It is worth noting that if the surfaces of constant pressure p_e = constant and those of constant density n = constant coincide, i.e. $p_e = p_e(n_e)$, then it follows from (137) that the magnetic field is frozen into the electron component.

For tokamak plasma it is convenient to use the reduced MHD equations. For this, we assume that $B = e_z B_T + e_z \times \nabla\psi$ and consider B_T to be constant. Since $c\nabla \times E = -(\partial B/\partial t)$, we obtain

$$E = -\nabla\phi + \frac{1}{c}\frac{\partial\psi}{\partial t}e_z. \tag{138}$$

Here ϕ is the scalar potential. If this expression is substituted for E into equation (137) for electrons and then the equation is multiplied by B, we obtain

$$\frac{\partial\psi}{\partial t} - \frac{cB}{B_T}(\nabla\phi - \frac{1}{en}\nabla p_e) = 0. \tag{139}$$

The electron temperature T_e may be considered to be constant along the magnetic lines, i.e. $B \cdot \nabla T_e = 0$. Therefore, equation (139) may be written as

$$\frac{\partial\psi}{\partial t} + [e_z \times \nabla\lambda] \cdot \nabla\psi = B_T\frac{\partial\lambda}{\partial z} \tag{140}$$

where

$$\lambda = \frac{c}{B_T}(\phi - \frac{T}{e}\ln n). \tag{141}$$

Now let us return to (136). In this equation the components on the right-hand side are larger than those on the left-hand side. Therefore approximately,

$$v_\perp = \frac{cE \times e_z}{B_T} = \frac{c}{B_T}e_z \times \nabla\phi. \tag{142}$$

Comparing this expression with (97) we find

$$\chi = \frac{c}{B_T}\phi. \tag{143}$$

Equations (140) and (142) together with equation (98) for the vorticity $\Gamma = \Delta_\perp\chi$ replace equations (98) and (99) of single-fluid hydrodynamics. The continuity equation should be added to them

$$\frac{\partial n}{\partial t} = -v \cdot \nabla n = -\frac{c}{B_T}(e_z \times \nabla\phi) \cdot \nabla n. \tag{144}$$

The new system of equations (98), (140) and (143) is more complicated than the two equations (98) and (99). For the special case of fast plasma motion the component with inertia in (98) is of importance. The potential ϕ in the expression (141) for λ is large, so that, approximately, $\lambda \simeq c\phi/B_T = \chi$. In this approximation the reduced MHD equations for a single-fluid and two fluids coincide.

New effects appear for a class of slow motions, when the inertia component in (136) may be neglected. For helical symmetry one may again introduce an auxiliary field $B_\perp^*$ and corresponding flux function, so that the solution of (98) is again

$$\Delta_\perp\psi^* = F(\psi^*). \tag{145}$$

In other words, we have come back to the tearing modes.

Suppose that the tearing modes are stabilized and the magnetic surfaces coincide with the initial nested toroidal surfaces: $\psi = \psi(r)$. Then it follows from (140) that λ is constant along the magnetic field lines. It means that a non-singular λ function is equal to $\lambda(r)$.

Now let us consider small perturbations of ϕ and n, so that $\phi = \phi_0(r) + \tilde{\phi}$, $n = n_0(r) + \tilde{n}$. Since λ depends only on r, it follows from (141) that

$$\tilde{\phi} = \frac{T_e}{e}\frac{\tilde{n}}{n_0} \tag{146}$$

and the linearized continuity equation (144) gives

$$\frac{\partial\tilde{n}}{\partial t} + \frac{c}{B_T}\frac{d\phi_0}{dr}\frac{1}{r}\frac{\partial\tilde{n}}{\partial\theta} = \frac{cT_e}{eB_T}\frac{dn_0}{dr}\frac{1}{r}\frac{\partial\tilde{n}}{\partial\theta}. \tag{147}$$

The second term on the left describes the electrical drift in the ϕ field. In the frame of reference which rotates in the azimuthal direction with the velocity of the electrical drift, this term disappears. Then for perturbations of the form $\exp(-i\omega t + im\theta - in\varphi)$, we obtain from (147) a dispersion equation for the frequency:

$$\omega = \omega^* \equiv \frac{cT_e}{eB_T}\frac{m}{r}\kappa \tag{148}$$

where

$$\kappa = -\frac{1}{n_0}\frac{\mathrm{d}n_0}{\mathrm{d}r}. \tag{149}$$

The expression (148) is the well-known drift frequency. The corresponding wave perturbation $\tilde{\phi}$, $\tilde{n}$ is called the drift wave. Let us notice some of its specific features. Let us find the electron drift velocity when $\boldsymbol{E} = 0$, $B_\perp \ll B_\mathrm{T}$:

$$v_{e\theta} = -\frac{c}{enB_\mathrm{T}}\frac{\mathrm{d}p_\mathrm{e}}{\mathrm{d}r}. \tag{150}$$

The plasma pressure gradient usually has the same direction as the density gradient, so that the drift wave propagates in the direction of the electron drift (150). Since the frequency ω^* is low enough, the question arises whether we could really neglect the ion longitudinal velocity $v_\mathrm{i} = \sqrt{T_\mathrm{i}/m_\mathrm{i}}$ as compared with the phase velocities. To find the longitudinal phase velocity one has to find first the longitudinal component of the wave number $k_\parallel = -(1/B)\left((m/r)B_\theta - (n/r)B_\mathrm{T}\right)$. We see that $k_\parallel = (m/r)(B_\theta/B_\mathrm{T})(1-(n/m)q(r))$. At a point r_s where $q = m/n$, $k_\parallel$ is zero, i.e. the phase velocity is infinite and hence our approximation is obviously fulfilled.

In the vicinity of the point r_s one may put $r = r_\mathrm{s} + x$, so that the expression for $k_\parallel$ takes the form

$$k_\parallel = -\frac{m}{r^2}\frac{B_\theta}{B_\mathrm{T}}Sx \tag{151}$$

where $S = (r/q)\,\mathrm{d}q/\mathrm{d}r$.

We see that the condition $\omega^* > k_\parallel v_\mathrm{i}$ is fulfilled only within the interval

$$x < \frac{\kappa r}{S}\frac{cT_\mathrm{e}}{eB_\theta v_\mathrm{i}}. \tag{152}$$

As an order of magnitude, the right-hand side is equal to $\rho_{i\theta}$, that is, to the ion Larmor radius in the poloidal magnetic field. Beyond this interval a drift wave damps rapidly due to the ion Landau-damping.

Thus, drift waves in tokamaks look like strongly r-localized perturbations which propagate azimuthally in the direction of the electron drift with the phase velocity about the same value. The main relation (146) is a result of the electron equilibrium along the magnetic field. Since the magnetic line fills all irrational magnetic surfaces, this condition is fulfilled along any direction on such a surface, but then it follows from (137) that the component of electron velocity normal to the magnetic surface, turns out to be zero. In drift waves electrons

simply move along the magnetic lines without crossing magnetic surfaces. On the contrary, ions move across the surfaces, but in such a way that the total flux through the magnetic surface is equal to zero in order to ensure plasma quasi-neutrality.

Thus, in the frame of ideal two-fluid magnetohydrodynamics, drift waves do not lead to any transport across magnetic surfaces.

It turns out that, when taking into account dissipation, drift waves may become unstable: a small imaginary component is added to frequency ω^* and such a growth rate corresponds to the drift-wave instability.

There are many mechanisms of drift-wave instabilities [155]. Let me indicate the best known. In a rarefied plasma the drift waves are destabilized by collisional transitions of trapped electrons into untrapped and vice versa: this mode is called a drift mode on trapped electrons.

If the ion temperature gradient is high enough, i.e. $\eta_\mathrm{i} = \mathrm{d}\ln T_\mathrm{i}/\mathrm{d}\ln n > 1$, the ion drift-temperature instability may develop. On the plasma edge, where the temperature is low and the role of dissipation grows, the instability on the resistivity gradient may build up. In the literature from Russia this instability is called a current-convective mode, and in English it is called a rippling mode. In addition to tearing modes discussed above the so-called microtearing modes can be unstable. These modes are sensitive to drift effects and have to be studied with the help of kinetic equations.

Drift-wave instabilities and drift-wave turbulence constitute a specific broad area of tokamak plasma physics. Many theoretical and experimental papers deal with this topic. Drift waves are definitely important for tokamak plasma especially in its periphery, but I would prefer to pass over this important branch of tokamak physics. On the one hand, it has not yet reached a state of maturity, and on the other hand, to discuss it thoroughly we could deviate from the most interesting plasma feature—its self-organization.

6 Plasma as a Complex System

High-temperature plasma, confined by a magnetic field, is an exceptionally unusual physical object. To begin with, it is an open dissipative system permanently supplied by a source of external energy in a rather orderly form. This energy dissipates in the plasma converting it into thermal energy. Then it diffuses slowly to the cold walls. While reaching the walls, the thermal flux releases a lot of entropy accumulated by intensive production of entropy in plasma itself.

Similar to other dissipative open systems of this type, non-linear phenomena build up in plasma, enhancing energy and entropy fluxes through the system. In a magnetized plasma these processes become especially multi-various due to the presence of long-distance forces. One should speak rather of a self-consistent system of particles and fields, than of an ensemble of charged particles immersed in the field.

Let us consider a simplified picture of tokamak cross section (figure 6.1). The plasma is maintained in a state of high temperature equilibrium with the help of an external power source. In the simplified version this power is launched into the central core of plasma. Then it is transported towards the walls in the form of a thermal flux. The wall temperature is definitely less than 0.1 electronvolts, i.e. 10^3 K, while the plasma core temperature has to be not less than 10^4 electronvolts. Thus we have at least 10^5 for the ratio of these temperatures. It means that the entropy related to a given portion of energy is a factor 10 higher inside the walls as compared with the entropy at the plasma core. In other words, energy transport is accompanied by entropy production with a large multiplication factor.

We consider first the hot plasma core. Of course, we could imagine the completely quiet plasma state when the collision transport dominate. This is, so to speak, a purely theoretical ideal. All the transport fluxes in this case have to follow the neoclassical theory

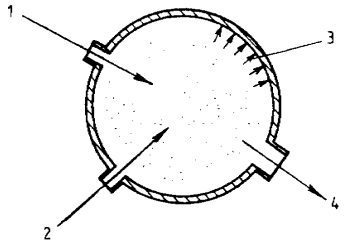

Figure 6.1 Tokamak plasma as an open dissipative complex system. External power (1) is launched inside the high temperature plasma core and then this power is transported to the room-temperature walls (3). With the pellet injection (2) the plasma flows towards the exhaust pumps (4). This flow refreshes the plasma and together with the energy flux maintains its 'life'.

which establishes the low limit for transport. The fluxes would be very low and plasma confinement extremely good.

However, this most quiet plasma state does not withstand invasion of many different non-linear cooperative agitations, which lead to amplification of the transport fluxes and hence to the increase of the rate of entropy production. The agitations can intercept some portion of the initial order and energy flux to maintain their own activity. If this activity embraces all the plasma core we can state that some coherent pattern develops which destroys the initial axial symmetry and produces something like global convection. This is a fully non-linear macroscopic instability.

On the other hand, there is local entropy production everywhere inside the plasma. This entropy generation is the by-product of the local plasma transport. We have local dissipation everywhere. This dissipation diminishes the order of energy and some local structures may appear. They amplify this dissipation to maintain their steady-state average level. Such structures can enhance the rate of local entropy production by increasing the transport fluxes feeding the structures themselves. This picture looks like anomalous transport.

Finally we have the possibility when both types of non-linear patterns can be present: some local turbulence may coexist with the coherent macroscopic modes. They can be linked with each other and then the long-range interaction between the different parts of the plasma column may lead to feedback coupling of the local transport coefficients and profiles. This phenomenon is called profile con-

sistency.

Now let us consider the edge plasma. Here again we have thermal and particle fluxes with a very large difference in temperatures of plasma and walls. This means that many non-linear phenomena can be present here. In practice it means that the edge plasma looks like a source of noise with a very high level. This noise can propagate inside the plasma core leading to transport enhancement.

The heating itself can be a source of additional noise generation. The most harmless is ohmic heating, when power is softly launched into the central plasma core with a smooth profile. The current density in tokamak plasmas is of the order of 1 MA m^{-2}. Therefore at a plasma density of the order of $10^{20}\,m^{-3}$ the drift current velocity of electrons is of the order of $10^5 m\,s^{-1}$ which is much less than the sound velocity. That is why the current itself cannot play a significant role in plasma noise generation, but different auxiliary heatings can serve as additional sources of noise. Neutral beams for instance produce a high energy tail in the distribution function and this non-equilibrium can lead to the so-called 'fish-bone' instability. There is some concern that similar phenomena can be present when the fusion reactor plasma is heated by alpha-particles. Thus the tokamak plasma represents a very complicated state of matter.

In fact, each laboratory or natural plasma is a complex physical system. The high-temperature tokamak plasma is even more sophisticated, in particular because Coulomb collisions are very rare and the classical channel of dissipation by means of collisions becomes insignificant.

A rational approach to study complex systems consists of a large number of experiments aimed at understanding empirical laws supported by development of a theoretical description and computer models. All this is actively used in modern tokamak studies. As experience with other complex systems shows, the general method of scaling and dimensional approach represents a powerful tool for their description.

6.1 Dimensional Approach

Methods of dimensional approach and similarity in physics are often closely related to each other. In order not to depart from the physics of ionized gases, we shall illustrate the major ideas of this approach by a simple example of gas flow in a tube.

Let us assume that in a long tube of radius a, gas with a mean velocity u flows under the influence of a constant pressure gradient. In actual gas-pipe lines the pressure gradient is maintained by inter-

mediate stations with gas blowers but this is not important in our case, and we are going to consider a constant pressure gradient ∇p. Practical engineers are interested in the dependence of velocity upon the pressure gradient, or, to be more precise, the pressure gradient dependence of the flux Φ, i.e. the amount of gas flowing per unit time. The function $\Phi = \Phi(\nabla p)$ can be found theoretically. However, this is a simple task for Poiseuille laminar flow only. For more interesting turbulent flows accurate methods of calculation are still absent. But this fact does not bother engineer-hydrologists, since reliable empirical laws exist which can be applied to tubes of any diameter by means of scaling relations.

Let us consider the way it is done. We assume that the gas consists of atoms or molecules of mass m and density n, at temperature T. Thus, together with tube radius, mean velocity and pressure gradient we have six parameters. The size of atoms is another feature which may be described by σ_c, the mean cross section for collisions. Thus, we have seven parameters in total. Therefore, if we want to find the $\Phi = \Phi(\nabla p)$ dependence we have to take into account five other parameters, i.e. the problem becomes rather complicated. Nevertheless we can be helped by a dimensional method.

It is known, that all the laws of physics are based on mechanics, and mechanics itself uses conventionally chosen units for mass, length and time. It is clear, that the objective laws of nature cannot depend on those units: these laws are invariant with respect to variations of measurement units chosen by man. This invariance is seen more precisely when non-dimensional combinations of dimensional values are used. Therefore, all the objective laws of physics may be presented as relations between non-dimensional parameters.

Only four non-dimensional combinations can be constructed from the available seven dimensional values in the gas pipeline case. Therefore, in the expression $\Phi = \Phi(\nabla p)$, which can be written in a non-dimensional form thereby coupling two dimensional parameters, only three extra parameters remain. In other words, we obtain a three-parameter family with which it is not difficult to fit experiments and to find empirical data for any combination of parameters.

Thus, let us form non-dimensional parameters, only four of which are independent. Selection of non-dimensional parameters is often a matter of opinion, and therefore, a certain physical judgment has to be involved. For instance, a mean velocity could be quite naturally combined with a pressure gradient

$$mnu^2/a \mid \nabla p \mid = F^2 \tag{153}$$

where F^2 is simply a notation for the left-hand side. The quantity mn is equal to the gas mass density ρ, and relation (153) may be

considered as an expression for the mean velocity

$$u = F(a \mid \nabla p \mid /\rho)^{1/2}. \tag{154}$$

Here F is a non-dimensional factor which is a function of the other three non-dimensional parameters. Let us consider other parameters which have a reasonable physical meaning. To begin with, let us form a non-dimensional combination $N = n\sigma_c^{3/2}$. This represents a characteristic of gas rarefaction, if $N \ll 1$ the gas is ideal from a thermodynamical point of view. As we see, the number N can be considered as an internal parameter. It is proportional to n and is in no way related to other non-dimensional parameters. If the 'rare gas' criterion is fulfilled then N drops out of the group of significant non-dimensional parameters. But it is still too early to say definitely that σ_c is of no importance: N may be multiplied by a large number and, therefore, to reach a proper judgment we should consider some other parameters as well.

Let us take into consideration the sound velocity which is proportional to the mean thermal velocity of atoms: $c_s = \sqrt{\gamma T/m}$, where γ is the adiabatic index. The ratio $M = u/c_s$ is non-dimensional and is called the Mach number. If $M \ll 1$, then the flow is definitely subsonic.

In order to conclude our consideration of non-dimensional parameters let us introduce $K = a/\sigma_c^{1/2}$, a number which is proportional to the ratio of tube radius to atom size. It is evident that for macroscopic flows $K \gg 1$, but, nevertheless, such a non-dimensional parameter does exist. It is easy to see that the numbers N, M and K do not depend on each other.

In addition to K and N, one may introduce another purely geometrical parameter $\Lambda = NK = n\sigma_c a$, which is equal to the ratio of the tube radius to the mean free path $\lambda = 1/n\sigma_c$. All the above-mentioned non-dimensional parameters have definite physical meaning and indicate regions of specific gas behaviour. The most interesting is the region of parameters where gas is rarefied, $N \ll 1$ and the tube is wide, i.e. $K \gg 1$. The product Λ of these two parameters may be either greater or less than unity. If $\Lambda \ll 1$, then we have Knudsen flow at a deep vacuum. Ordinary gas at pressures of the order of atmospheric pressure correspond to $\Lambda \gg 1$. Now let us compile another non-dimensional combination which is called the Reynolds number:

$$Re = \frac{una\sigma_c}{c_s}. \tag{155}$$

The Reynolds number (155) is equal to the product $M\Lambda$: it may vary over a broad range of values.

Experiments show that sub-sonic ($M \ll 1$) flow characteristics of the rarefied gas ($N \ll 1$) with low viscosity ($\Lambda = NK \gg 1$) depend only on the Reynolds number. In other words, $N, \Lambda = NK, M$, respectively, seem to drop out and only the Reynolds number is relevant. If so, we can set both M and Λ^{-1} to zero and only the Re parameter is variable.

Thus, in expression (154) the non-dimensional factor F depends only on Re. This means that similar gas flows may exist. Even without the gas changing, and thus assuming that $n\sigma_c/c_s$ is constant, a family of similar flows can be imagined with ua = constant and therefore with the same Re value.

After measuring the function $F(Re)$ in the experiment, we can evaluate a mean velocity with the help of (154) and, consequently, find the total flux Φ for any gas flow.

It is worth noting, that all similar flows with the same value of Re have similar profiles for the mean velocity distribution over the radius, since there are no other parameters which could affect the profile variations. Moreover, all the turbulence characteristics can be scaled keeping the Re number the same.

If we introduce one other parameter, namely, the tube roughness, i.e. the ratio of the roughness δ to the tube radius, then the factor F will depend on δ/a. At high Re numbers F ceases to depend on Re and depends on δ/a only, i.e. again only one parameter is relevant.

Similar considerations may be applied to other, more complex flows in gas hydrodynamics.

Let us simply note that dimensional analysis should always be based on reasonable physical parameters which are specific for each particular case. Such an approach can allow us to pick out the most relevant parameters and to drop the unimportant ones.

6.2 Dimensional Analysis of Tokamaks

Tokamak plasma is a more complex object than gas turbulent flow. Nevertheless, dimensional analysis [59–61] can also be used here.

Let us first consider an idealized case. Let plasma of circular cross section with major radius R and minor radius a be maintained in a steady-state by means of purely ohmic heating. Plasma has a mean density n, and we assume that mean electron and ion temperatures are equal, i.e. $T_e = T_i = T$.

Suppose that there are no impurities and there is a single-component plasma. Let I be plasma current, B_p the poloidal magnetic field at the plasma boundary, B_T, the toroidal magnetic field, m_e, the electron mass, m_i, the ion mass and c, the velocity of light.

Let us assume for a while, that atomic processes are not important i.e. radiation is low enough, and neutrals do not penetrate deep into plasma, so that 'the mantle' of partially ionized edge plasma is thin compared with a. Thus we can assume that recycling of particles takes place in a very thin layer as compared with the main plasma core. Under these conditions one can expect the existence of self-similar self-organized plasma states, if they have the same macroscopic non-dimensional parameters. When compiling these parameters one should be guided by physical arguments.

First let us write down all the dimensional parameters

$$a,\ R,\ B_{\mathrm{T}},\ B_{\mathrm{p}},\ m_{\mathrm{e}},\ m_{\mathrm{i}},\ e,\ c,\ n,\ T. \tag{156}$$

Here n and T are the mean values of density and temperature (in any sense of averaging). The velocity of light has appeared here since we are using CGSE units.

Thus, we have ten dimensional values. One may construct seven non-dimensional parameters with them. First let us write either the well-known, or rather obvious values

$$\begin{aligned} &A = R/a \qquad q_a = aB_{\mathrm{T}}/RB_{\mathrm{p}} \qquad m_{\mathrm{e}}/m_{\mathrm{i}} \\ &\beta = 8\pi p/B_{\mathrm{T}}^2 = 16\pi nT/B_{\mathrm{T}}^2. \end{aligned} \tag{157}$$

The parameter $m_{\mathrm{e}}/m_{\mathrm{i}}$ for pure deuterium plasma may be taken as constant. The range of the change in the aspect ratio, $A = R/a$, is usually not very large. The values of q_a and, β are very important and have a definite physical meaning. They have a somewhat larger range of variation.

Thus we have indicated four parameters (157) and we have to find another three. Similarly to gas flow, they could be: a parameter for 'ideal plasma' behaviour in a thermodynamic sense, the ratio of size to characteristic internal plasma length, and the dissipation parameter which contains collision frequency. When constructing these parameters one should imagine a fully ionized hot plasma.

The 'ideal plasma' parameter is a number N_{D} which is equal to the number of particles in a Debye sphere. If $N_{\mathrm{D}} \gg 1$, the plasma may be considered as ideal in a thermodynamic sense: the potential energy of the Coulomb interaction of particles turns out to be much less than their kinetic energy of thermal motion.

Omitting a numerical coefficient we have

$$N_{\mathrm{D}} = n(T/e^2n)^{3/2}. \tag{158}$$

As an internal characteristic length, let us accept the value

$$\Lambda = c/\omega_{\mathrm{pe}} = \sqrt{m_{\mathrm{e}}c^2/4\pi e^2 n}. \tag{159}$$

Then for a non-dimensional size parameter we can accept the number

$$\Pi = a^2/\Lambda^2 = 4\pi n a^2 r_0 \tag{160}$$

where $r_0 = e^2/m_{\mathrm{e}}c^2$ is the classical electron radius.

To characterize plasma dissipation one may use a non-dimensional collision frequency. Neoclassical theory involves a non-dimensional effective collision frequency $\nu*$

$$\nu^* = \left(\frac{R}{r}\right)^{3/2} qR/\lambda. \tag{161}$$

Here λ is the mean free path length for Coulomb collisions.

In (161) the quantities $q = q(r)$ and $\lambda = \lambda(r)$ are local, and related to a given radius r. For the global characteristics of the plasma column we will use some averaged value $\bar{\nu}*$.

As is known, the mean free path for Coulomb collisions depends strongly on the temperature, $\lambda \sim T^2/n$. This fact will be taken into account later on. Note, that the mean free paths for ions λ_{i}, and electrons λ_{e}, differ slightly from each other by a numerical factor. We will neglect this difference for a while. Thus, a full set of non-dimensional parameters for tokamak plasma of circular cross section looks as follows

$$A = R/a,\ q_a,\ m_{\mathrm{e}}/m_{\mathrm{i}},\ \beta,\ N_{\mathrm{D}},\ \Pi,\ \bar{\nu}^*. \tag{162}$$

It is easy to check that all seven parameters are independent of each other.

Let us also note, that it is possible to construct one other geometrical parameter which, at first sight, might play a certain role in the physics of tokamaks. This is the cross section of plasma, expressed in Larmor radii:

$$K = a^2/\rho_{\mathrm{i}}^2 = a^2e^2B_{\mathrm{T}}/2Tm_{\mathrm{i}}c^2. \tag{163}$$

Here $\rho_{\mathrm{i}} = v_{\mathrm{i}}/\omega_{\mathrm{ci}}$ is the ion Larmor radius, $v_{\mathrm{i}} = \sqrt{2T_{\mathrm{i}}/m_{\mathrm{i}}}$ is the mean thermal velocity, $\omega_{\mathrm{ci}} = eB/m_{\mathrm{i}}c$ is the ion-cyclotron frequency. The parameter in (163) is similar to the above-mentioned K parameter for a rarefied gas. It can be expressed as $K = 2m_{\mathrm{e}}\Pi/m_{\mathrm{i}}\beta$ using the parameters introduced in (162). For my part, I do not feel that the parameter K plays any role in tokamak plasma physics. Usually K^{-1} is very small and can be omitted from the set of important parameters.

The non-dimensional parameters define the internal physics of a complex system. They are indicators of the fundamental state of

such a system. As for dimensional parameters, they look like some projection of a given system on the external world. Being immersed in the external physical world, each complex system can possess a non-unique set of dimensional parameters. In other words, for a given set of dimensionless parameters the family of systems can exist with different sets of dimensional parameters. This phenomenon is called self-similarity. For instance, at a given Reynolds number for gas flow in a pipe-line only the product au is fixed, so that a one-parameter family of similar flows exists with the same au value.

In plasma three-dimensional parameters, namely, m_e, e and c are fundamental constants of nature. Hence only seven parameters out of the ten (158) are really variable. That is why if we fix all the parameters (162) the dimensional parameters will be fixed, and plasma will have no freedom for similarity. However, if some of the parameters drop out, then families of similar discharges exist, in which only the parameters left over are fixed. This approach is conveniently used when comparing ideal theoretical models with experiment [60].

The set (162) itself suggests variants of idealization aimed at a diminishing number of relevant parameters. It is obvious that the number N_D cannot be included in the set of important parameters: high-temperature plasma is ideal from the thermodynamical point of view, so that $N_D^{-1} \to 0$. Therefore, there is at least a single-parameter family of similar tokamaks. Examining the full set of independent parameters (162) we can imagine other idealizations when some of these parameters are not important. For instance, we can assume that collisions are not relevant when a very hot plasma is at hand. In the case of collisionless plasma $\bar{\nu}^* \to 0$, a family of similar tokamaks becomes double-parametric. Another assumption is related to the case when the plasma pressure is very low and β is extremely small. If we put $\beta \to 0$, one other free parameter of similarity enters.

However, both of these assumptions are of a rather abstruse character and may be interesting mainly for theoreticians. In any case collisions are definitely important for ohmic heating, which relates to collisional dissipation, while β is not an independent parameter but enters as a result of interplay between the heating and energy losses.

Hence the most natural assumption is $N_D^{-1} \to 0$. Note that N_D is also contained in the argument of the Coulomb logarithm but the latter is such a weak function of N_D that it can be considered as a constant. If N_D is dropped out of the set (162) then a one-parameter family of similar tokamaks has to exist.

Let us fix all the parameters in (162) except for N_D. Then one of the dimensional parameters is left free. It can be chosen as we

like. Let it be the magnetic field B. Because for given A and q_a the dimensionless parameters scale as

$$\beta \propto nT/B^2 \qquad \text{II} \propto na^2 \qquad \nu^* \propto an/T^2 \tag{164}$$

the dimensional values allow the following scaling

$$a \propto B^{-4/5} \qquad n \propto B^{8/5} \qquad T \propto B^{2/5}. \tag{165}$$

It is easy to check that the quantities in (164) are not changed when the scaling (165) is fulfilled.

The dimensionless parameters (162) look like internal characteristics of plasma. When atomic processes are not important these parameters and only these are responsible for the features of all phenomena in plasma. The physics of plasma with the same parameters is the same too. For the external observer there exists a one-parameter family (165) which represents the concrete realization of such a plasma.

Note, that according to (165) the plasma current $I \propto aB \propto a^{-1/4}$. In other words, the product $Ia^{1/4}$ can be considered as the main parameter of this family. This value labels the family of self-similar tokamaks. To a rough approximation the current is the most important plasma parameter for distinguishing tokamaks from each other.

The self-similar tokamaks are geometrically similar and have the same ratio of size to the internal parameters of length. The similarity inside the one family is also true of other physical values. In particular, this statement relates to the energy-confinement time. The product $\tau_E \omega_B$ is dimensionless so that the value $B\tau_E$ depends on the dimensionless parameters only. Instead of the $\tau_E \omega_B$ combination we could relate τ_E to the transit time, or to the Bohm confinement time. But all such combinations convert again to $B\tau_E$ if the similarity condition (165) is valid.

Thus according to (164) there are three dimensionless combinations. But the temperature is not an independent variable; it is controlled by the balance of ohmic heating power and transport losses. Hence, according to (165), we have only two independent combinations

$$Ba^{5/4} \qquad nB^{-8/5}. \tag{166}$$

$B\tau_E$ is dependent upon them. If we take, for instance, the family of similar tokamaks with $Ba^{5/4} =$ constant then the value of $B\tau_E$ is the function of a single parameter: $B\tau_E = F(nB^{-1.6})$

An experimental discussion of this statement will be given in section 8.3. If auxiliary heating is used in addition to ohmic heating then another dimensionless parameter P/P_{OH} appears where P is

the total heating power and P_{OH} is the ohmic heating power prior to additional heating. We will see later how this parameter can be used in the dimensionless approach.

6.3 Murakami and Hugill Numbers

Let us consider now atomic processes. This means that we involve an additional parameter $\hbar$, namely, Planck's constant. Correspondingly, we can construct a new non-dimensional parameter. It is known that dimensionless parameters can be constructed with the help of atomic constants alone. The combination $\gamma = e^2/\hbar c$, the fine structure constant, is dimensionless and equal to approximately 1/137. Of course this number does not help very much in application to plasma physics problems. To obtain a more convenient expression for the appropriate parameter we should consider the corresponding physical background again.

For convenience we may introduce atomic units for length, velocity and energy

$$r_a = \frac{\hbar^2}{m_e e^2} \qquad v_a = \frac{e^2}{\hbar} \qquad \epsilon_a = \frac{m_e e^4}{\hbar^2}. \tag{167}$$

To evaluate the role of atomic processes we should compare appropriate power losses with Joule heating power. It is much easier to proceed with the help of the following 'Gedanken experiment'. Let us assume that we have a plasma with a temperature of the order of $T \sim \epsilon_a$. At this temperature the plasma looks like a mixture of ionized and non-ionized gases. Let us assume that the density of both gases is of the same order of magnitude and is about $\bar{n}$, i.e. about the average plasma density in a tokamak. Now let us compare ohmic heating power with power losses produced by atomic processes.

Heating power per unit volume P_{OH} apparently is equal to ηj^2, where j is current density and η is electrical resistivity. The average current density is proportional to $cB_T/q_a R$, where c is the velocity of light (here we use again CGSE units). Electrical resistivity can be evaluated as

$$\eta = \frac{m_e \nu_{ei}}{e^2 n} = \frac{L\hbar^3}{m_e e^4} F(T_*) \tag{168}$$

where ν_{ei} is the electron–ion collision frequency, $T_* = T/\epsilon_a$ is the non-dimensional temperature, F is a factor of the order of unity at $T_* \sim 1$ and decreasing as $T_*^{-3/2}$ at higher temperatures. In (168) we emphasized the factor $L \sim 10$: it is the Coulomb logarithm which takes into account the long-range character of Coulomb collisions.

Thus, the average power of ohmic heating may be expressed as

$$P_{OH} = \frac{c^2 B_T^2}{q_a^2 R^2} \frac{L\hbar^3}{m_e e^4} F(T_*). \tag{169}$$

As for losses due to radiation and ionization, they can be written as

$$P_R = n^2 r_a^2 v_a \epsilon_a G(T_*) = n^2 \frac{e^2 \hbar}{m_e} G(T_*). \tag{170}$$

As can be seen, P_R increases as the square of the density and if P_R becomes comparable to P_{OH}, then atomic processes start to a play significant role. That is why as a characteristic of this role we may accept the quantity P_R/P_{OH} which can be expressed as:

$$P_R/P_{OH} = H^2 G(T_*)/F(T_*) \tag{171}$$

where

$$H = \frac{e\gamma n q_a R}{B_T \sqrt{L}} \tag{172}$$

$\gamma = e^2/\hbar c \simeq 1/137$ and L is a number of the order of 10.

In expression (171) G/F is of the order of unity at $T_* \sim 1$. Both functions G and F decrease with temperature, so that very roughly the right-hand side in expression (171) may be considered as a constant independent of T_*.

Thus, the role of atomic processes in a tokamak is defined by a non-dimensional parameter H which we call the Hugill number. If we put L equal to 12.3, H will have the following numerical value:

$$H = n q_a R / B_T \tag{173}$$

where the average density n is measured in units of $10^{20}\,\mathrm{m}^{-3}$, R in metres and B_T in tesla.

In addition to the Hugill number, the so-called Murakami number [62] is used

$$M = nR/B_T. \tag{174}$$

It is expressed in the same units. M is used for plotting the Hugill diagram (figure 3.9). We should note, that the straight rays from the origin of the coordinates on the Hugill plot of figure 3.9 correspond to the lines of constant H: $I/I_c = 1/q_a = M/H$. As is seen from (171), increasing the Hugill number, the role of the atomic processes also increases compared with ohmic heating. Radiation on the periphery of plasma may affect the current density profile and cause degradation of plasma confinement. That is the most important mechanism

that leads to the Hugill density limit [63], which corresponds to the critical value of $H_c \approx$ constant.

This density limit may also be expressed in the form of the Greenwald criterion [64], $\bar{n}_c =$ constant $\times j_s$, where j_s is the current density averaged over the plasma cross section. The Murakami limit, $n \sim B_T/R$, corresponds to the absolute density limit at the maximal permissible plasma current.

If in addition to ohmic heating some auxiliary heating is used then returning to (171), one may easily see that both density limits increase approximately as $n \sim \sqrt{P}$, where P is the total heating power.

The low-density limit on the Hugill plot (see line 1 in figure 3.9) can also be expressed in terms of the Hugill number. This limit relates to electron run-away at low density when the current electron velocity j/en approaches the thermal velocity $v_e = \sqrt{2T/m_e}$. The ratio j/env_e is approximately equal to $\sqrt{L/T_*}H^{-1}$. Here T_* is the dimensionless electron temperature expressed in atomic units. At temperatures of the order of several keV the value of j/env_e is of the order of $0.1H^{-1}$, so that strong electron run-away begins when the Hugill number decreases below a few tenths of unity.

6.4 Dimensional Analysis of Energy Confinement

The mechanisms of energy losses from tokamak plasma are rather complicated not only because there are several channels of energy leakage, but also due to the fact that major channels, namely electron and ion thermal conductivities, are usually anomalous, i.e. highly exceeding neoclassical values. Nevertheless, even in this case, one may try to apply methods of dimensional analysis in order to find out the main non-dimensional parameters which control transport. Although such an approach cannot replace real theory it can help to shed light upon the most important physical mechanisms of transport.

To be more precise, let us first try to consider empirical scalings for τ_E on the basis of dimensional analysis. To begin with, let us use the Hugill diagram once more so that even our starting point would be bound to the non-dimensional parameters. From a practical point of view, the most interesting region of plasma parameters is that of high densities and currents. Figures 6.2 and 6.3 show two examples of successfully attaining high densities, in JET by using beryllium coating of the chamber walls and in JT-60 with the help of pellet injection. It can be seen that the experimental points are inside the region of $q_{cyl} = q_{eff} > 2$ and $H < 3$. Experimental points of other

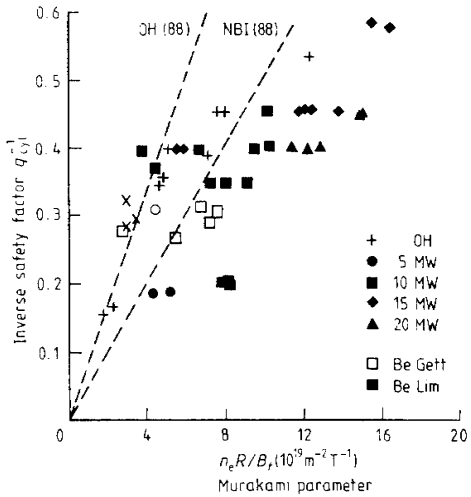

Figure 6.2 Hugill plot for JET with beryllium coating of vessel walls (1989) [102].

tokamaks are usually deep inside the limits of this region except in some cases when very low values of q were attained [19].

Let us emphasize once more that high densities here and later on are meant in the sense of a non-dimensional Murakami parameter. For instance, high absolute values of density in high-field tokamaks (ALCATOR, FT) do not have the same high values of Murakami parameter, as shown in figures 6.2 and 6.3.

For a discussion of scalings we begin with ohmic heating discharges. When the densities are not high enough so-called neo-ALCATOR scaling is valid

$$\tau_E = 7 \times 10^{-2} naR^2 q_a. \tag{175}$$

Scaling expressed in such a way has wrong dimensionality. The right-hand side of this equation is non-dimensional, but should have dimesions of time. In order to restore the dimensionality of (175) let us express it in the following way:

$$\tau_E = 0.4 \frac{\Lambda^{-2}}{v_0} aR^2 q_a \tag{176}$$

where $\Lambda^{-2} = 4\pi e^2 \bar{n}/m_e c^2$, $v_0 = 2 \times 10^7\,\mathrm{m\,s^{-1}}$.

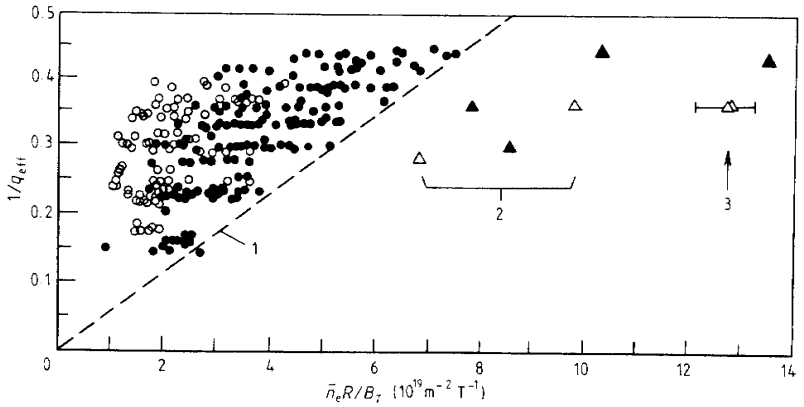

Figure 6.3 Operation region (Hugill plot) for JT-60 with pellet injection: 1—gas puffing; 2—minor pellets; 3—large pellets. Full circles—limiter, open circles—divertor [103, 147].

The quantity v_0 is the mean thermal velocity of electrons at 1 keV temperature, i.e. $v_e = v_0\sqrt{T}$, where T is expressed in keV. Thus, the ALCATOR scaling can be considered as a simplified empirical version of a more regular relation of type (176) with v_0 replaced by v_e, i.e. having a slightly unfavourable dependence on temperature. One should note that such dependence was clearly demonstrated by the T-11 device [15].

Neo-ALCATOR scaling with linear dependence upon density is valid only up to some critical density n_s above which a saturation and sometimes even slight decrease of τ_E with density is observed. The critical density value n_s at which the transition from one dependence to another occurs is given by the Shimomura relation [26]

$$n_s \simeq B_T\sqrt{A_i/2}/q_a R. \tag{177}$$

It means, that the transition line corresponds to the Hugill number $H_s = \sqrt{A_i/2}$, as shown in figure 6.4. Above the critical density the energy confinement time may be considered as neo-ALCATOR at $\bar{n} = n_s$, i.e.

$$\tau_E = 7 \times 10^{-2} a R B_T \sqrt{A_i/2}. \tag{178}$$

This statement does not affect the Frascati tokamak (FT) results [65] which will be discussed somewhat later.

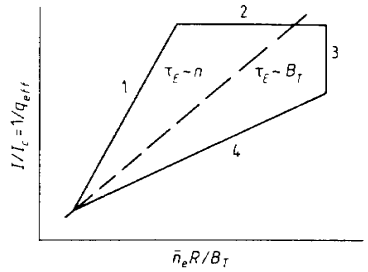

Figure 6.4 Boundary of the ALCATOR scaling on the Hugill diagram (broken line).

The question may arise as to whether the critical density value relates to ballooning instability. To answer it, we have to examine where the Troyon limit is situated on the Hugill plane. It is convenient to express β not in terms of average pressure but in terms of chord average of density and central temperature. To do so we choose some standard profiles for density and temperature: $T = T_0(1 - r^2/a^2)$, $n = n_0(1 - r^2/a^2)$. Then with $g = 2.8$ we can express the Troyon limit in the form

$$H_c = 7aB_T/T_0 \tag{179}$$

where T_0 is expressed in keV and H_c is the Hugill number at $\beta = \beta_c$.

We immediately see that at a fixed value of aB_T/T_0 the ballooning limit corresponds to H = constant. This line changes together with temperature and enters the $H < 3$ region only at high enough temperatures, so that the limit by ballooning modes is not relevant to the transition line $H_s = \sqrt{A_i/2}$ from linear to saturation dependence on density. In other words, the energy confinement time saturation with density is not related to ballooning modes (this is obvious directly from the experiments).

Let us consider now energy confinement scaling with auxiliary heating. It is convenient to start from the Goldston scaling

$$\tau_E = 3.7 \times 10^{-2} I R^{1.75} a^{-0.37} K^{0.5} P^{-0.5} (A_i/1.5)^{0.5}. \tag{180}$$

Here we use again MA, metres and MW units. The factor with A_i takes into account the isotope effect reflecting the fact that the original scaling was based on experiments with H and D mixture, $A_i = 1.5$.

Not to complicate matters, let us restrict ourselves to circular plasma, $K = 1$, and assume $A_i = 2$ (the case of deuterium). Moreover, as soon as we are not seeking for accuracy but looking for

parametric clarity let us round off the power indexes, so that, for dimensional analysis we accept a very simple dependence

$$\tau_E \simeq 6 \times 10^{-2} I R^{1.5} a^{-0.5} P^{-0.5} \tag{181}$$

which approximately agrees with (180) for large-size facilities. Taking into account that $P = W_T/\tau_E$ where $W_T = 2\pi^2 a^2 R\langle 3nT\rangle$ is the total thermal energy of plasma, then, squaring (181) and eliminating P we get the following simple relation

$$\tau_E \simeq 7 \times 10^{-2} \frac{R^2}{a\beta_p}. \tag{182}$$

Here $\beta_p = 16\pi\langle nT\rangle/B_p^2$ and $B_p = I/5a$.

The right-hand side of (182) again does not have proper dimensionality. We may proceed in the same way as we did with neo-ALCATOR scaling. Namely, let us express it as follows

$$\tau_E = 1.4 \times 10^6 \frac{R^2}{c_0 a\beta_p}. \tag{183}$$

Transition from neo-ALCATOR scaling (176) to additional heating scaling (183) occurs at

$$\Lambda^2 < 3 \times 10^{-7} a^2 \beta_p q_a. \tag{184}$$

Let us introduce into our consideration an average Larmor electron radius in the poloidal magnetic field B_p: $\rho_\theta = \sqrt{2Tm_e c^2/e^2 B_p^2}$.

This expression may be written as: $\rho_\theta = \Lambda\sqrt{\beta_p/2}$, where $\beta_p/2$ is the electron component in β_p. Equation (184) may be rewritten at $q \approx 4$ as

$$\Lambda < 4 \times 10^{-2} \sqrt{a\rho_\theta}.$$

In other words, when Λ diminishes the confinement gets poorer.

Now let us return to empirical scalings (175) and (182). The condition of transition from neo-ALCATOR scaling to L-mode scaling with additional heating, as we see, may be expressed as

$$\bar{n} a^2 \beta_p q_a > 1 \tag{185}$$

where $\bar{n}$ is expressed again in $10^{20}\,\mathrm{m}^{-3}$. This is a different version of (184).

Finally, we can find one other approximate relation for the point of transition from neo-ALCATOR to L-mode scaling. For this, let us take into account loop voltage, which in tokamaks is usually of the order of one volt. Thus, the ohmic heating power is proportional to the current. In such a rough approximation relation (181) can be written for ohmic heating as

$$\tau_E' = 6 \times 10^{-2} I^{0.5} R^{1.5} a^{-0.5} \tag{186}$$

where the prime denotes that τ_E' does not depend on density. This relation leads to another variant for transition from linear τ_E dependence of saturation density. Scaling (186) is relevant when the corresponding τ_E' value is less than that of (178), i.e. at

$$aB_T > \sqrt{IR/aA_i}. \tag{187}$$

This condition is fulfilled in facilities with ohmically heated plasmas at high magnetic field values. For instance, Goldston scaling (180) i.e. the more precise version of L-mode scaling, explains quite satisfactorily the FT experimental data with ohmic heating [65].

Now we can summarize the results of our considerations. Transition from linear ALCATOR scaling to saturation in plasmas with ohmic heating occurs at a fixed Hugill number. One may suppose that this transition relates to approaching the critical Hugill boundary, i.e. it is related to atomic processes. These processes may modify the current distribution profile to a less favourable one and may enhance transport.

When heating power is increased the Hugill limit shifts towards higher densities. The transition point from linear dependence upon saturation density will be shifted with power increase to lower density values, because the L-mode energy confinement time decreases with power. In large facilities which satisfy condition (187), the region of saturation of density corresponds to auxiliary heating scaling even with ohmic heating alone. That is why in large machines a neo-ALCATOR scaling is valid only at low densities so that Goldston scaling (with its modifications) should be considered as the basic one.

One more conclusion can be made on the basis of empirical data, namely that dissipation is not so important and $\bar{\nu}*$ can be omitted from the number of parameters responsible for transport. This does not mean that dissipation is definitely of no importance at all. The situation here is rather similar to gas flow in rough tubes at very high Reynolds number values, i.e. dissipation is not seen explicitly but is important for non-linear small-scale patterns.

One more remark. Simplified expressions (176) and (183) contain either macroscopic or electron parameters. This suggests that a major channel of energy losses could be the electron channel whereas

the ion channel adjusts to it unless the ion transport lowers down to the neoclassical value. Then why does Goldston scaling contain $(A_i)^{1/2}$? Some light is shed by the relation $n_s \sim (A_i)^{1/2}$ for the critical density of transition from linear τ_E^{OH} dependence on saturation. As soon as n_s corresponds to some fixed Hugill number and seems to be related to the processes at the plasma edge, the presence of the factor $(A_i)^{1/2}$ in scaling may be related to plasma edge phenomena. The lighter ions are, the more violently they move in turbulent fluctuations at the periphery and, in turn, more intensively excite the plasma core. The experimental data of ISX-B (where plasma confinement was improved by heavy impurity influx from the walls) support this point of view. Thus the edge plasma may be an essential character in tokamak transport phenomena. We will see in section 9.3 that mechanisms with ion mass dependence may exist even inside the bulk plasma.

7 Non-linear Plasma Activity

Tokamak plasma lives a very complicated life: many collective processes spontaneously develop and persist in it. Some of these processes are of a clearly obvious, regular nature and could be observed directly by means of different diagnostics. Others, like anomalous thermal conductivity, indicate the existence of some perturbations in plasma. Sometimes corresponding noise can be measured directly, for example, by means of electron density fluctuations. Below we will describe major types of non-linear activity both macroscopic, related to the MHD-perturbations, and kinetic, related to electron and ion non-equilibrium distribution functions.

The present chapter covers mainly regular processes in plasma.

7.1 Mirnov Oscillations

Mirnov and Semenov having installed a series of small magnetic probes in the T-3 tokamak, measured for the first time external magnetic oscillations [66]. Correlation analysis allowed them to identify m and n numbers of helical perturbations. That was the beginning of tearing mode investigations.

The most intensive tearing-mode build up is indicated at the initial phase of the discharge when the factor $q(a)$ at the plasma boundary increases monotonically with time. They look like perturbation bursts with different numbers $m \sim q(a)$. Each such burst is accompanied by energy loss from plasma, and even by local current disruption at the plasma periphery [67].

Such oscillation bursts can be described theoretically [68], as the result of a tearing-mode development when $q(r)$ dependence is non-monotonic. The bursts during current rise may be suppressed or even eliminated by gas puffing which creates more stable current density profiles.

Tearing modes may exist also in the steady-state phase of a discharge: a weak instability plays the role of supervisor which controls

the current distribution profile near its marginal shape. Internal tearing modes, as a rule, propagate azimuthally in the direction of electron drift. This is quite a natural feature, since the magnetic surfaces are frozen into electrons. Sometimes the tearing modes slow down or even stop completely—such modes are called locked modes. The presence of such a mode may be dangerous: a magnetic island formed in plasma ceases to feel the stabilizing role of the conducting chamber and may easily develop to large sizes; and large islands lead to disruptive instability.

7.2 Saw-tooth Oscillations

Saw-tooth oscillations were discovered in the ST facility by Von Goeler *et al* [69]. It was observed that in a stable phase of the discharge the central temperature experienced periodic oscillations of relaxation type. Since then saw-tooth oscillations have been registered in practically all tokamaks. This is a very important type of plasma non-linear activity not only because it noticeably decreases the plasma thermal insulation in large facilities but also because it is the key to understanding a more drastic phenomenon—the disruptive instability.

The process itself consists of periodically repeated phases of slow temperature rise at the centre of the plasma column with subsequent fast drop. Shortly before each temperature drop, oscillation-precursors are observed. They appear to be $m = 1$ mode. When temperature drops at the centre the temperature profile flattens, so that the temperature decreases inside some radius r_s and increases directly beyond this radius. The r_s radius is called the inversion radius.

After a drastic phase of temperature drop in the $r < r_s$ region, and increase beyond this region, a thermal wave propagates from the central region to the plasma periphery. This wave is often used for electron thermal conductivity measurements. The temperature profile flattening during saw-tooth oscillations in T-10 is shown in figure 7.1 where the normalized values of temperature and radius r_s are plotted. The sharp flattening of the temperature profile is called internal disruption.

A simple model of internal disruption was proposed by Kadomtsev [70]. This model is based on the fact that prior to the disruption the value $q(0)$ abates below unity everywhere inside the r_s radius corresponding to $q(r_s) = 1$. Here the development of $m/n = 1/1$ internal mode is possible. To describe this mode one may use the reduced MHD equations. The auxiliary transverse field $B_* = B_\theta - (r/R)B_T$ has

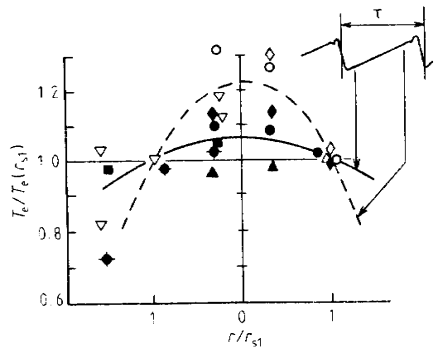

Figure 7.1 Electron-temperature-profile flattening at an internal disruption.

different signs on both sides of radius r_s, as shown in figure 7.2(a). If the plasma column inside r_s is perturbed according to the helical $m = 1, n = 1$ mode then in each cross section this perturbation looks like a simple displacement. As is seen in figure 7.2(b), a current layer with oppositely directed magnetic fields is formed. Due to finite conductivity in the ab current layer (figure 7.2(b)) the magnetic lines reconnect. As a result of this reconnection a moon-like island A is formed (figure 5.5(c)),which pushes the plasma column core outward. Thus, reconnection cannot be stopped unless the cylindrical symmetry of the magnetic surfaces is completely restored, as shown in figure 7.2(d). Now B_* has the same polarity everywhere, i.e. $q > 1$. But as a result, a cooler plasma occurs at the centre whereas a hotter one forms at the periphery. Thus, r_s radius indeed is an inversion radius. After each internal disruption a much slower phase of initial state restoration takes place. The central plasma region is heated up, part of the current penetrates into it, the $q(0)$ value drops again lower than unity, and the column becomes prepared for a new internal disruption.

This simple model explains the main effect—the relaxation nature of the oscillations with a slow phase of temperature increase at the centre and a subsequent phase of temperature-profile fast flattening. The reconnection of the magnetic field lines may be described by the Sweet–Parker model [71, 72]. Let us consider the current layer scaled up to larger size (figure 7.3). Its width is of the order of r_s, and thickness δ is determined by the magnetic field diffusion rate. As the field diffuses into plasma and magnetic lines reconnect, plasma is extracted from the layer. A kind of 'catapult' of strained magnetic

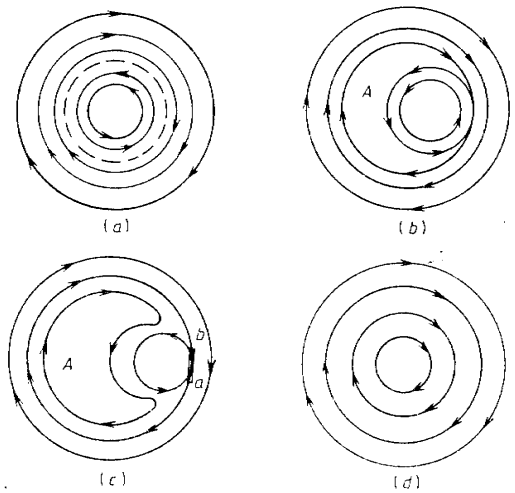

Figure 7.2 Process of reconnections on auxiliary transverse magnetic field B^*: (a) direction of magnetic lines relative to the surface with $B^* = 0$; (b) contact of surfaces with oppositely directed fields B^*; (c) reconnection of the current layer ab due to finite plasma conductivity; (d) final result of reconnections: auxiliary magnetic field is unidirectional.

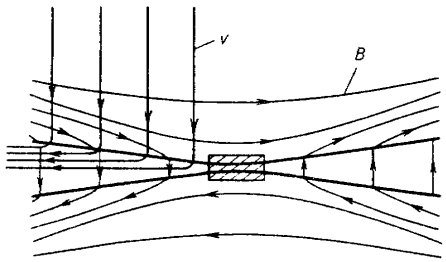

Figure 7.3 Plasma expulsion along the layer during reconnection.

lines is formed, which throws out the plasma from the layer into the moon-like region A of the magnetic island (figure 7.2(b)). An estimation of the reconnection rate can be be made in the following way.

Let Δt be the time taken for a layer renewal, i.e. the time taken to expel the plasma from the layer by magnetic lines. This time is of the order of $\Delta t \sim r_s/c_A^*$, where c_A^* is the Alfven velocity corresponding to the auxiliary magnetic field. During this time the magnetic lines diffuse a depth δ. Since $\delta^2 \sim c^2/4\pi(\eta\Delta t)$, where η is resistivity, we obtain

$$\delta \sim \left(\frac{c^2}{4\pi}\eta\frac{r_s}{c_A^*}\right)^{1/2}.$$

Now we can find the time of complete reconnection $\tau \sim r_s\Delta t/\delta$.

$$\tau \sim (\tau_A\tau_R)^{1/2} \tag{188}$$

where $\tau_A = c_A^*/r_s$, $\tau_R = 4\pi r_s^2/c^2\eta$.

A comparison of this simple model of laminar reconnection with experiment has shown that it describes the main features of the phenomenon quite satisfactorily. However, the accumulation of experimental data had indicated a great variety of possible forms of reconnection, which entailed the necessity of model improvement and, in some aspects, its serious modification.

To simulate numerically a 'saw-tooth' one should describe its two phases: the phase of slow profile restoration with $q(0) < 1$ and the phase of fast temperature flattening. To describe the first phase the neoclassical resistivity has to be taken into account. The fact is that only the transit particles contribute to the electron electrical conductivity so that electron trapping leads to a decrease of the density of current carriers. As a result, the resistivity is modified $\eta \cong \eta_{cl}(1 - 2\sqrt{\epsilon})^{-1}$, where η_{cl} is the classical Spitzer resistivity, $\epsilon = r/R$, and the multiplier in brackets takes into account the electron-trapping effect. Due to toroidal correction, the stationary temperature profile tends to sharpen: even for a flat temperature profile the resistivity at $\epsilon = 0$ is lower than that at some distance from the magnetic axis. The phase of current density restoration lasts for the resistivity time τ_R. If one assumes that r_s is proportional to R one may obtain [73], a very simple semi-empirical scaling for the period of saw-tooth oscillations

$$\tau_{ST} \simeq 10^{-2}R^2T_e^{3/2}/Z_{eff}. \tag{189}$$

Here R is the major radius in metres, T_e is the electron temperature in keV, Z_{eff} is the effective ion charge, τ_{ST} is in seconds. There are some other more accurate scalings for τ_{ST} [74], but (189) is the simplest one.

The second phase is the phase of the sharp temperature profile flattening i.e. an internal disruption. Three questions arise: what is

the trigger of the internal disruption (i.e. type of instability), how does the disruption develop and what is the time of disruption?

To discuss these questions one should turn back to the simplest model of complete reconnection and consider the simplifications made. In the framework of the reduced MHD-equations there is no ground for the initial instability: the internal $m = 1/n = 1$ snake is in neutral equilibrium until the process of reconnection starts. In some cases instability can be triggered when β_p inside radius r_s exceeds a certain critical value [59].

The real process of reconnection may substantially differ from the ideal picture of a quiet evolution of the 'moon-like' island descibed above. The fact is that every force tube 'catapulting' into A may drastically perturb plasma and create MHD-turbulence. If a turbulent zone is formed in region A then the B_* mean value may disappear due to mixing of magnetic lines. Then there is no force that would 'press' the internal core to the magnetic surface with the inverse magnetic field. In this case a partial reconnection can take place. Such 'saw-teeth' with incomplete reconnection were observed in TFR (Tokamak Fontenáy aux-Roses) and were interpreted by the authors [75] as a result of the development of MHD turbulence in the vicinity of the x point.

Further on, the stochasticity of the magnetic lines may appear due to the toroidicity which violates the ideal helical symmetry [76]. Both types of stochasticity may change significantly the resistivity value inside the current layer. If after crossing the current layer each electron does not return back to the same point, then, instead of a normal skin-layer, an anomalous skin-layer can develop. In this case in the expression for classical $m_e\nu_e/ne^2$ resistivity the electron collision frequency of ν_e should be replaced by an anomalous value i.e. by the characteristic inverse time of an electron single transit along a magnetic line of length qR with thermal velocity $v_e = \sqrt{2T/m_e}$ [77]. The replacement of ν_e by its anomalous value significantly increases the reconnection rate and makes it close to the observed one at the fastest internal disruptions.

A broad series of experiments on the study of saw-tooth oscillations was done in the T-10 facility [78]. A great deal of information has been obtained in experiments on large facilities [79,80]

7.3 Disruption Instability

The disruption instability was discovered in the earliest phase of experiments in tokamaks [8,10]. The first observations had shown major characteristics of this phenomenon: negative spike on the

Table 7.1 Comparative characteristics of different types of disruption.

Types of disruption	Saw-tooth	Minor disruption	Major disruption
$V(t)$	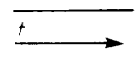	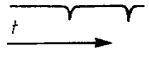	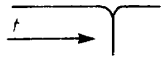
Voltage ΔV	—	−1−−10	−10−−500 V
$X(t)$			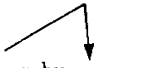
Soft x-ray ΔX	~ 10%	~ 20–80%	Drop by several times
$\Delta T_e(0)$	~ 10%	~ 20–50%	~90%
Δn_e	~ 1–4%	~ 10%	~ 30%
$\tilde{B}_\theta/B_\theta$	—	< 4%	~ 15–20%
m	1,0	(3),2,1,(0)	(3),2,1,0,3,4

loop voltage, positive current derivative and drastic decrease of the plasma major radius. They all indicate a sharp broadening of the current-carrying zone accompanied by partial release of the poloidal flux from plasma. The disruption is accompanied by strong MHD-oscillations and plasma energy loss. The disruption instability may lead to total plasma collapse; such a disruption is called a major disruption. Alongside this there are minor disruptions: partial loss of energy from plasma which may be repeated without total destruction of the column. Both minor and major disruptions together with internal disruption in saw-tooth oscillations represent similar phenomena but on a different scale. This is easily seen from table 7.1 where the comparative characteristics of these three types of disruption are shown [67].

Major disruptions are most dangerous. In a quiet discharge phase the disruptions develop while approaching the operating limits. Correspondingly, the disruptions may develop at the

— density limit,
— q_a limit,
— β limit.

The disruptions may also be initiated by careless handling of plasma:

— by a fast density rise,
— by a fast current rise, often while a locked mode is growing

— by changing the geometry from a limiter to the divertor with a separatrix;
— as a result of a large 'saw-tooth', especially at low q_a;
— by a mode activity localized at the plasma edge.

In addition, the disruptions may be initiated by casual circumstances, for instance, penetration into plasma of a fragment from the first wall etc.

Scenarios of disruptions are more or less similar varying with different factors of plasma destabilization.

In large tokamaks disruptions at the density limit go through four different phases

1. Constriction of a current channel due to radiation losses;
2. MHD-precursor, such as kink modes growth, particularly $m = 2/n = 1$ mode; sometimes this mode slows down with the frequency decrease, then it stops completely and forms a locked mode
3. Drastic energy loss—is a real disruption but at this stage the plasma can still be restored. If different modes, particularly $m = 1$, develop further, then MHD-activity affects all the column and a major disruption becomes unavoidable.
4. Current decay—it begins with current-profile flattening accompanied by a plasma current hump and negative loop voltage, then the current decays due to impurity influx and plasma cooling.

As a typical example, figure 7.4 displays the energy and current decay in JET. As we see, the energy quench is very fast—less than one millisecond. One can distinguish two phases of the quench.

Disruptions of other types (not at the density limit) have similar scenarios, but the MHD-precursor may be shorter in time.

The intimate cause of disruption is related to the ability of the poloidal magnetic field to release energy. If the plasma column shrinks and the $q(r) = 2$ surface becomes located outside the hot plasma boundary then a non-linear tearing mode may develop. Roughly speaking, a double-threaded helical bubble appears near the hot plasma boundary. This bubble tends to penetrate inside the plasma core and to tear it in two parts. Additional excitation of other modes which accompanies this process and leads to current-density profile flattening simply enhances the situation.

Another approach to describe the same phenomenon is based on the Taylor relaxation model (see section 9.2). This model was suggested for the reversed field pinch. It presumes reconnection of free magnetic lines in the plasma that can lead to energy relaxation constrained by the helicity conservation law. As a matter of fact the tokamak plasma is immersed in a very strong magnetic field which does not allow for the reconnection of free magnetic lines. However,

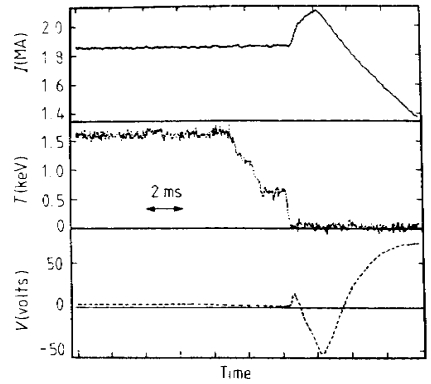

Figure 7.4 Current decay and the temperature quench during disruption in the JET tokamak [102].

when many modes are excited, i.e. during the disruption, such a possibility appears.

Applied to a tokamak plasma with $B_T \gg B_p$ the Taylor theory leads to a homogeneous current-density distribution which is most undesirable from the point of view of kink modes. Once it appears, this state is maintain by the Taylor mechanism until complete decay of plasma current. Thus, a major disruption looks like a total confusion of reconnections, whereas a minor one leaves untouched the magnetic structure of the central part of the column. In both cases regions with chaotic behaviour of magnetic lines appear which lead to an enormous electron thermal conductivity. Very high heat losses from plasma to the walls are produced.

Disruption in large tokamaks is a kind of modest accident: a large amount of energy is released to the walls. In addition to the thermal impact, the chamber experiences a mechanical impact due to electric currents flowing from plasma. Together with the toroidal magnetic field these currents create quite appreciable ampere forces.

In principle, the probability of disruptions can be reduced but, as a rule, this is a specific problem for each device.

7.4 Fan Instability

If fast particles are produced in tokamak plasma, both electrons and ions, then kinetic instabilities can develop. One of the first

kinetic instabilities discovered in the experiments [81] was called a fan instability. It is produced by run-away electrons i.e. electrons which cannot be stopped by Coulomb collisions and pass into a free acceleration regime. This effect is related to the fact that the cross section of Coulomb collisions decreases with the energy of the particle beam ϵ_b as ϵ_b^{-2}.

A considerable number of run-away electrons may appear when the electron energy acquired in a collision-free path represents a considerable fraction of thermal energy. Numerically, this condition may be expressed as $E < 0.1E_D$, where the value of the critical field

$$E_D = \gamma_D T_e / e\lambda_e \tag{190}$$

has been called the Dreicer field, γ_D is the numerical coefficient, λ_e is the electron mean free path.

Run-away electrons may appear near the left-side limit on the Hugill diagram (figure 3.9), and also at the initial stage of the discharge when the loop voltage is high enough. Run-away electrons are injected more violently by disruptions when local bursts of current density may appear. A major disruption further intensifies the rate of production of run-away electrons: the plasma temperature decreases and the electric field in plasma grows as $E \sim \eta \sim T_e^{-3/2}$, whereas the Dreicer field diminishes.

When many run-away electrons appear they may excite oscillations due to the so-called anomalous Doppler effect [82]. For excitation of waves the following resonance condition has to be fulfilled

$$\omega - k_\parallel v_\parallel = +\omega_{ce} \qquad \text{or} \qquad \omega - k_\parallel v_\parallel = -\omega_{ce} \tag{191}$$

where ω is the wave frequency, $k_\parallel$ is the projection of the wave vector on the direction of the magnetic field, $\omega_{ce} = eB/m_e c$ is the electron-cyclotron frequency.

The frequency $\omega' = \omega - k_\parallel v_\parallel$ is equal to the Doppler shifted frequency of the plane wave $\exp(-i\omega + ikr)$, which is seen by the electron in its moving frame of reference. When ω' coincides with the cyclotron frequency the resonance condition is fulfilled. The first relation (191) corresponds to the normal resonance and the second one to the anomalous Doppler effect.

To see the difference between these two cases it is convenient to use quantum-mechanics language. Let the electron emit just one quantum with energy $\hbar\omega$ and longitudinal momentum $\hbar k_\parallel$. Then the electron energy change is equal to

$$\delta\mathcal{E} = \delta\mathcal{E}_\parallel + \delta\mathcal{E}_\perp = -\hbar\omega. \tag{192}$$

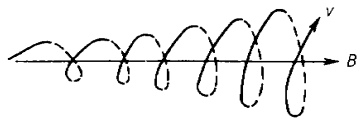

Figure 7.5 Conversion of longitudinal energy into transverse energy for a fan instability.

Due to momentum conservation the longitudinal energy change is equal to $\delta\mathcal{E}_\parallel = m_\parallel v_\parallel \delta v_\parallel = -v_\parallel \hbar k_\parallel$. Thus we have for the transverse energy change

$$\delta\mathcal{E}_\perp = -\hbar(\omega - k_\parallel v_\parallel). \tag{193}$$

For the case of the normal Doppler effect we have the usual picture where the emission of quanta leads to diminishing of the transverse energy, whereas for the anomalous Doppler effect just the opposite happens. Namely, the electron increases its transverse energy while radiating the electron-cyclotron wave in the anomalous Doppler effect.

The phase velocity $v_\varphi = \omega/k_\parallel$ of such a wave, as seen from (191), is less than the electron velocity. That is why the wave seems to have a negative energy in the electron frame of reference: an electron, as an oscillator with frequency ω_{ce}, does not lose but gains its perpendicular energy when the wave is excited at the expense of its longitudinal energy. This scenario resembles a fan opening (figure 7.5). As a result of the fan-type instability the high-frequency oscillation bursts are excited in plasma and they are accompanied by losses of fast electrons. It is just the leakage of fast electrons to the walls that makes the fan instability a dangerous one.

7.5 'Fish-bone' Instability

The 'fish-bone' instability was discovered in PDX during the transverse injection of fast neutral beams [86]. It was so named because regular bursts of Mirnov MHD-oscillations resembled the skeleton of a fish (figure 7.6).

Similar to the predecessors of a saw-tooth crash, the 'fish-bone' is a $m = 1$, $n = 1$ mode. Oscillation frequency in each burst decreases almost two-fold from the beginning of a burst to its end. In the PDX facility 'fish-bone' instability was observed at sufficiently high values of toroidal β, i.e. $\beta q_a \geqslant 5\%$. The instability leads to intensive loss of fast ions and thus worsens the efficiency of additional heating. Later on this instability was observed in practically all large facilities: JET,

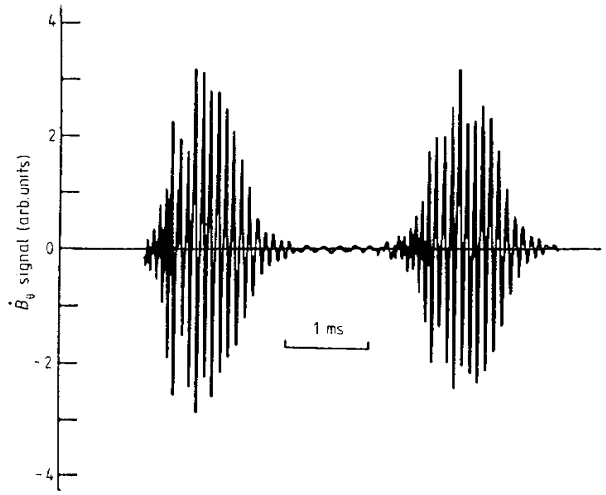

Figure 7.6 Oscillations of the poloidal-field time derivative as an indication of fish-bone instability [83].

TFTR, JT-60, DIII-D. The frequency of the excited mode is usually not high, of the order of $\sim 10^4$ Hz. The oscillations grow rather fast, then they decay somewhat more slowly and plasma is stabilized until the next burst.

Theoretically the 'fish-bone' instability is explained as a kinetic excitation of the internal helical mode by fast ions [84]. When β_p increases the internal helical mode reaches its excitation threshold so that its frequency slows down and the coupling of wave with ion precession may occur. For a more accurate analysis of instability the diamagnetic drift of the plasma thermal component should be taken into account [85]. Each spike of fish-bone activity starts with linear instability and then it transits into a non-linear regime when some portion of high-energy particles is expelled from plasma. The wave frequency is very low so that the particles can continue to be in resonance. When they are shifted along the major radius the particle energy diminishes and simultaneously these particles produce work in the averaged vertical electric field of perturbations. In other words the radially drifting particles can pump energy in oscillations, thus increasing their level. When the energy of resonant particles is exhausted the oscillations drop until the next spike of fish-bone activity.

A fish-bone instability is dangerous because it throws out a significant amount of fast ions trapped in plasma. There is a danger that a similar process may happen in future fusion reactors where

helical-mode destabilization may be excited by α-particles produced in the D–T reaction. That is the reason for a detailed investigation of this instability.

The results in DIII-D [86] were optimistic in this regard. Although the 'fish-bone'-oscillation bursts were sometimes observed in this facility at $\beta_p \geqslant 1,5$, $\bar{n}_e \leqslant 10^{20}\,\mathrm{m}^{-3}$, generally the plasma was stable.

7.6 Edge Localized Modes

In the ASDEX tokamak in the H-mode, an enhanced plasma confinement regime, oscillations affecting only the plasma periphery were discovered. They were called edge localized modes, or ELMS. They are characterized by a sudden H_α radiation growth in the divertor accompanied by fast decay of X-ray radiation from the plasma periphery and by a fast drop of β_p. Similar behaviour of these signals was observed in ASDEX during transition from H-mode to L-mode confinement. Roughly speaking, one may say that the ELM resembles a short pulse of H-L-H transitions. In fact the plasma losses in a single ELM may be even higher than in a quiet L-mode phase.

The characteristic features of a set of ELMS in ASDEX are shown in figure 7.7, taken from references [87,88]. The frequency of relaxation oscillations (figure 7.7) grows gradually, the amplitude decays, and towards the end of the ELM a transition from H- to L-mode confinement occurs. During ELM pulses one may observe helical perturbations of higher modes, $m = 3,4$, so that m/n is close to the value of q_a at the plasma boundary.

The relaxation nature of ELMS and the fact that they are accompanied by kink modes and energy loss from the plasma periphery resemble the characteristic features of internal disruption. One may say that ELM is something like an edge disruption.

Instabilities of ELM type have been observed in many facilities, e.g. PDX, DIII-D, JET. The presence of ELM oscillations does not mean that plasma should transit into the L mode: H modes with ELMS as well as without ELMS, have been observed in several facilities. Absence of ELMS in ASDEX led to the accumulation of heavy impurities in the central region of plasma, i.e. the H mode appeared to be too quiet and accumulating impurities as predicted by the neoclassical theory.

It seems that the optimal situation could be reached when a very low ELM activity without confinement degradation is maintained and the influence on the impurity content is already present. On DIII-D [89] and ASDEX [90] it was found that in ELM discharges with a

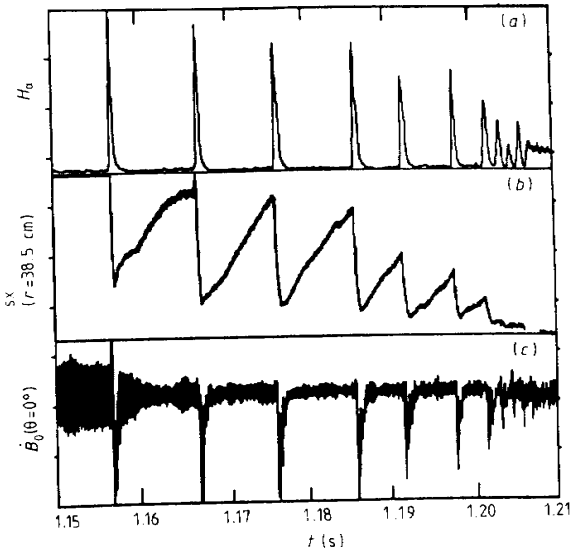

Figure 7.7 Oscillations in the ELM mode [87].

carefully optimized ELM repetition rate stationary conditions could be achieved.

7.7 MARFE

In the ALCATOR-C facility at very high plasma density another phenomenon was discovered which was called MARFE, for multifaceted asymmetric radiation from the edge. MARFE is a toroidal ring of a dense moderately cold plasma, located at the periphery of a plasma column on its inner contour. MARFE is easily observed due to its intense light radiation.

Later MARFE was discovered in a number of facilities. Plasma density in MARFE is high enough and is comparable with the central density of the main plasma. Its temperature is low, only several electron volts. That is why MARFE is an intense light source.

The physics of MARFE is similar to the physics of a solar prominence. It is known, that a protuberance on the sun represents a 'sheet' of dense plasma, suspended on magnetic field lines. Plasma temperature in a protuberance is much lower than in the surrounding corona. As a result, a plasma layer with intensive radiation builds up. The heat flux from the corona is not sufficient to heat a prominence to high temperatures. However, corona plasma pressure is sufficient to support the prominence in a state of hydrostatic equilibrium.

The same occurs in MARFE. Edge plasma is not very hot and its radiation increases when temperature decreases. If colder plasma appears, then it continues to be cooled down, and plasma pressure along the magnetic field increases cold plasma density and further enhances its radiation. A region of cold plasma—MARFE—is formed. Edge plasma 'compresses' MARFE cold plasma along magnetic field lines and feeds the energy for the subsequent re-radiation.

Thus, MARFE is the result of thermal-radiation instability of edge plasma [83–85]. It is obvious why MARFE is formed on the inner contour. This is just the region where magnetic lines have a higher connection length due to a higher value of the longitudinal field. In addition, plasma on the inner contour is more stable which is the reason why the process of cross-field heat transport to the wall is diminished there.

MARFE, similar to ELM, is a result of plasma self-organization processes in a tokamak. A phenomenon, similar to MARFE, i.e. compression of cold plasma with the subsequent power re-radiation is used in an open divertor geometry.

8 Plasma Thermal Insulation

Study of plasma thermal insulation has been the major objective of numerous experimental and theoretical investigations. Practically all transport processes are included here, i.e. ion and electron thermal conductivities, diffusion, impurity transport and viscous decay of the rotation. At the beginning of research there was a hope that experiments would allow us to determine all empirical expressions for kinetic coefficients which would then be explained theoretically. This hope was supported for a long time by the results from small and medium size tokamaks where the ion thermal conductivity was close to the neoclassical value; and as for electron thermal conductivity and diffusion there was hope that experiments might help to produce a universal formula applicable for all cases. These illusions were dispelled in the 1980s partially due to more detailed investigations in medium-size tokamaks, but, mainly, as a result of vast experimental data from large facilities.

A new quality emerged as a result of the discovery of various confinement regimes, which sometimes differ greatly from each other in respect of the values of thermal and diffusion fluxes. It became clear that in tokamak plasma profile effects play an important role: a greater role than at fixed kinetic coefficients. We should speak rather of the feedback coupling between profiles and kinetic coefficients. In other words, some kind of self-organization processes occur which control the plasma shape. To describe these more complex processes one has to abandon the simplest approaches like thermal transport with given thermal conductivity coefficients and proceed to more sophisticated physical models of self-organization.

8.1 Neoclassical Theory of Transport

The minimal level of transport fluxes is determined by Coulomb collisions. In a uniform magnetic field the coefficients of ion χ_i and

electron χ_e thermal conductivity, as well as the diffusion coefficient are determined very simply: $\chi_i \simeq \rho_i^2 \nu_i$; $\chi_e \approx D \simeq \rho_e^2 \nu_e$ where ρ_i and ρ_e are the mean Larmor radii, and ν_i ansd ν_e are the mean collision frequencies; χ_i is approximately $\sqrt{m_i/m_e}$ times higher than χ_e and D.

In a tokamak the situation becomes more complicated due to drift of particles in a non-uniform magnetic field. In a fundamental work by Tamm [4] the maximal enhancement of kinetic coefficients due to this mechanism was estimated: χ and D should not exceed the classical values corresponding to the case when only the poloidal magnetic field B_θ is present. In other words, the theoretical enhancement factor is not higher than $B_T^2/B_\theta^2 = q^2\epsilon^{-2}$, where $\epsilon = r/R$.

A more accurate theory by Galeev and Sagdeev [9,4], known as neoclassical theory, has shown that the real form of the enhancement factor is more complicated. A simplified version of this theory can be presented as follows.

To account for toroidal effects let us investigate first singly-charged particle motion in a tokamak magnetic field. To be more precise, let us study the motion of the guiding centre of the drift circle of radius $\rho = v_\perp/\omega_c$, where $\omega_c = eB/mc$ is the cyclotron frequency of the charged particle with mass m (here we use again CGSE-units which is more convenient for theoretical discussions).

Let us consider the toroidal magnetic surface of circular cross section with major radius R_0 and minor radius r (figure 8.1). We shall assume that $\epsilon = r/R$ is small. Then the magnetic field strength on this surface is approximately equal to $B = B_T(1 - \epsilon\cos\theta)$: on the external contour the field is somewhat weaker than on the internal contour. When a charged particle moves in a magnetic field its total energy $\epsilon = mv_\parallel^2/2 + mv_\perp^2/2$ is conserved ($v_\parallel$ is the longitudinal component, and $v_\perp$ is the transverse velocity component). In addition the transverse adiabatic invariant is also conserved

$$\mu_\perp = mv_\perp^2/2B = \text{constant}. \qquad (194)$$

While the Larmor orbit is moving from the external contour towards a stronger magnetic field, the transverse kinetic energy increases and the longitudinal energy decreases correspondingly. If the longitudinal energy is not high enough as compared with the transverse one, then a mirror effect may appear: the particle is reflected from a strong magnetic field. It is easy to see that reflection occurs for those particles which have $v_\parallel^2 < 2\epsilon v_\perp^2$ at $\theta = 0$. Indeed, at an angle increase $\Delta\theta = \pi$ the value of $v_\perp^2$ according to (194) would be increased by $2\epsilon v_\perp^2$ but if $v_\parallel^2$ is less than this value then the particle cannot penetrate into the strong magnetic field region. These re-

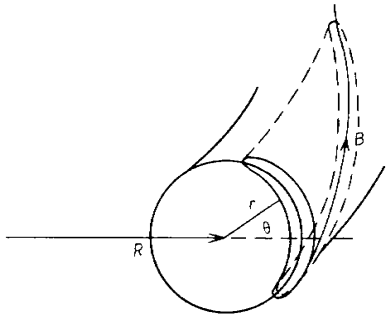

Figure 8.1 Trapped particle trajectories ('banana').

flected particles are called trapped particles, whereas particles with $v_\parallel^2 > 2\epsilon v_\perp^2$ are called transit particles.

Now let us consider magnetic drift. Two forces directed along the major radius affect the drift motion: the expelling force of diamagnetic Larmor motion $F_D = -\mu_\perp \nabla B = mv_\perp^2/2R$ and $F_c = mv_\parallel^2/R$, centrifugal force. These forces lead to drift with velocity v_d, so that the Larmor force $ev_d B/c$ compensates the expulsion forces. In other words,

$$v_d = \frac{v_\parallel^2 + v_\perp^2/2}{\omega_c R} \tag{195}$$

where $\omega_c = eB/mc$ is the cyclotron frequency. The drift velocity is directed along the vertical symmetry axis. Correspondingly, in the upper part of the torus the particles drift outside the magnetic surface, and in the lower part inside. As a result, the trapped particles perform a trajectory which looks like a 'banana' in the cross section projection. The 'banana' width is $\Delta \simeq v_d t$, where t is the transit time of one half of the 'banana'. For a typically trapped particle with longitudinal velocity $v_\parallel \sim v_\perp\sqrt{\epsilon}$ and total velocity of the order of the thermal velocity the banana width is

$$\Delta \simeq q\rho/\sqrt{\epsilon} \tag{196}$$

where $q = B_T r/RB_\theta$, $\rho = v_T/\omega_B$ and $v_T = \sqrt{2T/m}$.

The trajectories of transit particles also deviate from the magnetic surfaces. For particles which have just become transit ones, i.e. which are located in the vicinity of the separatrix (that, in its turn, separates trapped particles from transit ones), the $v_\parallel$ value is again of the order of $v_\perp\sqrt{\epsilon}$, so that their displacement along the minor radius is again of the same order as for trapped particles. However, for a

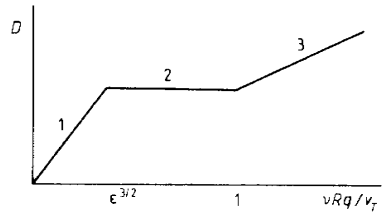

Figure 8.2 Schematic dependence of diffusion coefficient D and thermal diffusivity on the collisional frequency.

typical transit particle with longitudinal velocity of the order of a transverse one, this relationship looks like $\Delta \sim q\rho$.

With known particle trajectories it is possible to find corresponding kinetic coefficients by solving the kinetic equations with Coulomb collisions. For a rough estimation of transport coefficients, it is sufficient to find $\delta^2\nu_{eff}$ where ν_{eff} is the appropriate frequency of collisions and δ is a particle displacement between collisions. It is convenient to start with a rarefied plasma at high temperature, when the mean-free path $\lambda_{eff} = v_T/\nu_{eff}$ is high enough compared with qR. Trapped particles are the main contributors to transport in this case, so that one may speak about diffusion and thermal conductivity on the 'bananas'.

The schematic dependence of the coefficients of diffusion D and thermal conductivity χ upon the effective frequency of collisions is shown in figure 8.2. The region of very rare collisions is labelled '1'. Diffusion and thermal conductivity in this region are dominated by the collisions which correspond to transferring the particles from being trapped to transit ones and vice versa. Thus a single collision can produce a characteristic displacement of the order of $\Delta \simeq q\rho/\sqrt{\epsilon}$. Since for such a collision it is sufficient to change the longitudinal velocity by $v_\perp\sqrt{\epsilon}$ value then the corresponding frequency of collisions turns out to be much greater than the mean collision frequency because the process of Coulomb collisions has a diffusion nature in velocity space. Thus, it follows that

$$\nu_{eff} \simeq \nu/\epsilon \tag{197}$$

since the effective collision frequency exceeds the mean collision frequency by a factor of $(v_\perp/v_\parallel)^2$.

Bearing in mind, that the fraction of trapped particles is of the order of $\sqrt{\epsilon}$, the corresponding transport coefficients may be characterized by

$$\sqrt{\epsilon}\Delta^2\nu_{eff} = \epsilon^{-3/2}\nu q^2\rho^2. \tag{198}$$

This expression is valid both for ion and electron thermal conductivities: it is sufficient to insert the corresponding values for ν and ρ. It is easy to see that χ_i exceeds χ_e by a factor of $\sqrt{m_i/m_e}$. The diffusion coefficient D in neoclassical theory is of the same order of magnitude as the electron thermal conductivity, i.e. it is much less than the ion thermal conductivity.

The expression for transport on 'bananas' is valid only at low values of ν_{eff}, when the collision frequency of trapped particles is less than the bounce frequency i.e. at $\nu_{\text{eff}} > \sqrt{\epsilon} v_T/qR$. In terms of the dimensionless collision frequency

$$\nu^* = \nu\epsilon^{-3/2} qR/v_T \tag{199}$$

the 'banana' diffusion region in figure 8.2 is limited by the condition $\nu* < 1$.

In region 2, where $1 < \nu^* < \epsilon^{-3/2}$, the average collision frequency ν is less than the mean bounce frequency qR/v_T. Correspondingly, not all the particles contribute to the transport, but only slow-transit ones. Such particles suffer a displacement of the order of $\Delta \simeq q\rho v_T/v$ and their effective collision frequency is of the order of $\nu v_T^2/v^2$. Their relative number is of order of v/v_T, where the characteristic value of v can be found from the relation $\nu_{\text{eff}} \sim v/qR$. Thus their contribution to the transport can be estimated as $\Delta^2 \nu_{\text{eff}} v/v_T \sim q^2\rho^2 v_T/qR$ and gives the 'plateau' in figure 8.2. In other words, in this intermediate region, χ and D do not depend on collision frequency (naturally, to a rough approximation only).

The region of frequent collisions, 3, may be described hydrodynamically. It is called the Pfirsch–Schlüter region, after two physicists who were the first to investigate this problem theoretically. It is better to imply specific plasma convection which leads to diffusion as well as to convective thermal fluxes. Let us start with diffusion. In a straight cylinder with a longitudinal magnetic field the diffusion arises due to finite resistivity: to maintain the equilibrium current $j_\perp = -cB^{-1}\mathrm{d}p/\mathrm{d}r$, plasma should move with such a velocity to provide a Lorentz force evB/c which compensates the friction force $e\eta_\perp j_\perp$, where $\eta_\perp = m_e/e^2 n\tau_e$ is the transverse resistivity. From here we find the diffusion flux in a uniform field

$$nv = -n\frac{c^2}{B^2}\eta_\perp \frac{\mathrm{d}p}{\mathrm{d}r}. \tag{200}$$

In the toroidal magnetic field this value is modified by the additional flux due to longitudinal current which is called the Pfirsch-Schlüter current. This current is produced due to the $j_\perp$ current non-symmetry along θ. As we know, the expulsion force in the

direction of the major radius is equal to $2p/R$ per unit length of plasma tube with unit cross section. Therefore, an additional current $\delta j_\perp = \epsilon j_\perp \cos\theta$ appears. Since the current lines are continuous, i.e. $\mathrm{div}\boldsymbol{v}\boldsymbol{j} = 0$, a non-symmetrical component of poloidal current $\delta j_\perp$ should be compensated by a longitudinal current flowing along the magnetic field lines

$$j_\parallel = -\frac{B}{B_\theta}\delta j_\perp = \frac{2cr}{RB_\theta}\frac{\mathrm{d}p}{\mathrm{d}r}\cos\theta. \tag{201}$$

To maintain this current a longitudinal electric field $E_\parallel = \eta_\parallel j_\parallel$ and $E_\theta = E_\parallel B/B_\theta$ should exist in the plasma. This field leads to radial plasma convection with the velocity $v_r = cE/B = c\eta_\parallel j_\parallel/B_\theta$. This velocity changes according to a $\cos\theta$ law, and might appear not to lead to an average plasma flux across the magnetic surfaces. But this is not true: the element of toroidal surface is $\mathrm{d}S = 2\pi R\mathrm{d}\theta \simeq 2\pi R_0 r(1+\epsilon\cos\theta)\,\mathrm{d}\theta$, so that the radial velocity should be averaged over the angle θ with a weight $(1+\epsilon\cos\theta)$ in order to find the average flux. After averaging and adding (199) we obtain

$$nv = -n\frac{c^2}{B^2}\eta_\perp \frac{\mathrm{d}p}{\mathrm{d}r}\left(1 + \frac{2\eta_\parallel}{\eta_\perp}q^2\right). \tag{202}$$

For Coulomb collisions in H and D plasmas $\eta_\perp \simeq 2\eta_\parallel$, so that, as compared with a uniform magnetic field, the flux in toroidal plasma (202) is enhanced by a factor $(1+q^2)$. Thus, the neoclassical values of χ_i, χ_e and D are approximately as shown in figure 8.2. This rough picture is of a rather qualitative nature. A more accurate quantitative theory was developed by Hinton and Hazeltine [95] and later in the work by Chang and Hinton [96]. Their main result is a smoother transition between the 'banana' region, plateau and Pfirch–Schlüter regions.

Comparison of theory with experiment shows that the ion thermal conductivity is of the order of the theoretical value, but often differs from it by several orders of magnitude. As for the χ_e and D experimental values, they exceed the values predicted by neoclassical theory by two orders of magnitude.

8.2 Bootstrap Current

The neoclassical theory has clarified some other transport effects. For example, it allows one to calculate the diffusion of impurities. The impurity diffusion coefficient, obviously, has the same order of

magnitude as χ_i, since ion thermal conductivity looks like diffusion of hotter ions with respect to the backward flux of colder ions. Calculations of classical impurity transport were done in detail. Sometimes they agree with the experimental data. But more often a much cruder approach seems to be more correct: the same diffusion coefficient for all the impurity species.

Another effect, which is quite clear from the point of view of neoclassical theory, is a change of plasma longitudinal conductivity due to electron trapping. Roughly speaking, in rarefied plasma the number of current carriers changes, and therefore, the electron resistivity becomes higher as compared with the classical Spitzer resistivity by a factor of $(1-2\sqrt{\epsilon})^{-1}$

$$\eta = \eta_{\rm cl}(1-2\sqrt{\epsilon})^{-1} \qquad \eta_{\rm cl} \simeq 10^3 Z_{\rm eff} T_e^{-3/2} \ \ (\Omega\,{\rm m}). \tag{203}$$

The last expression is given in MKS units and T_e electron temperature, in keV.

We have to mention one additional effect, namely Ware pinching produced by trapped particles [97]. Its origin is the following. The trapped particle trajectories in the form of 'bananas' do not embrace the magnetic axis and do not feel the direct influence of the toroidal magnetic field. When a longitudinal electrical field E is applied, these particles start to drift in the poloidal magnetic field B_θ. The drift velocity is controlled by the balance of two forces, the electrical field force and the Lorentz force. Since the portion of trapped particles is $\sim \sqrt{\epsilon}$, the pinching velocity related to the whole plasma becomes equal to

$$v_{\rm W} \simeq -\frac{cE}{B_\theta}\sqrt{\epsilon}. \tag{204}$$

The neoclassical theory allows us to calculate this value over the whole frequency range, not only for the 'banana' region.

The most interesting effect discovered by neoclassical theory is the so-called bootstrap-current. Bootstrap-current was predicted on the basis of neoclassical theory in the work of Bickerton *et al* [98] (see also [99]). This is a current produced by plasma itself due to its diffusion expansion. This seems to be an effect opposite to Ware pinching, plasma expansion replaces longitudinal electrical field. The name 'bootstrap current' was suggested with 'Alice in Wonderland' in mind where the heroine managed to support herself in the air by her shoelaces.

Basically, bootstrap current is related to the presence of trapped particles, but is transported not only by trapped particles but mainly by transit ones. Trapped 'bananas' create a toroidal drift current due

to toroidal expulsion

$$j_{\rm T} \sim \epsilon^{3/2}\frac{c}{B_\theta}\frac{{\rm d}p}{{\rm d}r}. \tag{205}$$

Here the multiplier $\epsilon^{1/2}$ accounts for the contribution of trapped particles, and the other multiplier ϵ accounts for the fact that this current is produced by the toroidal expulsion.

Collisions between the trapped and the slowest transit electrons with effective frequency $\nu_{\rm eff} \sim \epsilon^{-1}\nu_{\rm ee}$ transfer the toroidal momentum to untrapped particles at a rate of $\sim \epsilon^{-1}\nu_{\rm ee}j_{\rm T}$. Due to the balance with ions a steady-state $j_{\rm BS}$ current of untrapped electrons is produced: $\sim \epsilon^{-1}\nu_{\rm ee}j_{\rm T} \sim \nu_e j_{\rm BS}$. Now we can estimate the bootstrap current

$$j_{\rm BS} \simeq -\epsilon^{1/2}\frac{c}{B_\theta}\frac{{\rm d}p}{{\rm d}r}. \tag{206}$$

In spite of the apparent clarity of this logic it is no more than simple mnemonics. As a matter of fact, expression (206) corresponds to the averaged drift velocity which is larger than the trapped-particle drift (205). This looks like a kind of contradiction. The stricter approach of neoclassical theory shows that the bootstrap current is closely related to diffusion [99]. Let us find the radial diffusion current $j_r \sim eDdn/dr$ which, according to (198), is of the order of $\epsilon^{-3/2}\nu q^2\rho^2 e dn/dr$. Multiplying it by the factor $1/cB_\theta$ we obtain the same estimation for the friction force, as follows from the arguments based on the momentum transfer.

Thus the bootstrap current is a very delicate phenomenon deeply related to collisional diffusion of the rarefied plasma. The detailed theoretical analysis [100] of the bootstrap current phenomenon was summarized by a very simple relation

$$I_{\rm BS}/I = 0.67\beta_{\rm p}\sqrt{\epsilon}.$$

where $\epsilon = a/r$ and I is the total plasma current.

The bootstrap current is a direct consequence of the 'banana' toroidal drift combined with the collisional diffusion. Being based on collisions of electrons near the separatix it is not sensitive to the anomalous behaviour of the transit particles. In other words, the mechanism for sustaining bootstrap current is more robust in regard to collective processes than the diffusion itself. Nevertheless, for a long time the bootstrap-current effect was not observed experimentally. It was observed for the first time in TFTR experiments [101], and then it was reproduced in a number of facilities. The highest effect was demonstrated first in JT-60 [103] and later in the JET facility. Since the current in plasma is $I \sim B_{\rm p}$, then the bootstrap

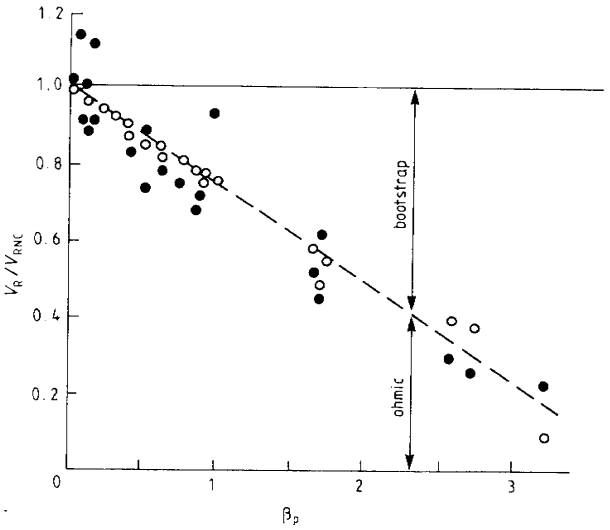

Figure 8.3 Bootstrap-current dependence on poloidal β_p [103].

to total current ratio j_{BS}/j should be proportional to the value of $\beta_p \sim 8\pi p/B_p^2$ according to (206). This very dependence was observed on JT-60 as is shown in figure 8.3. As we see, when $\beta_p \simeq 3$, the bootstrap current fraction accounts for 80% of the total current. In the JET facility it was only possible to realize transient regimes with a bootstrap current.

The presence of bootstrap current in tokamak plasma is a very encouraging feature. It facilitates creating a fully steady-state tokamak: less power would be required to maintain non-inductive current drive.

8.3 Confinement Modes

Several confinement modes have been discovered in tokamaks. In each of those modes a certain interrelation is observed among processes at the plasma edge and profile effects in the main core of hot plasma. Therefore, modes differ sometimes in the characteristics of the peripheral plasma, sometimes in their profiles and, in some cases, in both features. We shall review first of all the empirical data.

From a practical point of view the regimes of improved confinement are the most interesting, and those regimes have been studied

in depth (though much is left for a more detailed study). All the regimes of improved confinement are either continually linked with the regime of worse confinement (L mode), or arise due to the process of sharp transition, i.e. bifurcation. Therefore, it is quite natural to consider first a regime of basic confinement, i.e. L mode with its analogues and then to proceed to regimes of improved confinement. Let us start with ohmic confinement. Ohmic heating is characterized by the following modes:

- LOC (linear ohmic confinement) is a regime of ohmic confinement where the density is not very high, $n < n_s$. Here a linear relationship between energy confinement time and density, i.e. the neo-ALCATOR scaling, is valid;
- SOC (saturated ohmic confinement) is a regime of ohmic confinement at $n > n_s$, where the dependence of τ_E on density is saturated. SOC is an ohmic analogue of the L mode;
- IOC (improved ohmic confinement) is a mode of improved ohmic confinement, where the regime of linear ohmic confinement is significantly extended towards high densities. Initially, this regime was obtained in ASDEX by handling the plasma parameters accurately [104]. It looks like the ohmic analogue of H mode.
- the HDM (high density mode) was obtained in TUMAN-3 in an ohmic phase of the discharge [105] and is similar to the H mode;
- the P mode is a mode of improved plasma confinement both in the ohmic regime and with additional heating while injecting pellets—particles of frozen hydrogen. The P mode is related to $n(r)$ peaked profile and in this sense it is similar to the S mode.

The regimes with additional heating are characterized by the following modes:

- the L mode is the basic mode of non-improved confinement which occurs, so to speak, by itself, i.e. without additional effort. Plasma confinement in the L mode is satisfactorily described by Goldston scaling, or by its improved modifications.
- the H mode was first discovered in ASDEX [17]. It is the most popular mode of improved confinement with additional plasma heating. Just after this mode was discovered in ASDEX, the terms L (low) mode and H (high) mode were established.
- IL, the improved L mode in JFT-2M, resembles the H mode, but does not possess its characteristics at the plasma periphery.
- the S mode (or supershots) is the mode experimentally discovered in TFTR. It is the mode of improved confinement with strongly peaked distribution $n(r)$. In this respect it is similar

to the P mode with additional heating.

— the Z mode is the name for the improved confinement mode where the edge parameters are controlled by an influx of impurities. This mode was discovered in ISX-B and it is an interesting one because it helps to clarify the physics of improved confinement but it is certainly less attractive from a practical point of view.

In addition to the modes mentioned above, there exist combinations or slight modifications. For example, the PZ mode indicates a simultaneous presence of pellets and impurities; IDC-improved diverter confinement is a variation of IOC, but with the diverter and additional heating; detached plasma in TEXTOR is also a variation of IOC; S and B regimes in T-10 are very similar to the 'attached' and 'detached' regimes in TEXTOR. The VH mode found in the DIII-D tokamak was so named because it corresponds to a very high confinement regime and looks like a best version of the H mode without ELMS and saw-teeth.

It is convenient to start the discussion of the experimental data, from various confinement modes, with H mode, since, starting from its discovery in 1982 [17], intensive studies of different modes and their relationships have been made. Figure 8.4, which is now of historical interest, shows how strong the effect of the transition from the L mode to the H mode was. If τ_E degradation was clearly seen in the L mode at power increase, in the initial phase of the H mode (figure 8.4) this degradation is absent and the confinement time seems to resemble the neo-ALCATOR scaling. Subsequent experiments have shown that the degradation with power also takes place in the H mode, but τ_E is still 2 to 3 times higher than in the L mode.

The H mode is observed in the diverter as well as the limiter configurations. It possesses the following main characteristic features. Usually, at the L-H transition a slight electron temperature increase at the plasma edge leads to some kind of bifurcation, with the plasma reaching its new state: at its edge the temperature and density profiles sharply steepen and the global confinement increases so that at given P power the plasma thermal energy grows in time until a new stationary level is reached (there is no such a sharp transition in DIII-D). Not only energy confinement improves but particle confinement as well. There are significant changes at the plasma edge: edge temperature grows so that some kind of a pedestal is produced, the recycling decreases and H_α radiation intensity drops. A thermal barrier seems to be formed at the plasma edge: electron temperature rises almost up to 1 keV. On the DIII-D tokamak the presence of such a barrier and experimentally observed electric field $\sim 300\,\mathrm{V\,cm^{-1}}$ di-

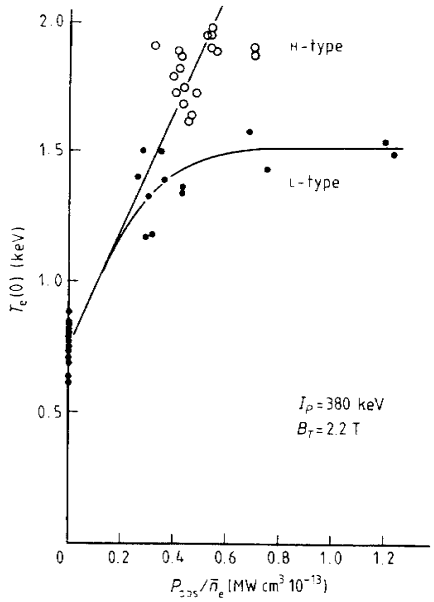

Figure 8.4 Electron temperature in L and H modes in ASDEX [17].

rected inside the plasma indicate good electron confinement in the edge plasma.

The L-H transition takes place only at high values of density and additional heating power. The density threshold is clearly seen in figure 8.5, where energy confinement times for L and H modes are compared in the ASDEX double-null DN diverter configuration. The threshold power density at the plasma edge needed for L-H transition is about (2–3) $10^{-2}\,\mathrm{MW\,m^{-2}}$ for different facilities. To establish a transition, additional heating is usually needed, but in TFTR and DIII-D H mode regimes were reached at ohmic heating alone. The confinement time for the H mode is usually 2–3 times higher than for the L mode, although more accurate scalings are available.

It is reasonable to discuss the modes with peaked density profiles together with the ohmic confinement regime. Figure 8.6 shows the ALCATOR-C initial data which served as a basis for neo-ALCATOR scaling, and the results of pellet injection which eliminated τ_E saturation with density. Figure 8.7 shows that TFTR pellet injection allows one to increase the ohmic density limit but it did not prevent

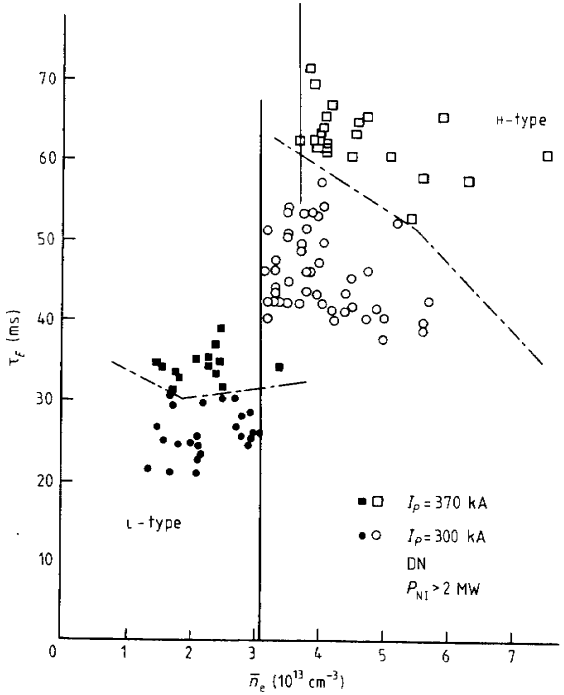

Figure 8.5 Density threshold for L-H transition in ASDEX [17].

the transition from the linear dependence of τ_E on density to the saturation regime, which has some similarity to the L mode. Supershots which lead to even higher peaking of density and temperature profiles permitted τ_E to increase by 2–3 times as compared with the L-mode scaling. In this respect the S mode resembles the H mode.

Figure 8.8 shows a continuous transition from the L mode to the S mode in TFTR. In this figure the enhancement factor is plotted on the ordinate axis, i.e. ratio of improved confinement time to the predicted confinement time of the L mode, and on the abscissa axis—peaking factor of density profile, i.e. the ratio of $n_e(0)$ density at the centre of the discharge to its $\langle n \rangle$ value averaged over the volume. As is seen, there is a clear correlation between these values. It turns out that H and S regimes are not completely different: recent experiments in TFTR [106] managed to produce a H mode from the supershot while maintaining a high peaking factor of profiles: a factor of $n(0)/\langle n \rangle \simeq 2$–3 and a factor of $p(0)/\langle p \rangle$ even higher, up to 5.

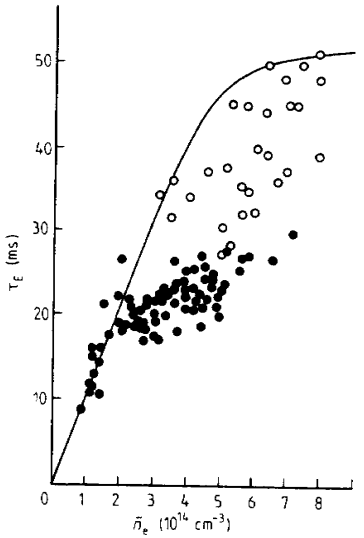

Figure 8.6 Confinement improvement in ALCATOR-C with pellet injection [17].

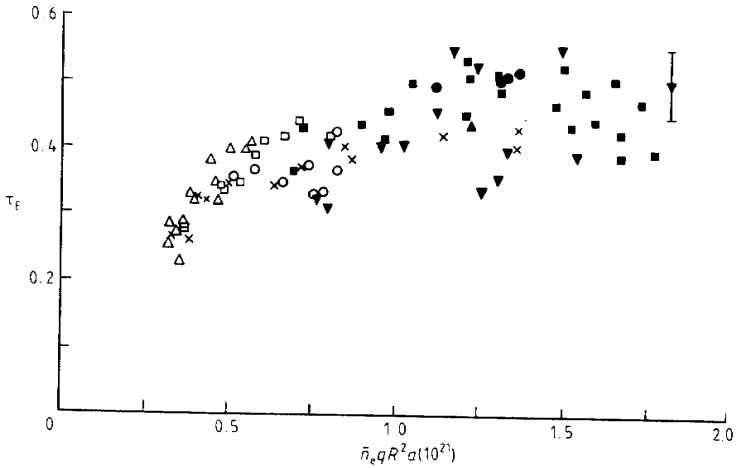

Figure 8.7 Saturation of τ_E with density in the TFTR ohmic regime [108].

Figure 8.9 shows the comparison of confinement times in a regular

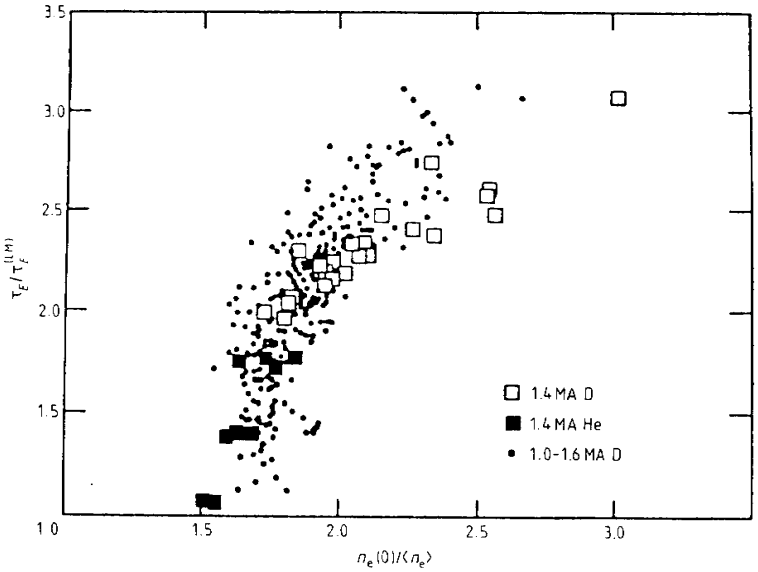

Figure 8.8 Plasma energy confinement improvement in TFTR as a result of density-profile peaking [139].

ohmic regime (LOC + SOC) and in the regime of improved confinement IOC in ASDEX. The authors have shown that discharges with τ_E saturation on density were observed at freshly-carbonized walls releasing large amounts of gas. However, if the walls were not carbonized or if they were carbonized and subsequently treated by a glow discharge in helium, then the confinement was improved while decreasing the gas puffing. At these conditions, together with modification of the diverter chamber aimed at decreasing the recycling, the improved ohmic confinement regime was realized. Figure 8.9 shows that the linear dependence on density is restored in IOC at much higher density values than the transition point from LOC to SOC. We cannot exclude the possibility that it is simply shifted into the region of higher densities—in the same way as with pellet injection.

As for the n_s transition point from LOC to SOC, it usually corresponds to the Hugill number value $H = H_s \simeq \sqrt{A_i/2}$. However, in devices with strong toroidal magnetic field the predicted SOC-value of energy confinement time might turn out to be higher than the corresponding L mode value. This happens when relation (187) is fulfilled. In this case the L-mode value of confinement time is valid at high densities even at ohmic heating. For example, figure 8.10

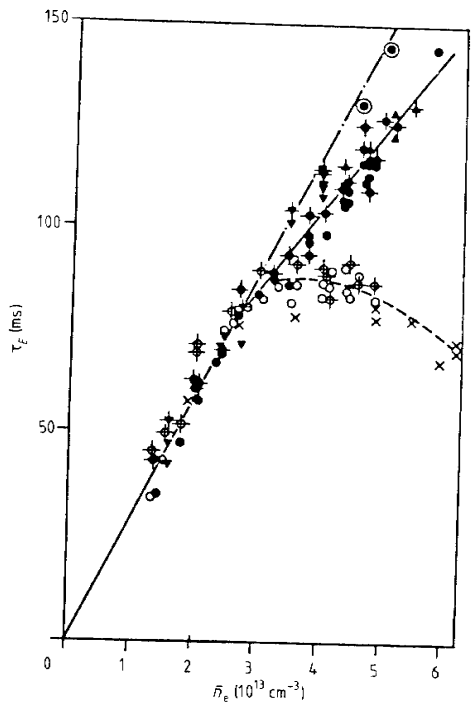

Figure 8.9 Improved ohmic confinement mode in ASDEX: the broken curve corresponds to the saturation mode; dots and circles—two different IOC modes [88].

shows good agreement between the experimental data in FT [60] and the predicted value of τ_E according the recipe given by Goldston [27]: $\tau_E^{-2} = \tau_{OH}^{-2} + \tau_{AUX}^{-2}$ where τ_{OH} is the energy confinement time in ohmic regime, and τ_{AUX} under additional heating. In this case the saturation in respect of density begins at lower values than n_s.

Many different modes of confinement can produce the impression that no conformity of laws exists at all. This is certainly not so. To display a hidden regularity it is reasonable to abandon the precise empirical formulas and to use an extremely simplified picture of figure 8.11 which schematically shows the energy confinement time dependence upon density for different modes of confinement.

The continuous line LOC–SOC corresponds to the ordinary ohmic confinement mode. The LOC part relates to neo-ALCATOR or T-11

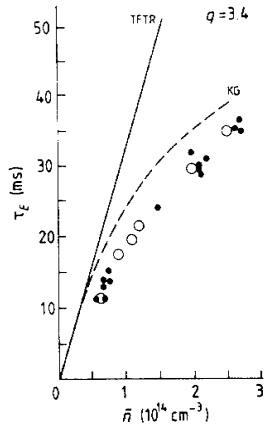

Figure 8.10 Dependence of τ_E on plasma density in FT tokamak: full line corresponds to ALCATOR scaling; dashed line to Kay–Goldston (KG) scaling in Goldston combination for τ_E [65].

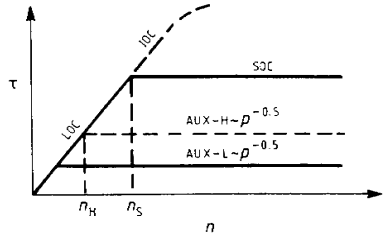

Figure 8.11 Simplified scheme of the different confinement modes. The LOC–IOC line (linear ohmic confinement plus improved ohmic confinement) corresponds to the best experimental confinement. Saturated ohmic confinement, SOC, and auxiliary heating confinements demonstrate degradation with power.

scalings. It is dominated by the electron channel of losses. At $n = n_s$ saturation with density takes place. When the density increases the neoclassical ion thermal conductivity can be important.

We can ask: what is the best plasma confinement that can be realized? Of course, the answer is a trivial one: the best confinement corresponds to neoclassical transport. This is the truth, but not the

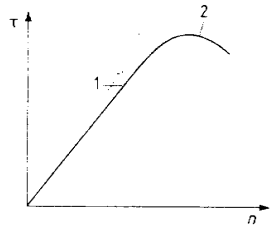

Figure 8.12 The best theoretical mode of confinement looks like a superposition of the superclassical confinement (1) and electron plus ion neoclassical confinements (2).

realistic truth. We know that electrons are always anomalous. Thus we have to accept for them not neoclassical but anomalous transport. I believe that the minimal value for electron transport is provided by T-11 scaling. I propose to call the corresponding expression (221) for the electron thermal conductivity superclassical. Thus the best energy confinement is displayed in figure 8.12. At low density electron superclassical transport dominates and as the density increases the ion neoclassical transport becomes more important.

The best mode of confinement, when the electrons correspond to neo-ALCATOR i.e. superclassical, and ions to neoclassical transports, is realized by the LOC–IOC line only. It does not mean that this best confinement mode cannot be reached when auxiliary heating is present. It means only that to reach this best confinement regime is not a simple matter. In some experiments, for instance, in a T-11 device, in ASDEX IOC mode and for P mode in ALCATOR (see continuous line in figure 8.6) the best confinement mode was realized. However, in most experiments the degradation of confinement is seen when the heating power is increased. It is better to say that this degradation has already begun in the SOC ohmic confinement mode. Additional heating simply reveals this degradation more clearly by means of its amplification.

The most typical mode of confinement is the L mode which is shown in figure 8.11 by a continuous line AUX-L. In rough approximation the AUX-L line can be considered as the SOC line decreased by the factor $(P_{OH}/P)^{0.5}$, where P_{OH} is the ohmic heating power. By the way, this simple procedure is known as T-10 scaling. As we see in figure 8.11 the density value for transition to saturation diminishes as compared with n_s as $n_s(P_{OH}/P)^{0.5}$. Thus with increase of the

auxiliary heating power the area of LOC scaling on the Hugill plot shrinks (see figure 5.3).

If the enhanced confinement mode, for instance, H mode, is realized then the corresponding AUX-H line in figure 8.11 is enhanced two-three times higher than the AUX-L line. If the L-H transition occurs at density lower than n_H we observe something like the restoring of the LOC mode with neo-ALCATOR scaling. But at $n > n_H$ the AUX-H mode corresponds again to saturated dependence upon density and the LOC confinement is not restored at all. If the transition to enhanced mode happens at not very high power or even at ohmic heating power then the AUX-H line can be situated higher than the SOC line. This takes place in the HDM which looks like the H mode in the ohmic heating regime.

In the high field tokamaks L-mode energy-confinement scaling predicts values lower than for SOC mode. In this case ohmic confinement will correspond to the LOC–AUX-L line but not to the LOC–SOC line. This regime takes place in a FT-device.

Thus, summing up the results of different confinement mode studies the following can be said. The linear ohmic mode with ALCATOR scaling is the best confinement. Unfortunately, at regular conditions with increasing density it transfers either into a saturated ohmic confinement mode, or into the L mode with Goldston-confinement scaling. Different improved confinement modes look like a LOC mode extended into the high density region with subsequent saturation. Accompanied by neoclassical ion thermal conductivity, improved modes increase confinement by a factor of 2–3 as compared with the L mode. For the H mode the possibility of improving confinement is associated with the formation of a thermal barrier for electrons on the plasma boundary. The H-mode temperature and density profiles can be broad, but at the plasma edge a high temperature pedestal builds up. The second possibility rests upon peaked density and temperature profiles: these are S, P and IOC modes. Combinations of these are also possible.

Now we see that only the best confinement regime LOC–SOC appears to be stipulated by some fixed transport coefficients. All other regimes, namely SOC, AUX-H, AUX-L, indicate that some self-organization-type phenomena can be present in tokamak plasma. They couple the transport fluxes with profiles and provide the non-linear transitions from one mode of confinement to another.

In support of this statement direct comparison of similar tokamaks can be made. Such an analysis was performed in [107] by Scott *et al.* They compared the non-dimensionally similar discharges with the same parameter $Ba^{5/4}$ = constant (see formula (166)). In such a family of similar discharges all plasma characteristics have to be

dependent on a single variable $nB^{-1.6}$, if atomic processes are not important. If the latter statement is not correct we have to include an additional parameter, namely, the Murakami number $M = nR/B$. For similar discharges having the same q and $Ba^{5/4}$ the M parameter is proportional to $nB^{-1.8}$. This is not very much different from $nB^{-1.6}$, so that, even with the atomic phenomena taken into account, there is effectvely only a single parameter which is variable in similar discharges.

Figure 8.13 gives the comparison of energy confinement time for similar tokamak discharges in dimensionless variables [107]. We see that the majority of points for three tokamaks of very different sizes are superimposed on each other in the non-dimensional variables. Only one exclusion exists—these are the TFTR points in figure 8.13(c). Now if we compare this picture with figure 8.6 for the energy confinement time in ALCATOR-C device we can see that the TFTR points in figure 8.13(c) just overlap with figure 8.6 points at the pellet injection. In other words, TFTR plasma corresponds to ALCATOR-C plasma with pellet injection. Thus two different modes of confinement are directly demonstrated in this non-dimensional representation.

Tokamak plasma is a complex physical system, which demands a set of non-linear equations for its description. It is known that non-linear equations can have not only a single solution but two, three or even several. This phenomenon is called the branching of solutions. Different branches of the mathematical model correspond to different states of a given physical system.

Thus we can say that the different modes of tokamak-plasma confinement correspond to different branches of the plasma state. The transition from one mode to another can be caused by a very tiny external perturbation or it can occur spontaneously as a result of some internal plasma activity.

8.4 Scalings

A large database on plasma-energy confinement in tokamaks may be summarized in simple empirical values for τ_E, which are called scalings. Such scalings are numerous: participants of different experimental teams are trying, as a rule, to establish empirical dependences which would permit them, first of all, to describe their own experimental data well enough. Applied to other facilities such scalings are not always correct. Nevertheless, step by step more or less universal scalings have been established. We will mention only some of these scalings.

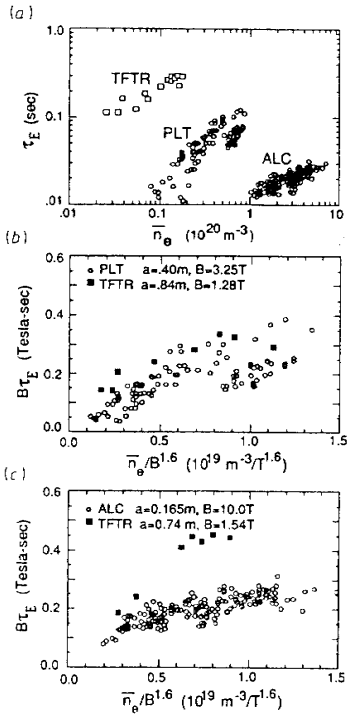

Figure 8.13 Comparison of energy confinement time versus density (a) in dimensional units for 3 tokamaks of very different sizes, (b) in dimensionless variables for dimensionally similar TFTR and PLT plasmas, (c) in dimensionless variables for dimensionally similar TFTR and ALCATOR-C plasmas [107].

In the LOC regime the experimental results are adequately described by neo-ALCATOR scaling

$$\tau_{\rm NA} = 0.07naR^2q, \tag{207}$$

where q is the effective safety factor with respect to kink modes, i.e. q a cylindrical equivalent the correct value of which for shaped plasma [135] can be simplified again

$$q \simeq \frac{5ab}{RI}B. \tag{208}$$

Here a is the minor radius in metres, R the major radius, I the current in MA, n the mean density in $10^{20}\,\mathrm{m}^{-3}$, $K = b/a$ the elongation

of the plasma cross section and B the field in T. The neo-ALCATOR scaling is valid only up to saturation density

$$n = n_s = \frac{B}{Rq}\sqrt{A_iK/2} \tag{209}$$

and transits above it into the Shimomura [110] scaling

$$\tau_s = 0.07aRB\sqrt{A_iK/2} \tag{210}$$

where A_i is the atomic number of ions.

With additional heating instead of (207) and (208), one should use the auxiliary heating scaling, and for transition from one regime to another the Goldston suggestion can be used

$$\tau_E^{-2} = \tau_{\rm OH}^{-2} + \tau_{\rm AUX}^{-2}. \tag{211}$$

The Goldston scaling for the L mode is as follows

$$\tau = 0.037IP^{-0.5}R^{1.75}a^{-0.37}K^{0.5}(A_i/1.5)^{0.5}. \tag{212}$$

Here P is the plasma heating power in MW. An isotope correction factor is added to reflect the fact that empirical data for Goldston-scaling referred to the nearly-equal mixture of hydrogen and deuterium. After Goldston many different scalings were proposed: Kay–Goldston [108], Rebut–Lallia [109], Odajima–Shimomura [110] etc. The general feature of all these scalings is confinement degradation with power. In power-law scalings this degradation is close to $\tau_E \sim P^{-0.5}$. For instance, in very simple T-10 scaling

$$\tau_{\rm T-10} \simeq \tau_{\rm OH}(P/P_{\rm OH})^{-\alpha} \tag{213}$$

the energy confinement corresponds to the diminished ohmic heating value. The power index α in (213) is not very different from 0.5. According to (213) the AUX-L line in figure 8.11 corresponds simply to the LOC–SOC line lowered by the factor $(P_{\rm OH}/P)^{0.5}$. This recipe can be accepted for the case when instead of the soc line we have in fact the ohmic L-mode line (as in a FT device, for example). But when the soc-line corresponds to Shimomura scaling, it is not so evident that (213) can be applied. When accepted (213) means simply that its accuracy is not sufficient to discriminate both scalings in medium-size machines.

Detailed analysis of all scalings for auxiliary heated plasma was undertaken by the ITER team [28]. It was shown that the difference between different scalings relates to the very weak dependence upon

two parameters, one of which corresponds to aspect ratio and the other to $q_{\rm eff}$. Many different scalings were summed up as the ITER-89 scaling

$$\tau_E^{\rm ITER89-P} = 0.048 I^{0.85} R^{1.2} a^{0.3} K_x^{0.5} n^{0.1} B^{0.2} A_{\rm i}^{0.5} P^{-0.5}. \qquad (214)$$

Here K_x means separatrix elongation and all parameters are expressed in MKS units, accepted by us in other empirical formulas. The expression (214) is somewhat complicated. Perhaps it could be corrected further in future. For theoretical discussion it is more convenient to simplify (214) by expressing B through I, dropping the density dependence and by rounding off the power indexes

$$\tau_{\rm EL} \simeq 6 \times 10^{-2} I R^{1.5} K^{0.5} (A_{\rm i}/2)^{0.5} P^{-0.5}. \qquad (215)$$

This simplified empirical value differs from the simplified version of Goldston scaling only by the absence of dependence upon the minor radius. The (215) scaling corresponds to the L mode of confinement. For the H mode the energy-confinement time is larger by a factor of about two. Sometimes, as in the VH mode for instance, this factor is equal to about three.

There are also scalings for the H mode. We shall mention here a very simple scaling of Schissel *et al* [111]. With further simplifications by rounding off the numbers it can be represented in the form

$$\tau_{\rm EH} \simeq 0.1 I R^{1.5} (A_{\rm i}/2)^{0.5} P^{-0.5}. \qquad (216)$$

Here the isotope effect is taken into account with the usual assumption that $\tau_E \sim A_{\rm i}^{0.5}$. The authors of paper [111] claim that (216) does not contain the dependence on K. As is seen from comparison of (215) and (216) the H-mode confinement time is almost twice greater than the L-mode confinement time.

In addition to power laws, the experimental data may be described by a linear off-set scaling. This means that the plasma thermal energy may be written as

$$W = W_{\rm OH} + \tau_{\rm inc}(P - P_{\rm OH}). \qquad (217)$$

Here $W_{\rm OH}$ is the thermal energy of the plasma at ohmic heating, $P_{\rm OH}$ is the ohmic heating power before additional heating, $\tau_{\rm inc}$ is the so-called incremental confinement time for which experimental scalings were proposed. As compared with the power law the linear off-set scaling contain twice as many fitting parameters and which is why it is less convenient for extrapolation to larger devices.

8.5 Thermal Conductivity, Diffusion and Viscosity

It would be much more pleasant to deal with ion and electron temperature conductivities as well as with the kinetic coefficients of diffusion and viscosity instead of τ_E global energy-confinement time. Unfortunately, the experimental information concerning these coefficients is not as comprehensive as information on τ_E; moreover, the spread of experimental data is more pronounced. As for the theory, it cannot yet calculate kinetic coefficients on the basis of turbulent processes in the self-organized plasma with a sufficient degree of confidence. Nevertheless, certain conclusions can be drawn on the basis of existing knowledge.

Foremost, experiment shows that energy loss is dominated by thermal transport in the bulk plasma outside the zone with saw-tooth oscillations. The convection contribution by the diffusion flux turns out to be lower. Total thermal fluxes for electrons and ions are normally determined in the following way

$$\Gamma_{\rm e,i} = -n_{\rm e,i} \chi_{\rm e,i} \frac{\partial T_{\rm e,i}}{\partial r}. \qquad (218)$$

Thus, $n_{\rm e,i}\chi_{\rm e,i}$ plays the role of thermal-conductivity coefficients. In other words, a certain difference exists compared with the commonly accepted definition for thermal-conductivity coefficients in other branches of physics: $\kappa = C\chi$, where C is the specific heat. Since the plasma thermal energy is equal to $3(n_e T_e + n_i T_i)/2$, then according to common practice, $1.5 n_{\rm e,i}\chi_{\rm e,i}$ should play the role of thermal conductivity coefficients. However, the relationships (218) are routinely used in plasma physics.

Thermal diffusivity coefficients are more convenient for comparison with theoretical expressions, and besides that, it is easier to compare them with scalings for τ_E. One may roughly assume that

$$\tau_E \simeq a^2/4\chi \qquad (219)$$

where χ is the half-sum of thermal diffusivities $\chi_{\rm e}$ and $\chi_{\rm i}$.

According to experiments, ion and, to a greater extent, electron thermal diffusivities are increasing functions of the minor radius. Roughly speaking, plasma is confined inside the magnetic surface with $q \sim 2$, the confinement is worse beyond this region. Thermal diffusivity coefficients are essentially increased at the plasma periphery (except H mode).

The ion thermal diffusivity sometimes drops to the Chang–Hinton neoclassical value of $\chi_{\rm CH}$. But more often it exceeds this value by 3 times or even more. The electron thermal diffusivity is almost always

anomalous and usually exceeds neoclassical values by two orders of magnitude. It may go down almost to the neoclassical value only in the H mode inside the high-temperature thermal barrier at the plasma edge.

To have some notion of the magnitudes of χ_e and χ_i one has to keep in mind that their experimental values are of the order of $1\,m^2\,s^{-1}$, deviating in both directions by several times. For example, there is a rough INTOR scaling which assumes that

$$\chi_e \simeq 0.5/n \tag{220}$$

Here χ_e is measured in $m^2\,s^{-1}$, and the local density in $10^{20}\,m^{-2}$. The approximation (220) corresponds to the assumption that the electron thermal conductivity $n\chi_e$ is constant over the cross section. In reality, the electron thermal conductivity rises strongly towards the periphery, but even a rough simulation with (220) sometimes gives acceptable results. For (220) to agree with a neo-ALCATOR scaling, one would have to insert an additional multiplier into this relationship containing the r/qR^2 product, but it seems that such a complication lacks physical sense.

Much greater physical sense leads to the empirical value of χ_e proposed by Merezhkin and Mukhovatov on the basis of experimental data obtained at the T-11 facility

$$\chi_{MM} \simeq \frac{\epsilon^{7/4}}{qRnr_0}\sqrt{\frac{T_e}{2A_i m_e}}. \tag{221}$$

This expression is written in CGSE units, $\epsilon = r/R$, $r_0 = e^2/m_e c^2$ is the electron classical radius, T_e is the electron temperature, A_i is the atomic weight. I suggest we call expression (221) superclassical thermal diffusivity. The reason for this is that it contains classical values only while $\Lambda = \sqrt{4\pi n r_0}$ which is called the London length and is well-known in superconductivity physics.

The relationship (221) was found empirically, but it agrees with Ohkawa's idea [123] who pointed out that experiments in tokamaks correlate with an assumption that

$$\chi_e \sim (c^2/\omega_{pe}^2)v_e/qR \tag{222}$$

where $\omega_{pe} = \sqrt{4\pi e^2 n/m_e}$ is the plasma frequency, $v_e = \sqrt{2T_e/m_e}$ is the mean electron thermal velocity.

Expression (221) is better than (220) both in the physics sense and because of a much steeper profile along r due to the multiplier $\epsilon^{7/4}$. It is clear that the superclassical value cannot be considered as

a universal, empirically found thermal diffusivity coefficient: relation (221) corresponds more or less to neo-ALCATOR scaling, but does not describe other confinement modes. Thus, χ_{MM} is a lower limit of anomalous electron thermal conductivity, as if it were an analogue of χ_{CH}, the neoclassical value for ions.

Now let us discuss diffusion which has been studied in detail in many experiments. The experimental results can be roughly summarized as follows: the diffusion coefficients for all the plasma components are approximately equal to each other and have a value of the order of

$$D \simeq \tfrac{1}{4}\chi_e. \tag{223}$$

As a matter of fact, the multiplier in front of χ_e may slightly change from 1/5 to 1/2 for different plasmas.

As for the viscosity, it may be related to the decay of the differential rotation along the major φ azimuth as well as along the minor θ azimuth. However, rotation of tokamak plasma along the minor azimuth is practically forbidden: at such a rotation the plasma would be compressed and expanded periodically due to changes of its local major radius. Ion–ion collisions prevent this process and dampen rotation.

Thus, only rotation along φ may exist. This rotation is generated, for instance, during a non-balanced injection of fast neutrals. Plasma rotation is undesirable: if plasma 'runs away' from the neutral beam, then the velocity of the beam relative to plasma decreases, and, consequently, the power introduced into the plasma decreases as well.

The rotation damping due to viscosity may be characterized by the global time of rotational momentum decay τ_φ. In exact analogy to τ_E, the τ_φ value may be called rotational momentum lifetime. The experiments show that with rare exception

$$\tau_\varphi \simeq \tau_E. \tag{224}$$

This fact clearly contradicts neoclassical theory. In neoclassical theory when the rotation velocity is low compared with the speed of sound, the relation $\tau_\varphi \gg \tau_E$ is expected, since the momentum is transported by transit ions only and the collision amplification effect due to the particles which are close to trapping, becomes insignificant. If the rotation velocity is high, the τ_φ neoclassical value becomes significantly smaller and reaches τ_E. However, direct comparison of the theoretical neoclassical value of τ_φ with TFTR experiments [112] has not shown a satisfactory agreement even in this case.

Thus, to summarize the state of the art of the investigation of tokamak transport processes, one may say the following. The set

of all transport processes (i.e. thermal conductivity, diffusion and viscosity) points to the fact that they are determined by collective, turbulent processes, and only at very quiet conditions may they go down to neoclassical values.

9 Plasma Self-organization

Tokamak plasma is an exceptional physical object, artificially created in laboratory conditions. Plasma parameters are most impressive—temperature up to hundreds of millions of degrees, i.e. an order of magnitude higher than at the centre of the Sun, currents up to several million amperes with loop voltage less than 1 V—and all this when particle density is five orders of magnitude less than atmospheric. But the most amazing parameter is the long-time existence of hydrogen plasma which fills practically the whole chamber and remains sufficiently pure. Moreover, in spite of relative 'brittleness' with regard to strong perturbations, plasma quite easily adjusts to 'minor inconveniences', i.e. to relatively small external perturbations. A more detailed study of these properties reveals the existence of different self-organization mechanisms which enhance 'survival' of plasma at a level close to the optimal one.

9.1 Profile Self-consistency

The effects of plasma self-organization in a tokamak are numerous—in fact all non-linear processes are related to these very phenomena. Therefore, we shall start the discussion with an effect, although very obvious from first acquaintance with plasma, but still neglected for a long time as one of the essential features of plasma. Here we are speaking about 'profile consistency'. This term was introduced by Coppi [22] who paid attention to the fact that electron temperature profiles as functions of the minor radius are strikingly similar to each other in very different facilities.

An inattentive person may take this fact for granted and spend no effort in additional analysis. Indeed, plasma temperature attained by Joule heating should obviously be maximal in the centre and drop to very low values on the walls.

Moreover, intensive plasma cooling due to atomic processes at the periphery produces a 'bell-shaped' profile (figure 9.1) which, in its

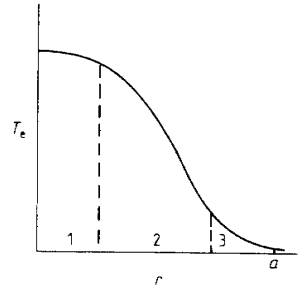

Figure 9.1 Three different plasma regions: 1—saw-tooth activity; 2—confinement region; 3—edge plasma.

turn, makes the temperature profile seem to be universal. However, one should not draw hasty conclusions.

Let us investigate more closely the plasma column cross section. As is seen from figure 9.1, one may distinguish three zones in which transport processes play the dominant part: 1—saw-tooth oscillations; 2—heat transfer; 3—atomic processes. It is just zone 2 which is responsible for magnetic confinement. The volume of zone 1 depends on the q value at the plasma column boundary, i.e. q_a. If q_a is reduced, then the inversion radius r_s of saw-tooth oscillations grows, and, consequently, the saw-tooth contribution to the total heat transfer also increases. In large and middle-size tokamaks the zone of saw-tooth oscillations does not disappear completely even at high q_a values: the central value $q(0)$ continues to be slightly less than unity even in these cases. Thus, the plasma column seems to be 'supported' by a certain current density at the centre, so that $q(0) \simeq 1$. As the total current grows, the current channel simply broadens. This very fact noticeably affects the profile's 'self-consistency'.

In fact, if one takes a certain point $r = a_*$, where $q(r)$ starts to grow considerably with r, it is natural to assume that a significant portion of current flows inside this radius. But then, a_*^2 should be proportional to total current. Now let us introduce non-dimensional radius $\rho = r/a_*$ where a_* is expressed as

$$a_* = \sqrt{RI/5B_T}. \tag{225}$$

In other words, a_* is the radius, inside of which the total plasma current with homogeneous current density and $q = 1$ inside the current channel could be placed.

In a tokamak steady-state phase of discharge the current density is proportional to $T_e^{3/2}$, since it is equal to $j = \sigma E$, and the electrical conductivity $\sigma \sim T_e^{3/2}$. Therefore, if j and T_e profiles decay beyond

$r = a_*$, then similar profiles, dependent only on $\rho = r/a_*$, may exist. In other words, they resemble self-similar profiles which are functions of q, but not directly of r.

Self-similar profiles reflect somewhat better the sense of 'profile self-consistency', but their resemblance to the experimental profiles is not very decisive, since $q(0)$ settles at a value of about unity and q_a values are maintained to be not very high at the plasma boundary. This fact alone together with 'bell-shapeness' makes the profiles look similar.

More evidently the effect of profile self-consistency was demonstrated by the direct experiments on T-10 [113]. The T-10 tokamak is equipped with a powerful set of gyrotrons which permits the introduction of about 2MW power at the electron-cyclotron resonance, at any chosen major radius.

Figure 9.2 shows the dependence of ECR-heating efficiency upon the value of power consumption: in fact this is an increment of plasma energy content during ECR heating as a function of the resonance position at point R. It can be seen that, in a certain interval of R the plasma energy increment does not depend on the point of power consumption, and beyond this interval the effectiveness reduces quickly, although the resonance point is still far from the plasma column boundary, $a = 32$ cm. According to the experiments, the electron temperature profile remained constant at the resonance point variation inside the region of effective heating. The pressure profiles remained even more rigid. The rigidity of the pressure profile increases with the parameter n/I, so that one could speak of reaching some optimal or canonical profile [113, 114] at large n/I values.

9.2 Optimal Profiles

The physical cause of 'profile self-consistency' can be understood on the basis of tearing-mode activity when profiles are not optimal from the point of view of their stability. The effects may appear when the plasma global state exerts influence on its local characteristics.

Unfortunately, the linear theory of stability does not help very much in obtaining a simple enough picture for the plasma self-consistent global state. Some energy principle seems to be more attractive. This approach was developed by Taylor to describe the plasma relaxed state in the reversed field pinch [115]. It is based on the assumption of complete reconnection of magnetic field lines. In a tokamak such a reconnection may occur only in the region of

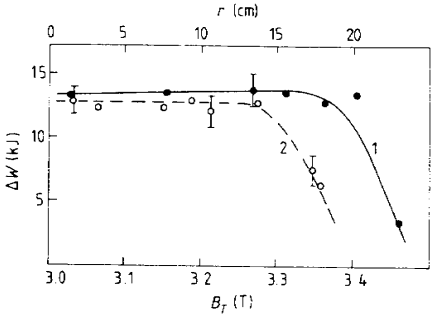

Figure 9.2 Increment of plasma energy with ECR-heating as a function of resonance position ($n_e = 3 \times 10^{19}\,\mathrm{m}^{-3}$, $P_{HF} = 820\,\mathrm{kW}$): 1—plasma current $I = 270\,\mathrm{kA}$; 2—plasma current $I = 170\,\mathrm{kA}$ [113].

saw-tooth oscillations or during severe disruption process. That is why some special arguments are required for the tokamak plasma.

The relaxed state may be described as a certain minimum of energy under specific constraints.

In a reversed field pinch the 'helicity' is just such a constrained factor, which is determined as

$$K = \int \boldsymbol{A} \cdot \boldsymbol{B} 2\pi r \, \mathrm{d}r \tag{226}$$

where $\boldsymbol{B}$ is the magnetic field vector, $\boldsymbol{A}$ is the vector potential of the magnetic field. It is K that is conserved at local reconnections of magnetic-field lines.

The logic to constrain the helicity is the following. With the help of MHD equations it is possible to show that integral (226) over any volume inside the magnetic surfaces is conserved if the resistivity is zero. For finite resistivity this is not so because magnetic field lines can reconnect. But when the resistivity is low the K-value has to be conserved approximately if the integral in (226) is taken over the full volume of plasma. The reconnection leads simply to redistribution of magnetic field line tubes but not to decay of K. In finding the energy minimum it is necessary to find the extremum of the functional $\mathcal{E} + \lambda K$, where $\mathcal{E}$ is the magnetic field energy and λ is a Lagrange multiplier.

The procedure leads to the solution with the force free magnetic field

$$\nabla \times \boldsymbol{B} = \alpha \boldsymbol{B} \qquad \alpha = \text{constant}. \tag{227}$$

It follows from this relation that

$$B_z = B_0 J_0(r) \qquad B_\theta = B_0 J_1(r).$$

Here J_0, J_1 are the Bessel functions. Near the axis B_θ is much smaller than B_z. Thus from the point of view of tokamak ordering, $B_T \gg B_\theta$, the force free solution leads to the homogeneous current density distribution

$$B_z \simeq B_0 = \text{constant} \qquad B_\theta \simeq B_0 \alpha r.$$

Such a state with an energy minimum at K = constant could correspond to the disrupting plasma only when no restrictions are imposed in respect of magnetic field line reconnections.

For tokamaks the energy variational approach was proposed almost simultaneously in three papers: Hsu and Chu [116], Biskamp [117] and Kadomtsev [118]. Formally, it relates to requirement of an extremum of plasma and poloidal magnetic field energy

$$\mathcal{E} = \int \left(\frac{B_\theta^2}{8\pi} + \frac{p}{\gamma - 1} \right) 2\pi r \, \mathrm{d}r \tag{228}$$

under an additional constraint

$$I = \int j 2\pi r \, \mathrm{d}r = \text{constant} \tag{229}$$

and the assumption that the plasma pressure p and the current density j are functions of q or $\mu = 1/q$.

Let us explain what this means. Because the toroidal magnetic field energy is conserved, the expression (228) represents the total energy inside the plasma column. Without additional constraints, this energy would go down to an absolute minimum, i.e. to zero. However, this is not possible in a tokamak plasma because the magnetic field is frozen into highly-conducting plasma.

In a tokamak, global reconnection of magnetic lines takes place only at current disruption. In a steady state phase overall reconnection is forbidden, but some small local zones of reconnection may appear. A typical example is saw-tooth oscillations in the vicinity of the plasma column axis—this is a reconnection process repeated periodically. More accurate experimental studies have shown that 'fine saw-teeth' were detected in the vicinity of rational points $q = m/n$ with not large m and n numbers. These are also periodically repeated reconnections, but on a smaller scale.

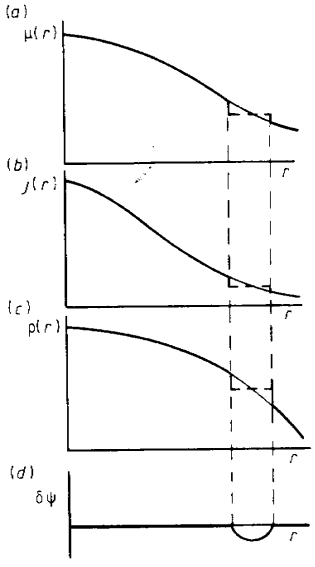

Figure 9.3 Local plateau formation on profiles $\mu = 1/q$, j, p at $m = 0$, $n = 0$ variation of $\delta\psi$.

In order to find out whether these reconnections are favorable from the energy point of view, one may compare two states: before and after reconnections. When the energy of the final state is lower, the reconnections may develop even if some intermediate potential barrier exists to prevent the release of magnetic energy of kink modes. Perhaps this very barrier leads to the relaxation-type feature of saw-tooth oscillations when the energy is slowly accumulated to be released subsequently in the saw-tooth crash.

Let us assume that in the vicinity of some rational point, as a consequence of non-linear tearing mode development, a tubular layer with stochastic magnetic field of reconnected magnetic lines is formed. Plasma in this layer can smooth out pressure along the magnetic lines, so that a local pressure plateau can be formed. This is shown in figure 9.3(b). Since there is no pressure gradient in this area, a force-free magnetic field is produced, i.e. j current flows along the magnetic field lines

$$\boldsymbol{J} = \alpha \boldsymbol{B}. \tag{230}$$

We can assume that all the stochastisized layer is filled by a single magnetic line. This leads to two effects: firstly, the q value (or μ) also reaches a plateau due to averaging of rotational transform angle, and, secondly, a plateau is formed in the current density. The second statement is related to the fact that from (230) and $\nabla \cdot \boldsymbol{j} = 0$ it follows that $\boldsymbol{B} \cdot \nabla \alpha = 0$, i.e. α is constant inside the stochastic region. But in a tokamak the toroidal component of magnetic field is much higher than the poloidal and this means homogeneity of longitudinal current in the stochastic layer. Thus, when a stochastic layer is formed a plateau develops on $\mu(r)$ as well as on pressure and current densities, as shown in figure 9.3. In order to find out how the energy changes under an additional constraint of $I =$ constant, one should find the variation of $F = \mathcal{E} + \lambda I$ functional, where λ is a Lagrange multiplier. As we see, F plays the role of free energy which can be released when the stochastic layer is formed. By variation from initial distribution to the plateau, (see figure 9.3), the following expressions can be used: $\delta p/\delta\mu = p'/\mu'$, $\delta j/\delta\mu = j'/\mu'$ where primes indicate derivatives over r. In other words, one may put $p = p(\mu)$, $j = j(\mu)$ in the variations considered.

One should note, that the final state is considered to be stochastisized. Therefore, formally keeping cylindrical symmetry (i.e. $m = n = 0$), we actually mean a local disruption-type transition. That is why the current density should not be considered as related to magnetic field by a normal expression with axial symmetry

$$j = \frac{c}{4\pi r}\frac{\mathrm{d}(rB_\theta)}{\mathrm{d}r}. \tag{231}$$

It is just the current density which is the most sensitive to field stochastization. If we express j through the magnetic field, then, at the frozen field outside the stochastic layer, the total current would be automatically conserved, and the corresponding term would be immediately excluded from the free energy variation.

Since

$$\mu = \frac{RB_\theta}{rB_\mathrm{T}} = \frac{R}{rB_\mathrm{T}}\frac{\mathrm{d}\psi}{\mathrm{d}r} \tag{232}$$

and ψ flux is conserved outside the stochastic layer, the functional $F = \mathcal{E} + \lambda I$ may be varied over ψ on the assumption that $p = p(\mu)$ and $j = j(\mu)$.

Supposing $\delta\psi$ is localized in the vicinity of a rational point (see figure 9.3(d)), then after variation and integration by parts we obtain

$$\delta F = -\int Q\delta\psi\,\mathrm{d}r \tag{233}$$

where

$$Q = \frac{R}{4B_\mathrm{T}}\frac{\mathrm{d}}{\mathrm{d}r}\left(\frac{B_\mathrm{T}^2}{R^2}r^2\mu + \frac{4\pi}{\gamma - 1}\frac{\mathrm{d}p}{\mathrm{d}\mu} + 4\pi\lambda\frac{\mathrm{d}j}{\mathrm{d}\mu}\right). \tag{234}$$

If $Q = 0$ we obtain a neutral equilibrium state with respect to stochastic layer formation. And since, according to figure 9.3(d), $\delta\psi < 0$ for the variation considered we see that $Q < 0$, i.e. a faster decrease of p and j with radius as compared with the relaxed state, corresponds to free energy gain, i.e. to energy reduction during the stochastic layer formation.

In order to find relaxed state profiles, let us choose the simplest dependence of p and j on μ

$$p = p_0\mu^2 \qquad j = j_0\mu^2. \tag{235}$$

The μ value is naturally considered to be equal to unity at the centre since the saw-tooth oscillations belong to the class of relaxation processes under consideration. Therefore p_0 and j_0 are the corresponding values at the centre of the plasma column.

Inserting these expressions into the $Q = 0$ relationship we obtain

$$\mu = (1 + \rho^2)^{-1} \qquad p = p_0(1 + \rho^2)^{-2} \qquad j = j_0(1 + \rho^2)^{-2} \tag{236}$$

where

$$\rho = r/a_* \qquad a_*^2 = RI/5B_\mathrm{T} \qquad j_0 = 5B_\mathrm{T}/\pi R.$$

The current density profile (236) turns out to be consistent with relation $j/j_0 = (1/2r)(\mathrm{d}/\mathrm{d}r)(r^2\mu)$ relation, which follows from (231) relating j to B. This is why (235) is the only reasonable choice.

Comparison with experiments [118] shows that profile $p = p_0(1 + \rho^2)$ agrees well with experimental data, as shown in figure 9.4. As a matter of fact from figure 9.4 it follows that experimental profiles are somewhat steeper than the optimal one on the plasma periphery.

The JET profile, which differs greatly from the optimal one due to a large zone of saw-tooth oscillations, is not shown in figure 9.4. Lazzaro with co-authors [119] considered a relaxation model on the assumption of the existence of a broad zone of saw-tooth oscillations. Inside this zone the relaxation on free reconnections forms the profile of $\mu = 1$, and outside this zone, $r > r_\mathrm{s}$, the variational principle again agrees with the profiles of type (235), where μ again behaves as $(a_0^2 + r^2)^{-1}$, a_0^2 being a constant not yet defined.

Thus, for JET it is natural to assume

$$\mu = \begin{cases} 1 & \text{if } r < r_\mathrm{s} \\ (a_0^2 + r_\mathrm{s}^2)/(a_0^2 + r^2) & \text{if } r_\mathrm{s} < r < a. \end{cases} \tag{237}$$

At the plasma edge $\mu_\mathrm{a} = q_\mathrm{a}^{-1} = RI/5B_\mathrm{T}a^2 = a_*^2/a^2$, i.e. the experimentally prescribed value. Therefore, according to (237) there exists a relationship between a_0^2 and r_s^2

$$\mu_\mathrm{a}(a_0^2 + a^2) = a_0^2 + r_\mathrm{s}^2. \tag{238}$$

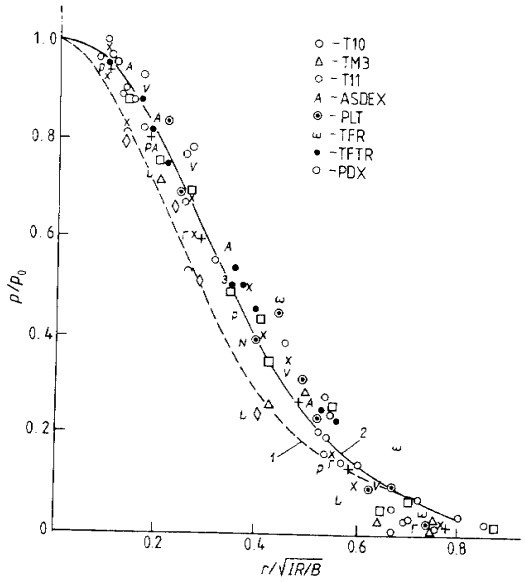

Figure 9.4 Comparison of the plasma pressure distribution profiles with the experimental data: 1—$p = p_0(1 + \rho^2)^{-2}$; 2—$p = p_0(1 + \rho^2)^{-6}$.

At $r_\mathrm{s} = 0$ we have $a_0^2 = a_*^2(1 - \mu_\mathrm{a})^{-1}$ and at $a_0 \to 0$ we obtain a maximal possible value $r_\mathrm{s}^2 = \mu_\mathrm{a}a^2 = a_*^2$. From (237) and the relationship (231) between j and B_θ it follows that

$$j = j_0 \begin{cases} 1 & \text{if } r < r_\mathrm{s} \\ a_0^2\mu^2/(a_0^2 + r_\mathrm{s}^2) & \text{if } r_\mathrm{s} < r < a \end{cases} \tag{239}$$

where $j_0 = 5B_\mathrm{T}/\pi R$. For the profiles (237) and (239) one can estimate the value of free energy $F = \mathcal{E} + \lambda I$, by excluding the Lagrange multiplier using the $Q = 0$ relationship, where Q is given by (234). It turns out that F has a maximum at $r_\mathrm{s} = 0$ and reaches its minimum at r_s which is a bit less than a. Therefore, the JET profile corresponds to this F minimum, whereas the ASDEX profile corresponds to the relaxed state with $r_\mathrm{s} \to 0$.

Another model for optimal profile treatment was proposed by Taylor [125]. To describe the plasma state with the stochastized magnetic field lines he suggests that one considers plasma current to consist of many current filaments. Let each current-carrying filament

have the same elementary current j_s. Let (x_i, y_i) be the coordinates of the filament i in the cross section z = constant. We use notation $\psi_s(\boldsymbol{r}, \boldsymbol{r}_i)$ for the elementary poloidal flux at the point $\boldsymbol{r}$ from the ith filament with coordinate $\boldsymbol{r}_i$ in the cross section z = constant.

Then we have the equations for the $(x_i,\ y_i)$ coordinates

$$j_s \frac{\mathrm{d}x_i}{\mathrm{d}z} = -\frac{1}{B}\frac{\partial H}{\partial y_i} \qquad j_s \frac{\mathrm{d}y_i}{\mathrm{d}z} = \frac{1}{B}\frac{\partial H}{\partial x_i}. \tag{240}$$

Here

$$H = \tfrac{1}{2}\sum_{i,j} j_s^2 \psi_s(\boldsymbol{r}_i, \boldsymbol{r}_j).$$

As we see H plays the role of a Hamiltonian for the $(x_i,\ y_i)$ points considered as 'propagating in time z'.

We can use the standard statistical approach to the dynamical system (240). In particular, we can look for a 'stationary' thermal equilibrium. If many 'material points' are present we can use an averaged self-consistent value of H, so that the derivatives in (240) can be replaced by the derivatives of

$$j_s \psi(\boldsymbol{r}) = \sum_j j_s^2 \psi_s(\boldsymbol{r}, \boldsymbol{r}_j)$$

at the point $\boldsymbol{r}$. We obtain the model of particle motion in the 'gravitational' potential ψ with j_s playing the role of the mass of a particle.

If the Boltzmann distribution is reached, then

$$j = j_0 \exp(-\beta\psi). \tag{241}$$

Here $\beta = j_s/T_*$, j_0 is the central current density and T_* is some artificial 'temperature' which measures the level of magnetic-field-line stochasticity. The T_* value has no relation to the plasma temperature. Using relation (111) between j and ψ we have

$$\Delta_\perp \psi = \frac{4\pi}{c} j_0 \exp(-\beta\psi). \tag{242}$$

The solution of this equation with cylindrical symmetry looks like the canonical profile, $j = j_0(1 + r^2/a_*^2)^{-2}$. The constant a_* increases together with the artificial temperature T_*.

Thus a very simple model of current filament pattern leads to the same optimal current density profile in the stochasticized magnetic field as the variational principle. We shall discuss this feature in section 9.4.

The profile resilience phenomenon can be described quantitatively with the help of a very simple model for computer simulation [153]. This model is based on the idea that in addition to the usual heat transport flux, which is proportional to the temperature gradient, enhanced electron and ion fluxes can appear when the profiles deviate from the canonical ones. If the heat flux increase is large the optimal profile will be controlled by this feedback coupling between the profiles and non-linear transport fluxes.

This model gives quite a good numerical simulation of the experiments on optimal profile retention. It can be further extended to describe numerically the transition from the L to H mode and to hot ion and/or hot electron modes.

For this it is sufficient to assume that at a strong deviation of the real electron and ion pressure profiles from the optimal ones the effect of heat-flux increase with the deviation ceases to act. This fact can be taken into account by introducing a so-called 'forgetting factor' in the expression for the additional heat fluxes associated with the deviations from the canonical profiles.

This model leads naturally to the possibility of L-H transition when the pressure profile near the plasma edge becomes much sharper as compared with the canonical one. Another experimental fact, namely the existence of so-called hot ion and/or electron modes is again modelled sufficiently well as a result of the decrease of the effective transport coefficient when the deviations from the canonical profile are large enough.

Physically this simple model can be explained as a result of some kind of suppression of plasma turbulence or impediment for transit in the regime with the stochastized magnetic field lines when the pressure profile deviation from the canonical one exceeds some critical value.

Let us underline once more that this transport model is a strongly non-linear one. That is why it is very convenient for modelling phenomena of transitions between different confinement modes.

9.3 Spontaneous Breakdown of Symmetry

We intend to show that the high-temperature plasma in a tokamak, being practically in the collisionless regime, destroys by itself the symmetrical pattern of nested toroidal surfaces [108–111]. This breakdown of symmetry is similar to other examples of physical phenomena involving broken symmetry, such as ferromagnetism, type-II superconductivity, rotating He II and so on. However, there is an essential difference, because in a tokamak plasma the breakdown of

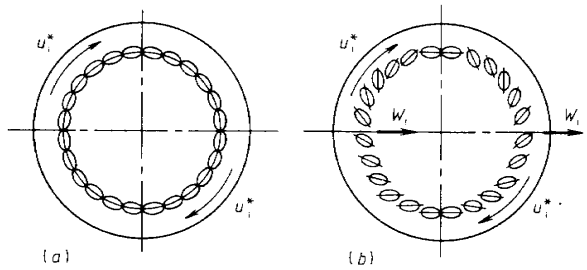

Figure 9.5 Magnetic island structures: (*a*) in the cylindrical plasma column; (*b*) toroidal variant of island structure which can be pumped by ions.

symmetry occurs in a highly non-equilibrium state and has the appearance of a self-organization phenomenon.

Let us start with a small perturbation of cylindrical symmetry. If the amplitude of the magnetic field perturbations is very low, it can be considered as a superposition of Fourier modes like $\exp(im\theta - in\varphi)$, where m, n are the azimuthal numbers, θ is the poloidal angle and φ is the toroidal angle. Each mode can be considered as very small everywhere except at the so-called rational surface where $q(r_s) = m/n$. Here q is the local safety factor, $q(r) = B_T r/B_\theta R$, B_T is the toroidal magnetic field, B_θ is the poloidal magnetic field, r is the minor radius and R the major radius.

Near the rational surface a small magnetic perturbation leads to a distortion of the initially symmetrical magnetic configuration (figure 3.7) and a helical pattern of filaments is produced (figure 9.5). Let us consider a single pattern in greater detail. We shall start with a perturbation in the case of a straight cylinder, using a cylindrical frame of reference with the variables r, θ, $z = R\varphi$. The perturbation is assumed to be helical and so is dependent on r, $m\theta - n\varphi$, t.

To describe the plasma motion we can use a set of reduced two-fluid MHD equations (139)–(143).

Thus, we use the so-called tokamak ordering, in which B_T is considered to be very large and ion motion is allowed in the transverse direction only. Thus we have $\mathrm{div}\boldsymbol{B} = \mathrm{div}\boldsymbol{B}_\perp = 0$ so that a poloidal magnetic flux can be introduced

$$\boldsymbol{B} = B_T \boldsymbol{e}_\varphi + \boldsymbol{e}_\perp \times \nabla\psi. \tag{243}$$

From the Maxwell equation for the electric field we find

$$E = -\nabla\phi' + \frac{\boldsymbol{e}_\perp}{c}\frac{\partial\psi}{\partial t}. \tag{244}$$

Here ϕ' is the electric field potential. In addition to ϕ' we shall use a notation ϕ for the normalized potential: $\phi = e\phi'/T_e$.

The electrons can be considered as being in equilibrium

$$\frac{1}{n}\nabla(nT) = -e\boldsymbol{E} - \frac{e}{c}\boldsymbol{v}_e \times \boldsymbol{B}. \tag{245}$$

The electron temperature can be considered as a constant along the magnetic field lines, so that

$$\boldsymbol{B} \cdot \nabla T_e = 0. \tag{246}$$

If we now substitute expression (244) for the electric field in equation (245) and then take its component in the magnetic field direction, we obtain

$$\frac{\partial\psi}{\partial t} + (\boldsymbol{e}_\varphi \times \nabla\lambda)\cdot\nabla\psi = B_T \frac{1}{R}\frac{\partial\lambda}{\partial\varphi} \tag{247}$$

where

$$\lambda = \frac{c}{B_T}\left(\phi' - \frac{T}{c}\ln n\right). \tag{248}$$

In the electron continuity equation we can use for the longitudinal component $v_{e\varphi}$ the relation

$$nv_{e\varphi} = -j/e = -\frac{c}{4\pi e}\Delta_\perp\psi. \tag{249}$$

The transverse component of the electron velocity can be found from equation (245), so that the density continuity equation takes the form

$$\frac{\partial n}{\partial t} + \frac{c}{B_T}(\boldsymbol{e}_\varphi \times \nabla\phi')\cdot\nabla n = \frac{c}{4\pi e B}(\boldsymbol{B}\cdot\nabla)\Delta_\perp\psi. \tag{250}$$

We shall assume that the transverse dimension of the filament structure is much less than the mean ion Larmor radius but larger than the mean electron Larmor radius. For such very short wavelength perturbations we have to use the Vlasov kinetic equation for ions instead of MHD equation. However in the first approximation the ions can be considered as being in equilibrium with the Boltzmann distribution function, so that for the density we can use the expression

$$n = n_0(1 - \kappa x - e\phi'/T_i) \tag{251}$$

where $\kappa = -(\mathrm{d}\ln n_0/\mathrm{d}x)$, T_i is the ion temperature and $x = r - r_s$ is the distance from the rational surface where $q(r_s) = m/n$. Substituting this relation for the density in equations (247), (248) and

(250), we obtain a closed set of two equations for the functions ψ and $\phi = e\phi'/T_e$

$$\frac{\partial\psi}{\partial t} + v^*\frac{1}{r}\frac{\partial\psi}{\partial\theta} = \frac{1+\tau}{\tau}D_B(\boldsymbol{B}\cdot\nabla)\phi \tag{252}$$

$$\frac{\partial\psi}{\partial t} - v^*\tau\frac{1}{r}\frac{\partial\phi}{\partial\theta} = -L(\boldsymbol{B}\cdot\nabla)\Delta_\perp\psi. \tag{253}$$

Here we have introduced the notation

$$v^* = \frac{cT_e}{eB_T}\kappa \qquad D_B = \frac{cT_e}{eB_T} \qquad \tau = T_i/T_e \qquad L = c\tau/4\pi e n_0 B_T. \tag{254}$$

Equations (252) and (253) can be used to describe non-linear plasma perturbations with helical symmetry. The set of equations (252) and (253) has an energy integral, and to find this we must multiply the first equation by $\Delta_\perp\psi$, the second by $(1+\tau)D_B\phi/\tau L$, integrate them over the cross section and sum the results. We then have

$$\mathcal{E} = \mathcal{E}_\psi + \mathcal{E}_\phi = \int\left(\frac{1}{8\pi}(\nabla_\perp\psi)^2 + \frac{1}{2\tau^2}p_0\phi^2\right)2\pi r\,\mathrm{d}\theta\,\mathrm{d}\varphi\,\mathrm{d}r \tag{255}$$

where $p_0 = n_0(T_e + T_i)$, $\phi = \tau e\phi'/T_i = -\tau\tilde{n}/n_0$, $\tilde{n}$ being the density perturbation. The total energy $\mathcal{E}$ consists of magnetic energy $\mathcal{E}_\psi$ and electrostatic energy $\mathcal{E}_\phi$.

We shall consider later the stationary rotating pattern of the helical island-chain structure in which all the variables are functions $f(\theta - n\varphi/m - uv_*t)$, u being the dimensionless phase velocity. For such perturbations we can estimate the quantity $\phi \sim \kappa\tau k\tilde{\psi}/k_\parallel B$ where $k_\parallel$ is the wave number along the magnetic field. With the help of this relation we can estimate the coupling between $\mathcal{E}_\psi$ and $\mathcal{E}_\varphi$: $\mathcal{E}_\psi \simeq \mathcal{E}_\varphi kw/\beta_\theta$, where $k = m/r$ is the wave number, w the transverse dimension of the helical island chain, and β_θ the ratio of the plasma pressure to the poloidal magnetic field pressure.

We are interested in the so-called soft modes in which $mB_\theta/r - nB_T/R$ is small. This means that $x = r - r_s$ is small too. Let us now introduce an artificial magnetic field $\boldsymbol{B}^*$, whose θ component is

$$B^*_\theta = B_\theta - nB_T r/mR \simeq -B_\theta Sx/r \tag{256}$$

where S is the so-called 'shear': $S = (r/q)\mathrm{d}q/\mathrm{d}r$. We shall introduce in addition the flux function ψ^*, so that $\boldsymbol{B}^* = \boldsymbol{e}_\varphi \times \nabla\psi^*$. Near the rational surface the equilibrium value of ψ^* is

$$\psi^* = -\frac{B_\theta}{2}\frac{S}{r_s}x^2. \tag{257}$$

Equations (252) and (253) will not be changed if the variables $\boldsymbol{B}^*$ and ψ^* are used instead of $\boldsymbol{B}$ and ψ, and the derivative $\partial/\partial z$ can be omitted when $\boldsymbol{B}^*$ and ψ^* are used. Now let us introduce the following normalized variables:

$$\psi_\alpha = \frac{r_s}{B_\theta S}\psi^* \qquad \phi_\alpha = \frac{1+\tau}{\kappa\tau}\phi. \tag{258}$$

Omitting the index α, we obtain in place of equations (252) and (253)

$$[\nabla\phi\times\nabla\psi]e_\varphi = (u-1)\frac{\partial\psi}{\partial y} \tag{259}$$

$$-[\nabla(\Delta\psi)\times\nabla\psi]e_\varphi = (u+\tau)\gamma\frac{\partial\psi}{\partial y} \tag{260}$$

where the constant $\gamma = [4\pi nT_e/(1+\tau)B_\theta^2](\kappa r_s/S)^2$ and the variable y is determined by the expression $y = r(\theta - n\varphi/m - uv_*t)$. The equilibrium function ψ_0 is given by $\psi_0 = -x^2/2$.

Equation (259) can easily be solved

$$\phi = (u-1)x + P(\psi) \tag{261}$$

where $P(\psi)$ is an arbitrary function of ψ. With the help of relation (261), equation (260) can be written in the form

$$\Delta_\perp\psi = -\gamma(u+\tau)x\frac{\mathrm{d}P}{\mathrm{d}\psi} + F(\psi) \tag{262}$$

where $F(\psi)$ is an arbitrary function of ψ.

We shall seek a solution of these equations in the form of a periodic island chain. For this purpose we can write

$$\psi = \psi_0 + \tilde{\psi} = -x^2/2 + \alpha\cos(ky) \tag{263}$$

where α is the perturbation amplitude and k is the wave number $k = m/r_s$. The amplitude α might itself be dependent on y, but in our approximation we can omit the higher harmonics in y; in other words, we can assume that α is independent of y and is a function only of x. Let us also agree to regard $\alpha(x)$ as approximately equal to its maximum value, $\alpha_0 = \alpha(x=0)$ within the magnetic islands. The curves for ψ =const, including the island structure, are shown in figures 5.6 and 9.5. These curves in fact represent the cross section of the new magnetic surfaces for helical symmetry. Since the electrons

and ions follow a Boltzmann distribution, we have what might be described—by comparison with simple cylindrical equilibria—as a broader class of equilibria.

From equation (263) it can be seen that magnetic islands form at the points $ky = 2\pi l$ where l is an integer including $l = 0$. The value of $\psi = \psi_s$ on the separatrix (separating the islands from the toroidal magnetic surfaces) can be found as the value of ψ for $x = 0$, $y = \pi$

$$\psi_s = -\alpha_0. \tag{264}$$

Accordingly, the half-width of the magnetic island, w, can be determined if we put in equation (188) $\psi = \psi_s$, $y = 0$, $x = w$:

$$w = 2\sqrt{\alpha_0}. \tag{265}$$

Thus, the island width increases with perturbation amplitude as the square root of the amplitude.

We need to construct a solution, at least an approximate one, of the non-linear equation (262) taking into account relation (261). In tackling this problem it is natural first to consider the region far from the islands where a linear approximation is valid. It is more convenient to linearize (259) and (260) on the assumption that $\tilde{\psi}$ and $\phi = \tilde{\phi}$ are small quantities periodically dependent on y. Neglecting quadratic terms, we obtain

$$x\tilde{\phi} = (u-1)\psi \tag{266}$$

$$\Delta_\perp \tilde{\psi} = -\frac{\gamma(u+\tau)}{x}\tilde{\phi} = -\frac{\Gamma}{x^2}\tilde{\psi} \tag{267}$$

where $\Gamma = \gamma(u-1)(u+\tau)$. As we can see, equation (267) has the form of a Schrödinger equation with a potential $U = -\Gamma/x^2$. Since $\Delta_\perp = (\mathrm{d}^2/\mathrm{d}x^2) - k^2$, our task reduces to seeking a bound state with energy k^2 in the potential well $U(x)$, which outside the island structure behaves as Γ/x^2.

If $\Gamma < 1/4$, then in the region of small x there are no solutions with nodes, and hence we can seek a single ground state. For large x the Laplacian $\Delta_\perp \to 0$, so that our approximate solution takes the form

$$\tilde{\psi} \simeq \alpha_0 \mathrm{e}^{-kx}\cos ky. \tag{268}$$

We may adopt the approximation that equation (267) is true for x greater than the average half width of the island structure, that is $x > w/2$. If the potential U is taken to be equal to $-\Gamma/x^2$ for

$x > w/2$, and if for $x < w/2$ we use the same linear equation but with $U = 0$, then for small Γ we can use the matching condition

$$\Delta' = -2k = -\int_{-\infty}^{-\infty} U\,\mathrm{d}x \simeq \frac{4\Gamma}{w} \tag{269}$$

where

$$\Delta' = \frac{1}{\tilde{\psi}}\frac{\partial\tilde{\psi}}{\partial x}\bigg|_{x>0} - \frac{1}{\tilde{\psi}}\frac{\partial\tilde{\psi}}{\partial x}\bigg|_{x<0} \equiv -2k$$

is the difference between the logarithmic derivatives of the asymptotic solutions, familiar to us from tearing-mode theory. And so, in accordance with expression (269), the half-width of the island is defined in terms of Γ:

$$kw \simeq 2\Gamma = 2\gamma(u-1)(u+\tau). \tag{270}$$

If Γ is small, i.e. if the phase velocity u of the island chain is close either to the electron drift velocity ($u = 1$) or the ion drift velocity ($u = -\tau$), then the islands are narrow, with small kw.

More exact relationships can be obtained with the help of an approximate solution of the non-linear equation (267), taking expression (261) into account. The function ϕ should tend to zero far from the island structure, since there is no equilibrium electric field in the frame of reference we have chosen, and since ψ tends to $\psi_0 = -x^2/2$ at large x the function $P(\psi)$ for large x must be close to $\mp(u-1)\sqrt{-2\psi}$, where the different signs before the root refer to the regions on either side of the separatrix. Thus, in order for the root to vanish at the separatrix, the function $P(\psi)$ must be proportional to $\sqrt{2(\psi_s - \psi)}$, where ψ_s is the value of ψ at the separatrix. Hence

$$\phi = x(u-1)\left[1 - \sqrt{2(\psi_s - \psi)/x^2}\right]. \tag{271}$$

This expression refers only to the region outside the separatrix where $\psi < \psi_s$. Within the separatrix we consider $\psi = \alpha_0 \cos ky$, so that in accordance with expressions (261), (271) we can match both solutions simply by putting $P(\psi) = 0$ inside the islands

$$\phi = x(u-1) \qquad \text{at} \qquad \psi > \psi_s. \tag{272}$$

In other words, the square root in expression (271) vanishes at the separatrix and continues to be zero in the region within the separatrix. Thus, we know $P(\psi)$, which can be substituted in equation (262). Within the separatrix $P = 0$, so that $\Delta_\perp \psi = F(\psi)$

there. In the approximation we have adopted, $\alpha = \alpha_0 =$ constant within the separatrix $\psi = -x^2/2 + \alpha_0 \cos ky$. Since α_0 is of the same order as w^2, the second term in the expression for $\Delta_\perp \psi$ is negligible as compared with unity in $w^2k^2 \ll 1$ and we can put $F(\psi) \simeq -1$, i.e. the equilibrium value. Outside the separatrix where $\psi < \psi_s$, the expression found above for $P(\psi)$ can be substituted in equation (262). As a result we obtain

$$\Delta_\perp \psi = \Gamma \left[\frac{x^2}{2(\psi_s - \psi)} \right]^{1/2} + F(\psi). \tag{273}$$

Far from the island, $\Delta_\perp \psi$ tends to its equilibrium value, which is equal to minus unity, so that from equation (273) we get an extremely simple expression for the function F, namely $F(\psi) = -1 + \Gamma$. Now equation (262) can be used for a more exact calculation of the matching condition in (269). In order to find the matching condition, we integrate the right-hand side of expression (273) over x. The integral of the root on the right-hand side together with a corresponding contribution in F is equal to $-\Gamma x$, where $x = 2\sqrt{a_0 |\cos ky|}$ is the position of the separatrix. In order to single out the terms that are proportional to $\cos ky$, we average both sides of equation (273) with a weighting function $\cos ky$ and integrate the left-hand side from zero to x, and the right-hand side from x_s to x. In this way we find a more exact matching condition

$$kw = \frac{16}{3\pi}\Gamma = \frac{16}{3\pi}\gamma(u-1)(u+\tau). \tag{274}$$

This condition is similar to condition (270) obtained in a simple linear approximation. Relationship (274) can be considered as an equation for determining the magnitude of the dimensionless phase velocity u. For small kw, u is either somewhat greater than unity or somewhat less than $-\tau$. In other words, the phase velocity is either somewhat greater than v^* for waves travelling along the electron drift or somewhat less than $-\tau v^*$ for waves travelling along the ion drift. The magnitude by which the phase velocity exceeds the corresponding drift velocity is proportional to kw, where w is the half-width of the island, and inversely proportional to γ, i.e. to the poloidal β_θ.

When dissipation is taken into account, both types of island structure begin to evolve with time. Let us first consider the case of a dense cold plasma which, though it bears no relationship to a tokamak plasma, is instructive from the standpoint of understanding the role of dissipation.

We take into account on the right-hand side of equation (245) a friction force of electrons with respect to the ions equal to $-m_e\nu_e \mathbf{v}_e$, where ν_e is the average frequency of electron–ion collisions. Accordingly, on the right-hand side of equation (247) for the flux function ψ an additional term $\Lambda^2\nu_e\Delta_\perp\psi$ will appear where

$$\Lambda^2 = c^2/\omega_{pe}^2 = c^2 m_e/4\pi e^2 n. \tag{275}$$

If we repeat the operations which led to the energy definition in expression (255), we will see that $\mathcal{E}$ is not conserved but rather damps

$$\frac{\partial \mathcal{E}}{\partial t} = -\frac{\Lambda^2 \upsilon_e}{4\pi} \int (\Delta_\perp \tilde{\psi})^2 2\pi r \, d\theta \, d\varphi \, dr = -\eta \int (\tilde{j})^2 2\pi r \, d\theta \, d\varphi \, dr \tag{276}$$

where $\eta = m_e\nu_e/e^2 n$ is the resistivity and $\tilde{j}$ is the perturbation of the current density: $\tilde{j} = c\Delta_\perp\tilde{\psi}/4\pi$. Since $\Delta_\perp\tilde{\psi} \sim \Gamma\tilde{\psi}/x^2$ outside the separatrix, the right-hand side of equation (276) is proportional to $\Gamma^2\alpha_0^2 w^{-3} \sim w^3$, and the energy to the square of the amplitude, i.e. $\sim w^4$. Accordingly, expression (276) leads to a monotonic decrease of the island width

$$\frac{\partial}{\partial t}(kw) = -\text{ constant}\,\Lambda^2 k^2 \nu_e. \tag{277}$$

Thus, in a dense plasma the magnetic surfaces undergo a form of self-repair as their short-wave perturbations damp with time.

In a tokamak plasma this does not happen: the magnetic islands do not damp, but rather tend to increase with time. The point is that a tokamak plasma tends to be collisionless, and Landau damping resonance effects come into play instead of Coulomb collisions. To describe these we have to use the Vlasov kinetic equations with self-consistent fields. As we will see, the exchange of energy between the wave and the electrons is weakened owing to the formation of a plateau on the electron distribution function in the region of electron resonance with the wave. The ion distribution function, on the other hand, is distorted very little because the transverse size of the island structure is substantially smaller than the average Larmor radius of the ions.

Let us assume that island structures with a characteristic width w and a characteristic wave number k fill the whole cross section of the plasma in a quite densely contiguous pattern. The perturbation of the poloidal magnetic field in each island structure is given by the relation $\tilde{B}_\theta \sim w^2 k B_\theta / r$. This perturbation extends over a width $\Delta x \sim 1/k$. The magnetic field energy density of these closely packed

structures at a distance of $\sim w$ from each other amounts to $\mathcal{E}_\psi \sim \tilde{B}_\theta^2/8\pi wk \sim w^3 k B_\theta^2/8\pi r^2$.

As to the energy associated with the electric field $\mathcal{E}_\phi$, it is localized on a length of $\sim w$ since the electric potential perturbation decreases as $1/x$ when x increases. Accordingly, we have $\mathcal{E}_\phi \sim nT(e\tilde{\phi}'/T)^2$, where $\tilde{\phi}'$ is the amplitude of the electric field potential perturbation.

Since $\mathcal{E}_\phi \sim \mathcal{E}_\psi \beta_\vartheta / kw$, we find that $e\tilde{\phi}'/T \sim w/a$. For simplicity we make no distinction here between T_e and T_i.

Let us now consider an ion with Larmor radius $\rho \sim v_\perp/\omega_{ci}$. In its motion over a Larmor circle, this ion intersects $N = \rho/w$ island structures. At each of these island structures the ion may receive a momentum increment along the y axis of the order of

$$m_i \Delta v \sim k e \tilde{\phi}' w / v_\perp \tag{278}$$

where $w/v_\perp$ is the time of crossing the structure and $k\tilde{\phi}'$ is the electric field perturbation. Owing to a change in the magnitude of the perpendicular y component of the velocity, the centre of the Larmor circle is shifted by $\sim \Delta v/\omega_{ci}$. Let ω^* be the characteristic frequency of the oscillations we are considering. Since the interaction phase persists for a time $\Delta t \sim 1/\omega^*$, in multiple crossings of a given island structure over a time $\Delta t \sim 1/\omega^*$ the ion accumulates a total shift δ, which is ω_{ci}/ω^* times greater than in the case of a single passage across the island

$$\delta \sim \frac{\omega_i}{\omega^*} \frac{e\tilde{\phi}'}{m_i v_\perp} \frac{kw}{\omega_i}. \tag{279}$$

This shift is produced by a single island structure. In fact, the ion interacts not with a single structure but with $N = \rho/w$ neighbouring structures. If the partial shifts are not phased, they can be considered as random shifts, so that the total shift of the ion along the x axis amounts to $\delta_* \simeq \delta N^{1/2} = \delta(\rho_i/w)^{1/2}$. The phenomenon of the accumulation of many single shifts is very important: the total shift does not decrease strongly with the wave number, so that even very short wave length patterns can play an essential role in plasma transport.

If we have $N = \rho/w$ waves with mean oscillation frequency ω^* and with a frequency difference of the same order of magnitude, we can consider this pattern as a quasiperiodic process with a very large period, Ω^{-1}, where $\Omega = \omega^*/N$. The time Ω^{-1} is N times greater than ω_*^{-1}. If the shifts are again summed in a random fashion, the maximum shift $\delta_{max} = \delta_* N^{1/2}$ will be

$$\delta_{max} = N\delta = \rho\delta/w \simeq a\frac{e\tilde{\phi}'}{T} \sim w. \tag{280}$$

Here we have assumed that the drift velocity ω^* is of the order $kT/m_i\omega_{ci}a$.

We see that in a quasiperiodic perturbation with frequency Ω the ion is shifted over a distance $\sim w$. Hence, in a time Ω^{-1} the ion is shifted by the width of the island structure and can enter a different non-linear resonance. In other words, Chirikov's stochasticity criterion is marginally fulfilled. Accordingly, in a system of densely packed island structures the ions can undergo stochastic diffusion across the magnetic field. Since the ions are marginally stochastic, the corresponding mechanism of diffusion and ion thermal conductivity is very sensitive and can be easily self-regulated by the degree of contact among the island structures—in other words, for a given arrangement of the island structures, by the perturbation amplitude ψ.

The process with frequency $\Omega = \omega^*/N$ is extremely slow, and for this reason each ion retains its adiabatic invariant on average. Consequently, in a homogeneous magnetic field the transverse ion energy is conserved. If the field is inhomogeneous, then a shift towards the weaker field diminishes the ion energy, so that the ion may transfer a part of its energy to the waves. In other words, a shift of ions towards increasing major radius leads to pumping of the island structure energy.

To understand the possibility of noise pumping by a single ion we can consider a very simplified picture of figure 9.6. Let us assume that we have some mixture of drift waves with the fluctuating electric fields. Next we assume that the ion can be shifted in the major radial direction over some length δ in the averaged electric field. This is an averaged drift, which has already been considered in Chapter 2.

Let the ion energy be equal to $\mathcal{E} = \mathcal{E}_\perp + \mathcal{E}_\parallel$. Then due to conservation of the adiabatic invariant and the toroidal momentum the averaged energy change of ion is $\delta\mathcal{E} = -2\mathcal{E}_\parallel\delta/R - \mathcal{E}_\perp\delta/R$, where δ is the shift. When δ is positive, the ion energy diminishes.

Let the ion be shifted radially at the inner and later on at the outer position, as shown in figure 9.6. The net ion displacement along the minor radius after averaging due to the longitudinal ion motion can be zero. But the total energy loss is not zero (it is easy to see that, due to the relation μ = constant, only the longitudinal energy can be lost in the case shown in figure 9.6). Thus in toroidal geometry the ion can directly pump the noises and lose its energy without net displacement across the magnetic surfaces, if perturbations have suitable symmetry. Of course the picture in figure 9.6 is too idealized. It is more realistic to imagine that the noise pumping is accompanied by net ion diffusion. In this case the toroidal expulsion of diamagnetic ions can serve as a noise pumping mechanism.

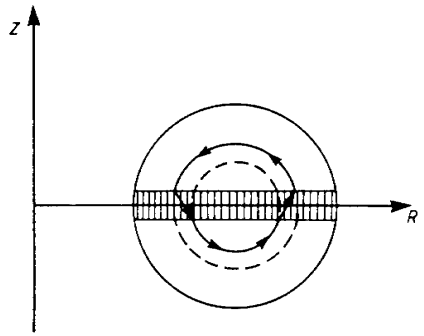

Figure 9.6 If the drift turbulence fills the hatched area and the phases of perturbations allow for ions to be shifted radially while crossing this area, then a single ion can transform some part of its energy into the energy of noise. This transformation is based on the conservation of azimuthal and magnetic momentum.

Let us consider this possible pumping mechanism in greater detail. If the island structures are touching each other, each island can be inclined with respect to the y axis by a small angle γ. Then, simultaneously with the shift along the x axis, the ion will be shifted along the y axis as well. As a result, the time of interaction with the island structure changes and becomes equal to $\Delta t \sim (1 + \gamma k\delta)\omega^*$, where $\gamma\delta$ is the shift along the y axis. Correspondingly, the value of the shift in expression (279) changes and becomes equal to

$$\delta \sim \frac{kw}{\omega^*} \frac{e\tilde{\phi}'}{m_i v_\perp}(1 + \gamma k\delta). \tag{281}$$

When $\gamma \neq 0$, a systematic ion shift in the radial direction occurs. Let us assume that the ions themselves can sustain an average value of γ in such a way that pumping of magnetic field perturbations could take place. It is possible to show [156] that in the case of a single island chain the toroidal configuration looks like figure 9.5(b), but being turned over an angle $\pi/2$. Thus the single chain cannot produce both an averaged flux and fluctuation pumping: many interacting chains are needed. We assume that pumping itself can slightly turn each island-chain in such way that the final picture looks like a superposition of the initial one and of that shown in figure 9.5(b). Since γ is small, we can find at first the linear part with respect to δ and then insert the value thus found in additional brackets evaluating the quadratic term in (281). Its averaged value corresponds to a systematic ion drift along the major radius over a time $1/\omega^*$.

The shift defined by expression (281) is produced by a single island structure, whereas the ion, in its motion along the Larmor circle, intersects $N = \rho/w$ such structures. Thus, the total systematic ion flux can be estimated with the help of relation

$$W_i = n\langle v\rangle \simeq n\omega^* N\langle\delta\rangle \simeq \gamma\kappa k^2 w^3 v_i n \tag{282}$$

where $\kappa = -\mathrm{d}(\ln n)/\mathrm{d}r$ comes from the expression for ω^*, and v_i is the mean thermal velocity of the ions.

The flux $n\langle v\rangle$ is directed along the major radius (see figure 9.5(b)). Accordingly, the islands are tilted in such a way that γ has opposite signs on the inner and outer contours (see figure 9.5(b)). In other words, γ varies as $\cos\theta$. This means that, to be continuous, $\gamma = \gamma_a\epsilon\cos\theta$, where $\epsilon = r/R_0$ and γ_a = constant. If we are seeking an average value of the flux through a toroidal surface of radius r, then $\langle v\rangle$ has to be averaged with a weighting function $(1+\epsilon\cos\theta)$ in order to take into account the θ-dependence of the surface element $\mathrm{d}s = 2\pi R\mathrm{d}\theta = 2\pi R_0(1+\epsilon\cos\theta)r\,\mathrm{d}\theta$. Accordingly, we obtain

$$\Gamma_n = \langle(1+\epsilon\cos\theta)W_i\rangle_\theta \simeq \frac{\epsilon^2}{2}\gamma_a\kappa k^2 w^3 v_i n. \tag{283}$$

Although the flux Γ_n is found to be proportional to the density gradient, as $n\kappa = -\mathrm{d}n/\mathrm{d}r$, it is still more proper to speak not of diffusion but of free convection of plasma.

The flux defined in expression (283) transfers not only particles but also ion thermal energy. The expression for the heat flux Γ_i takes a form similar to expression (283)

$$\Gamma_i = \frac{\epsilon^2}{2}\gamma_i\kappa k^2 w^3 v_i n T_i \tag{284}$$

where the coefficient γ_i allows for the fact that the heat flux can be greater than the particle flux, so that γ_i can be greater than γ_0. Furthermore, the product $\gamma_i\kappa$ can depend on the temperature gradient.

When the ions are shifted along the major radius, their transverse energy diminishes as $1/R$ owing to conservation of the transverse adiabatic invariant and the longitudinal energy decreases as $1/R^2$ owing to conservation of the azimuthal momentum. For this reason, the flux defined in expression (283) is responsible for noise pumping with a power

$$\frac{\partial\mathcal{E}}{\partial t} \simeq \frac{W_i T_i}{R} \simeq \gamma_i\frac{r\kappa}{R^2}k^2 w^3 v_i n T_i. \tag{285}$$

This energy pumping must be correlated with momentum pumping. The wave momentum can be obtained by dividing the wave energy by the phase velocity $v_\phi = -\omega^*\tau/k = -v^*\tau$. Accordingly, the momentum pumping is equal to $(-1/v^*\tau)\partial\mathcal{E}/\partial t$. Due to wave momentum pumping the ions experience a reaction force directed opposite to the rotation of the island structure, which in fact means that a friction force is acting upon them. As a result an ion flux Γ_n appears, since the friction force acting on the ions is balanced by the Lorentz force $-eBc^{-1}\Gamma_n$. From the momentum balance condition $(-1/v^*\tau)\partial\mathcal{E}/\partial t = -eBc^{-1}\Gamma_n$, taking into account expressions (283) and (284), we find $\gamma = \gamma_a r\kappa/2$. Since all the expressions are very approximate, we can simply say that $\gamma_i \sim \gamma_a$. In other words, the ion heat flux is of the order of the convection flux: $\Gamma_i \sim T_i\Gamma_n$.

Let us now consider the behaviour of the electrons. To describe them we can use a drift-kinetic equation

$$\frac{\partial f}{\partial t} + v(\boldsymbol{b}\cdot\nabla)f + \frac{c}{B}(\nabla\phi'\times\nabla f)e_\varphi = \frac{e}{m_e}E\frac{\partial f}{\partial v}. \qquad (286)$$

Here f is the electron distribution function with respect to longitudinal velocity v, $\boldsymbol{b} = \boldsymbol{B}/B$ and E is the longitudinal component of the electric field: $E = \partial\psi/c\partial t - \boldsymbol{b}\cdot\nabla\phi'$. For helical symmetry the expression $(\boldsymbol{b}\cdot\nabla)$ again becomes equal to $(\boldsymbol{B}^*/B)\cdot\nabla$, and we can use ψ^* instead of ψ, dropping the asterisk again.

Let us use a frame of reference rotating with the phase velocity of the wave, v_ϕ. Then, introducing the helical momentum $P = mv + e\psi/c$, we can express kinetic equation (286) in a simpler form

$$\partial f/\partial t = (\nabla H\times\nabla f)e_z \qquad (287)$$

where f is considered as a function of P and the Hamiltonian H is

$$H = \frac{c}{2m_e cB}(P - \frac{e}{c}\psi)^2 - \frac{c}{B}\phi' + xv_\phi. \qquad (288)$$

According to these equations, the electrons move along the lines H = constant, keeping P = constant. We see that island structures are also formed on the drift surfaces near the resonance points where $\omega = k_\parallel v$. Since the longitudinal wave number $k_\parallel$ has opposite signs on opposite sides of the point $r = r_s$, drift islands appear on electrons having different signs of v on opposite sides of the resonance point. On the drift islands, plateau-type distributions at P = constant are easily formed, since a rarefied plasma does not have time to dissipate

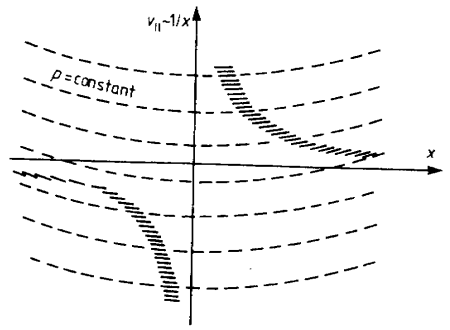

Figure 9.7 Plateau formation on the electron distribution function in phase space. The plateau develops along the dotted lines P = constant.

through collisions (see figure 9.7). Hence, the formation of a single island structure is not prevented by electron collisionless damping.

As a result, many island chains continue to grow until they begin to interfere with each other; the interaction between the island chains via electrons begins only when they touch each other. Once the drift surfaces are in contact, the electron drift trajectories become stochastic and the electrons are able to transfer a longitudinal momentum across the plasma (figure 9.7). Hence, anomalous resistivity, η_a, appears which leads to the saturation of island structure growth by ion pumping. As a matter of fact, it would be more correct to speak not of resistivity but of viscosity, because the averaged resistivity related to the averaged current density remains the same. The anomalous resistivity η_a can be evaluated if we assume that an anomalous collision frequency ν_a appears

$$\nu_a \simeq k_\parallel v_e \simeq (v_e/qR)kw. \qquad (289)$$

Now we can estimate the magnetic diffusion coefficient: $D_a = c^2\eta_a/4\pi = \Lambda^2\nu_a \sim \Lambda^2 kwv_e/qR$.

We can find a more accurate value for η_a in the linear approximation

$$\eta_a = \frac{m_e}{e^2 n}\sqrt{\pi T_e/2m_e}|k_\parallel|. \qquad (290)$$

This expression would be true if a Maxwellian electron velocity distribution were restored fairly quickly either by collisions or by exchanges of electrons between neighbouring island structures.

Let us now use the total energy balance

$$\partial\mathcal{E}/\partial t = 2\gamma_L\mathcal{E}_\phi - (v_e/qR)F_e\mathcal{E}_\psi. \qquad (291)$$

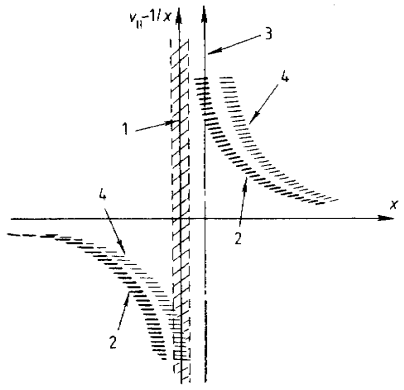

Figure 9.8 Contact between the plateaux of two neighbouring island chains in phase space: 1—rational surface and island chain (hatched area) of the first wave; 2—plateau on $f_e(v_\parallel)$; 3—second rational surface; 4—plateau formation due to the second island chain.

Here γ_L is a growth rate produced by ions, and with the factor $F_e = \Lambda^2 k^2 F'$, where $F' < 1$, we have taken into account the possibility of self-adjustment of wave damping by the electrons. Factor F_e increases with k as k^2 so that shorter waves decay faster. If there is a family of island chains their average energy decay will be dominated by waves with the maximum k values, but the wavenumber k cannot be larger than Λ^{-1}. Thus, for the average decay rate we can assume $\langle \Lambda^2 k^2 \rangle \sim 1$, so that $F_e \sim F'$. The factors F_e, and F'_e may be very small, but with increasing oscillation amplitude and closer contact between the islands the factors F'_e and F_e increase. Since the factor F_e is capable of self-adjustment, it automatically establishes itself at a value such that the island structures are maintained in a steady state (on average). Thus, even with weak ion wave pumping broken magnetic field symmetry in a tokamak plasma can be maintained. The magnetic surfaces break down to a slight extent, being filled with a large number of helical magnetic structures. This pattern looks similar to the picture, previously suggested by Rebut *et al* [109] using qualitative arguments.

Since the islands are formed by current filaments located on both sides of each island outside the separatrix, it is fair to say that the plasma is filled with a huge quantity of current filaments. These filaments are arranged in such a way that the currents flow parallel to the lines of force on the rational magnetic surfaces $q(r) = m/n$,

where the island centres are located. Note that in fact the current filaments are located not inside the magnetic islands but in a layer with a thickness of the same order as the island width, i.e. w. Since the currents in the plasma are screened over a thickness of the order of Λ, there exists a minimum dimension of island width, i.e. $w \geqslant \Lambda$.

Let us note further that the longitudinal phase velocity of the waves, $\omega_* \tau / k_\parallel$, is extremely large on the resonance surface $k_\parallel = 0$ and becomes of the order of the thermal electron velocity only at a distance $x \geqslant \rho_\theta$ from the resonance surface (where ρ_θ is the electron Larmor radius in the poloidal magnetic field). Only at this distance does the mechanism of island structure damping by electrons come into play; the quantity ν_a can be considered zero at $x < \rho_\theta$. Consequently, very small structures with $wk < 1$ and $k\Lambda \rangle 1$ show extremely weak damping even in the linear approximation, i.e. without any allowance for the plateau effect in phase space on the electron distribution function. Summing up, we can say that the magnetic structure is generated in such a way as to enable the electrons at any moment to switch on the anomalous transport mechanism. That is why the electron transport is so sensitive to any external perturbation and to non-linear phenomena in the edge and bulk plasmas.

9.4 Physics of Transport

The breakdown of magnetic symmetry and the formation of a large number of mutually contiguous helical structures leads to anomalous electron heat conduction. If the mean width of the structures is w, the anomalous thermal conductivity can be evaluated as $\chi_e \sim \nu_a w^2$. Let k be the mean wave number of the island structures. Then the thermal conductivity of the electrons can be written in the form

$$\chi_e = w^3 k \Phi_e v_e / qR \qquad (292)$$

where the tuning factor Φ_e takes account of the degree of contact among the island structures.

Let us first consider the case of weak contact, which can occur at low level of wave pumping by the ions. In this case a steady state is reached at $F_e \ll 1$ when the island structures are just beginning to come into contact with each other. The factor Φ_e in formula (292) is correspondingly small. Let us try to estimate it.

For this purpose we assume that in toroidal geometry a stochastization of the lines of force near the separatrix occurs in a layer comprising a fraction $\epsilon = r/R$ of the island width w. If an exchange of electrons between neighbouring island structures were to

take place in this layer, then both heat and longitudinal momentum could be transferred across this field. The cross-field transport involves preferentially slow passing electrons which carry practically no longitudinal momentum. The fraction of such electrons is $\sim \epsilon$. If we accept that $kw \sim 1$, $w^2 \sim 4\pi\Lambda^2 \sim 1/r_0 n$, we get the estimate

$$\chi_e \sim \epsilon^{3/2} \frac{v_e}{qRnr_0} \tag{293}$$

where $v_e = 2\sqrt{T_e/m_e}$, and $r_0 = e^2/m_e c^2$ is the classical electron radius. This quantity is close to the superclassical value (221) obtained on $T-11$ and is in line with the formula for χ_e suggested by Ohkawa [123]. The transport of longitudinal momentum affects those electrons which carry the momentum, i.e. those with a longitudinal velocity $v \sim v_e$. For these electrons there may be a very small transverse exchange and the factor F_e can then have a value substantially less than Φ_e. Variations in the factor F_e will not affect the heat transport described by relation (293) which is associated exclusively with slow passing electrons. In other words at low level of ion pumping the relation (293) is almost constant when ion pumping has a value in the main part of its range of variation.

Expression (293) corresponds to the minimum level of electron transport in a fairly quiet plasma, albeit one with slightly distorted magnetic field symmetry.

When the magnetic surfaces are only slightly disturbed, the ion dynamics is not very strongly modified. Thus, along with the scaling in (293) we would expect neoclassical ion heat conductivity to accompany electron thermal conductivity of the T-11 level. A regime of this kind corresponds to neo-ALCATOR or IOC scaling of a tokamak plasma with ohmic heating.

If ion pumping becomes more powerful, then the mechanism of enhanced transport appears which is naturally linked with L-mode confinement. This mode is created by the same island structures, but with closer contact. To understand the physics of this more powerful transport regime, we must take into account the ion pumping of magnetic perturbations by the mechanism described above.

With pumping according to (285), the magnetic noise energy balance equation takes the form

$$\frac{\partial \mathcal{E}}{\partial t} = F_i \frac{a v_i}{R^2} k^2 w^2 nT - F_e \frac{v_e}{qR} \frac{w^3 k}{a^2} \frac{B_\theta^2}{8\pi}. \tag{294}$$

where $F_i = \gamma_i \kappa w$ is a small ion control factor, and v_i and v_e are the ion and electron thermal velocities.

With high pumping power we may assume that the islands are pumped up to a level $wk \sim 1$. In this approximation for the average steady state we obtain an estimate of the characteristic island width

$$\frac{w^2}{a^2} \approx \frac{F_i}{F_e} \frac{qa}{R} \beta_\theta \sqrt{\frac{m_e}{m_i}}. \tag{295}$$

The ratio F_i/F_e depends implicitly upon k and w. However, relying on experimental data we can accept that this dependence is weaker than the strong F_i/F_e sensitivity to the level of stochastization. In this approximation F_i/F_e can be considered as a tuning factor.

Substituting this value for w^2 in the electron thermal diffusivity expression, we obtain

$$\chi_e = \Phi_e \frac{v_e}{qR} w^2 = \mu_e \frac{v_i a^3}{R^2} \beta_\theta. \tag{296}$$

Here the factor $\mu_e = F_i \Phi_e / F_e \ll 1$, since F_i is a small parameter. If the electron loss channel dominates, we can estimate the energy confinement time as $\tau_E \sim a^2/4\chi_e$, where a is the plasma minor radius and χ_e is some averaged value of the electron thermal conductivity. With the help of the energy balance equation, $3nTV = P\tau_E$, where V is the plasma volume and P is the heating power, we can express τ_E through the plasma parameters

$$\tau_E = C I R^{1.5} a^{-0.5} A_i^{0.25} P^{-0.5}. \tag{297}$$

Here I is the plasma current and A_i is the atomic mass number. The factor C is a slowly varying function of some of the plasma parameters and can be considered approximately as a constant.

The scaling (297) is similar to the so-called L mode of confinement.

Thus the strongly stochasticized ion regime corresponds to L-mode confinement. According to expression (294), the island width w in an L-mode regime is a certain fraction of a. If the plasma density decreases, the length Λ increases and at some density value the relationship $\Lambda \ll w$ will no longer hold true. From this density value downward neo-ALCATOR scaling is valid (this transition was discussed in [124]).

Thus we have shown that a spontaneous breakdown of magnetic symmetry takes place in a practically collisionless high-temperature tokamak plasma. This breakdown of symmetry looks like plasma self-organization: magnetic island chains fill the whole plasma cross section and are in contact with each other. The transverse size of these islands is much smaller than the mean ion Larmor radius but larger than the electron Larmor radius.

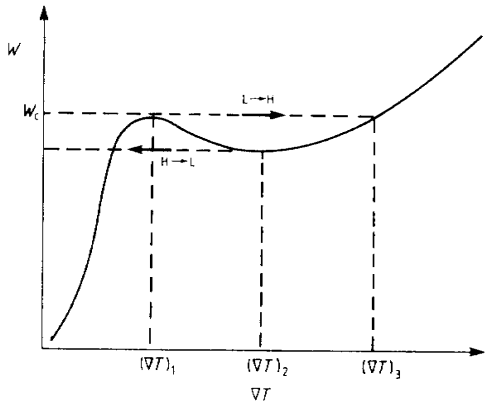

Figure 9.9 Thermal flux to the wall as a function of the edge plasma temperature gradient [117]. Depression of thermal conductivity is produced by turbulence suppression due to shear rotation of plasma [128].

Both ions and electrons are marginally stochastic in such a pattern. The magnetic noise is maintained by the ions owing to their convection in the direction of the weaker magnetic field. As they are essentially stochastic, the ions can pump island structures, propagating in the direction of the ion magnetic drift.

Both ions and electrons can tune their levels of transport, so that this mechanism is very sensitive to the profiles, boundary conditions and so on. This is why I have deliberately avoided trying to find, theoretically, a numerical factor C in expression (297) for the scaling. The great sensitivity of transport to external influences provides a clue to understanding why almost the same expressions—similar to expressions (297)—are valid for both L and H modes of confinement.

Another result which follows from the mechanism considered above is the possibility of continuous transition from scaling with auxiliary heating to neo-ALCATOR scaling when the density decreases. Neo-ALCATOR scaling is, as it were, the best mode of confinement which can be realized with the quietest plasmas.

Up to now we have discussed cooperative phenomena in the bulk plasma. Experiments show that strong non-linear phenomena develop in the edge plasma as well. Here a very strong non-linear activity is observed which looks like MHD-turbulence of the electrostatic drift type. The L-H transition phenomenon is related to this edge plasma activity.

The most plausible explanation for L-H transition is based [115–

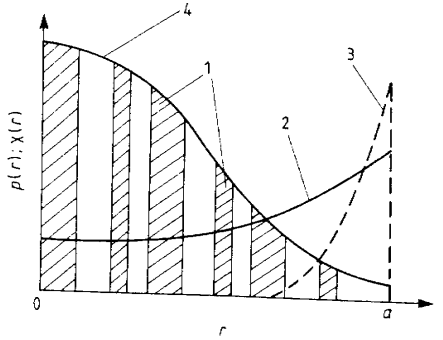

Figure 9.10 Schematic diagram of the plasma transport self-organization: 1—thermal flux produced by deviation from optimal profile; 2—bulk plasma transport; 3—transport at the plasma edge; 4—pressure profile.

118] on the idea of boundary plasma stabilization by differential rotation, which can damp the edge plasma turbulence. The edge plasma becomes quieter, and this effect can diminish the bulk plasma transport if it is sensitive to external noise pumping.

The theory was developed in parallel with experiments [129–133] which are in correlation with the theoretical approaches. The general theoretical idea is illustrated by figure 9.9, taken from Hinton's paper [117]. It shows the edge thermal flux dependence upon the plasma temperature gradient near the edge. This dependence can be a non-monotonic one if an electric field builds up which can stabilize the edge turbulence—and diminish the thermal flux. If one starts to increase the thermal flux, for instance, by injection of additional power into the bulk plasma, the temperature gradient also increases up to the critical value W_c of the thermal flux. After this the temperature gradient jumps to the higher value $(\nabla T)_1$. It is just an L-H transition, when the 'thermal barrier' is developed near the chamber wall. When W diminishes, the backwards transition H-L takes place at a somewhat lower value $(\nabla T)_2$. Thus hysteresis appears which is observed sometimes in experiments.

Now we can conclude discussion of the plasma transport self-organization phenomenon by a very simplified picture as in figure 9.10. It shows the plasma pressure profile in accordance with the 'profile-consistency' principle. The different mechanisms of thermal conductivity are shown in the same figure. The first one is exaggeratedly shown as stripes near the rational points. This mechanism controls the profile itself and saw-teeth are the most striking

representative of these partners.

The next is the bulk transport which is produced as a result of magnetic symmetry break-down. This mechanism defines global scaling for the energy confinement time. Accompanied by a slight current filamentation it can assist profile consistency formation by a mechanism similar to that considered by Taylor [125]. We have to assume simply that the filamented portion of current looks like a mixture of strings playing the role of a filament ensemble. Finally, we have a very strong activity at the edge which controls the transition from one mode of confinement to another and its influence extends well over the bulk plasma.

Cooperative action of these three mechanisms of enhanced transport with addition of neoclassical transport is responsible both for global plasma confinement and feedback couplings between profiles and fluxes. Their interplay controls the plasma self-organization phenomena including the existence of different modes of confinement.

10 Heating and Current Drive

The simplest method of plasma heating is ohmic heating: the current circulating in plasma needed for its equilibrium simultaneously heats plasma due to its ohmic resistivity. Ohmic heating is used in all small-size tokamaks. In larger tokamaks it serves to prepare initial plasma with not very high temperature. At higher temperatures ohmic heating is not effective since plasma resistivity decreases as temperature grows. To reach higher temperatures additional plasma heating is required. At the present time numerous methods of plasma heating have been developed, e.g. beam injection of neutral atoms of high energy, electromagnetic waves, adiabatic plasma compression along the minor and major radii. RF-heating embraces a wide range of frequencies and corresponds to various plasma oscillation modes: ion-cyclotron resonance (ICR), electron-cyclotron resonance (ECR), lower-hybrid resonance (LH) and Alfven waves (AW). Many heating methods including neutral injection can be used for non-inductive current drive [135].

10.1 Ohmic Heating

Plasma specific resistivity is very low: at multi-keV temperatures it is much lower than that of copper. In practical units the specific resistivity according to Spitzer is equal to

$$\eta \simeq 3 \times 10^{-8} Z_{\rm eff} T_{\rm e}^{-3/2} \qquad (\Omega\ {\rm m}). \tag{298}$$

Here $T_{\rm e}$ is electron temperature, in keV, $Z_{\rm eff}$ is the effective ion charge number. The rapid decrease of resistivity with increasing temperature makes ohmic heating ineffective at temperatures above a few keV. However, low resistivity has an advantage: at high temperatures the U loop voltage should be significantly lower than the common value of the order of 1 volt for tokamaks with moderate electron

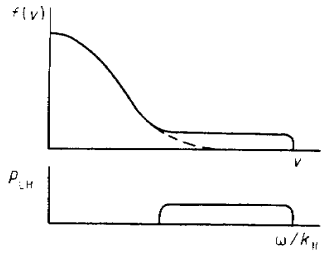

Figure 10.1 Electron distribution function modification by low-hybrid waves.

temperatures. Lower U values mean that there is a possibility of prolonged ohmic current drive at one and the same consumption of Volt-seconds. There are three effects which may slightly increase loop voltage: the presence of impurities leading to Z_{eff} increase, the neo-classical effect of current-carrier decrease, and reconnection of magnetic lines, particularly, in saw-tooth oscillations.

10.2 Lower Hybrid Resonance

Plasmas can be heated efficiently by waves with frequencies near the geometric mean of ion and electron gyro frequencies

$$f_{\text{LH}} = 0.65B\sqrt{A_{\text{i}}} \qquad \text{(GHz)} \tag{299}$$

where A_{i} is the atomic number. For these frequencies (a few GHz), the index of refraction for the plasma is large, highly anisotropic and depends strongly on density. As a result, the plasma reflects the wave, thereby precluding direct heating. Rather, it is necessary for a slow wave to tunnel through the edge plasma. A grill—a system of juxtaposed waveguides—is used for the launching of waves into plasma. The launcher should be placed very close to the plasma.

The waves in the region of lower-hybrid resonance are very convenient for current generation. The current generation physics is explained by figure 10.1 that shows how the energy electron 'tail' grows due to resonance absorption of lower-hybrid waves with phase velocity spectra shown in the same figure.

The wave with the phase velocity $v_\phi = \omega/k_\parallel$ establishes a local plateau on the electron distribution function due to the simple resonance $\omega - k_\parallel v = 0$. Adjusted to each other many local 'steps' on

the distribution function produce an extended plateau as shown in figure 10.1. The plateau formation can be described theoretically with the help of quasilinear theory. We see that the electron current generation relates to a somewhat more complicated physical mechanism than the simple transfer of longitudinal momentum from waves to electrons. The high-energy tail generation leads to more effective current drive than simple 'pushing' of the electron distribution by momentum transfer. The reason is that the high energy electrons have a much lower collision frequency with the thermal electrons than thermal electrons themselves. Thus the full distribution function of figure 10.1 is 'centred' by the collisions in such a way that the main electron velocity is not zero.

The 'tail' electrons slow down finally on the plasma electrons and ions due to binary Coulomb collisions. The effectiveness of the current drive is determined by the balance of power gained from the waves and lost due to pair collisions of tail electrons with the thermal particles.

The current drive method by lower-hybrid waves has been used in many facilities. The best results with an efficiency of $\gamma_{\text{CD}} = 0.34$ and total current up to about 2 MA were obtained in JT-60 [134]. The corresponding experimental data are shown in figure 10.2. The results with the efficiency of $\gamma_{\text{CH}} = 0.34$ were obtained while injecting 2-4.5 MW of power of lower-hybrid waves with density up to $\bar{n}_{\text{e}} = 0.3 \times 10^{20}\,\text{m}^{-3}$ and a current $I = 1$–1.75 MA. Note that, for steady current drive in the ITER tokamak, an efficiency of $\gamma_{\text{CD}} = 0.5$ is required.

Unfortunately, this method is not suitable for current drive in the central part of the plasma with high density and should be supplemented by other waves or neutral injection.

10.3 Ion-cyclotron Resonance

Electromagnetic waves in the range of ion-cyclotron resonance

$$f_{\text{ci}} = 15BZ/A_{\text{i}} \qquad \text{(MHz)} \tag{300}$$

penetrate plasma easily enough and are absorbed near the resonant layer of plasma, where the wave frequency coincides with one of the harmonics of gyro frequency. This method is well developed: heating physics is clear and efficient antennas for the launch of RF-power into plasma have been developed. To improve wave propagation in plasma as well as their effective absorption in the resonant layer, the method of minorities has been used. If the absorption occurs on

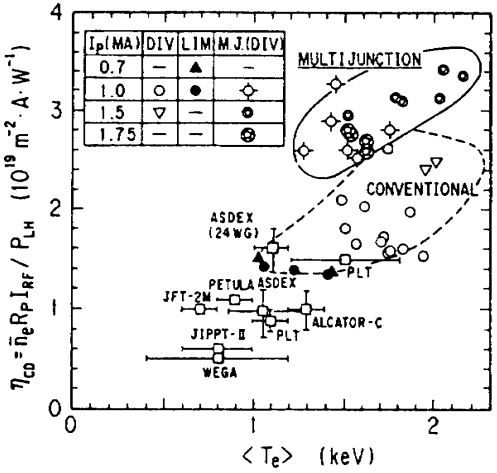

Figure 10.2 Summary of the low-hybrid current drive efficiency in JT-60 and other tokamaks [134, 147].

the ions of the minority species, then the ions are heated up to high energies, and the heating mode resembles fast ion injection.

To maintain current drive by waves which are directed along the toroidal column, one can use two possibilities. If a uni-directional fast ion tail could be generated in plasma, then the current is generated similarly to that by neutral injection. In the second possibility damping of cyclotron waves occurs on electrons at resonance on electron transit frequency. Theoretically $\gamma_{CD} \sim 0.2$–0.4 efficiency has been predicted, but additional experiments are required to support the theory.

10.4 Electron-cyclotron Resonance

This heating method is based on the absorption of RF-waves of ordinary or extraordinary polarization and with frequency near the electron gyrofrequency

$$f_{ce} = 28B \qquad \text{(GHz)} \tag{301}$$

or higher harmonics.

The absorption occurs in the region of Doppler resonance where $\omega - n\omega_{ce} = kv_{\parallel}$. In the case of propagation nearly perpendicular

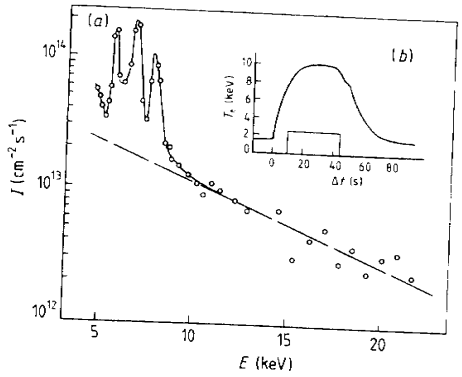

Figure 10.3 Heating with ECRH in T-10: (*a*) time integrated x-ray spectrum over the heating pulse; the dashed line is a fit to the spectrum obtained, assuming an electron temperature on the axis of 8 keV and a typical radial profile; (*b*) time evolution of the electron temperature on the axis measured by ECE.

to the magnetic field the resonance may broaden by the relativistic dependence of the electron mass on its energy.

Similarly to the lower hybrid current drive the main idea of current drive by ECR consists of such a deformation of the electron distribution function that its steady state would correspond to non-zero net longitudinal velocity. For instance, let resonance condition $\omega = \omega_{ce} + k_{\parallel}v$ correspond to the resonance of electrons with velocity $v > 0$ of the order of thermal velocity. These electrons are accelerated by the wave in such a way that their transverse velocity increases. The 'depleted region' left by these electrons in the distribution function will be filled by thermal electrons, both with positive and negative values of v. Thus the net number of electrons with $v > 0$ is increased so that a negative electron current is generated. Here again a net current is produced since high-energy electrons have much lower collision rates than thermal electrons.

The advantage of this method is in the use of waveguides without the introduction of any special plasma facing components (however, reliable windows transparent in this frequency region are needed).

The ECR-method has gained broad development after new RF-waves generators—gyrotrons—had been created. Figure 10.3 shows the results of T-10 electron component heating, where up to 10 keV temperature was obtained with the help of a powerful set of gyrotrons.

At the present time new methods of electron plasma component heating in strong magnetic fields—free electron lasers and cyclotron auto resonant masers (CARM)—are being developed.

In principle, ECR-waves may also be used for current drive. The current drive mechanism is related to the anisotropy of the electron distribution function, which occurs at the scattering and slowing down of ECR-heated electrons. These experiments are in progress now [136, 137].

10.5 Neutral Injection

Neutral injection as an effective means of high-temperature plasma heating was suggested a long time ago and is used at present: many large tokamaks have powerful injectors for plasma heating and current drive. The physical process consists of injecting a beam of high-energy neutral particles into plasma. The neutral beam atoms become ionized by charge exchange and by inelastic collisions with electrons and ions. Then the high energy ions are confined by the magnetic fields and slowed down by binary collisions with the background plasma, which is consequently heated. The fraction of energy transferred to ions and electrons depends on the E_f beam energy: if $E_f > 15T_e$, then the electrons are heated preferentially and if $E_f < 15T_e$, the ions are. The penetration depth of fast neutrals into plasma depends on the beam energy and plasma density. In the energy range from 20 to 200 keV per nucleon it can be approximated as

$$\lambda \simeq 5.5 \times 10^{-3}(E_f/A_f)n_e^{-1} \qquad \text{(m)}. \tag{302}$$

Here E_f/A_f is the energy of the beam particles in keV per nucleon, n_e is mean electron density in $10^{20}\,\mathrm{m}^{-3}$.

To increase the beam absorption by plasma tangential injection is used. The penetrating beam may be directed either in the same direction as the current (co-injection), or in the opposite direction (counter-injection). Using only one direction of injection leads to plasma rotation with a consequent decrease of heating effectiveness: plasma 'runs away' from the beam, so that the energy of the beam relative to plasma decreases. To avoid this effect a balanced injection co- and counter the current direction was used in TFTR.

Neutral injection may be used for current drive. Initially the concept of this current drive scheme was proposed by Ohkawa [138]. His idea was as follows. If a neutral beam is directed in a tangential direction, then after ionization it can produce a positively charged ion beam. It looks like a tail on the ion distribution function. Formally, we can find the corresponding beam current I_b, but in fact it is not

the electric current: the electrons are carried together with ions so that the whole plasma then rotates. What is required is the electron drift with respect to ions.

The simplest way to do this is to inject neutrals with ion charge number Z_b different from the average plasma ion charge number Z_{eff}. The electron drag by each ion is proportional to Z^2 per ion or to Z per the given charge density. Thus an ion tail with $Z \neq Z_{\mathrm{eff}}$ will drag electrons and net electron current is equal to $I = I_b(1 - Z_b/Z_{\mathrm{eff}})$. When $Z_b > Z_{\mathrm{eff}}$ this current is oppositely directed to I_b. This is the simplest mechanism of current drive by neutral beams.

If Z_b is not very different from Z_{eff}, as in the case of deuterium beam injection in pure deuterium or deuterium–tritium plasmas the more delicate mechanism of current drive may exist. The ion distribution function has again a high energy tail and the electron distribution function in equilibrium can have non-zero averaged velocity in the ion frame of reference. This is a result of the collision cross section dependence upon the energy. The net effect is much smaller but may be sufficient for a current drive in the high-temperature plasma when the averaged current drift velocity is less than the ion thermal velocity.

This method is convenient for existing tokamaks due to the fact that the beam of neutral particles penetrates plasma deeply enough, so that it can be used for current drive inside the central core of the plasma column. Driven currents in the range of 1 MA were demonstrated in TFTR [139] and JET [140] by means of neutral injection, and in the range of 0.5 MA in DIII-D [141]. Current drive efficiency in units of $10^{20}\,\mathrm{m}^{-2}\,\mathrm{MA/MW}$ equals

$$\gamma_{\mathrm{CD}} = \bar{n}_e IR/P. \tag{303}$$

It reached the values of $\sim 3 \times 10^{-2}$ (in TFTR) in agreement with the theoretically predicted value. Theory predicts an efficiency one order of magnitude higher in fusion reactor plasma. But the energy of beam particles has to be increased to guarantee their penetration deeply into plasma.

10.6 Other Schemes of Heating

In small and medium-size facilities other heating modes are used, e.g. adiabatic plasma compression, Alfven wave heating, 'helicity' injection, [142–144] etc. Adiabatic compression is a simple method of pulsed plasma heating. It uses a variable magnetic energy only and is quite convenient for small size tokamaks. Both minor and major radii compressions were tested in small and medium size tokamaks.

Alfven waves are again quite convenient for smaller tokamaks . This method of heating can also be used for current drive with good efficiency. But in large size tokamaks this scheme looks somewhat complicated demanding a large additional coil structure.

In future fusion reactors plasma will be heated by fast alpha-particles which are the product of D–T reactions. Theoretically, the possibilities of using alpha-particle power for the current generation are being studied.

11 The Burning Plasma

The burning plasma [145] can be heated by the fusion reaction products. In a D–T plasma these are alpha-particles with high energies. Single alpha-particles can be trapped by the tokamak magnetic fields. According to calculations, only a small fraction of alpha-particles may be lost due to toroidal drift (bearing in mind the toroidal magnetic field non-uniformity) at a plasma current over 3 MA. However, effects of collective behaviour of alpha-particles are not to be excluded.

The most attractive regime of a fusion reactor is that close to steady-state burn, when the reaction can be self-sustained without external additional power. A self-sustained fusion reaction has been the cherished dream of many physicists during many years of fusion research. However, a completely self-sustained fusion reaction may not be an optimal solution. Firstly, to control the burn it is desirable to have additional power that would allow us to adjust the reaction rate. Secondly, the best operation mode is steady-state operation of a fusion reactor. To implement this mode one should introduce power to maintain current drive.

In any case the power of alpha-particles would be high enough, and, therefore, their influence on plasma behaviour would also be high. The most dangerous are those collective phenomena that could lead to loss of fast alpha-particles from plasma before they are slowed down in plasma. Alpha-particles may generate many waves in plasma. The most dangerous are the effects of 'fish-bone'-type instability and internal Alfven modes excitation.

Theoretically, one of the dangerous mechanisms is the excitation of the so-called TAE-modes (toroidal Alfven eigenmode) [146]. Their physics is explained in figure 11.1, which shows the dependence on radius r of the frequency of local kink Alfven modes with low numbers of m, n. Since the oscillation frequency depends on the radius, the waves at various points on the radius will 'spread' in phase, so that local waves 'wrinkle up', $k \to \infty$, and then propagate along the

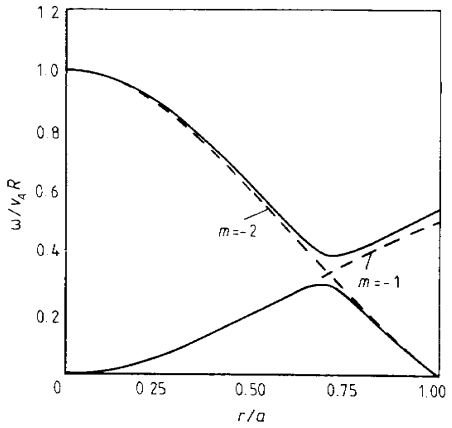

Figure 11.1 Toroidal Alfven eigenmode spectrum in a tokamak.

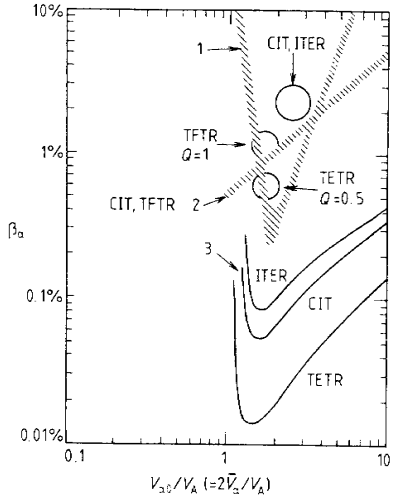

Figure 11.2 Reactor plasma instability thresholds: 1—ballooning mode; 2—fish-bone instability; 3—TAE mode [145].

radius due to finite Larmor radius effects. However, two modes, as can be seen from figure 11.1, may cross-over, and in the presence of

toroidicity they are linked to each other, so that a 'gap' is formed. This is the condition when a TAE-mode may occur. Near the point of former cross-over, global waves appear which can grow. Here we have a kind of fibre-glass analogue which has a refraction index higher than in the surrounding medium. This means, that due to 'total internal refraction' there is a possibility of Alfven wave 'waveguide' propagation. This is the very TAE-mode which may persist in plasma for a long time and interact with alpha-particles.

Figure 11.2 shows the excitation thresholds for fish-bones and TAE-modes depending on the alpha-particle β_α as a function of the ratio of its velocity to the Alfven phase velocity. The β_α value is the ratio of the alpha-particle pressure to the magnetic field pressure. β_α grows together with the D–T reaction power and the plasma temperature since at higher temperatures the process of alpha-particle thermalization slows down.

Figure 11.2 shows that thresholds increase with the size of the facility so that in ITER, for example, these modes could be harmless.

The present level of fusion research is close to being sufficient for plasma burning and the construction of an experimental fusion reactor.

12 Conclusion

For those readers who, like me, prefer to look through the Introduction and Conclusion before deciding whether it is worthwhile reading all the text, I shall try to summarize the main content of this book.

The tokamak is a Russian invention due to two Nobel Prize winners, Andrei Sakharov and Igor Tamm. The word 'tokamak' itself is simply an abbreviation for the more precise specification of this invention: 'toroidal chamber with magnetic coils'.

A tokamak is the simplest configuration for plasma magnetic confinement. It looks like a simple toroidal vacuum chamber immersed in a toroidal magnetic field. The torus itself can be considered as a closed secondary loop in a magnetic transformer with an iron core (see figure 3.4). When the primary coil is energized a secondary current is induced in the plasma coil produced by the gas break-down.

In the simplest case of ohmic discharge the plasma persists for a short time only when a unidirectional inductive electric field is maintained inside the vacuum chamber. The plasma current has to be high enough: the poloidal magnetic field produced by this current provides the plasma equilibrium along the major radius, assisted by an additional vertical magnetic field.

The inductive electric field maintains the current and provides ohmic heating power mainly inside the high-temperature plasma core. This power is sufficient to heat the plasma core up to a temperature of the order of tens of millions of degrees. The power is supplied in a sufficiently ordered form so that the entropy per unit energy is very low.

The plasma energy is transported towards the cold walls by thermal conductivity. The closer to the walls the lower is the plasma temperature and therefore the entropy flux increases rapidly towards the walls. It means that the entropy production rate increases rapidly with approach to the walls. In other words, a tokamak plasma is a typical open system with energy flux through it accompanied by intensive entropy production inside it.

It is known that many dissipative open systems of such a kind reveal different modes of self-organization: some part of energy flux and entropy production rate can be intercepted and used by the system to complicate its internal structure. Many new secondary coherent structures and turbulent chaotic noise may be produced by such mechanisms. The plasma is especially volatile matter with a very low dissipation rate so that secondary structure production is inherent to it. As experiments show, the tokamak plasma is a complex physical system with many mechanisms of self-organization evolving simultaneously. These mechanisms control the plasma behaviour. We have to underline that these mechanisms are strongly non-linear so that to investigate and to understand them and their interplay is not a simple matter. Fortunately, a lot of experimental data with theoretical discussions have been accumulated in previous years and we have now a safe base for tokamak plasma physics.

The first and the most striking indication of non-standard plasma behaviour is the electron thermal conductivity. Experiments show that the electron thermal conductivity is two orders of magnitude higher than the classical value produced by particle collisions. This fact indicates that some cooperative processes are present in plasma.

To explain the anomaly several attempts have been made based on the consideration of the so-called drift modes, that is, slow waves with very long wavelengths along the magnetic field lines. However, all such mechanisms lead either to Bohm-like or to gyro-Bohm transport which is strongly dependent upon the value of the magnetic field. Experiments do not display such strong dependence. That is why drift waves cannot provide a reasonable explanation in spite of the fact that the absolute value of transport predicted by them is not very different from the experimental values.

As for me, I believe that the explanation is a different one but it is not drastically different from the drift waves approach. As it is argued in section 9.3. I suggest we accept that the tokamak magnetic structure is spontaneously broken. This breakdown of symmetry could be termed microtearing modes, but I would prefer not to use this word simply to avoid the habitual way of imagining at first some ideal symmetrical geometry and to investigate its instability with respect to small magnetic surface deformations. Let us accept that the magnetic symmetry is destroyed initially and can be considered as filled by many island-chain structures rotating in the ion drift direction. Such structures have electric field perturbations and ions have the ability to pump these structures directly due to toroidal curvature of tokamak plasma. This possibility is illustrated by figure 9.6, where it is shown that a single ion can perform the work in the averaged vertical electric field near the median plane. The work

is accompanied by ion shift in the major radius direction and with the corresponding diminishing of ion energy.

Thus the pumping of perturbations by ions maintains the broken symmetry. As it is argued in section 9.3, a very delicate balance can be reached when both electrons and ions are in the regime of stochastic motion. Ions pump the noise while electrons damp it and as a result a self-organized structure is produced with strongly anomalous electron behaviour and with moderately enhanced ion transport.

The electron current density is slightly filamented to assure the existence of magnetic-island structure and this feature itself can lead to the effect of current profile control. Indeed the tokamak plasma demonstrates a very impressive peculiarity, namely so-called 'profile consistency'. It looks like a tendency to retain optimal radial distribution profiles of plasma pressure and temperature. These profiles resist any attempts to modify them for instance by a change of external power deposition profile.

These profiles may change suddenly with simultaneous plasma transition from one to another mode of confinement. The best known examples are the so-called L (low) and H (high) modes of confinement. They differ by several times with respect to the energy confinement time. This fact shows the tokamak plasma is a strongly non-linear system. Such systems can have a non-single-valued state of equilibrium. In other words, the non-linear equations which describe their behaviour can display branching of their solutions. Such branching corresponds to different modes of confinement with different plasma profiles.

Several approaches might be suggested to describe this complicated matter. The most perfect one consists in a detailed investigation of all the elementary non-linear mechanisms which lead to plasma self-organization. We have to analyse all plasma instabilities in linear and non-linear regimes, to find the characteristics of microturbulence, to classify all saw-tooth phenomena near the magnetic axis, to classify and describe all non-linearities near the plasma edge including turbulence suppression by differential plasma rotation etc. Then we could try to combine all the findings into one integrated picture of complex plasma behaviour. All these efforts are under way.

In parallel with this ambitious activity simpler approaches would be welcome which are based either on simple physical arguments or on specially developed numerical models. Such approaches are discussed in section 9.2 in connection with the 'profile consistency' phenomenon. The first one is based on the energy variational principle. It compares the energies of two neighbouring states: an initial

one and one with a turbulent stochastic layer. If the energy variation is zero, the initial state is marginally unstable with respect to a perturbation which stochastizes magnetic field lines and can produce enhanced transport. The corresponding profiles can be considered as limiting ones prescribed by the profile consistency principle.

If it is assumed that enhanced transport is produced by a local deviation from the optimal profile, then a very simple transport model can be suggested which describes the feature more precisely. With an additional assumption that with a strong deviation from the optimal profile the stochastic mode cannot be developed and transport 'forgets' that the optimal profile exists, more complicated phenomena like L–H transition or the central 'hump on profile' development can be described by this simple computer model. A quite different approach to understand the optimal profile phenomenon is based on the physical model of plasma current filamentation.

Many violent non-linear phenomena can develop near the plasma edge where the plasma physics is complicated by different atomic processes. Many examples of such non-linear phenomena are known now from different tokamaks.

The most familiar ones are edge localized modes (ELM)s and multifaceted asymmetric radiation from the edge (MARFE) .

In spite of the many plasma instabilities and non-linearities, the tokamak concept demonstrates the ability to heat and to confine high-temperature plasma. Experimental efforts have led to the safe confinement of plasma with high pressure of the order of one tenth of the magnetic field pressure. Experiments have clarified the area of stable plasma operation. On the current density plane this operation region is given by the so-called Hugill plot (figure 3.9).

The operation limits appear at low and high density values and at plasma current increase. The most interesting from the practical point of view is the region of high density and large current. On the Hugill plot this is the upper right corner of the operation area. Here plasma handling has to be very careful, negligent operation can cause current disruption, i.e. by complete plasma destruction. Experiments show that a high-temperature plasma, with parameters acceptable for a future reactor, can be maintained for a long time in large facilities when the plasma is handled delicately.

For a fusion reactor completely stationary plasma operation is preferable. To realize steady-state operation a non-inductive current drive is needed. Assisted by the bootstrap current, i.e. current generation by the plasma itself, different schemes of current drive are under investigation providing the possibility of mastering this mode of operation for future fusion reactors.

Tokamak plasma physics has reached a mature state now. A ma-

jor effort by experimentalists and theoreticians has resulted in establishing the physical basis of a tokamak high-temperature plasma confined by strong toroidal and poloidal magnetic fields. A clear understanding of many physical processes in plasma has been achieved. Many processes in plasma are well-simulated by computer codes. The database established in preceding years has proved sufficient for the design and the subsequent construction of an experimental thermonuclear reactor, ITER, for instance.

Studies have revealed that the tokamak plasma is a very complex physical object with numerous internal feedback links and different forms of self-organization. Therefore, to master all the potential of the plasma physical properties aimed at its optimal utilization in future fusion reactors one should conduct further research aimed at detailed studies of all fine physical processes that exist in high-temperature tokamak plasma. This research will be carried out on a more sophisticated experimental basis and using more advanced diagnostics. We may believe that these investigations will lead eventually to a practical assessment of fusion energy and to the creation of fusion power in the next century.

References

[1] Sakharov A D 1990 *Fear and Hope* (Moscow: Interverso) pp 155–163 (in Russian)

[2] Tamm I E 1958 Theory of magnetic thermonuclear fusion reactor (Part 1) *Plasma Physics and Problems of Controlled Fusion* vol 1 (Moscow: AN SSSR) (in Russian) pp 3–19

[3] Sakharov A D Theory of magnetic fusion reactor (Part 2) *Plasma Physics and Problems of Controlled Fusion* vol I (Moscow: AN SSSR) pp 20–30 (in Russian)

[4] Tamm I E Theory of magnetic fusion reactor (Part 3) *Plasma Physics and Problems of Controlled Fusion* vol 1 (Moscow: AN SSSR) pp 31–41 (in Russian)

[5] Bezbatchenko A L, Golovin I N, Kozlov P I, Strelkov A S and Yavlinsky I A Electrodeless high-current discharge in a toroidal chamber with longitudinal magnetic field. *Plasma Physics and Problems of Controlled Fusion* vol 1 pp 116–133 (in Russian)

[6] Leontovich M A and Shafranov V D On the stability of a flexible conductor in a longitudinal magnetic field *Plasma Physics and Problems of Controlled Fusion* vol 1 pp 207–213 (in Russian)

[7] Shafranov V D On the stability of a plasma column in the presence of a longitudinal magnetic field and conducting casing *Plasma Physics and Problems of Controlled Fusion* vol 1 pp 130–143 (in Russian)

[8] Gorbunov E P and Razumova K A 1963 Effect of strong magnetic field on magnetohydrodynamic stability of plasma and confinement of charged particles in the tokamak device *Atomic energy* **15** 363–370 (in Russian)

[9] Galeev A A and Sagdeed R Z Transport phenomena in rarefied plasma in toroidal magnetic traps *ZhETF* **53** 338–359 (in Russian)

[10] Artsimovich L A 1972 Tokamak Devices *Nuclear Fusion* **12** 215–252

[11] Artsimovich L A 1967 On the prospects of controlled fusion research *Usp. Fiz. Nauk* **91** 365–379 (in Russian)

[12] Kadomtsev B B 1967 Plasma instability and controlled fusion reactions *Usp. Fiz. Nauk* **91** 381–387 (in Russian)

[13] Vlasenkov V S *et al* 1977 Fast-Neutral-Beam Injection Experiments in T-11 *6th Int. Conf. on Plasma Physics and Controlled Nuclear Fusion Research, (Berchtesgaden, 1976)* vol 1 (Vienna: IAEA) pp 86–94

[14] Parker *et al* 1985 Progress in Tokamak Reseach at MIT *Nucl. Fusion* **25** 1127–36

[15] Leonov V M, Merezkin V G, Muchovatov V S, Sannikov V V and Tilinin G N 1981 Ohmic-heating and neutral beam injection studies

on the T-11 tokamak *8th Int. Conf. on Plasma Physics and Controlled Nuclear Fusion Research (Brussels, 1980)* vol 1 (Vienna: IAEA) pp 394–403

[16] Blackwell B *et al* 1983 Energy and impurity transport in ALCATOR-C Tokamak *9th Int. Conf. on Plasma Physics and Controlled Nuclear Fusion Research (Baltimore, 1982)* vol 2 (Vienna: IAEA) pp 27–40

[17] ASDEX team 1989 The H-mode in ASDEX *Nuclear Fusion* **29** 1880–992

[18] Artsimovich L A and Shafranov V D 1972 Tokamak with non-circular cross section of plasma coil *Pis'ma v ZhETF* **15** 72–6

[19] Barsukov A G *et al* 1983 Investigation of plasma confinement and injection heating in the T-11 tokamak *9th Int. Conf. on Plasma Physics and Controlled Nuclear Fusion Research (Baltimore, 1982)* vol 1 (Vienna: IAEA) pp 83–94

[20] Hawriluk R J *et al* 1987 TFTR Plasma Regimes *Plasma Physics* **1** 51–64

[21] Bush C E *et al* 1990 Limiter H-mode experiments on TFTR *13th Int. Conf. Plasma Phys. and Controlled Nucl. Fus. Res. (Washington, October 1990)* vol 1 pp 309–23

[22] Coppi B 1980 Nonclassical transport and the 'principle of profile consistency' *Comments Plasma Phys. Contr. Fusion* **5** 261–9

[23] Bell V G 1989 An overview of TFTR confinement with intense neutral beam heating *Plasma Physics* **1** 27–40

[24] Alikaev V V *et al* 1988 Effect of power profile fed to the plasma on the efficiency of ECR heating in T-10 *Fizika Plazmy* **14** 1027–45

[25] Alikaev V V *et al* 1985 Electron cyclotron heating plasma confinement in the T-10 tokamak *Plasma Physics and Controlled Nuclear Fusion Research* **1** 419–32

[26] Shimomura Y *et al* 1985 Empirical scaling of energy confinement time of L-mode plasma and optimized mode and some consideration of reactor core plasma in tokamak *Japanese Atomic Energy Research Institute* JAERI-M 87-080

[27] Goldston R J 1984 Energy confinement scaling in tokamaks *Plasma Phys. Contr. Fusion* **26** 1A 87–103

[28] Yushmanov P N *et al* 1990 Scalings for tokamak energy confinement *Nucl. Fusion* **30** 1999–2006

[29] Zarnstorff M *et al* 1988 Transport in TFTR supershots *12th Int. Conf. on Plasma Physics and Controlled Nuclear Fusion Research (Nice, France, 12–19 October 1988)* vol 1 (Vienna: IAEA) pp 183–91

[30] Aikawa H and JT-60 team 1988 Recent progress in JT-60 experiments *12th Int. Conf. on Plasma Physics and Controlled Nuclear Fusion Research (Nice, October 1988)* vol 1 (Vienna: IAEA) pp 67–81

[31] Kadomtsev B B and Pogutse O B 1973 Nonlinear helical plasma perturbations in the Tokamak *ZhETF* **65** 575–89 (in Russian)

[32] Rosenbluth M N *et al* 1976 Numerical studies of nonlinear evolution of kink modes in tokamaks *Phys. Fluids* **19** 1987–96

[33] Izzo R *et al* 1983 Reduced equations for internal kinks in tokamaks *Phys. Fluids* **26** 3066–78

[34] Strauss H R 1976 Nonlinear, three-dimensional magnetohydrodynamics of noncircular tokamaks *Phys. Fluids* **19** 134–40

[35] Strauss H R 1983 Finite-aspect-ratio MHD equations for tokamaks *Nucl. Fusion* **22** 649–55

[36] Sykes A and Wesson J A 1976 Relaxation instability in tokamaks *Phys. Rev. Lett* **37** 140–3

[37] Weller A *et al* 1987 Density perturbations at rational q-surfaces following pellet injection in JET *14th European Conf. on Controlled Fusion and Plasma Physics (Madrid, 1987)* Part 1 pp 25–8

[38] Gusiatnikova V I, Samokhin A V, Titov V S, Vinogradov A M and Yumagujin V A 1989 Symmetries and conservation laws of Kadomtsev–Pogutse equations *Acta, Applicantal Mathematical* **15** 23–64

[39] Coppi B, Galvao R, Pelat R, Rozenbluth M and Rutherford P 1976 Internal resistive screw modes *Fiz. Plazmy* no 2–6 961–6 (in Russian)

[40] Kadomtsev B B 1963 Hydrodynamic plasma stability *Voprosy teorii plazmy* no 2 (Moscow: Gosatomizdat) p 132 (in Russian)

[41] Kadomtsev B B 1958 *On the hydrodynamics of low-pressure plasma* (Moscow: AN SSSR) no 4 pp 16–24 (in Russian)

[42] Pogutse O P and Yurchenko E I 1982 Ballooning effects and plasma stability in tokamaks *Voprosy teorii plasmy* (Moscow: Energoizdat) **11** 56–118 (in Russian)

[43] Shafranov V D and Yurchenko E I 1967 Flute instability criterion for plasma in toroidal geometry *ZhETF* **53** 1157 (in Russian)

[44] Mercier C 1987 *Lectures in Plasma Physics* (Brussels and Luxembourg: Euratom) EUR 5127EN

[45] Mikhailovskii A B and Shafranov V D 1973 On hydromagnetic stability of Spitzer figure 8-type Stellarators with high pressure plasma *Pis'ma v ZhETF* (in Russian)

[46] Mikhailovskii A B and Shafranov V D 1974 Self-stabilization effect of high-density plasma in toroidal traps *ZhETF* **66** 190–199 (in Russian)

[47] Navratil G A *et al* 1990 Study on high poloidal beta plasmas in TETR and DIII-D *13th Int. Conf. on Plasma Physics and Controlled Nuclear Fusion Research (Washington, October 1990)* vol 1 pp 209–18

[48] Troyon F *et al* 1984 MGD-limits to plasma confinement *Plasma Phys. Contr. Fusion* **6** 209

[49] Coppi B, Filreis J and Mark J W 1979 Topology and physics on internal modes in magnetically confined plasmas *7th Int. Conf. on Plasma Physics and Controlled Nuclear Fusion Research (Innsbruck, 1978)* vol 1 (Vienna: IAEA) pp 793–8

[50] Sykes A M *et al* 1979 MHD theory of ballooning modes applied to JET, and the effect of anisotropic pressure on ballooning modes *7th Int. Conf. on Plasma Physics and Controlled Nuclear Fusion Research, (Innsbruck, 1978)* vol 1 (Vienna: IAEA) pp 625–36

[51] Mercier C 1979 MHD stability criteria for localized displacements *7th Int. Conf. on Plasma Physics and Controlled Nuclear Fusion Research, (Innsbruck, 1978)* vol 1 (Vienna: IAEA) pp 701–13

[52] Taylor T S *et al* 1990 Profile optimization and beta discharges in DIII-D *13th Int. Conf. on Plasma Physics and Controlled Nuclear Fusion Research (Washington, October 1990)* vol 1 pp 177–94

[53] Lazarus E A *et al* 1990 Stability of high elongation plasmas in the DIII-D Tokamak *13th Int. Conf. on Plasma Physics and Controlled Nuclear Fusion Research (Washington, October 1990)* vol 3

[54] Kadomtsev B B, Pogutse O P and Yurchenko E I 1982 Non-linear MHD equations and dissipative ballooning modes *9th Int. Conf. on Plasma Physics and Controlled Nuclear Fusion Research (Baltimore, 1982)* vol 1 (Vienna: IAEA) pp 67–75

[55] Hender T C, Crassie K and Zehrfeld H P 1989 Resistive ballooning modes in the second stable regime *Nucl. Fusion* **29** 1459–67

[56] Tang W M, Connor J W and White R B 1981 Finite-gyro-radius stabilization of ballooning modes in a toroidal geometry *Nucl. Fusion* **21** 891–892
[57] Bussac M W *et al* 1975 Internal kink modes in plasmas with circular cross sections *Phys. Rev. Lett* **35** 1638–41
[58] Nave M FF and Wesson F 1988 Stability of the ideal M=1 mode in tokamak *Nucl. Fusion* **28** 297–301
[59] Kadomtsev B B 1975 Tokamaks and dimensional analysis *Fiz. Plasmy* **1** 531–5 (in Russian)
[60] Connor J W and Taylor J B 1977 Scaling laws for confinement *Nucl. Fusion* **17** 1047–55
[61] Connor J W Invariance principles and confinement *Plasma Phys. Contr. Fusion* **30** 619–50
[62] Murakami M *et al* 1976 Some observations on densities in tokamak experiments *Nuclear Fusion* **16** 347–8
[63] Stoff P E and Hugill F *et al* 1977 High density discharges with gettered torus walls in DITE *8th European Conf. on Controlled Fusion and Plasma Physics, (Prague, 1977)* vol 1 p 37
[64] Greenwald M *et al* 1986 *A New Look at Density Limits in Tokamaks PFC/JA-86-22* (Plasma Fusion Center, Massachusetts Institute of Technology)
[65] Alladio F, De Marco F and Pieroni L 1987 Confinement ohmically heated plasma *14th European Conf. on Controlled Fusion and Plasma Physics (Madrid, 1987)* **1** 61–4
[66] Mirnov S V and Semenov I B 1978 Initial stage of discharge in tokamak devices *Fiz. Plasmy* **4** 50–60 (in Russian)
[67] Mirnov S V 1983 *Physical Processes in Tokamak Plasmas* (Moscow: Energoatomizdat) (in Russian)
[68] Dnestrovsky Yu N, Kostomarov D P and Popov A M 1979 Dynamics of magnetic islands in the case of non-monotonic current profile in a tokamak *Fiz. Plazmy* **5** 519–26 (in Russian)
[69] Von Goeler S, Stodiek W and Sauthoff N 1974 Studies of internal disruptions and M=1 oscillations in tokamak discharges with soft-x-ray technigues *Phys. Rev. Lett* **33** 1201–3
[70] Kadomtsev B B 1975 On disruption instability in tokamaks *Fiz. Plazmy* **5** 710–5
[71] Sweet P A 1958 *Electromagnetic Phenomena in Cosmic Physics* (London: Cambridge University Press) 123–35
[72] Parker E N 1957 *J. Geophys. Res* **62** 509
[73] Park W and Monticello D A 1989 Sawtooth oscillations in tokamaks *Preprint PPPL-2601* (Princeton University)
[74] McGuire K and Robinson D C 1979 Sawtooth oscillations in a small tokamak *Nucl. Fusion* **19** 505–7
[75] Samain A *Introduction to Tokamak Physics* (Association Euratom-CEA)
[76] Lichtenberg A J 1984 Stochasticity as the mechanism for the disruptive phase of the M=1 tokamak oscillations *Nucl. Fusion* **24** 1277–89
[77] Wesson J A 1990 On sawtooth reconnection *13th Int. Conf. on Plasma Physics and Controlled Nuclear Fusion Research (Washington, 1990)* vol 2 pp 79–85
[78] Bagdasarov A A *et al* 1979 Studies on ohmic heating in T-10 *7th Int. Conf. on Plasma Physics and Controlled Nuclear Fusion Research, (Innsbruck,1978)* vol 1 (Vienna: IAEA) pp 35–49

[79] JET TEAM 1990 Sawteeth and their stabilization in JET *13th Int. Conf. on Plasma Physics and Controlled Nuclear Fusion Research, (Washington, October 1990)* vol 1 pp 437–51
[80] Fredrickson E *et al* 1990 Partial and full reconnection during sawtooth activity and disruptions *13th Int. Conf. on Plasma Physics and Controlled Nuclear Fusion Research (Washington, October 1990)* vol 1 pp 559–71
[81] Alikaev V V, Razumova K A and Sokolov Yu A 1975 Instability connected with the beam of runaway electrons in TM-3 Tokamak *Fiz. Plazmy* **1** 546–55 (in Russian)
[82] Kadomtsev B B and Pogutse O P 1967 Electric conductivity of plasma in strong magnetic field *ZhETF* **53** 2025–33 (in Russian)
[83] Bell M, Aruhasalam V, Bitter M *et al* 1981 Recent PDX Results *10th European Conf. on Controlled Fusion and Plasma Physics* **2** 16–20
[84] Chen L *et al* 1984 Excitation of internal kink modes by trapped energetic beam ions *Phys. Rev. Lett.* **54** 1122–5
[85] Coppi B and Porcelli F 1986 Theoretical model of fishbone oscillations in magnetically confined plasmas *Phys. Rev. Lett.* **57** 2272–5
[86] Heidbrink W W and Sager G 1990 The fishbone instability in the DIII-D tokamak *Nucl. Fusion* **30** 1015–25
[87] Von Goeler S, Kluber O, Fussmann G, Gernhardt F and Kornherr M 1989 MHD activuty during ELMS *IPP 111/143* (Max-Planck Institut für Plasmaphysik)
[88] Aratari R *et al* 1988 ASDEX—experimental results and comparison with theoretical studies *Max-Planck-Institute für Plasmaphysik, Annual report* **5** 62
[89] Burrell K H *et al* 1989 *Plasma Phys. Contr. Fusion* **1** 1649
[90] Vollmer O *et al* 1990 *Controlled Fusion and Plasma Phys., Proc. 17th Conf. (Amsterdam , 1990)*
[91] Lipschultz B *et al* 1984 Marfe: an edge plasma phenomenon *Nucl. Fusion* **24** 977–88
[92] Drake JF 1987 Marfes: radiative condensation in tokamak edge plasma *Phys. Fluids* **30** 2429–33
[93] Lipshultz B 1987 Review of Marfe phenomena in tokamaks *J. Nucl. Mater.* **145–147** 15–25
[94] Galeev A A and Sagdeev R Z 1973 'Neoclassical' theory of diffusion *Voprosy teorii plazmy* (Moscow: Atomizdat) **7** 205–73 (in Russian)
[95] Hinton F L and Hazeltine R D 1976 Theory of plasma transport in toroidal confinement systems *Rev. Mod. Phys.* **48** 239–308
[96] Chang C S and Hinton F L 1982 Effect of finite aspect ratio on the neoclassical ion thermal conductivity in the banana regime *Phys. Fluids* **25** 1493–94
[97] Ware A A 1970 Pinch oscillations in unstable tokamak plasma *Phys. Rev. Lett* **25** 1 916–9
[98] Bickerton R J, Connor J W and Taylor JB 1971 Diffusion driven plasma current and bootstrap tokamak *Nature* 229 110–13
[99] Kadomtsev B B and Shafranov V D 1971 Stationary tokamak *Plasma Physics and Contr. Nucl. Fusion Res.* (Vienna: IAEA) 479–89 (in Russian)
[100] Cordey L G, Challis C D and Stubbertield 1988 *Plasma Phys. Contr. Fusion* **30** 1625
[101] Bell M *et al* 1989 An overview of TFTR confinement with intense neutral

beam heating *12th Int. Conf. on Plasma Physics and Controlled Nuclear Fusion Research (Nice, October 1988)* vol 1 (Vienna: IAEA) pp 27–40

[102] Adams J *et al* 1989 Latest JET results and future prospects *12th Int. Conf. on Plasma Physics and Controlled Nuclear Fusion Research (Nice, October 1988)* vol 1 (Vienna: IAEA) pp 41–65

[103] Aikawa H *et al* 1989 Recent Progress in JT-60 Experiments *12th Int. Conf. on Plasma Physics and Controlled Nuclear Fusion Research (Nice, October 1988)* vol 1 (Vienna: IAEA) 67–81

[104] Muller E R *et al* 1988 Improved confinement at high densities in ohmically heated and gas refuelled divertor discharges in ASDEX *Plasma Phys.* **1** 19–21

[105] Akatova T Yu *et al* 1990 Investigation of improved confinement regimes and density limit in tthe TUMAN-3 tokamak *13th Int. Conf. on Plasma Physics and Controlled Nuclear Fusion Research (Washington, October 1990)* vol 1 pp 509–22

[106] Bush C E *et al* 1990 Limiter H-mode experiments on TFTR *13th Int. Conf. on Plasma Physics and Controlled Nuclear Fusion Research (Washington, October 1990)* vol 1 pp 309–24

[107] Scott S D *et al* 1989 Local transport measurements during auxiliary heating in TFTR *12th Int. Conf. on Plasma Physics and Controlled Nuclear Fusion Research (Nice, October 1988)* (Vienna: IAEA) **1** 27–40

[108] Kaye S M and Goldston R J 1985 Global energy confinement scaling of neutral beam heated tokamaks *Nucl. Fusion* **25** 65–9

[109] Rebut P H, Lallia P P and Watkins M L 1988 Chaotic magnetic topology and heat transport in tokamaks *JET Report* JET-P(88)05

[110] Odajima K, Shimomura Y 1988 Energy confinement scaling based on offset linear characteristics *JAERI-M 88-068* (Japanese Atomic Energy Research Institute)

[111] Schissel D *et al* 1990 H-mode energy confinement scaling from the DIII-D and JET tokamaks *JET Report.* JET-P(90)16

[112] Scott S D *et al* 1989 Current drive and confinement of angular momentum in TFTR *12th Int. Conf. on Plasma Physics and Controlled Nuclear Fusion Research (Nice, October 1988)* (Vienna: IAEA) **1** 655–68

[113] Vasin N L, Esipchyk Yu V, Razumova K A and Sannikov V V 1987 'Canonical' and 'limiting' profiles in a tokamak *Fiz. Plazmy* **13** 109–13 (in Russian)

[114] Esipchuk Yu V and Kadomtsev B B 1986 Optimal current density distribution in a tokamak *Pis'ma v ZhETF* **43** 573–575 (in Russian)

[115] Taylor J B 1974 Relaxation of toroidal plasma and generation of reverse magnetic fields *Phys. Rev. Lett* **33** N 19 1139–41

[116] Hsu J Y and Chu M S 1986 On the tokamak equilibrium profile *GA-A18275 GA Technologies*

[117] Biskamp D 1986 *Preprint IPP 6/258 Max-Plank-Institute für Plasmaphysik*

[118] Kadomtsev B B 1986 Self-organization in tokamak plasma *Izv. VUZov* **29** 1032–40 (in Russian)

[119] Lazzaro E *et al* 1988 Relaxation model of H-modes in JET *JET Report* P(88) 48

[120] Scott B D and Hassam A B 1987 Analytical theory of nonlinear drift-tearing mode stability *Phys. Fluids* **30** 90–101

[121] Qu W X and Callen J D 1985 Nonlinear growth of a single neoclassical MHD tearing mode in a tokamak *University of Wisconsin Plasma Report 85-5 October 1985*

[122] Carrera R, Hazeltine R D and Kotschenrenther M 1986 Island bootstrap current modification of the nonlinear dynamics of the tearing mode *Phys. Fluids* **29** 899–901

[123] Ohkawa T A 1978 Transport Model for Alcator Scaling in Tokamaks *Phys. Lett* **67A** 35–8

[124] Kadomtsev B B 1985 Tokamak energy confinement 1, 2 *Comments Plasma Phys. Controlled Fusion* **9** 227–37

[125] Taylor J B 1990 Natural Profiles and Transport in Tokamaks *IAEA Meeting on Tokamak Transport PPPL (USA, 8-10 October 1990)* (Vienna: IAEA)

[126] Itoh S and Itoh K 1988 Model of the H-mode in tokamaks *HIFT-158 Hiroshima University*

[127] Taylor R J 1990 Forced poloidal rotation *IAEA Meeting on Tokamak Transport PPPL (USA, 8-10 October 1990)* (Vienna: IAEA)

[128] Hinton F L 1990 Thermal confinement bifurcation and the L- to H-mode transition in tokamaks *IAEA Meeting on Tokamak Transport PPPL (USA, 8-10 October 1990)* (Vienna: IAEA)

[129] Taylor R J *et al* 1989 H-mode behavior induced by cross-field currents in a tokamak *Phys. Rev. Lett.* **63** 2365–68

[130] Weynants R R *et al* 1990 H-mode behaviour induced by radially outwards fields imposed in TEXTOR *13th Int. Conf. on Plasma Physics and Controlled Nuclear Fusion Research (Washington, October 1990)* vol 1 pp 473–82

[131] Hickok R L *et al* 1990 Turbulent Fluctuations and Transport in TEXT *13th Int. Conf. on Plasma Physics and Controlled Nuclear Fusion Research (Washington, October 1990)* vol 1 pp 229–34

[132] Grobner R J *et al* 1990 Role of the edge electric field and microturbulence in the L-H transition *13th Int. Conf. on Plasma Physics and Controlled Nuclear Fusion Research (Washington, October 1990)* vol 1 pp 453–60

[133] Burell K H *et al* 1990 Physics of the L to H transition in the DIII-D tokamak *Phys. Fluids* B **2** (6) 1405–10

[134] Imai T *et al* 1990 Lower hybrid current drive and higher harmonic ICR heating experiments on JT-60 *13th Int. Conf. on Plasma Physics and Controlled Nuclear Fusion Research (Washington, October 1990)* vol 1 pp 645–57

[135] Fisch N J 1987 Theory of Current Drive in Plasmas *Rev. Mod. Phys.* **59** 175–230

[136] Prater R *et al* 1989 Electron cyclotron heating experiments in DIII-D tokamak *12th Int. Conf. on Plasma Physics and Controlled Nuclear Fusion Research (Nice, October 1988)* vol 1 (Vienna: IAEA) pp 527–40

[137] Alikaev V V *et al* 1991 ECCD experiments on T-10 *Proc. 18th European Conf. on Controlled Fusion and Plasma Phys.* 3–7 III 361–4

[138] Ohkawa T A 1970 New method of driving plasma current in fusion devices *Nucl. Fusion* **10** 185–8

[139] Meade D M *et al* 1990 Recent TFTR results *13th Int. Conf. on Plasma Physics and Controlled Nuclear Fusion Research (Washington, October 1990)* vol 1 pp 9–24

[140] Rebut P H and the JET Team 1990 Recent JET results and future

prospects *13th Int. Conf. Plasma Phys. and Controlled Nuclear Fusion Research (Washington, October 1990)* vol 1 pp 27–52
[141] Nagami M JT-60 Team 1990 Recent experiments in JT-60 *13th Int. Conf. on Plasma Physics and Controlled Nuclear Fusion Research (Washington, October 1990)* vol 1 pp 53–68
[142] Kirov A *et al* 1990 Current drive by Alfven waves (helicity injection) *13th Int. Conf. on Plasma Physics and Controlled Nuclear Fusion Research (Washington, October 1990)* vol 1 pp 831–7
[143] Darrow D *et al* 1990 Results of the helicity injection experiments for tokamak current drive *13th Int. Conf. on Plasma Physics and Controlled Nuclear Fusion Research (Washington, October 1990)* vol 1 pp 839–46
[144] Avinash K and Kaw P K 1990 High frequency surface helicity injection in toroids with moving boundaries *13th Int. Conf. on Plasma Physics and Controlled Nuclear Fusion Research (Washington, October 1990)* vol 1 pp 847–54
[145] Furth H P *et al* 1990 Burning plasmas *Nucl. Fusion* **30** 1799–816
[146] Cheng C Z 1990 Alpha particle destabilization of the toroidicity-induced Alfven eigenmodes *Rep. Princeton Plasma Phys. Lab PPPL-2717*
[147] Kadomtsev B B, Troyon F C and Watkins M L 1990 Tokamaks *Nucl. Fusion* **30** 1675–94
[148] Wesson J A 1987 *Tokamaks* (Oxford: Oxford Science Publications)
[149] ITER 1990 Conceptual design *Interim Report* (Vienna: IAEA)
[150] Gilleland J R *et al* 1989 ITER concept definition *Nucl. Fusion* **29** 1191–212
[151] ITER Physics Group 1990 *ITER Physics Design Guidelines: 1989 (Int. Thermonuclear Experimental Reactor)* (Vienna: IAEA) (February) p 43
[152] Bortnikov A V *et al* 1980 T-12 divertor experiment *8th Int. Conf. on Plasma Physics and Controlled Nuclear Fusion Research (Brussels, 1980)* vol 1 (Vienna: IAEA) pp 687–96
[153] Yu N Dnestrovskij *et al* 1991 Canonical profiles transport model for improved confinement regimes in tokamaks *18th European Conf. on Controlled Fusion and Plasma Physics* vol 1 pp 413–20
[154] White R B 1989 *Theory of Tokamak Plasmas* (Amsterdam: North-Holland) pp 373–5
[155] Kadomtsev B B and Pogutse O P 1967 Turbulence processes in toroidal systems *Voprosy teorii plazmy* no 5 209–350 (in Russian)
[156] Kadomtsev B B 1991 Plasma transport in tokamaks *Nucl. Fusion* **31** 1301–14
[157] Manheimer W M 1989 *MHD and Microinstabilities in Confined Plasma* (Bristol: Hilger)
[158] Cairns R A 1991 *Radiofrequency Heating of Plasmas* (Bristol: Hilger)
[159] Litvak A G 1991 *High-Frequency Plasma Heating* (Bristol: Hilger)
[160] JET Team 1992 Fusion energy production from a deuterium–tritium plasma in the JET tokamak *Nucl. Fusion* **32** 187–204

Index

Alfven waves, 23
Alpha particles, 191
ASDEX device, 29

Ballooning instability, 36, 81
Barrel-type equilibrium field, 28
Beta limit, 37
Blanket, 56
Bohm diffusion, 43
Bootstrap current, 53, 129
Break-even, 47
Burning plasma, 190

Canonical profile, 153
Complex physics system, 90
Conductivity, 50
Confinement modes, 132
Current drive, 49, 53
Cyclotron frequency, 12

D–T reaction, 10
DIII–D device, 29
Debye sphere, 96
Density limits, 35
Diamagnetic moment of a charged particle, 16
Diffusion of plasma, 147
Dimensional analysis, 92
Disruption instability, 38, 114
Divertor, 29
Drift frequency, 88
Drift instabilities, 85

ECR heating, 153, 186
Edge localized modes (ELM), 121
Edge plasma, 47
Energy confinement time, 11, 15
Equilibrium magnetic field, 27
Equilibrium of plasma, 24, 57

Fan instability, 117
Fish-bone instability, 119
Flute instability, 77
FT device, 104

Goldston scaling law, 105
Giro–Bohm diffusion, 45
Grad–Shafranov equation, 61

H-mode of plasma confinement, 7
Hugill number, 36, 101
Hugill plot, 35

ICR heating, 185
Impurities, 48
Inductance of plasma, 27
Inductor, 24
Internal kink mode, 85
ITER, 7

JT-60 device, 8

Kink instability, 65
Kruskal–Shafranov limit, 34

L-mode of plasma confinement, 7
Langmuir frequency, 51
Larmor radius, 12
Lawson criterion, 11
Linear off-set scaling, 146
London length, 148
Loop voltage, 24
Lower hybrid resonance, 184

Magnetic bubbles, 70
Magnetic confinement, 11
Magnetic islands, 46, 75
Major radius of plasma, 25
MARFE, 122
Merezhkin–Mukhovatov scaling, 41
Minor radius of plasma, 25
Mirnov oscillations, 38, 109
Murakami number, 36, 101

Neo-ALCATOR scaling, 7, 41
Neoclassical theory of transport, 42, 124
Neutral injection, 186

Ohkawa relation, 148
Ohmic heating, 183
Operation limits, 35
Optimal profiles, 153

PDX device, 119
Plasma shaping, 29
Poloidal magnetic field, 25
Profile consistency, 39
Profile resilience, 161

Quench (thermal), 116
Q-value, 47

Reconnection of magnetic field lines, 111
Reduced MHD-equations, 66
Resistivity of plasma, 76, 100
Rotational transform, 31
Rutherford regime of tearing mode, 76

Safety factor, 32
Saw-tooth oscillations, 110
Scrape-off layer (SOL), 62
Self-organization, 39, 151
Separatrix, 29
Shafranov shift, 60
Shear, 44
Shimomura scaling, 104
Similar tokamaks, 99, 142
Spontaneous break-down of symmetry, 45, 161
Supershots, 39

T-10 device, 153, 183
T-15 device, 8
Tearing instability, 72
TFTR device, 8
Thermal conductivity, 147
Thermal diffusivity, 147
Tokamak reactor, 54
Tore supra device, 8
Toroidal Alfven eigenmode (TAE), 191
Toroidal magnetic field, 25
Triangularity, 6
Troyon limit, 37

Viscosity of plasma, 150
Volt-seconds, 24

Ware-pinching, 52